Nucleation, Growth and Acoustic Properties of Thin Film Diamond

Michael D. Whitfield

This thesis is submitted for the degree of Doctor of Philosophy

Department of Electronic and Electrical Engineering
University College
University of London

SEPTEMBER 1998

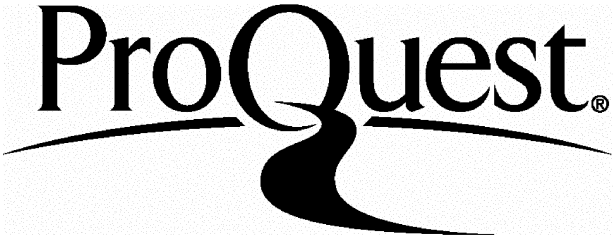

University of London

Abstract of Thesis

NUCLEATION, GROWTH AND ACOUSTIC PROPERTIES OF THIN FILM DIAMOND.

Michael D. Whitfield

The unusual combination of extreme properties possessed by diamond could potentially benefit a wide range of applications. Thus far practical utilisation of this material has remained difficult and consequently limited; natural and synthetic crystals are unsuitable forms for many uses, particularly electronic applications which ideally require large area, single crystal substrates. Emerging CVD methods for the growth of thin film diamond offer a practical alternative; although nucleation on non-diamond substrates during CVD growth is in general poor, recently introduced negative substrate biasing has shown that very high nucleation densities and limited forms of heteroepitaxy can be achieved. However, although development has been rapid many problems remain; in particular, the underlying mechanisms of biased nucleation and growth on non-diamond substrates are not well understood. Furthermore, the successful development of a new material such as CVD diamond relies on a balance between fundamental research and exploitation of its benefits in the form of applications; at present there are only a few such examples for CVD diamond.

This thesis addresses these issues by considering the bias enhanced nucleation of CVD diamond on silicon and *tungsten* substrates together with a study of the acoustic properties of the material. Bias enhanced nucleation and growth of (100) diamond on tungsten substrates has been characterised using secondary electron microscopy and Raman spectroscopy. Optical emission spectroscopy has been used to study the influence of substrate bias on the microwave plasma during diamond nucleation. Surface acoustic wave (SAW) devices have recently emerged as promising near term applications for *currently* available CVD diamond, however little is known about the propagation of acoustic waves in this material. A detailed study of the influence of film characteristics on acoustic propagation in free standing CVD diamond films has been undertaken using the techniques of laser ultrasonic analysis.

Acknowledgements

To my parents and family, here's what has been keeping me so busy lately. I hope having finished this doorstop I will be on your doorsteps a little more often now !

Of course there are a few others I need to thank here who have helped along the way but without the financial support of the EPSRC and my friends at DERA-Malvern via a CASE award there would be no need to write this in the first place and library shelves would be lighter. While thinking of the DERA I remember Don Rodway, sadly departed, for an introduction to the art of microwave chambers; and Dr. Jim Savage for being my industrial mentor these past years. Also my thanks to the technical staff at DERA for practical help with substrates and electronics.

While thanking collaborators I don't forget Liam and Colm over there at NMRC Cork for many lessons in Laser Ultrasonics, and rather more on the difference between the real stuff they serve over there and that ditchwater that passes for Guinness in London.

Here in London I am grateful to the numerous people at UCL who have helped me; particularly the Clean room staff, Kevin Lee, David Prescott and more recently Chris Nice; and the helpful chaps in the workshop, who always managed to make the thing no matter how feeble the sketch ! My thanks also to all others who have lent advice or bits of kit in the course of my work.

I have of course received untold help and support, well that's what they would call it, from the varied members of the Diamond Electronics Group who have provided a down to earth philosophy to counter our lofty ideals way up there in the greenhouse (or icebox, depending on season) on the 11^{th} floor; Duncs, the vacuum GURU for pearls along the 'if it ain't bust, don't fix it' line and lengthy appraisals of the advantages of bikes over cars... Robert for an endless (seemingly) supply of jokes, you'd call them ? Lisa for her cheery optimism and remarkable ability to convert alcohol to heat; Bhas, for his philosophical musings... oh, and for the Mickey Mouse you have so kindly bought back from Disney World just recently...no need to be so oblique; Simon, for the best training in cleanroom techniques and for an even better one in the art of cynical sarcasm; Looi, for enthusiastic and enlightening discussions on the why's and wherefore's of diamond transistor physics; but take it easy there your diligence is commendable but you don't want to *keep missing the sights* in Brighton; and also of course to our energetic leader and friend Richard B Jackman, without whom there would be no Diamond Electrons Group; whose boundless optimism defies the laws of finance but sadly not the laws of physics, even with aid of plenty of the good stuff ! and remember, *not everything makes sense in black and white*; so bear that in mind as you read this thesis.

Finally, last but not least, my deeply felt thanks to Alison, for her love, support and friendship which has kept us together as we have battled ? *not too strong I think*, towards our common goal...two doorstops !

MW, September 1998 (London)

Contents

Chapter 1

Introduction

Until rather recently the growth of a thin film form of diamond by chemical vapour deposition methods (CVD) remained little more than an interesting demonstration of metastable thermodynamics. Slow and difficult growth combined with poor understanding of the mechanisms had ensured that the diamond obtained by these methods remained of little technical significance. This was despite the acknowledged unique combination of extreme properties likely to ensure the superior performance of diamond, compared to competing materials, in many fields of application [Yoder 1994]. However, intensive research and development over recent years has now yielded a CVD process capable of producing significant quantities of high grade, low cost thin film diamond material. Realisation that the properties of this material are now becoming accessible is driving the rapid development of an increasing range of valuable technical and commercial applications.

The sustained development of any new or novel material is a difficult and slow process. Success requires the solution of basic materials science problems together with commercial exploitation for practical and profitable near-term applications. In these respect CVD diamond is not an exception and despite the considerable recent progress numerous problems remain to be overcome. Understanding of the diamond nucleation and growth processes remains relatively crude. Two important issues are the low nucleation densities typical on non-diamond substrates and the related question of achieving heteroepitaxy; the latter is a virtual requirement if commercially successful, fully active electronic devices are to be realised from this material. True heteroepitaxy of diamond has not been conclusively demonstrated on accessible substrates and even the best films remain polycrystalline in nature. This property is responsible for much of the non-ideal performance exhibited by these films when compared with predictions based on the properties of the natural material.

A key recent development has been the process of bias enhanced nucleation (BEN) in which a negative substrate bias of typically 200 volts is applied to the substrate during the nucleation phase prior to film growth [Yugo 1990]. BEN can result in substantial increases of around 10^6 in the nucleation density on non-diamond substrates and under certain circumstances can promote the growth of highly oriented films which exhibit a limited degree of epitaxy with the underlying substrate. When combined with (100) textured growth, very high quality CVD diamond films can be grown using this technique; these highly oriented diamond (HOD) films show improved electronic characteristics and are promising candidates for the development of realisable active electronics. However, the underlying mechanisms of BEN remain poorly understood in terms of both surface and gas phase processes which it presumably modifies and this presently restricts further progress towards heteroepitaxy using this technique.

This thesis presents the results of studies in which the two key areas in the development of a new material, which were mentioned above, are addressed i.e.material science and applications development. The work comprises studies undertaken to characterise some of the effects of BEN, in particular its influence on the regions of the microwave plasma close to the substrate surface. Understanding of the BEN mechanisms is necessary if the BEN process is to be controlled and optimised to provide the best possible CVD films for commercial exploitation. The development of realisable applications has been addressed in this thesis by a study of the effects of film characteristics, such as quality and morphology, on the propagation of acoustic waves in a range of examples of current free standing CVD diamond films. Recent publications [Nakahata 1995] strongly suggest that surface acoustic wave (SAW) devices are likely to become an important near term application for diamond films and the current study should provide information which can be utilised during the design of such devices. Attention is drawn to a class of acoustic devices known as flexural plate wave (FPW) devices for which CVD diamond may prove to be suited.

With these aims in mind chapter two provides an introduction to diamond, its extreme properties and current methods of synthesis. CVD growth methods are described and the mechanisms of nucleation, biased nucleation and growth on non-diamond substrates are discussed. Finally in this chapter, application issues for thin film diamond are considered.

The nucleation and growth work reported in this thesis was carried out using microwave plasma enhanced CVD in the form of a resonant chamber reactor. Chapter three provides a detailed account of the basic processes occurring within the plasma supported in these types of reactor and describes experimental techniques used during the current studies. The experimental work begins in chapter four, which presents the results of a comprehensive study of biased nucleation and growth on polycrystalline and single crystal forms of tungsten. Chapter five describes the results of optical emission studies of the effect of substrate biasing on atomic hydrogen, hydrocarbon species and electron temperature in the plasma together with the effects of reactor pressure and methane fraction. These studies indicated that the bias most strongly influences the regions directly above the substrate including the appearance of a thin secondary glow near to the substrate surface and lead to further OES studies at higher spatial resolutions to examine in more detail the near surface region; these studies are described in chapter six. From a process control perspective it is well known that the effects of BEN can be rather variable; in chapter seven the results of an atomic force microscopy study, to establish if simple laser reflectometry can be used as an in-situ optimisation probe for BEN, are described. The relationship between bias and orientation of the resulting nuclei are explored in terms of the ion flux from the plasma and the changes in the reflectometry signal from the biased surface. Although fundamental studies are important, applications must not be neglected if diamond films are to achieve full potential. In chapter eight the results of the first laser ultrasonic study of acoustic wave propagation in a range of free standing diamond films are reported; this study is timely in view of the likely development of CVD diamond SAW devices noted earlier. Finally, chapter 9 provides an overall summary of the work presented in the previous chapters together with a discussion of the implications for further studies.

References

Nakahata H., Higaki K., Hachiago A., Fujii S., Shikata S. and Fujimori N., [1995], *IEEE Trans. on Ultrasonics, Ferroelectrics and Frequency Control*, **42**, 362.

Yoder M.N., [1994], in *Synthetic Diamond: Emerging CVD Science and Technology*, (eds. Spear H.E. and Dismukes J.P.), John Wiley and Sons Inc., New York.

Yugo S., Kanai T. and Muto T., [1990], *Vacuum*, **41**, 1364.

Chapter 2

Current Status: Nucleation, Growth and Applications.

Diamond is an unusual material combining a range of extreme properties; until recently it was only available in the natural form or as relatively small stones produced by high-temperature-high pressure industrial techniques. Consequently despite its unusual properties the technical uses of diamond have remained limited. More recently Chemical Vapour Deposition (CVD) methods have been developed which permit the growth of *thin film* forms of diamond; such films are now readily accessible at economic cost and exciting applications exploiting the unique properties of diamond can be realistically considered. This chapter provides a brief introduction to diamond, its unusual mechanical and electronic properties and the methods by which the different forms of diamond are produced. The current status of nucleation and growth are summarised with particular attention given to the Bias Enhanced Nucleation (BEN) method. A *brief* summary of CVD diamond film applications concludes this introduction to the CVD diamond field.

2.1 Introduction.

This chapter presents an introduction to diamond, including its structure, properties, synthesis and applications. The discussion begins with natural diamond, which serves as a benchmark against which the success of 'artificial' diamond synthesis can be assessed. We are primarily interested in the growth of diamond by CVD means so after briefly mentioning the alternative means for synthesis the discussion moves swiftly on to consider the more common ways by which CVD growth of this remarkable material can be achieved. The heteroepitaxial nucleation of diamond is difficult because of diamond's high surface energy compared to most practical substrate materials; of the various nucleation methods, biasing is most directly relevant to the work described in this thesis and will be discussed in some detail together with a summary of nucleation models. Following successful nucleation the diamond film must be grown out to a useful thickness for whichever application is being considered; therefore a brief discussion of some of the general principles of growth is given. Finally, a short description and discussion of some of the many possible applications for which diamond can be considered is given. The brevity of this final section belies its importance; the author is of the opinion that applications and the development of 'real' uses for this versatile material are critically important if it is to become 'accepted' by the industrial community as a realistic and valuable alternative for the solution of practical problems.

Clearly it is impossible to give a complete and comprehensive review of the entire CVD diamond research effort, which has been undertaken to date in a single chapter. All of the areas discussed in the following pages have been well reviewed by other authors and the reader should consult the references given in the main text if a more detailed treatment is sought

2.2 Diamond

Diamond is a naturally occurring crystalline form of carbon consisting of a lattice of tetrahedrally bonded carbon atoms with sp^3 type bonding and a nearest-neighbour interatomic distance of 1.54 Angstroms [Wilks 1991].

The chemical bonds are extremely strong and their density at 3.5×10^{23} cm^{-3} is the highest among all known crystalline structures; as a result diamond is the hardest naturally occurring material. Its name is derived from the Greek *adamas* which means 'unconquerable, invincible '. Although most well known for being the hardest material, diamond combines a number of unusual and extreme properties; it is an excellent semiconductor, it is optically transparent and diamond is also the strongest and most thermally conductive of all naturally occurring materials. These remarkable properties have, during latter part of this century, been the driving force behind considerable research efforts aimed at the large scale technical utilisation of a material which had previously been appreciated mainly for its aesthetic beauty. This has lead to the development of a high-pressure-high-temperature (HPHT) process for making synthetic diamonds and more recently chemical vapour deposition (CVD) processes which have enabled the growth of thin film diamond on both diamond and non-diamond substrates.

2.2.1 Structure of Diamond.

Diamond is an allotrope of carbon. Carbon is a group IV element with an atomic number of 6; it has a $(1s)^2$ $(2s)^2$ $(2p)^2$ electronic structure. It can be more energetically favourable for the four valence electrons to be distributed with one in the s-orbital and one in each of the three p-orbitals. The s and p levels may mix to form four equivalent hybridised sub levels which are capable of covalent bonding [Kittel 1986]. Carbon may crystallise in a number of forms determined by the bonding type, which in turn depends on external conditions. For example, sp (carbyne), sp^2 (graphite) or sp^3 (diamond). Mixed bonding e.g. sp^2 and sp^3 can occur which leads to the diamond-like-carbon (DLC) class of materials; also it is possible to obtain amorphous random-like networks of e.g. sp^3 dominated material, which display no discernible crystallinity. The sp^3 hybridisation results in a tetrahedral configuration, in which each atom is covalently bonded to its four nearest neighbours. This is the diamond lattice, shared by materials such as silicon and germanium, which can be viewed as two interpenetrating face-centred-cubic (fcc) lattices, displaced one from the other by a quarter of the cube diagonal. The diamond lattice is characterised by a nearest neighbour distance of 0.154450 nm and a lattice constant of 0.356683 nm at 298K [Bakon 1993].

The diamond lattice is illustrated in figure (2.1), which shows the two interpenetrating fcc lattices as black and white circles respectively.

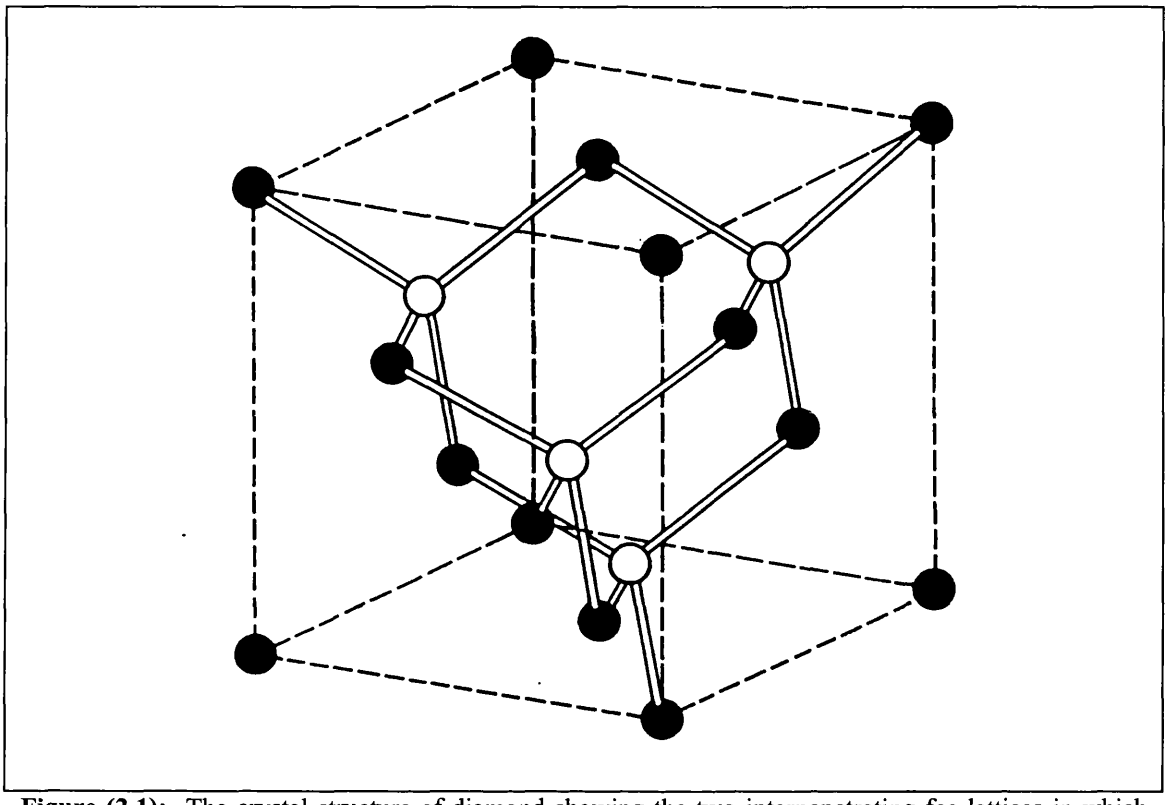

Figure (2.1): The crystal structure of diamond showing the two interpenetrating fcc lattices in which one lattice (white circles) has been displaced by one quarter the body diagonal of the other (black circles); [redrawn from Kittel 1986].

The underlying lattice structure together with growth conditions determines the visible crystal type, i.e. the bounding facets of as grown crystals depend upon the competition between the growth rates in different crystallographic directions and the growth rates depend strongly on the external conditions. For a natural diamond crystal free to grow in all directions the dominant forms are bounded by the family of eight {111} planes and result in the classic octahedral shape usually associated with diamond. However, depending on conditions, {100} and {110} facets can be present and result in a complex range of morphologies including cubes and cubo-octahedral types. Twinning and re-nucleation can add to the complexity of the observed crystal shapes; diamond morphology has been well reviewed by a number of authors and further details can be found elsewhere [e.g. Bruton 1978, Clausing 1998].

2.2.2 Properties of Diamond

The high atom density of the diamond lattice and lightness of the carbon atom together with its very strong covalent bonding give rise to a range of mechanical and electrical properties which by comparison with many materials are extreme. Consideration of these properties, either singly or in combination, suggests that diamond can be expected to provide high performance in many areas of application and in some cases may exceed the performance of competing materials by orders of magnitude. For example, the combination of high transmittance and strength suggest that diamond would be an ideal material for infra-red windows, for use in aeroplanes and missiles. The current generation of materials such as zinc selenide (ZnSe) are relatively soft and can withstand only limited damage before becoming effectively opaque [Kline 1991]. Damage, in this context, includes that from collisions with innocuous sounding substances such as rain! The combination of high transmittance and the high thermal conductivity indicates that many of the problems associated with high power density laser windows, would benefit from the use of diamond. Applications in visible blind UV radiation detectors and acoustic wave filters could also benefit and there are many others which have been suggested [Yoder 1994]. The mechanical properties of diamond are summarised in table (2.1) [Bachmann 1991] and electrical properties are given in table (2.2).

Property	Value	Comparison	Applications
Hardness $Kg.mm^{-2}$	12000 - 15000	Hardest Material	Drill bits, Polishing, Cutting tools, Surgical Knives.
Friction Coefficient	0.2 (in air)	Very low in air, higher if kept under vacuum	Lens coatings, bearings, tools, hard disks, sliding parts.
Young's Modulus Nm^{-2}	1.2×10^{12}	Highest Mechanical strength, twice the value of alumina	Stiff membranes for lithography, masks,radiation windows,audio tweeter domes, micromachining.
Sound Velocity km. s^{-1}	18.2	1.6 times value for alumina	As above.
Thermal Conductivity $Wcm^{-1}K^{-1}$	20	Value for type IIa natural diamond is 4 x that for copper.	Highly efficient electrically insulating heat sinks for high power/ VLSI electronics.
Thermal Expansion Coefficient K^{-1}	8.0×10^{-7}	Value at room temperature close to silica	Thermally stable substrates for e.g. x-ray lithography masks, power laser windows.
Chemical Inertness	Inert	inert, resistant to all acids and bases at room temperature.	Coatings for reactor vessels, sample containers, analytical instruments,medical prosthesis

Table (2.1): Selected mechanical properties of diamond extracted from [Bachmann 1991].

Property	Silicon	GaAs	Diamond
Dielectric Constant	11.9	12.8	**5.7**
Electron Mobility ($cm^2.V^{-1}.s^{-1}$)	1500	8500	**2000**
Hole Mobility ($cm^2.V^{-1}.s^{-1}$)	600	400	**1800**
Saturation electron velocity ($cm\ s^{-1}$)	10^7	$2x10^7$	**$2.7x10^7$**
Breakdown Field ($V.cm^{-1}$)	$0.3x\ 10^6$	$0.4\ x\ 10^6$	**10^7**
Intrinsic resistivity (Ω.cm)	10^3	10^9	**10^{16}**
Work function (eV)	4.8	4.7	**4.8 (p-type) -ve (111)**
Bandgap (eV)	1.1	1.43	**5.45**

Table (2.2): Electrical properties of diamond shown compared to silicon and gallium arsenide, [extracted from Yoder 1993, Morkoc 1994]

Although the extreme properties of diamond have been acknowledged for many years, it is only recently, with the development of a CVD process for the controlled growth of diamond, that it has been possible to consider more fully the exploitation of much of the potential suggested in tables (2.1) and (2.2). Previously the applications of diamond have been restricted by the size, shape, reproducibility and cost of the natural material and a very limited ability to modify the material to suit the need at hand. These difficulties were alleviated to some extent by the development in the 1950's of a reproducible, high pressure high temperature (HPHT) process for the synthesis of diamond and subsequently a very large market for industrial diamonds has been created. However despite this, most applications have tended to exploit only the excellent mechanical properties such as strength and thermal conductivity. The total market for natural and synthetic (HPHT) diamond has been estimated at 65% for abrasives, 20% for micron powders, 10% for drilling and 5% for toolstones [Bakon 1993]. However, in the last 20 years the *metastable* growth of diamond, which was first reported in the early 1950's by Eversole and co-workers of the Union Carbide Corporation, [Spear 1994] has undergone extremely rapid development. There is now available a CVD process for the metastable growth of diamond which is clean, fast and controllable; takes place at modest temperatures and pressures and allows for controlled impurity doping. Thin (μm's) or thick (mm's) large area films of polycrystalline diamond can now be grown from simple gaseous constituents, such as

methane and hydrogen, to a purity which exceeds that of the very best natural crystals. Many of the extreme properties suggested in tables (2.1) and (2.2) can now be made available in an engineering material at accessible and reasonable cost.

2.2.3 Synthesis of Diamond.

Diamond is not a stable form of carbon at normal temperatures and pressures; it is metastable. This effectively means that if 'hot' carbon atoms are brought together and allowed to cool they prefer to condense as graphite and other forms of non-diamond carbon. If diamond is heated, *in vacuo,* to a temperature exceeding ~1800°C, then it will begin to spontaneously convert into graphite. Strictly speaking there is a conversion rate for this reaction at any finite temperature, although at room temperature it takes place so slowly that it requires millions of years to convert any significant amount of diamond to graphite. If this were not so, no significant diamond deposits would still exist to be mined. The conditions under which diamond becomes the thermodynamically preferred state of carbon can be appreciated from consideration of the diamond-graphite phase diagram such as the Berman-Simon curve shown as figure (2.2) [Wilks 1991].

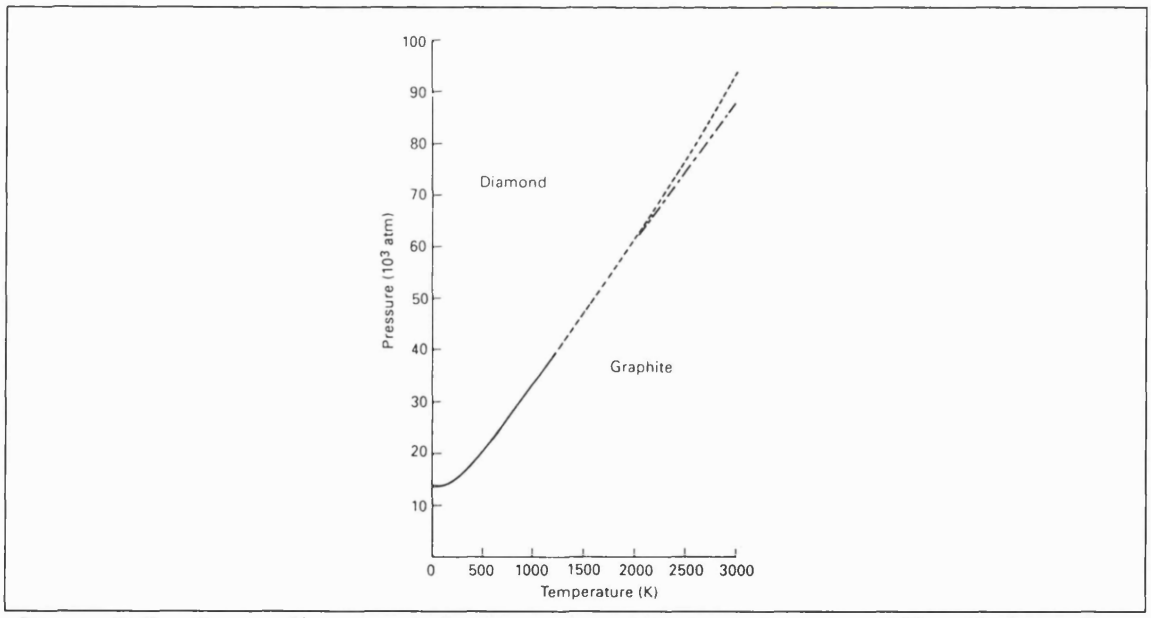

Figure (2.2): Berman-Simon graph for diamond-graphite thermodynamic stability, [Redrawn from Wilks 1991].

(i) Natural diamond

Diamond grows naturally under conditions of high temperature and pressure which exist at sufficient depths within the Earth's crust. The diamond bearing rocks are brought to the surface by volcanic activity and then may be eroded and re-deposited in sedimentary rocks by environmental processes. Natural diamond exists in many forms with differing qualities and purity depending on the conditions under which it was initially formed. A system has been developed which divides naturally occurring diamonds into four broad categories; this classification system is summarised in table (2.3) [Wilks 1991].

Type	Abundance	UV absorption edge	IR absorption edge	Nitrogen content
Ia	~ 98% (natural)	~ 330nm	2.5-10 μm	N to 0.3%, A and B aggregates; low levels of single N atoms in single substitutional sites
Ib	~ 0.1% (natural) most HPHT			
IIa	~ 2%	~220 nm	2.5-6 μm transparent > 6μm	Very low N level.
IIb	< 0.1%			Extremely low N; semiconducting (Boron acceptors)

Table (2.3): The classification of natural diamond crystals, [adapted from Wilks 1991]

Naturally occurring diamonds are currently mined mainly in Africa, the former USSR and Austrailia [Bakon 1993] and can be classified according to table (2.3). Type I diamonds contain some nitrogen impurities and exhibit a characteristic UV absorption edge at ~330 nm. Type Ia contain mainly nitrogen aggregates and account for ~98% of the mined material. Type Ib contain mainly single substitutional nitrogen and account for ~0.1%. Type II diamond are characterised by very low nitrogen levels, leading to a near bandgap UV absorption edge at ~220 nm and account for ~2% of natural diamonds. Type IIb diamond are extremely rare type II diamonds with unusually low nitrogen levels together with some additional boron impurities which have been shown to give rise to p-type semiconducting behaviour, [Collins 1971].

(ii) High pressure high temperature growth of diamond

Consideration of the phase diagram shown in figure (2.2) implies that under suitable conditions of temperature and pressure the production of a synthetic form of diamond should be possible. Following the discovery, in the late 18^{th} century, that diamond is a crystalline form of carbon, together with the development of chemical thermodynamics, Bundy and co-workers at General Electric reported the first successful attempt to synthesise artificial diamond at a temperature-pressure regime in which diamond was the thermodynamically preferred form of carbon [Davidson 1994]. Growth methods, which take place in the diamond region of the phase curve, shown in figure (2.2), are referred to as high-pressure high-temperature (HPHT) techniques. The method invented by Bundy *et al.* was rapidly developed and today there are a number of HPHT techniques which can be classified as: (i) direct conversion, (ii) metal solvent catalyst, (iii) shock wave conversion and (iv) diamond seed crystal growth. The method used depends on a combination of the intended application and various economic costs; metal catalyst methods can improve growth rates significantly. If high purity is desired the seed crystal methods can yield diamond comparable in quality to the best natural stones at growth rates of 2-3 mg hr^{-1}. Further discussions can be found elsewhere; [Bakon 1993, Wilks 1991].

HPHT produced diamonds are mainly used in abrasive and cutting applications and while boron doping is possible, the resulting material has poor uniformity and tends to be subject to impurities from the HPHT process; this is not a realistic way to produce bulk quantities of electronic grade material. Many other potential applications such as protective coatings and thermal substrates are also severely limited by the form of HPHT material.

(iii) Chemical Vapour Deposition of Diamond

The metastable growth of diamond with respect to graphite was first reported by Eversole of the Union Carbide Corporation in the 1950's. In 1962 Angus recognised the importance of atomic hydrogen to the process via the suppression or preferential etching of co-deposited non-diamond phases. In the 1970's and early 80's Russian groups demonstrated growth on non-diamond substrates for the first time. Up until this

point growth rates were unfeasibly low and metastable diamond synthesis was little more than a scientific curiosity with few prospects for widespread applications. However, at the beginning of the 1980's, the Japanese National Institute for Research in Inorganic Materials (NIRIM), developed improved activation and deposition techniques based on microwave and hot filament coupled plasmas, which enabled them to produce improved films and more importantly much higher growth rates, [see Davidson 1994 for a tabulated history and references]. This was a key development and subsequently the field has expanded rapidly; many different deposition techniques have been developed and there is now a considerable world-wide community engaged in research of many aspects of CVD diamond growth which is now the most versatile method for producing this unusual material.

There is only a small free energy difference between diamond and graphite; around 0.03 eV/atom at 298 K and atmospheric pressure [Angus 1989]. Therefore there is always a finite probability that both phases will form during synthesis by whatever method. To promote the formation of diamond the growth conditions must be adjusted to ensure that the growth rate of graphite and other non-diamond carbons is very low. This requirement has been considered in terms of the minimum thermodynamic, chemical and kinetic factors which each of the multitudinous deposition techniques must provide if diamond is to grow successfully; Koba [1993] has listed the important features:

(i). Bulk transport and activation of a carbon gas phase to produce species suitable for the formation of diamond precursors.

(ii). Transport of activated gas phase species to the substrate surface; adsorption of precursors onto the growth surface.

(iii). Diffusion and reaction of precursors on the surface to allow film growth.

(iv). The presence of an sp^2 suppressing gas species in sufficient concentrations to ensure that the dominant phase surviving deposition is sp^3 bonded material. Usually this requirement is satisfied by a high concentration of atomic hydrogen which performs a number of critical roles in the growth environment including: the preferential etching of graphite (~50 times faster than diamond), stabilisation

of the growth surface and generation of radical sites, providing a route for continued growth of the sp^3 like surface [Angus 1989, Bachmann 1991].

2.2.4 CVD Growth Techniques

Many techniques are able to satisfy the requirements needed to ensure the preferential growth of diamond under metastable conditions. The most common can be broadly divided into (i) hot filament CVD, (ii) plasma enhanced CVD and (iii) combustion CVD; these methods have been extensively reviewed in the literature e.g. [Zhu 1991, Bachmann 1993, Bachmann 1998].

(i) Hot-filament chemical vapour deposition (HFCVD)

Originally reported by Matsumoto *et al* [1982], this is one of the simplest methods of CVD in which metal filaments, electrically heated to ~2000°C, dissociate and activate a suitable precursor gas, typically a 1% CH_4 in H_2 mix. The substrate, usually silicon, is situated ~1 cm from the filament. Other typical chamber conditions are pressure ~40-100 Torr, total gas flow ~100 sccm; under such conditions growth rates of 1-10 $\mu m\ hr^{-1}$ have been obtained. Deposition area is limited only by the filament shape and design; the method is ideal for scale-up and is capable of coating complex shapes [May 1995].

Problems with the HFCVD method include; conversion of the refractory metal filament to a carbide leading to brittle fracture and failure, contamination of the film with filament metal can also occur which is detrimental to the semi-conducting properties of the film. A typical HFCVD experimental arrangement is shown in figure (2.3) [redrawn from Matsumoto 1982].

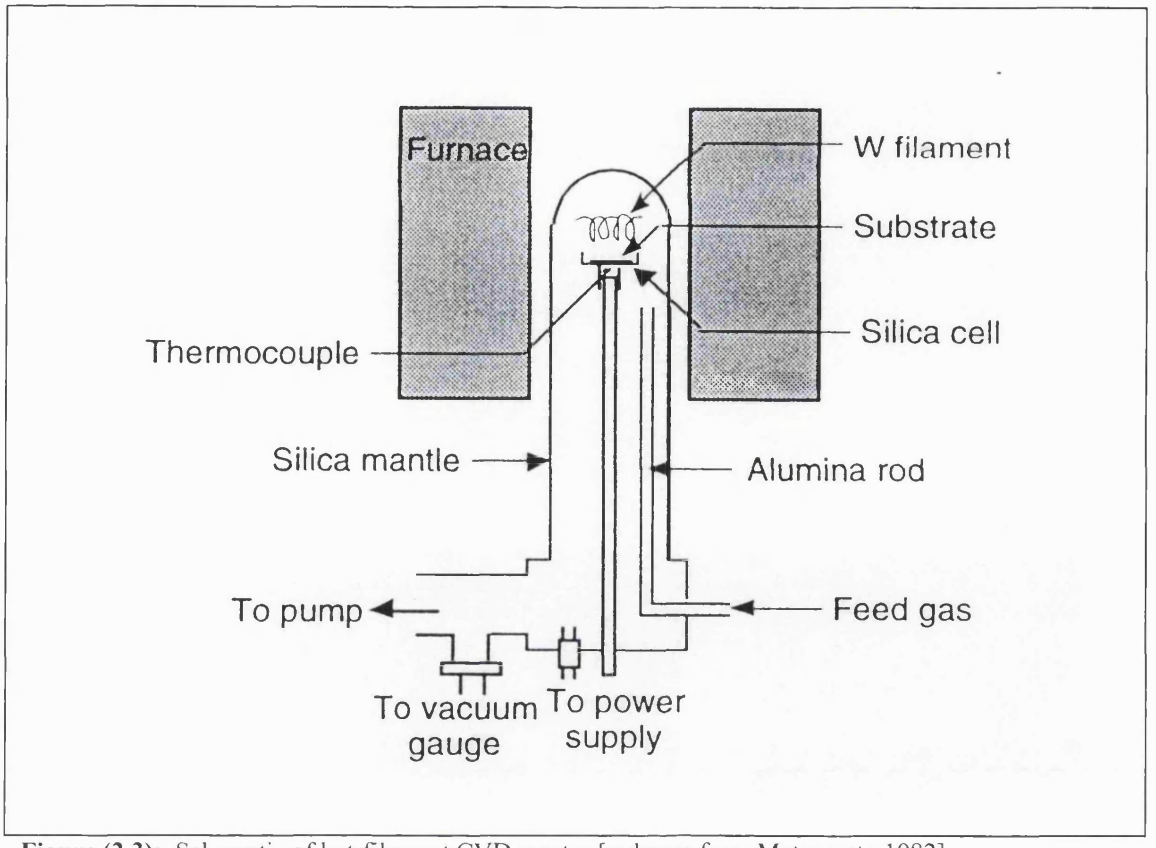

Figure (2.3): Schematic of hot-filament CVD reactor [redrawn from Matsumoto 1982].

(ii) Plasma enhanced chemical vapour deposition.

Proposed in 1981 by Spitsyn [1981], a number of plasma systems have subsequently been developed. These all rely on the dissociation of a suitable gas precursor by electric fields to generate a plasma containing a mixture of neutrals, ions, electrons and radicals which, under the correct conditions, supply the required growth species for diamond film growth on a nearby substrate. Microwave (MW), radio-frequency (RF) and direct current (DC) fields have all been successfully employed in such systems. Plasma systems are also characterised by pressure which determines the degree of thermal equilibrium within the plasma; higher pressure systems (> 200 Torr) are in near thermal equilibria and full dissociation may occur within such environments leading to very high growth rates. The various forms of plasma enhanced deposition systems have been well reviewed elsewhere [Bachmann 1998]. The most common and successful of these are the 2.45 GHz microwave activated systems, which it has been argued were largely responsible for the huge research effort of the last fifteen years which has moved CVD diamond growth from a curiosity to an industrially relevant technique [Bachmann 1998]. The most common forms of the 2.45 GHz system are

briefly described below; more detailed descriptions can be found in the suggested references. A detailed discussion of the ASTeX resonant cavity form of the microwave system is given in chapter 3, together with a discussion of the processes which occur within the microwave activated plasma.

The choice of specific frequencies for RF and MW systems is mainly driven by the ready industrial availability of components which comply with national regulations; 2.45 GHz is particularly convenient as the ~12 cm wavelength leads to waveguide components etc. which are reasonably compact, while a cheap supply of suitable magnetron power sources are available due to the use of this frequency for the domestic microwave oven. First developed by the NIRIM group, in a tubular silica chamber form, figure (2.4a), typical deposition conditions are similar to hot-filament reactor conditions e.g. pressure 20-100 Torr, substrate temperature ~800 °C, 1% CH_4 in H_2, total gas flow ~100 sccm; under these conditions, with a 1kW magnetron supply, growth rates of ~ 1-5 μmhr^{-1} can be achieved. The design, while reasonably easy and cheap to set up, suffers from problems of reliability and silica contamination from the reaction tube which typically contacts the plasma. An improved system introduced by Bachmann [1993] is the 'Bell Jar' reactor shown in figure (2.4b) which was subsequently developed into the well known ASTeX High Pressure Microwave System (HPMS) system which is described in more detail later in this thesis. The 'Bell Jar' design is a resonant cavity system which allows growth over larger areas and significantly reduces wall contamination in the as grown film. An interesting alternative is electron-cyclotron resonance (ECR) systems in which the electron gyration frequency coincides with the driving microwave frequency. A typical set-up is shown as figure (2.4c); 2.45 GHz ECR systems have been examined in detail by Kawarada [1987] as a possible route to achieving large, uniform, high density plasmas compared with resonant cavity systems. However, efficient ECR requires low pressures, typically less than 0.1 mbar. Under these conditions growth rates and crystal sizes are observed to be rather poor and it has been concluded that such systems although showing initial promise are best suited to the deposition of mixed phase films for use as low wear coatings [Bachmann 1998].

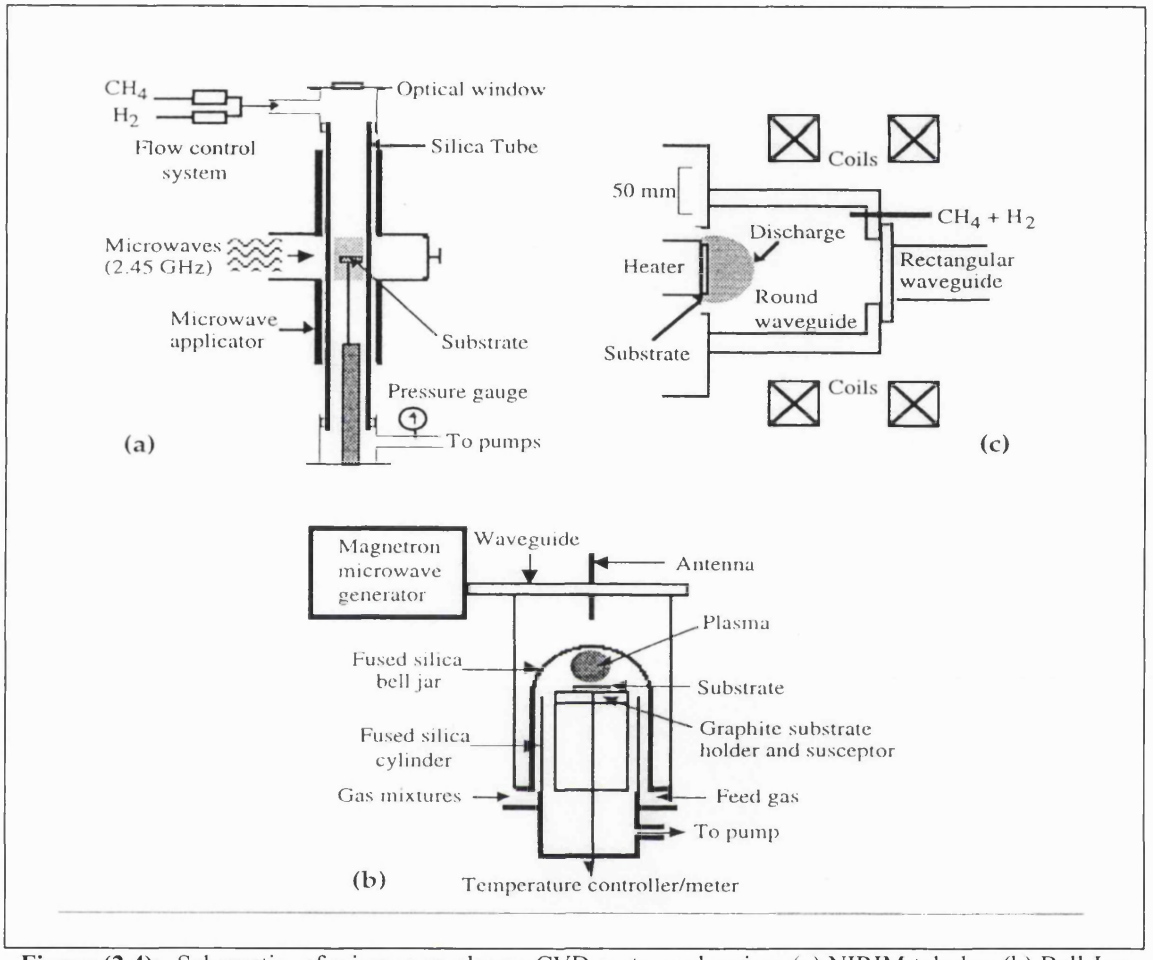

Figure (2.4): Schematic of microwave plasma CVD systems showing; (a) NIRIM tubular; (b) Bell Jar; and (c) ECR coupled; arrangements [redrawn form Zhu 1991].

(iii) Combustion Flame CVD.

A novel method developed by Hirose, [1988] called combustion flame CVD utilises a simple oxy-acetylene welding torch and a water cooled substrate holder; a typical set-up is shown in figure (2.5). A high gas pressure and high temperature means that the flame acts as a thermal plasma with a low degree of ionisation. For this reason much of the hydrogen and oxygen liberated in the combustion process is present in the form of atomic species which together with carbon species from the dissociation of acetylene provides the conditions for diamond growth. The acetylene-oxygen ratio is critical and is usually around unity; the substrate is typically placed in the inner bright flame rather than the oxidising outer flame which would convert carbon to gaseous carbon dioxide. Gas temperatures are of the order of 3000 ^{o}C, while substrate temperatures are maintained at

800-1000 ^{o}C. Very high growth rates of up to 140 μmhr^{-1} can be attained in typical combustion flame systems. Main problems are with substrate temperature, process stability and film quality which are all difficult to control. It is surprising that such a simple method works and clearly illustrates the diversity of CVD growth methods.

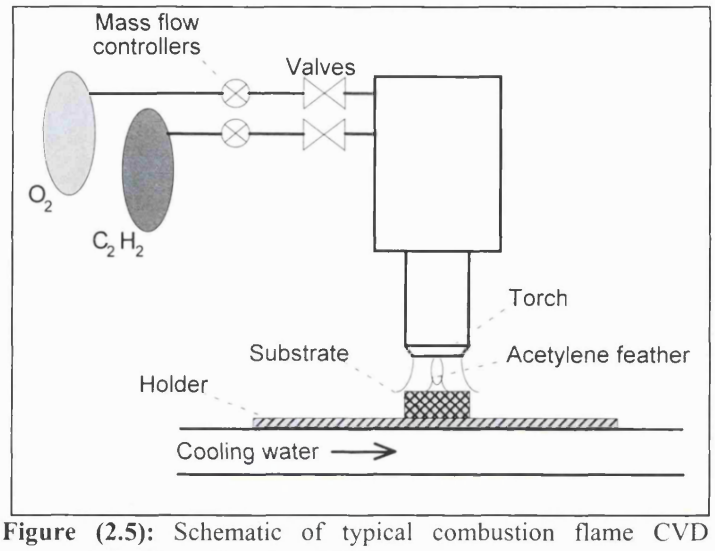

Figure (2.5): Schematic of typical combustion flame CVD apparatus [redrawn from Zhu 1991].

Only a few of the many techniques successfully used to grow diamond have been described here. Useful summaries of the various diamond growth techniques have been given in reviews by Bachmann [1993,1998], while a tabulated comparative summary has been given by Chan [1996]. The deposition method chosen ultimately depends on a combination of the application requirements for the diamond film together with economic considerations. For example, in pure research the resonant cavity 2.45 GHz system will no doubt continue to dominate over the medium term, for its stability, large comparative research base, modest cost and convenient size; while industry can be expected to accelerate the development of high power density, large area deposition systems, such as arc-jets and RF plasma torches, for their scale up potential and high growth rates. Currently, it is the cost of CVD diamond production which prevents its uptake in many high volume applications, rather than material quality considerations. A measure of the success of the CVD research effort can be appreciated when it is realised that the industrial diamond producers, such as Norton Diamond Inc. (USA), are now able to grow uniformly over a 10 inch substrate wafer, at a cost per carat, which has been reduced by two orders of magnitude in the last ten years.

2.3 Nucleation

The ultimate goal of CVD diamond growth is successful heteroepitaxial growth; that is the growth of single crystal diamond over a large area on a single crystal, non-diamond substrate. This approach is necessary because large area single crystal diamond substrates to act as blanks for the subsequent growth of a thin film which could then be sliced to form wafers are not readily available. Unfortunately there are also no alternative substrates available which are lattice matched to diamond with similar surface energy and thermal expansion coefficient; consequently progress in true heteroepitaxial growth has been limited thus far. A notable exception is cubic-boron nitride (c-BN) on which epitaxy has been achieved [Koizumi 1990], however c-BN is even harder to grow than diamond and substrates larger than ~1mm diameter are difficult to obtain; the current status of heteroepitaxial growth has been reviewed recently by Bozeman [1998]. An interesting alternative approach to obtain 'near single crystal' templates has been reported by Geis *et al.* [1991a], in which oriented, single crystal seeds ~100 μm in size were placed into etch pits on a silicon surface. These were then overgrown to form relatively thick films containing very low angle grain boundaries; such plates can then be used as templates for the further growth of high quality films which are subsequently cut or lifted off. However it is very difficult and expensive to make such templates and grain boundaries always occur because it is virtually impossible to align perfectly the seed crystals. So although this approach may be useful in the near term for low volume, high value applications it unlikely to be a realistic solution for the mass production of high quality single crystal substrates which are the ideal requirement of many applications, for example electronic devices.

Before growth of any sort can be considered, the film must first be nucleated on the substrate. The nucleation mechanisms of diamond on non-diamond substrates are not well understood and in general the process is difficult; these mechanisms are the subject of considerable experimental and theoretical work and numerous possibilities have been considered. The nucleation of diamond has been well reviewed in the literature; useful summaries have been given by Liu and Dandy [1995] and Bozeman, Stoner and Glass [1998]. The difficulty with nucleation is probably due to a combination of: the high surface energy of diamond compared to most available substrates, low sticking probability

for the diamond precursors and competition from other non-diamond phases which would also like to grow on the substrate. Because of its high surface energy diamond nucleates and grows in a Volmer-Weber mode which leads to continuous films via the three dimensional growth of nucleation sites [Volmer 1926]. Clearly if the nucleation density is low this results in very rough films, furthermore growth is very slow until the nuclei coalesce and the growth mode changes to a 2-D layer mode; e.g. Frank-van der Merwe [Frank 1949]. To obtain reasonably smooth films and respectable growth rates, a high nucleation density is required and this means that some type of nucleation enhancement process must be employed. It has also been observed that nucleation density is much higher on polycrystalline substrates compared to single crystal substrates and that substrates can be divided into carbide and non-carbide forming materials on which the details of the nucleation mechanisms may differ.

Enhancement methods which have successfully been used to promote the nucleation of diamond can be broadly divided into: abrasive, seeding and biasing. The typical unaided nucleation density on pristine silicon, the most commonly used substrate, is ~10^5 cm^{-2} from which it can be estimated that for a growth rate of around 0.5 μm hr^{-1} film coalescence time will be on the order of 60 hours excluding any incubation period required. At coalescence the nuclei will be rather large and consequently the film will start with a high surface roughness which will get worse with increasing thickness.

2.3.1 Conventional Enhancement Mechanisms

Scratching with both diamond and non-diamond abrasives has been shown to enhance the nucleation density by several orders of magnitude [Liu 1995]. Diamond abrasives give the highest enhancement and it is thought that one mechanism may be homoepitaxial nucleation on diamond seed particles left in the substrate. An additional mechanism is probably nucleation on damage regions which may have a higher surface energy than the undamaged surface. On silicon, enhancement to nucleation densities as high as 10^{10} cm^{-2} have been shown; studies have indicated that nucleation density is approximately inversely proportional to the size of the abrasive particles. Scratching methods include wet and dry abrasion and ultrasonic agitation in a suspension of the abrasive material. Scratching however, can contaminate and damage the substrate, which can be detrimental to the subsequently grown film; an alternative method involves seeding or coating the substrate

with a carbon containing or carbonaceous material. Enhancement in this way has been achieved with a range of materials including; carbon fibres, graphite powders, hydrocarbon oils and a-C:H films; however the methods are poorly characterised and few general conclusions can be drawn with regard to likely nucleating species [Bozeman 1998].

Although these treatments are attractive in that they are inexpensive, simple and effective, they are not well suited to optical or electronic applications as they either contaminate or damage the substrate; furthermore the treatment of non-planar geometries can be difficult, especially if abrasives are used. These methods also suffer from being in the main *ex-situ* and are not amenable to simple quantitative control with respect to the subsequent nucleation density achieved.

2.3.2 Bias Enhanced Nucleation (BEN)

A very promising alternative is electrical substrate biasing, which causes minimal substrate damage, can be carried out *in-situ* and can be easily controlled through the bias voltage and time; its progress can be monitored by tracking the development of the bias current with time and by simple laser diagnostics on the nucleating substrate. Typical nucleation enhancements up to ~10^{11}cm^{-2} have been obtained on pristine silicon and it has been estimated, based on critical nuclei size, that a maximum nucleation density up to 10^{14}cm^{-2} may be achievable using BEN [Yugo 1996]. Further details and discussion can be found in recent reviews [Bozeman 1998 and references therein; Liu 1995] and in the introduction and discussion sections of chapters 4,5,6 and 7 in this thesis.

During bias enhanced nucleation (BEN), a negative bias of ~100-250 V is applied to the substrate relative to the chamber or a second electrode within the chamber. The methane fraction is often increased to ~3-5%; substrate temperature can be increased to ~850-900 °C and the reactor pressure reduced to ~15-20 Torr to obtain a more uniform plasma; however the precise details show considerable variation and typically have to be optimised for a given reactor and conditions. BEN has been shown to have two very important effects:

(i). A strong nucleation enhancement on many types of substrate; typically on pristine silicon the nucleation density increases from ~10^5 cm^{-2} to ~10^{11} cm^{-2}.

(ii). Under certain conditions, which are rather critical, limited epitaxy of the diamond nuclei with the substrate can be observed; most commonly studied on silicon the effect has also been seen on other substrates. If BEN is combined with (100) textured growth, then highly oriented (100) textured diamond films, termed HOD films, can be grown which show significantly improved characteristics compared to other films.

BEN is widely considered to be the most important nucleation technique available for promoting nucleation on non-diamond substrates; at present it is the only realistic way to obtain highly oriented and textured diamond films which display improved electronic properties [Stoner 1993] arising from the low angle grain boundaries characteristic of these types of film. BEN was first reported by Yugo [1990] and since then has been the subject of extensive investigation by many groups; a review of *selected* contributions is given here. Early reports concentrated on biasing studies in hot filament reactors using either biased filaments or additional wire electrodes between the hot-filament and the substrate [Yugo 1991, Lee 1990, Chang 1992]. A threshold bias at around -100 V was observed below which little nucleation enhancement seemed to occur. Enhancements of 3-5 orders of magnitude were reported and suggested explanations included; sheath effects, altering the balance of electron and ion bombardment of the substrate; enhanced H_2 dissociation, leading to elevated near surface atomic hydrogen concentrations which could reduce sp^2 formation; and active species generation near to the substrate by accelerated H^+ ions. Considerable insight as to the substrate effects of BEN were provided by a very detailed and systematic study by Stoner *et al.* [Stoner 1992] who introduced biasing to MPECVD and studied its effect, *in vacuo,* on pristine silicon using an unusually wide range of probes including; XPS, AES, XPS-EELS, Raman, SEM and TEM. They observed the removal of surface oxides and the generation of SiC and α-SiC on the silicon surface and subsequent deposition of an amorphous carbon layer. They proposed simple models to explain their observations involving the nucleation of diamond on the SiC layers; the details of these models are considered in the next section. Wolter [1994] subsequently demonstrated the importance of carbide formation by investigating the effect of BEN on carbide forming and non-carbide forming substrates. Only small enhancements in nucleation density were found for copper, which does not form a carbide but which is a better lattice match to diamond. Carbide forming substrates which were studied included silicon and a number of the refractory metals; the authors demonstrated that BEN nucleation enhancement followed

the carbon affinity of the substrate; although silicon proved to be an exception which the authors suggested may be due to crystal structure effects. The first BEN oriented nuclei were reported by Stoner and Glass [1992] on pure β-SiC substrates in which ~50% of the nuclei exhibited preferential orientation with respect to the underlying substrate. On silicon, BEN oriented nuclei were first demonstrated in 1993 [Wolter 1993]; 30% of the nuclei were oriented with respect to the (100) silicon substrate following a newly introduced pre-bias *carburisation* stage which gave rise to limited areas of highly oriented (100) textured diamond film following subsequent growth. The authors suggested that the carburisation stage formed an epitaxial SiC layer and reduced the nucleation time thus minimising the detrimental effects of long biasing times which could damage the oriented nuclei. Subsequently it has been shown that a carburisation layer is not essential to the generation of BEN oriented nuclei [Jubber 1996]. Many groups have subsequently studied the generation of HOD films using BEN and current films can achieve HOD over large areas (> 30 cm^{-2}) [Floter 1998] compared to very limited areas of the early reports (~mm^2 or less).

2.3.3 Models for Diamond Nucleation.

(i) Conventional Nucleation.

Nucleation on non-diamond substrates has been classified into; nucleation on an intermediate diamond-like amorphous carbon [Singh 1994]; metal carbides [Lux 1991] or graphite [Lambrecht 1993] formed during the incubation period at the substrate surface by interaction with gas phase species. The thickness of the intermediate layer ranges from Angstroms e.g. 6Å for carbon on platinum [Belton 1992], to microns, e.g. 1.5-3 μm for Mo_2C on Mo [Bou 1992]. The representative nucleation mechanisms are shown in figure (2.6 a-c) as summarised by Liu [1995]; brief details are given in the text accompanying the figure; further details can be found in the review by Liu and references therein [Lui 1995] and [Bozeman 1998].

The models shown in the figure assume the existence or formation of 'nucleation sites'; it is generally assumed that these occur via the generation of some kind of carbonaceous precursors; the identity and mechanisms are at present unclear. A number of possibilities have been suggested, including hydrogenated sp^2 bonded carbon structures [Angus 1993]

and a mechanism in which rhombohedral graphite sheets are transformed into (111) diamond-like structures [Sandre 1994].

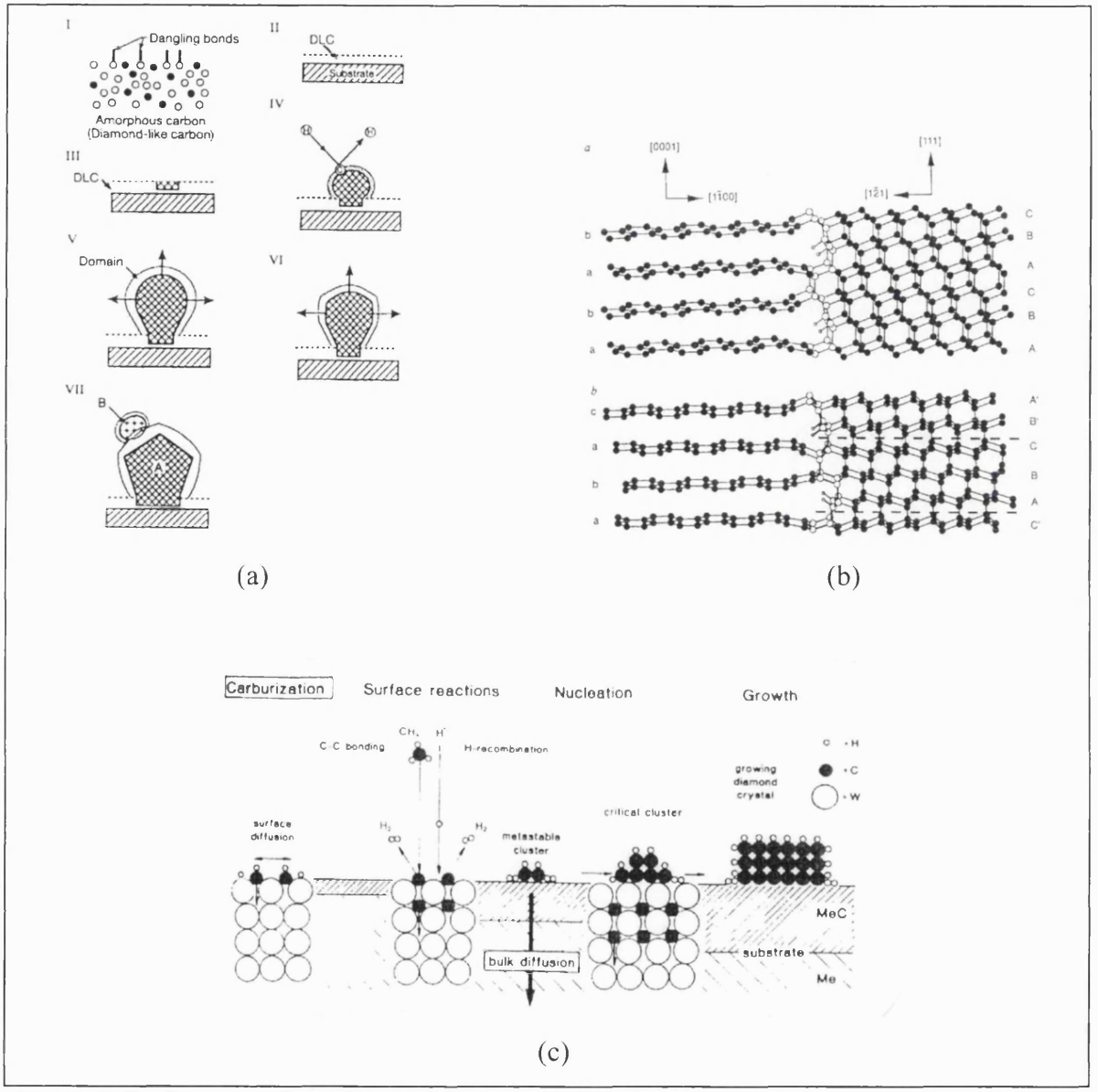

Figure (2.6): Summary of non-bias nucleation mechanisms thought to account for nucleation of diamond on most substrates;
(a) on a DLC interlayer; (I) formation of carbon cluster, bonding change from sp^1 to sp^2, (II) sp^2 converts to sp^3, (III) amorphous phase crystallises, (IV–VI) growth and faceting of diamond crystals (VII) secondary nucleation and growth.
(b) on graphite; Condensation of graphite followed by hydrogenation of the {1100} prism planes along edges of graphite particles; diamond nucleation at emerging stacking fault – almost perfect interface. Upper:- cubic diamond on perfect hexagonal graphite, Lower:- twinned diamond nucleus adjoining a graphite stacking fault. Twin boundaries – dashed lines, H-atoms – open circles, C-atoms solid circles and
(c) on a carbide interlayer; Carburisation consumes available C to form carbide surface; C surface concentration below diamond nucleation minimum; carbide layer thickness increases; C transport rate decreases, C surface concentration increases; Diamond nucleus forms when either surface C concentration reaches critical level or C cluster attains critical size. [redrawn from Lui 1995].

(ii) Models of Bias Enhanced Nucleation.

Given the uncertainty regarding the precise mechanisms of nucleation on non-diamond substrates *without* the aid of bias, all models purporting to explain bias nucleation must be considered as highly speculative. Many plausible explanations have been given but no definitive experiments have been conducted which would allow a confident choice amongst the proponents to be made; recent experiments seem to claim a key enabling role for energetic ions accelerated across the bias sheath to the substrate [M^{c}Ginnis 1995, Schreck 1996], however doubts have subsequently been articulated regarding these claims [Kulisch 1996, Bozeman 1998].

A definitive model requires a much more detailed understanding of *all* the effects which a large substrate bias incurs to both the substrate and nearby plasma environment. With this in mind a *selection* of the various models/explanations which have been proposed to account for the observed effects of the BEN process are briefly summarised below; for full details the reader should consult the review articles which have already been listed together with the original references and the *current literature*, as BEN is a highly active area of research.

Model 1

Much of the early biasing work e.g. [Yugo 1990, Lee 1990 and Chang 1992] can be combined to create a simple model which attempts to explain biasing using the following steps:

(i). Negative biasing increases the energy and flux of H· bombardment to the substrate, possibly increasing the near surface active species due to H· collisions.

(ii). Ion etching by H^+, may suppress or remove sp^2 bonded carbon on the surface, while sputtering by H^+ may promote various forms of SiC on the surface.

(iii). Negative bias may reduce the electron flux *to* the surface reducing substrate damage; this may aid the formation of sp^3 carbon and suppress sp^2carbon.

(iv). Electron emission *from* the surface may enhance the generation of H· from H_2 near to the surface.

(v). Diamond may nucleate on the SiC forms mentioned in (ii) or on sp^2 bonded carbon at the surface.

(vi). Excessive acceleration of ions may lead to etching of deposited diamond.

(vii). Successful nucleation appears to be a fine balance between erosion and growth processes mediated by atomic hydrogen.

This model is rather qualitative and lacks detail. There is some question over the mechanism responsible for the enhancement of H· generation, i.e. is enhancement due to electrons from the surface or ions to the surface. The assignment of SiC as being instrumental in nucleation was very speculative when considered against the evidence available from the early papers, although the presence of SiC phases consistently appears in the later models.

Model 2

Developed by Stoner *et al.* [Stoner 1992] following very careful and detailed studies of bias nucleation using *in vacuo* techniques. Their model is based on experimental observations of the formation and etching of SiC phases during the bias period; considerable evidence is presented in their paper and the model summarised below also incorporated observations made by previous workers.

(i). Before bias the surface contains some physisorbed oxygen and hydrocarbon contamination in the form of amorphous carbon.

(ii). The bias converts the amorphous carbon to SiC or etches it away and converts the oxygen to SiO.

(iii). Further biasing then etches away the oxide causing SiC islands to grow, the silicon is supplied by diffusion from the substrate. Excess concentration of carbon at the surface is created by either: (a) A high carbon flux arising from accelerated H· mediated dissociation of carbon species at the surface, or (b) preferential etching of Si from the surface SiC.

(iv). Carbide islands locally reach a critical thickness at which further growth ceases due to silicon shortage (diffusion limited); excess carbon is then free to form small clusters; Ion (H^+) bombardment may enhance surface carbon mobility.

(v). An unknown process occurs which allows some carbon clusters to become favourable for diamond nucleation, (presence of sp^3 bonded carbon ?); as more SiC reaches critical thickness (~90 angstroms) free carbon becomes available to form nucleation sites.

(vi). Continued biasing etches the surface but not the more stable diamond nuclei; local etching roughens the SiC surface. If silicon is preferentially etched then the increased carbon concentration in that area can give rise to nucleation on areas thinner than the critical thickness.

(vii). Etching, cluster formation and nucleation continue until the surface is covered with diamond nuclei; which then grow to form a closed film.

At the time this model was developed oriented nucleation during bias had not been observed so the primary aim was to attempt to explain the very large increase in nucleation density which was seen on pristine silicon using BEN. This work established the existence of a SiC layer and concluded that it played an important role during BEN but was unable to attribute the nucleation enhancement solely to the existence of this material on the substrate surface.

Model 3

Milne and co-workers [Milne 1995] studied localised epitaxy with and without a pre-bias carburisation stage and determined that carburisation was not necessary for epitaxy during BEN as β-SiC is also formed during bias; however they state that its inclusion can reduce the incubation time prior to nucleation enhancement. A two stage model was proposed which specifically addressed the role of carburisation and the low nucleation enhancement observed during the critical early bias phase; the model is summarised below:

(A) Carburisation:

(i). Removes oxides and contaminants which can reduce epitaxy and/or nucleation.

(ii). Forms a SiC layer which *may* contain β-SiC at the interface or embedded in an amorphous phase. The complexity of this layer has been confirmed by the authors using FTIR spectroscopy and shown to be a mixture of amorphous and crystalline material containing various sized grains.

(B) Biasing:

(i). *Without* (A) β-SiC may form during negative biasing.

(ii). *With* (A) the bias may form β-SiC by conversion of α-SiC created by (A) and/or etching which reveals an epitaxial β-SiC at the silicon interface.

(iii). Growth of β-SiC occurs on epitaxial islands and on exposed silicon.

(iv). Diamond nuclei form on β-SiC.

In common with most models no detailed mechanism for nucleation is suggested, however later work indicated that the bias layer contains both sp^2 and sp^3 C-H bonding groups and that bias could influence the distribution of these groups [John 1994]. Furthermore growth conditions could efficiently etch the original bias deposited nucleation layer, suggesting that buried sp^3 nucleation sites might subsequently be uncovered to provide sites for growth.

Model 4

Gerber *et al.* [Gerber 1994] have proposed a very different model based on the theory of subplantation in which high energy carbon ions originating in the plasma sheath create local densification in an amorphous carbon layer causing sp^2 bonds to reconfigure in an sp^3 form generating suitable nucleation sites for diamond growth, the model is summarised below:

(i). Biasing accelerates positive ions (e.g. H^+, CH^+,CH_2^+, CH_3^+ etc.) to the surface.

(ii). A nucleation maximum was observed for a mean ion energy ~90 eV.

(iii). Subplantation is employed to explain the creation of nucleation sites: (a) carbon atoms with sufficient energy are forced into interstitial positions with close nearest neighbouring carbon atom distances; (b) interacting atoms tend to hybridise as sp^3 C-C bonding sites; (c) too little energy and the ion fails to penetrate, sticking to the

surface forming sp^2 C-C bonding; (d) if the ion has too much energy the excess is dissipated as heat resulting in localised graphitisation.

(iv). In this way a two component film forms on the surface containing sp^2 and sp^3 carbon.

(v). Atomic hydrogen preferentially etches sp^2carbon.

(vi). Provided the sp^3clusters exceed a critical size they survive the H· etching to serve as nucleation centres for subsequent growth.

(vii). The correlation of bias with nucleation density is explained in terms of the energy dependent balance between sp^2 and sp^3 sites due to internal local density changes caused by subsurface implantation of C-ions.

This is an interesting model as it attempts to provide a detailed mechanism for the creation of sp^3 sites whereas most attempts to explain the bias process implicitly assume the existence of these crucial precursors. However, it does not seem to provide any mechanism for orientation especially as the formation of an amorphous carbon layer is assumed into which ions subplant; furthermore the model relies on a flux of relatively high energy ions (~ 80-90 eV) and there is yet little evidence to support the existence of such high energy heavy ions, which might not be expected in the collision dominated environment of a typical MW-diamond plasma; indeed Monte Carlo modelling of the bias sheath suggests much lower ion energies of ~15 eV can be expected [M^{c}Ginnis 1995].

Model 5

The final model described here arises from very recent work carried out by Stockel *et al.* [1998a] who used TEM, XRD, SEM and photoelectron spectroscopy to study bias nucleation on a silicon substrate using an approach, similar to the experiments described in chapter 7 of this thesis, in which they studied the spatial variation of nucleation across the substrate, which provides a sort of 'time resolved' view of the BEN effect. This work is of particular interest as they advocate a key role for the secondary plasma in the BEN nucleation process; this secondary plasma appears during biasing between the main MW plasma and the substrate and its presence has been noted by a number of workers [e.g. Kulish 1996, Schreck 1996, M^{c}Ginnis 1995] and is also the subject of experimental study

in this thesis. Their model is rather complex so the original reference should be consulted for full details, only a summary is given here; the numbered steps should be referred to the diagram shown as figure (2.7) extracted from their paper:

(a). Within the first few minutes of bias nearly epitaxial β-SiC crystals (~10nm) develop on the silicon surface; simultaneously, radicals and ions, (mostly hydrogen) accelerated across the sheath, etch the surface; Si is etched faster than SiC.

(b). SiC crystals form a closed polycrystalline film within ~10 minutes to a thickness (~10 nm) determined by a balance of temperature and diffusion coefficients; individual crystals retain their epitaxial relationship to the substrate. Fast carbon species subplant and supersaturate the SiC layer; diamond nucleation centres (structure unclear) form in the subsurface in registry with the SiC.

(c). Continual etching brings the diamond nuclei to the surface; nuclei continue to be formed beneath the surface in the SiC layer; if biasing is ceased at this point oriented diamond can be grown; continued biasing leads to secondary nucleation and twinning of existing crystallites.

(d). Growth at point (c) leads to epitaxial diamond with a range of crystallite sizes which arises because the etch process is continuous, even when there is no bias, and continually exposes new previously buried nuclei.

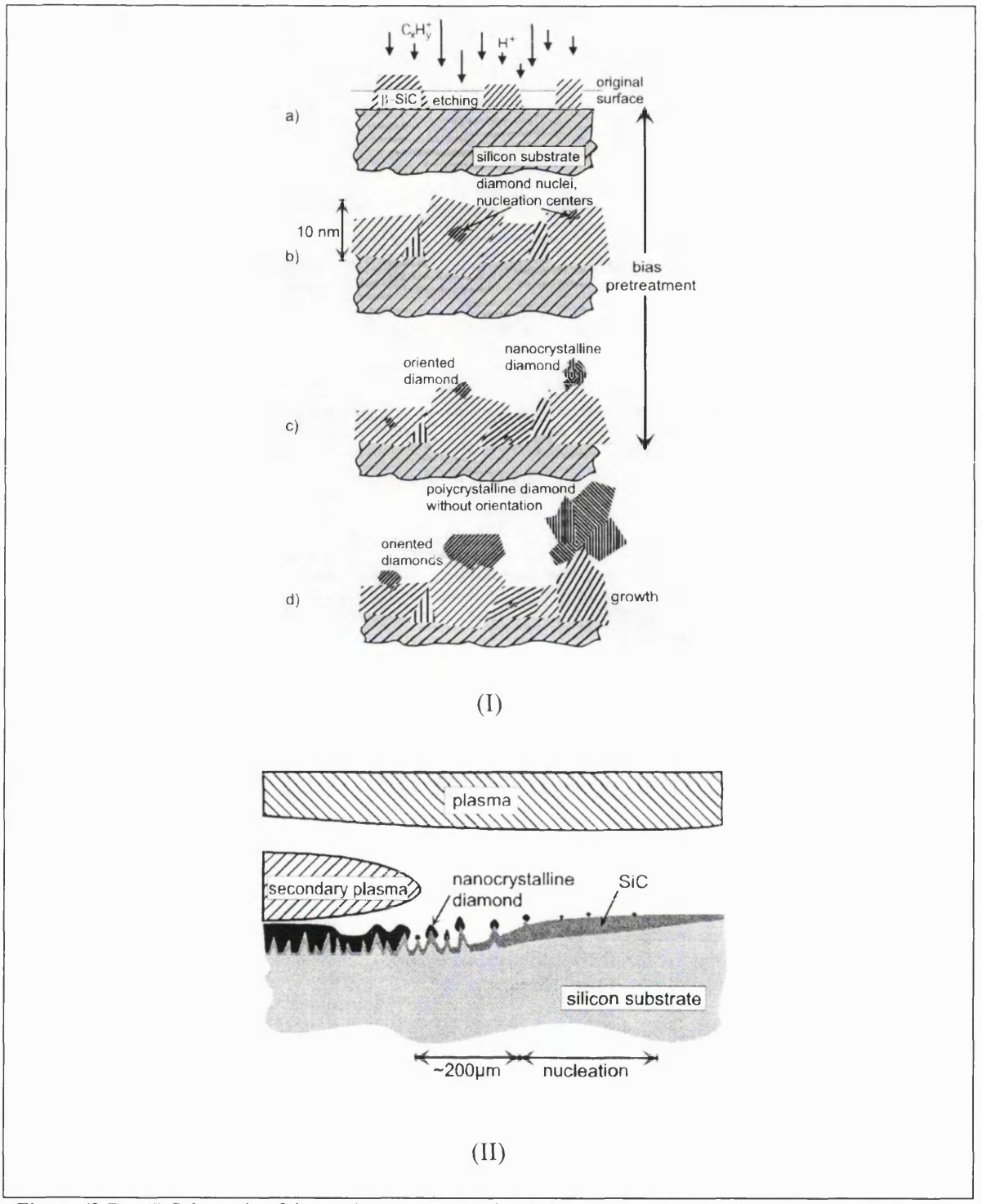

Figure (2.7): (I) Schematic of the model proposed by Stockel *et al.* to explain biasing, the steps labelled (a)-(d) correspond to the labelled steps in the text; included below in (II) is an indication of the substrate state in front of the secondary plasma as it advances across the substrate during the BEN process; Extracted from [Stockel 1998a].

This is a dynamic model that relies upon a balance between the continual etching of both the silicon and the SiC layer and the subcutaneous formation of epitaxial nuclei ahead of the advancing secondary plasma. Considerable evidence is presented to support each step

of this model and the existence of a near continuous β-SiC layer has also been observed by others [Jubber 1996]. However, the authors admit that their model does not explain the apparent direct registry which has sometimes been observed between silicon and diamond grains *without* an intermediate layer present [Jiang 1995, Jia 1995]. They also speculate that the subplantation mechanism described here in 'Model 4' might provide a mechanism for the creation of the 'unknown' nucleation precursor sites. Further work by this group [Stockel 1998b] provides a hint at the possible identity of these nucleation sites; experiments showed that most forms of carbon (e.g. microcrystalline graphite, hydrogenated amorphous carbon and turbostratic carbon) were rapidly destroyed by the fierce etching processes occurring in the vicinity of the secondary plasma. However, the formation of fine (~nm's) fibrous, hollow carbon tubes during biasing were resistant to the same etching processes. Under conditions of no bias it appears that diamond can nucleate on the ends of these carbon tubes

As stated previously it is apparent from the variety of the models summarised above that the mechanisms of bias nucleation remain open to interpretation. A number of common threads can be discerned; for example, epitaxy appears to be closely related to the presence of a β-SiC layer or sites; strong etching of the bias deposited layers to reveal nucleation sites appears in most of the models which is implicitly attributable to bias induced changes in the nearby plasma, including the development of the bias sheath - which is a region of high fields. The final model assigns a critical role in this respect for the secondary plasma which develops just above the substrate. Not surprisingly most of the models lack a direct explanation for diamond nucleation with the exception of model 5 which invokes subplantation to create sp^3 bonded carbon sites. It seems likely that none of the models described above is entirely correct and it can be speculated that a successful description will include elements from several to account for all the effects caused by the application of a substrate bias.

The full benefits of substrate bias and a measure of the considerable progress which has been achieved in recent years can be appreciated by considering the three SEM's shown in figure (2.8 a-c) which show a random polycrystalline film, a (100) textured film and an optimised highly oriented diamond film nucleated using BEN. Several groups have now reported HOD growth over large areas - greater than 30 cm^2 - and it is important to note

that as expected this form of material shows electronic properties which are much improved over randomly oriented, mixed morphology material [Stoner 1993].

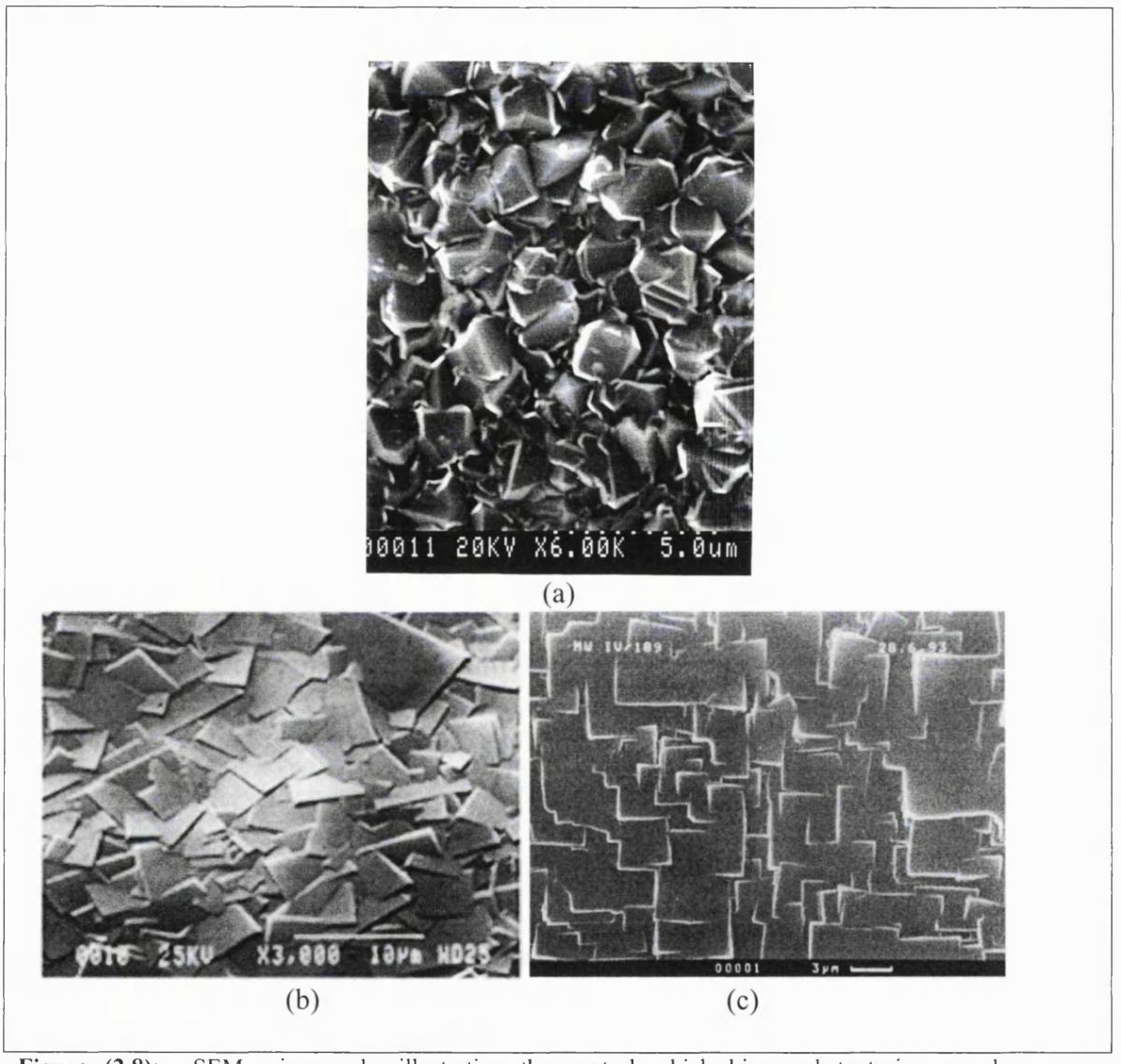

Figure (2.8): SEM micrographs illustrating the control which bias and texturing can have over polycrystalline diamond films; (a) randomly oriented, (b) (100) textured and (c) highly oriented and textured (100) HOD film.

2.4 Growth

Compared with the situation for nucleation a clearer understanding has been achieved for the growth of diamond under CVD conditions. A simplified generic model which accounts for the growth of a diamond surface from hydrocarbon gas phase precursors in the presence of atomic hydrogen is broadly accepted; however the chemical and kinetic details of the precise mechanisms which facilitate this model are the subject of considerable

controversy and ongoing research; a discussion at this level of detail is outside the scope of this work and the interested reader is directed to extensive summaries which have been given elsewhere; [Goodwin and Bulter 1998; Spear and Frencklach 1994 and references therein].

Diamond growth is complicated by the important role of surface chemistry in determining the relationship between gas phase precursors and growth phase species. Direct observation of surface chemistry is difficult as most surface spectroscopies are not well suited to use under CVD conditions. Typical diamond growth substrate temperatures are well above that required to remove physisorbed species but are well below the Debye temperature (~1860°C), in contrast to virtually all other crystal growth processes which usually occur at around twice the Debye temperature. This suggests that adspecies mobility on the growing surface is rather low and underlines the likely importance of the surface chemistry; however it has been noted that a high flux of surface atomic hydrogen may influence the surface mobility [Goodwin 1998]. The chemistry of diamond growth is complex compared to most deposition systems because of competition for deposition between different bonding forms of carbon and the high number of chemical reactions possible in organic systems compared to typical inorganic CVD systems. This complexity has been discussed by Spear and Frenklach [1994] and summarised in the diagram reproduced from that source in figure (2.9).

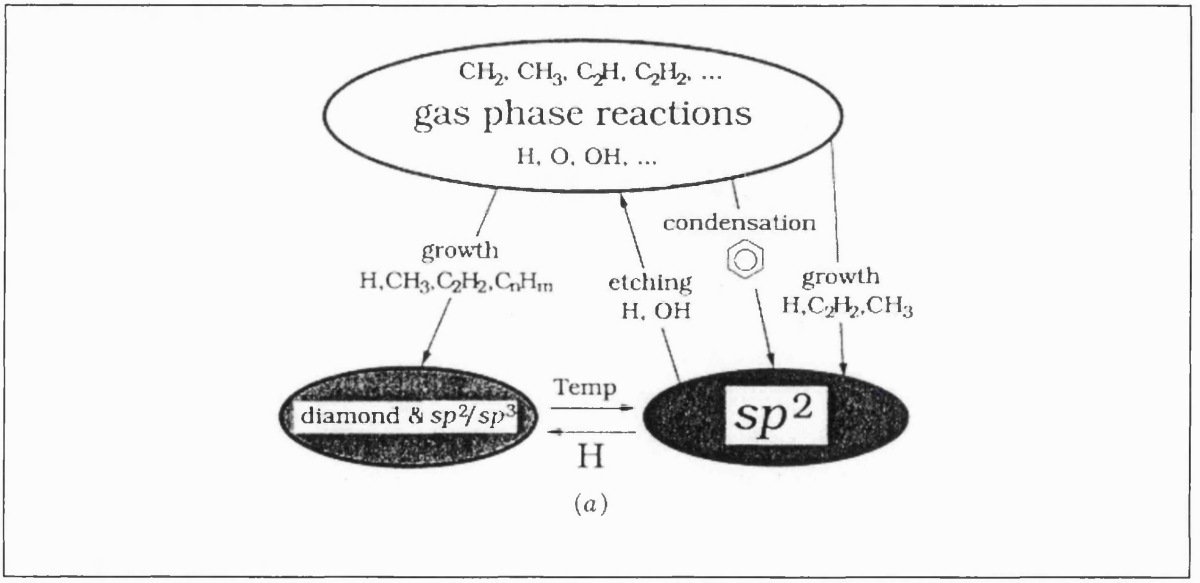

Figure (2.9): Schematic illustration of the chemical species and reaction pathways leading to various forms of deposited carbon [redrawn from Spear 1994].

Despite the complexity evident in figure (2.9) the main species and their roles in the growth process have to some extent been determined, allowing a simple generic picture of growth to be presented; however the mechanistic details remain the province of controversial debate. In hydrogen-methane systems, which are the most commonly encountered CVD environments, it has been accepted that the most likely precursors in the gas phase are CH_3 and C_2H_2 radicals. Under conditions where methane is a feed gas CH_3 is favoured due to its abundance, indicated by equilibrium gas phase calculations and measurements, together with its high reactivity and sp^3-like configuration. Other conditions may favour C_2H_2 and viable mechanisms have been suggested, see Spear [1994 and references therein]. The critical role of atomic hydrogen in the generation of precursor gas species and mediation of surface chemistry is well recognised [Bachmann 1998, Goodwin 1998]. Atomic hydrogen: (i) rapidly and preferentially etches co-deposited sp^2 and sp forms of non-diamond carbon [Angus 1988]; (ii) stabilises the growing surface by satisfying dangling carbon bonds; preventing surface reconstruction to sp^2 and sp structures;[*e.g.* Pate 1986] and (iii) rapidly generates radical sites on the H-saturated surface without which hydrocarbon precursors would be unable to attach to the surface; this occurs via abstraction reactions like: $C_dH + H \rightarrow C_d\bullet + H_2$; where the dot indicates a radical on the bulk diamond bonded carbon surface, [Spear 1989]. It has also been suggested that atomic hydrogen can promote the production of gas phase growth precursors and suppresses some forms of polyaromatic hydrocarbons which may generate unwanted sp^2 precursors [Frenklach 1989]. Figure (2.10) shows schematically a simplified generic model of growth which allows a bulk carbon diamond bonded surface, stabilised by atomic hydrogen in an sp^3 configuration, to grow by the incorporation of hydrocarbon radicals (e.g. CH_3) via surface reactions mediated by a high flux of the atomic hydrogen radical.

Several problems are apparent from the model shown; one is the high rate of attack by atomic hydrogen of any hydrocarbon successful in bonding to the surface; to be reasonably stable additional bonds with neighbouring carbon bonds are necessary, this introduces questions with respect to the likelihood of this occurring together with problems regarding the spacing of radical sites versus the relatively large size of most hydrocarbons required to adsorb to such sites if growth is to proceed. Many complex mechanisms have been proposed and studied to explain how hydrocarbon species may be correctly incorporated

into the lattice and the reader is directed to the references given at the start of this section for detailed discussions.

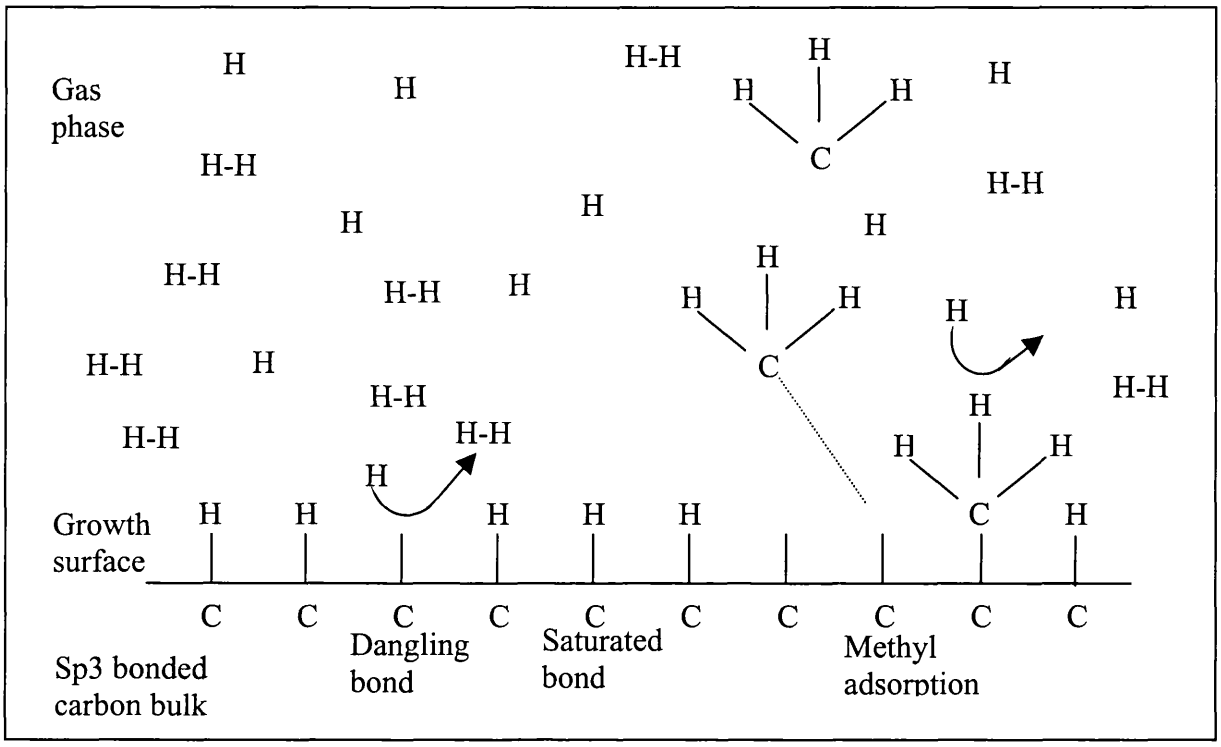

Figure (2.10): Generic model describing the growth of a diamond surface from the incorporation of CH_3 hydrocarbon radicals via surface chemistry mediated by a high atomic hydrogen flux; Left to right – surface bonds are saturated and stabilised by atomic hydrogen, H-abstraction creates dangling bonds, a fraction capture CH_3 radical groups from the gas phase, forming stable surface groups.

2.5 Applications

The aesthetic value of large high quality natural diamond gemstones is well known. The bulk of smaller and lower quality natural diamond together with virtually all HPHT diamond are used in abrasives and cutting applications of one form or another [Wilks 1991]. The uses of these types of diamond have been well reviewed elsewhere and are of little interest here where the primary concern is CVD diamond. Therefore no further discussion will be given and the interested reader is directed to reviews by [Wilks 1991, Hay 1998, Subramanian 1998] and references therein. The potential uses for CVD diamond can be broadly divided into mechanical and electronic applications together with niche applications which do not fall naturally into either group.

2.5.1 Electronic applications.

The use of diamond for various electronic applications has been examined by a number of authors including; [Baliga 1982, Collins 1989, Shenai 1989, Geis 1991b]. An up-to-date review of the current status of active devices has been given by Dreifus and Fox [1998]. The potential of diamond for use in the areas of high power, high frequency and high temperature electronics can be appreciated by considering certain 'figures of merit' (FOM) which have been developed to rank semiconductor materials according to their idealised, ultimate performance. Three such measures are the Johnson [1965], Keys [1972] and Baliga [1982] FOM. These attempt to rank semiconductors in terms of power-frequency, thermal and power loss performance respectively. FOM's are often normalised to silicon as a benchmark; a comparison of diamond with more well known semiconductors including a high temperature competitor, silicon carbide (SiC), is given in table (2.4). The implications of such FOM's with respect to achievable devices should be considered with care, the figures are guides and the subsequent rankings should not be regarded as absolute, for example it is unlikely that CVD diamond transistors will be made to be three orders of magnitude faster than the fastest silicon devices.

	Figure of Merit		
Material	**Keyes**	**Johnson**	**Baliga**
Silicon	1.0	1.0	1
Gallium Arsenide	0.5	6.9	13
6H Silicon Carbide	5.1	262	106
Diamond	**32**	**8206**	**6751** (p-type)

Table (2.4): Semiconductor figures of merit at 300K normalised to silicon; extracted from [Baliga 1989, Shenai 1989]

The ideal requirements for the realisation of active devices from a semiconductor are; (i) single crystal electronic properties, (ii) provision of insulating regions, (iii) availability of p and n-type material and (iv) formation of ohmic, schottky and insulating contacts. Currently these requirements with exception of (i) can *reasonably* be met by thin film CVD diamond allowing the fabrication of a large number of 'proof-of-principle' devices by many groups in the diamond research community. State of the art highly oriented and

textured films show promising electrical characteristics which, while not ideal, are a considerable improvement over mixed polycrystalline films; although true epitaxy remains the 'ultimate goal' for high performance electronic applications. Undoped diamond has an extremely high observed resistivity > 10^{15}-10^{16} Ω-cm; current CVD material can exceed these values by a factor of ~100 at 1000°C [Vandersande 1995]. P-type doping of the intrinsic material can be achieved using boron which acts as an acceptor (E_a~0.37 eV) and is readily incorporated from a suitable source during growth or can be ion implanted. Very recently unambiguous n-type doping has been achieved by the NIRIM group [Koizumi 1997] using phosphorus, although the donor level formed is rather deep at ~0.43 eV for conventional uses. A form of surface doping has also recently been reported in single crystal and CVD forms of diamond [Karawada 1996]. The doping is p-type, (as determined by Hall measurements), appears to be associated near surface hydrogen and shows very high mobilities at relatively high carrier concentrations in contrast to boron which gives low mobilities at similar carrier concentrations. The subjects of n-type and surface hydrogen doping are currently controversial; none-the-less a number of impressive electronic structures have already been demonstrated using the latter effect. Ohmic, Schottky and insulating contacts have been realised and extensive research regarding the properties of these contacts has been carried out, although complete understanding is yet to be achieved. Ohmic contacts can be made by: delta doping, surface reaction (i.e. use of carbide forming metals), and damage methods [Tachibana 1995]. Most metals will form Schottky contacts to diamond provided careful surface preparation is used; a hydrogen terminated surface has recently been demonstrated to reduce strongly Fermi level pinning by surface states allowing variation of the barrier height with metal electronegativity [Hayashi 1997]. For boron doped materials, a low doping level is usually used to obtain good Schottky contacts; however, a general observation is that currently the precise nature of the metal-diamond Schottky interface is not well understood. Only limited work has been carried out on insulating contacts but both intrinsic diamond and silicon dioxide have been successfully used.

As the discussion above indicates, most of the enabling requirements for the fabrication of active devices can be reasonably well satisfied by currently available CVD diamond material; as a consequence, a great deal of work has been carried out by various groups and the details of many ' proof-of-principle devices' have been published; an extensive and current tabulation has been given by Dreifus [1998]. On single crystal diamond; diodes,

MiSFETS, MOSFETS and MESFETS with respectable performance, comparable to early SiC devices, have been demonstrated operating at temperatures up to 550° C. Drain-Source currents of ~15 mA and transconductances as large as 1.3 mS/mm have been observed. Progress has been sufficient to permit the demonstration of simple all diamond circuits including a common-source amplifier, and NAND and NOR logic operating up to 400°C. Modulation doped FET operation has also been demonstrated. Most boron doped devices do not operate effectively at room temperature due to the high activation energy (0.37 eV) of the boron dopant; however impressive room temperature operation has been achieved from MESFET devices utilising the recently discovered p-type surface doping layer which may be associated with near surface hydrogen [Karawada 1996].

On polycrystalline CVD material active devices have been less successful; the very rough surfaces present formidable fabrication problems, while the high density of defects and grain boundaries are extremely detrimental to the promising electronic properties of ideal diamond. Despite these problems most of the devices demonstrated on homoepitaxial, single crystal material have also been demonstrated on boron doped polycrystalline CVD material, although performance is typically inferior by several orders of magnitude [Dreifus 1998]. However, a hydrogen surface doping layer has also been observed on CVD material [Looi 1998a] and very promising MESFET devices with pinch-off and full saturation, operating at *room temperature* with transconductance ~0.14 $mSmm^{-1}$, have been fabricated on this material [Looi 1998b]. The use of the HOD material which has demonstrated superior electronic properties compared to randomly oriented material [Stoner 1994] would be expected to improve these figures further. It should be noted that the near surface hydrogen doping approach is unsuited to high temperature operation as this layer so far only appears stable to temperatures of ~300 °C [Looi 1998b]. For improved high temperature operation the most promising approach may be to use large grain size, boron doped HOD material, which for small device dimensions may appear 'pseudo-single crystal-like'. Depletion mode MOSFET devices, operating at ~400°C, transconductance ~76 μSmm^{-1} and showing saturation and pinch-off, have been fabricated on this material [Stoner 1994].

Despite these successes some pessimism with regard to the commercial realisation of active electronic devices on diamond has been expressed [Collins 1992, Buckley-Golder

1992]. Doubts have concentrated primarily on problems such as: lack of a low activation energy dopant, poorly developed processing techniques, quality of CVD diamond growth and the lack of suitable *large area* substrates for heteroepitaxial growth. Other problems include: only niche applications exist to drive research, high development costs, poor availability of modelling tools which can handle the diamond semiconductor; and strong competition from existing materials such as silicon, gallium arsenide and for high temperature applications SiC - which is considerably further developed than diamond [Dreifus 1998].

2.5.2 Material Applications.

Material applications are defined here as those making passive use of the mechanical properties of the material such as its thermal conductivity, strength, hardness etc. and utilising relatively large quantities of the material. Such applications include: abrasives, polishing of optical components, wear coatings, cutting and grinding tools, thermal heat spreaders, optical windows, x-ray windows, microsurgery scalpels and others. The materials applications of diamond have been well reviewed elsewhere e.g. [Seal 1994, Ravi 1994, Wilks 1991, Subramanian 1998, Hay 1998] and are not discussed further here. As far as CVD diamond is concerned the effective use of the material in various of these applications depends on the ability to control the form and properties of the material together with the cost of production and in these respects there has been more progress than has been the case for electronic properties. For example, the CVD process is now sufficiently developed that grain size can be controlled over the nano to 100 -micron range; sp^2/sp^3 fraction varied from DLC, to diamond with purity higher than the best natural crystal; while the morphology can be chosen from random to highly textured, flat (100) material. The material can be grown on a range of substrate materials and forms, from flat surfaces to three dimensional objects, including fine wires. In other words, to a reasonable degree CVD diamond can be engineered to suit a given application. For example, black low optical quality diamond, which none-the-less exhibits very high thermal conductivity, can be deposited at high growth rates and modest costs for use in thermal spreader applications. The growth conditions can be altered and highly transparent, high strength material deposited at higher cost for missile and laser window applications. Applications can be divided into low value added products such as coatings, heat sinks, abrasives etc. and high value added products such as optical windows, detector coatings and medical

applications; [Ravi 1994]. A number of authors have made detailed cost/benefit and market projection studies for man-made diamond including the CVD form [e.g. Singer 1998, Busch 1994, Russell 1994]; at the risk of over simplification a fair summary is that, while for many of the applications mentioned above the material properties of current CVD grown material are adequate and in some cases more so, the single most important barrier to uptake is cost. CVD is energy intensive and expensive; projected medium term costs of ~$3-20/carat can be compared with HPHT costs of ~$0.20/carat for 50 micron grits; for the lowest value applications CVD material is therefore unlikely to be competitive. However, there is considerable scope for improvement in the deposition technology and the outlook for medium and high value products is more favourable [Singer 1998].

2.5.3 Novel and Niche Applications.

These are defined here as uses in which a form of *device* is fabricated, which is in some respects active and which utilises one or more of the unique or extreme properties of diamond to the benefit of the device; for example, high frequency resonant sensors which rely on the extreme mechanical properties of the material together with simple piezoresistive changes for the operation of a measuring device. Similarly, visible blind UV detectors; diamond field emission displays and cold cathodes; micro-electro-mechanical (MEMS) devices; dynodes, environmental and medical sensors; surface acoustic wave devices (SAWS); can all be considered to be novel or niche applications. While true fully active CVD diamond electronic devices, such as transistors, may be some way from commercial viability, this author believes that niche applications represent the likely route to near term commercial use of CVD material for *devices* as opposed to the fully passive material applications discussed previously. In evidence one can cite visible blind UV photodetectors [M^{c}Keag 1995] which are currently being manufactured by Centronics Ltd.; while electronically simple, these photodetectors represent the first commercially available devices made from CVD diamond. While the UV detector may be a rather specialised application not all the devices listed above are; Sumitomo Electronics Corporation have invested considerable effort to develop very high frequency CVD diamond SAW devices with probable applications in next generation mobile phone systems [Nakahata 1995]. An implantable CVD diamond glucose sensor is under development which utilises the bicompatibility and stability of diamond [Troupe 1998]. The potential medical market for

a successful glucose sensor is of the order of 10-12 million, based on the known incidence of diabetes. Another huge potential market is the electrochemical industry; it has been realised that boron doped CVD diamond is an excellent electrode material with a number of novel benefits including an unprecedented lifetime in corrosive and otherwise hostile environments. The common thread between these applications is that all combine relatively simple electrical behaviour with one or other of diamond's extreme properties to provide devices which are difficult or impossible to fabricate in other material systems. UV detectors are a good example; common semiconductors such as silicon, gallium arsenide and germanium cannot easily be made visible-blind because these materials have relatively small bandgaps; they are not therefore likely to be able to compete with CVD diamond UV detectors if a rugged, low cost solid state detector is needed. Full descriptions of the devices just discussed can be found in the given references while more general listings and reviews can be found elsewhere [Prelas 1998].

2.6 Summary.

Previously, exploitation of the exceptional properties of diamond has been restricted by the inconvenient form in which the natural form was available and by difficulty engineering the material to suit the application being considered. For abrasive and cutting applications HPHT synthesis has alleviated the situation and provided a cheap supply of diamond grits, which have allowed these industries to expand rapidly. However, HPHT methods are inaccessible, complex and entirely unsuited to the synthesis of forms the material which could allow industry to access the semiconducting and optical properties of diamond in a useful way. The development of a chemical vapour deposition technique operating at modest temperatures and pressures has completely altered this situation in recent years. Diamond can now be grown in a thin film form easily and relatively cheaply using reasonably simple equipment with modest set-up costs; many different substrates can be grown on and a number of film characteristics including; purity, grain size, morphology and active dopant levels, can be repeatably controlled, offering for the first time the ability to engineer this material to fit the requirements of a range of applications previously considered inaccessible.

This chapter has attempted to provide an introduction to the field of diamond; its unique combination of extreme properties, methods of synthesis and potential applications. The structure of diamond and its consequent electronic and material properties were described and compared to other typical materials. The conditions which are normally required for the formation of diamond were considered in the context of developing a synthetic means for the manufacture of diamond. Attention was focussed on CVD methods of producing this material and on the processes of growth and nucleation which determine the success of the CVD process. Although enormous progress has been made in the last 25 years since Angus first suggested the significance of atomic hydrogen to the CVD process, there is still much that is not understood about how this growth process functions at the mechanistic level. In particular the details of nucleation on non-diamond substrates are rather poorly understood at present, diamond is difficult to nucleate on most substrates and typically enhancement treatments must be used; these were summarised. The most promising technique is the recently developed bias enhanced nucleation (BEN) which shows very high nucleation densities, limited epitaxy and is also amenable to quantitative control in contrast to most other enhancement treatments. Although a great deal of study has been undertaken, clear understanding of the mechanism underlying the BEN treatment remains lacking, many models have however been proposed and a number of these were listed.

While fundamental studies are important in the development of a new material, practical success also depends on the development of realistic applications and these can then in turn drive forward the research field. With this in mind, the final section of this chapter has examined briefly some of the applications for CVD diamond and some of the issues which may determine it likely uses in the near term. It should be clear from the preceding discussions that much fundamental study remains to be done before the CVD growth process is fully understood. In particular the promising bias nucleation method require considerable further study if full advantage of bias is to be made. From the device applications point of view it is likely that near term commercial applications will be satisfied by the development of novel and niche devices, with fully active electronic applications awaiting the solution of the materials problems highlighted during the discussion. One of the most important recent developments has

been the successful fabrication of diamond surface acoustic wave devices, which may offer a near term bulk application for current CVD films. These represent a 'real' device application but yet do not require fully developed electronic properties, instead relying on a combination of modest electrical performance coupled with the extreme acoustic properties of diamond. With these points in mind this thesis sets out to explore the bias nucleation process and study the acoustic properties of CVD diamond; in other words to address both the more fundamental questions and to help develop the applications of the CVD diamond material.

2.7 References

Angus J.C. and Hayman C.C., [1988], *Science*, **241**, 913.

Angus J.C., Buck F.A., Sunkara M., Groth T.F., Hayman C.C. and Gat R., [1989], *MRS Bulletin*, **October**, 38.

Angus J.C., Li Z., Sunkara M., Wang Y., Lee C., Lembrecht W.R. and Segall B., [1993], *Second International Conference on the Applications of Diamond Films and related Materia,* MYU, Tokyo, pp 153.

Bachman P.K., article "*Diamonds from the Vapour Phase*", in *Physics World*, April 1991.

Bachmann P.K. [1998], in *Handbook of Industrial Diamonds and Diamond Films*, eds. Prelas M.A., Popovici G. and Bigelow L.K., (Marcel Dekker Inc.), New York, USA.

Bachmann P.K., [1993], in *Thin Film Diamond*, (eds. Lettington A. and Steeds J.W.), Chapman & Hall, London, UK.

Bakon A. and Szymanski A., [1993], *Practical Uses of Diamond,* Ellis Horwood, West Sussex, UK.

Baliga B.J., [1982], *J. Appl. Phys.*, **53**, 1759.

Baliga B.J., [1989], *IEEE Electron Device Lett.*, **10**, 455.

Baliga B.J., [1989], *J.Appl. Phys.*, **53**, 1759.

Belton D.N. and Schmieg S.J., [1992], *Thin Solid Films*, **212**, 68.

Bou P., Vandenbulcke R., Herbin R. and Hillion F., [1992], *J. Mater. Res.*, **7**, 2151.

Bozeman S.P., Stoner B.R. and Glass J.T., [1998] in *Handbook of Industrial Diamonds and Diamond Films*, eds. Prelas M.A., Popovici G. and Bigelow L.K., (Marcel Dekker Inc.), New York, USA.

Bruton E., [1978], *Diamonds*, Chiton Book Co. 366.

Buckley-Golder I.M. and Collins A.T., [1992], *Diam. and Relat. Mater.* **1**, 1083.

Busch J.V. and Dismukes J.P., [1994], in *Synthetic Diamond: Emerging CVD Science and Technology*, (eds. Spear H.E. and Dismukes J.P.), John Wiley and Sons Inc., New York.

Chang J.J. and Mantei T.D., [1992], *J. Appl. Phys.*, **71**, 5742.

Clausing R.E., [1998], *Handbook of Industrial Diamonds and Diamond Films*, eds. (Prelas M.A., Popovici G. and Bigelow L.K.), Marcel Dekker Inc., New York, USA.

Collins A.T. and Williams A.W.S., [1971], *J. Phys. C: Solid St. Phys.*, **4**, 1789.

Collins A.T., [1989], *Semicon. Sci. Technol.*, **4**, 669.

Collins A.T., [1992], *Mater. Sci. Eng.* **B11**, 257.

Davidson J.L., [1994] in *Synthetic Diamond: Emerging CVD Science and Technology*, (eds. Spear H.E. and Dismukes J.P.), John Wiley and Sons Inc., New York.

Dreifus D.L. and Fox B.A., [1998], Chapt. 29 in, *Handbook of Industrial Diamonds and Diamond Films*, eds. Prelas M.A., Popovici G. and Bigelow L.K., (Marcel Dekker Inc.), New York, USA.

Floter A., Guttler H., Schultz G., Steinbach D., Lutz-Elsner C., Zachai R., Bergmaier A. and Dollinger G., [1998], *Diam. and Relat. Mater.* **7**, 283.

Frank F.C. and van der Merwe J.H., [1949], *Proc. R. Soc. London Ser. A*, **198**, 205.

Frenklach M., [1989], *J. Appl. Phys.*, **65**, 5142.

Geis M.W., [1991b], *Proc. of IEEE*, **79**, 669.

Geis M.W., Smith H.I., Argoitia A., Angus J., Ma G.-H.M., Glass J.T., Robinson C.J. and Pryor R., [1991a], *Appl. Phys. Lett.*, **58**, 2485.

Gerber J., Weiler M., Sohr O., Jung K. and Ehrardt H., [1994], *Diam. and Relat. Mater.*, **3**, 506.

Goodwin D.G. and Butler J.E., [1998], in *Handbook of Industrial Diamonds and Diamond Films*, eds. Prelas M.A., Popovici G. and Bigelow L.K., (Marcel Dekker Inc.), New York, USA.

Hay R.A. and Galimberti J.M., [1998], in *Handbook of Industrial Diamonds and Diamond Films*, eds. Prelas M.A., Popovici G. and Bigelow L.K., (Marcel Dekker Inc.), New York, USA.

Hayashi H., Watanabe S.,Yamanaka S., Sekiguchi T., Okushi H. and Kajimura K., [1997], *Diam. and Real. Mater.*, **6**, 303.

Hirose Y, [1988], *First Int. Conf. New Diamond Science and Technology*, Tokyo Japan, Oct. 24-26, 1988.

Jia C.L., Urban K. and Jiang X., [1995], *Phys. Rev B* **52**, 5164.

Jiang X. and Jia C.L., [1995], *Appl. Phys .Lett.* **67**, 1197.

John P., Milne D.K., Drummond I.C., Jubber M.G., Wilson J.I.B. and Savage J.A., [1994], *Diam. and Relat. Mater.*, **3**, 486.

Johnson E.O., [1965], *RCA Review*, **26**, 163.

Jubber M.G. and Milne D.K., [1996], *Phy. Stat.Sol. (a),* **154**, 185.

Kawarada M., Mar K. and Kiraki A., [1997], *Jpn. J. Appl. Phys.* **62**, L1032.

Keyes R.W., [1972], *Proc. IEEE*, **2**, 225.

Kittel C., [1995], *Introduction to solid state physics*, John Wiley and Sons Inc., New York.

Kline C.A., [1991], *SPIE, Opt. Eng.*, **38**,204.

Koba R.J., [1993], in *Diamond Films and Coatings*, (ed. Davis R.F.), Noyes Publications, Park Ridge, USA.

Koizumi S., Murakami T., Inuzuka T. and Suzuki K., [1990], *Appl. Phys Lett.,* **57**, 563.

Koizumi S., Ozaki H., Kamo M., Sato Y. and Inuzuka T. [1997], *Appl. Phys Lett.,* **71**, 1065.

Lambrecht W.R.L., Lee C.H., Segall B., Angus J.C., Li Z. and Sunkara M., [1993], *Nature*, **364**, 607.

Lee Y.H., Richad P.D., Bachmann P.K. and Glass J.T., [1990], *Appl. Phys Lett.,* **56**, 620.

Liu H. and Dandy D.S., [1995], *Diam. and Relat Mater.* **4**, 1173.

Looi H.J., Pang L.Y.S., Wang Y., Whitfield M.D. and Jackman R.B., [1998a], *Diam. and Relat. Mater.,* **7**, 565.

Looi H.J., Pang L.Y.S., Whitfield M.D. and Jackman R.B. [1998b], *IEEE Elect. Device Lett.*, **19**, 112.

Lux B. and Haubner R., [191], in *Diamond and Diamond-like Films and Coatings*, (eds. Clusing R.E., Horton L.L., Angus J.C. and Koidl P.), Plenum Press, New York, pp 579.

Masumoto S., Sato Y., Tsutsumi M. and Setaka N., [1982], *J. Mater. Sci.* **52**, 219.

May P.W., Rego C.A., Ashfold N.M.R., Rosser K.N., Lu G., Walsh T.D., Holt L.,Everitt N.M. and Partridge P.G., [1995], *Diam. and Relat. Mater.,* **4,** 794.

McGinnis S.P, Kelly M.A and Hagstrom S.B, [1995], *Appl. Phys. Lett.*, 66, 311.

M^{c}Keag R.D., Chan S.S.M. and Jackman R.B., [1995], *Appl. Phys. Lett.*, **67**, 2117.

Milne D.K., Roberts P.G., John P., Jubber M.G., Liehr M. and Wilson J.I.B., [1995[, Diam. and Relat. Mater. **4**, 394.

Morkoc H., Strite W.S., Gao G.B., Lin M.E., Sverdlov B. and Burns M., [1994], *J. Appl. Phys.* **76**, 1363.

Nakahata H., Higaki K., Hachiago A., Fujii S., Shikata S. and Fujimori N., [1995], *IEEE Trans. on Ultrasonics, Ferroelectrics and Frequency Control*, **42**, 362.

Pate B.B., [1986], *Surf. Sci.*, **165**, 83.

Prelas M.A., Popovici G. and Bigelow L.K. (eds), [1998], *Handbook of Industrial Diamonds and Diamond Films*, (Marcel Dekker Inc.), New York, USA.

Ravi K.V., [1994], Chpt. 14 in *Synthetic Diamond: Emerging CVD Science and Technology*, (eds. Spear H.E. and Dismukes J.P.), John Wiley and Sons Inc., New York.

Russell C.J., [1994], in *Synthetic Diamond: Emerging CVD Science and Technology*, (eds. Spear H.E. and Dismukes J.P.), John Wiley and Sons Inc., New York.

Sandre E., Bonnot A. and Cyrot-Lackman, [1994], *Diam. and Relat. Mater.* **3**, 448.

Seal M., [1994], in *Synthetic Diamond: Emerging CVD Science and Technology*, (eds. Spear H.E. and Dismukes J.P.), John Wiley and Sons Inc., New York

Shenai K., Scott R.S. and Baliga B.J., [1989], *IEEE Trans. Electron Devices,* **36**, 1811.

Singer A.T and Busch J.V., [1998] in *Handbook of Industrial Diamonds and Diamond Films*, eds. Prelas M.A., Popovici G. and Bigelow L.K., (Marcel Dekker Inc.), New York, USA.

Singh J., [1994], *J. Mater. Sci.* **29**, 2761.

Spear K.E and Frenklach M., [1989], in *Diamond and Diamond-like Films*, The Electrochemical Society, Pennington, NJ, 122.

Spear K.E. and Frenklach M., [1994], in *Synthetic Diamond: Emerging CVD Science and Technology*, (eds. Spear H.E. and Dismukes J.P.), John Wiley and Sons Inc., New York

Stockel R., Janischowsky K., Stammler M., Ley L., Albrecht M. and Strunk H.P.,[1998b], *Diam. and Relat. Mater.*, **7**, 147.

Stockel R., Stammler M., Janischowsky K., Ley L., Albrecht M. and Strunk H.P., [1998a], *J. Appl. Phys.*, **83**, 531.

Stoner B.R, Ma G.H.M, Wolter S.D and Glass J.T, [1992], *Phy. Rev. B*, **45**,11067.

Stoner B.R. and Glass J.T., [1992], *Appl. Phys. Lett.*, **60**, 698.

Stoner B.R., Kao C.-t, Malta D.M. and Glass R.C., [1993], *Appl. Phys. Lett.*, **62**, 2347.

Stoner B.R., Malta D.M., Tessmer A.J., Holmes J.S., Dreifus D.L., Glass R.C., Sowers A and Nemanich R.J., [1994], in *Diamond-Film Semiconductors,* **2151,** 2, Society of Photo-Optical Instrument Engineers.

Subramanian K and Shanbhag V.R., [1998], in *Handbook of Industrial Diamonds and Diamond Films*, eds. Prelas M.A., Popovici G. and Bigelow L.K., (Marcel Dekker Inc.), New York, USA.

Tachibana T. and Glass J.T., [1995], in *Diamond: Electrical Properties and Applications,* (eds. Pan L.S. and Kania D.R), Kluwer Academic Publishers. pp 319.

Troupe C.E., Drummond I.C, Graham C., Grice J., John P., Wilson J.I.B., Jubber M.G. and Morrison N.A., [1998], *Diam. and Relat. Mater.*, **7**, 575.

Vandersande J.W. and Zoltan L.D., [1995], *Diam. and Relat. Mater.*, **4**, 641.

Volmer M. and Weber A., [1926], *Phys. Chem.*, **119**, 277.

Wilks J. and Wilks E., [1991], *Properties and Applications of Diamond*, Butterworth-Heinmann, Oxford, UK.

Wolter S.D., Stoner B.R., Glass J.T., Ellis P.J., Buhaenko D.S., Jenkins C.E. and Southworth P, [1993], *Appl. Phys. Lett.,* **62**, 1215.

Yoder M.N., [1993], in *Diamond Films and Coatings*, (ed. Davis R.F.), Noyes Publications, New Jersey, USA.

Yoder M.N., [1994], in *Synthetic Diamond: Emerging CVD Science and Technology*, (eds. Spear H.E. and Dismukes J.P.), John Wiley and Sons Inc., New York.

Yugo S., Kanai T. and Muto T., [1990], *Vacuum*, **41**, 1364.

Yugo S., Kanai T. Kimura T. and Muto T., [1991], *Appl. Phys. Lett.*, **58**, 1036.

Yugo S., Semoto K. and Kimura T., [1995], *Diam. and Relat Mater.*, **5**, 25.

Zhu W., Stoner B.R., Williams B.E. and Glass J.T, [1991], *Proc. IEEE,* **79**, 621.

Chapter 3

Experimental Methods and Theory.

This chapter presents descriptions and background discussion of the main experimental techniques which have been used during the course of the current studies, including relevant theory where appropriate. A discussion of the CVD resonant cavity reactor and processes occurring in the microwave plasma generated within the chamber is also given.

3.1 Introduction.

The following sections in this chapter describe the main experimental techniques employed during the course of the work reported in this thesis. Where relevant, additional material is also given; in particular following the discussion of the MEPCVD chamber a detailed summary of the CVD plasma environment has been included to provide a background for the discussions in chapters 5 and 6 of the results of optical emission studies made on a diamond plasma. Simple methods and set-ups which were employed, e.g. voltage or current measurement, are described in the experimental sections of the relevant chapters. Each experimental technique is introduced together with a brief background and description. The general principles are then described and where appropriate schematics of simplified arrangements are given together with a discussion of the applications to the field of diamond research; additional details of actual experimental set-ups are given in the experimental sections of the chapters in which they were used.

3.2 Microwave Enhanced Plasma Chemical Vapour Deposition

3.2.1 Introduction.

Microwave Enhanced Plasma Chemical Vapour Deposition (MEPCVD) refers to a class of reactor type which utilise 2.45 GHz microwave radiation to ignite a plasma at modest pressures, typically 10-100 Torr, in a gas composition suitable for diamond deposition e.g. hydrogen-methane. It has been claimed, with justification, that it was the introduction of the microwave reactor together with the hot filament reactor which precipitated the recent worldwide research effort and elevated CVD diamond deposition to the status of an industrially significant technology [Bachmann 1998]. The microwave class of device includes the original NIRIM tubular reactor, the "Bell Jar" reactor, ASTEX HPMS, and Wavemat reactors as well as magnetised and ECR coupled plasma sources and high pressure plasma torches; other designs have been suggested. Further discussion of some of these options has been given elsewhere in

this thesis; comprehensive reviews can be found elsewhere, [e.g.Bachmann 1998, Zhu 1991 and references therein].

3.2.2 Microwave Reactors.

The original microwave reactor, now called the NIRIM reactor after the NIRIM (National Institute of Research into Inorganic Materials) group in Japan who introduced it [Kamo 1983] was based on a 4cm quartz reaction tube situated directly in the path of microwaves via bores in a rectangular waveguide supplying power from typically a 1kW magnetron unit. At low pressures and powers for a hydrogen-methane mix (typically few mb, ~200W, ~1% CH_4/H_2) the microwaves ignite a plasma discharge within the tube consisting of a mixture of electrons, ions, radicals and neutrals characterised by translational and rotational energies which correspond to thermal temperatures of several thousand degrees. At typical operating pressures (10-100 Torr), such plasmas are at the boundary between non-isothermal and isothermal behaviour at which the gas temperature begins to approach the electron temperature and the plasma tends toward a state of local thermodynamic equilibrium (LTE). Under such conditions various deposits, ranging from graphite to diamond, will condense on a 'cold' substrate placed in the plasma. 'Cold' is in this context is relative to the effective plasma temperature and for diamond growth is typically around 800°C. The factors which determine the rate and kind of material deposited on the substrate are a rather complex function of plasma and substrate conditions; however in many microwave chambers a 1% CH_4 in H_2 at ~30 Torr, ~100 sccm total flow, at a microwave power of a few hundred watts and substrate temperature around 800°C results in a deposit with a high sp^3 fraction which can be considered as a diamond film.

The NIRIM reactor suffers from a number of problems including; difficult scale-up, serious contamination arising from sputtering of the tube walls which are very close to the plasma and difficulty in fully de-coupling the substrate and plasma temperatures. In 1987 the "Bell Jar" reactor was introduced by Bachmann and Smith together with the ASTeX company in the USA, [Bachmann 1993]. This design solves most of the above problems by removing the glass tube reaction chamber from the rectangular waveguide and replacing it with a quartz bell-jar chamber housed within a resonant cavity formed

from a large diameter circular waveguide coupled via an antenna rod to the rectangular guide supplying the microwave power. In this arrangement the microwave fields form a standing wave within the resonant cavity which vary in intensity; careful design of the chamber and positioning of the substrate holder results in a stable discharge which when struck takes the form of an spheroidal plasma ball which is located just above the substrate. The plasma is remote from the chamber walls which removes the problem of contamination, while the much larger size of the resonant cavity permits easy incorporation of substrate heating and cooling facilities allowing a much greater de-coupling of substrate and gas phase temperatures. The bell-jar reactor was subsequently developed by ASTeX into their well known High Pressure Microwave Source reactor (HPMS). The basic mode of operation is identical to the bell jar but in the HPMS the quartz bell is replaced by a flat quartz window which forms the top of a double-skin water cooled vacuum chamber reaction vessel which replaces the perforated metal circular waveguide of the bell-jar reactor. The HPMS chamber utilises standard high vacuum chamber technology and includes ports and windows for diagnostics together with an access door which accommodates samples up to 10 cm in diameter and simplifies sample replacement. A typical system includes gas flow and metering facilities, substrate heating and/or cooling, substrate temperature monitoring by thermocouple and waste gas removal by various methods; typically rotary and/or turbo pumps. Often the substrate holder arrangement is designed to allow the substrate to be electrically isolated from the remainder of the chamber and includes biasing facilities. Power supplies are typically 1, 1.5 or 5 kW magnetron type microwave units. This type of resonant chamber reactor is extremely stable and can operate continuously for the several weeks necessary to grow the highest quality >1 mm thick optical windows currently being developed for military and laser applications [Bachmann 1998].

Two MEPCVD chambers were used during the current study; these consisted of a 1.5 kW 2.45 GHz ASTeX HPMS system and a very similar unit designed and supplied by RFA Ltd. The RFA system is virtually identical to the HPMS, the main differences are the location and arrangement of some observation ports and the substrate heating method which is via low voltage AC current heating of a graphite heater element

instead of an RF source and graphite susceptor as used in the HPMS reactor. A simplified generic diagram based on the HPMS ASTeX reactor is shown in figure (3.1) in which the main components are identified. Both reactors were equipped to allow independent substrate biasing and included facilities to monitor bias voltage and bias current to better than ±0.5V and ± 0.1 mA.

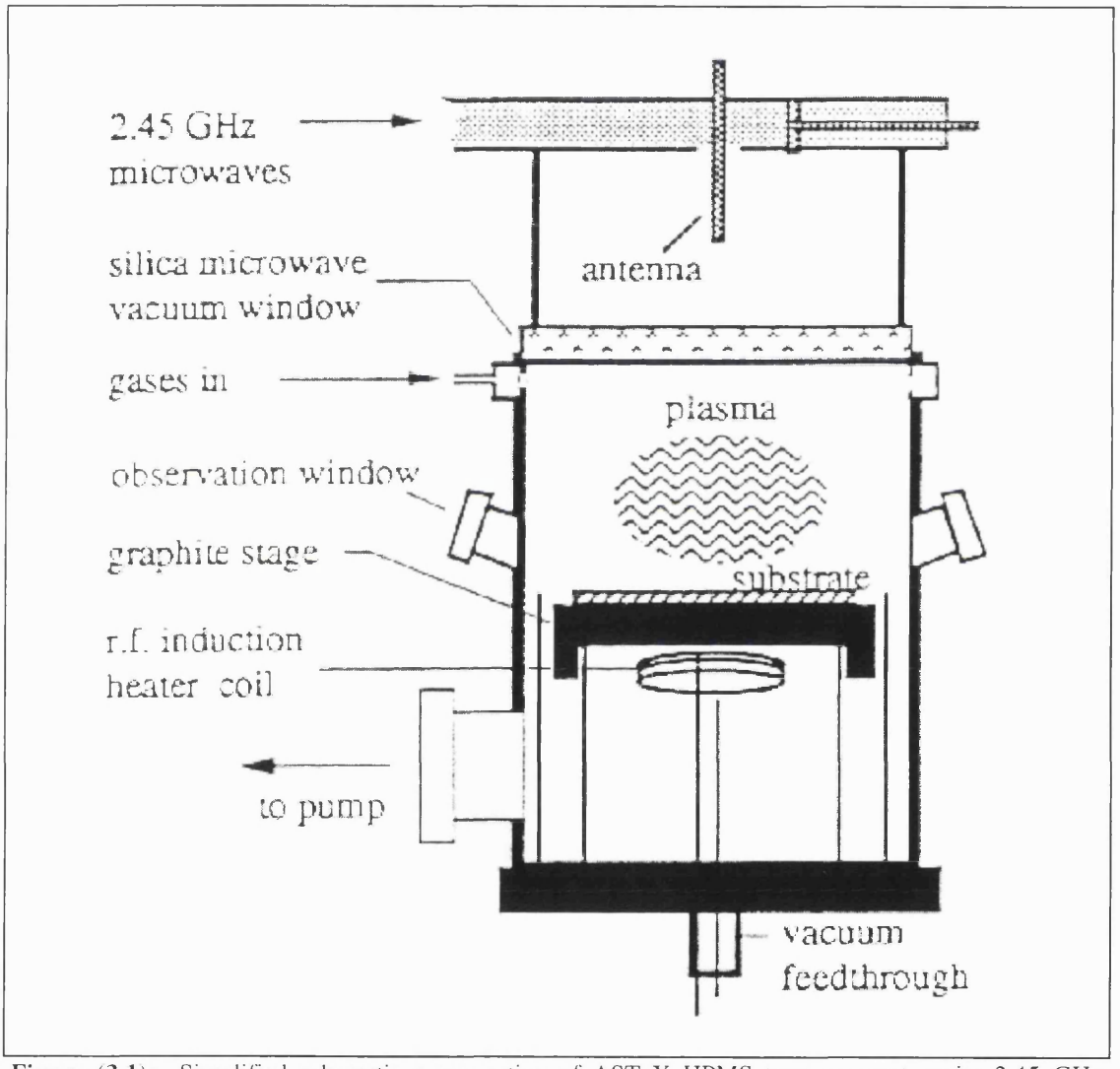

Figure (3.1): Simplified schematic cross-section of ASTeX HPMS type resonant cavity 2.45 GHz microwave reactor showing the main chamber arrangement [Redrawn from Bachmann 1998]

The two ports shown are designed to allow optical reflection studies of the substrate. On both the reactors used in these studies two additional CF-70 observation ports were available which allowed viewing normal to the reactor axis of the substrate-plasma region. Photographic and OES studies were carried out via these additional ports which are not shown on the figure. High purity gases (H_2, CH_4 and Ar) better than

99.995 % pure (BOC and Air Products) were used throughout the studies described in this thesis.

The 1.5 kW HPMS design is probably the most common research reactor in use today, however the design shown in figure (3.1) while addressing many of the issues of the earlier designs still suffers from two important problems. The first of these is that on a power-pressure plot the discharge is only stable within a corridor of conditions which becomes wider as power and pressure increase. Outside this corridor the plasma is unstable and can jump to the quartz window which will ultimately fail if exposed to the plasma for sufficient time. The second problem is that the (approximately) spherical symmetric discharge results in species and energy flux to the substrate which are radially non-uniform [Bachman 1998]. The highest density is at the substrate centre and the result is that substrate deposits show a radial dependence on growth rate and phase purity which decreases in an approximately gaussian manner towards the substrate perimeter. For large area, typically industrial, applications this problem can be alleviated to some extent by running at lower pressures and/or higher powers e.g. 5 kW.

3.2.3 The CVD Process.

Clearly the successful nucleation and growth of diamond in an environment such as that provided by the HPMS reactor depends on the detailed chemical and physical processes occurring in the plasma-substrate system. These are coupled, enormously complex and are the subject of a considerable ongoing research effort; a complete description of the microwave diamond nucleation and growth process is currently impossible. To take the plasma as an example; in a *simplified* model Bou *et. al.* [1992] considered 106 chemical reactions, 20 ionising reactions and 23 ion-neutral reactions in an attempt to examine the influence of electron density and temperature on the major species in the discharge! Of course simplifications and assumptions can be made depending on the goal of a given analysis and useful progress is rapidly being made. The current state of knowledge with respect to the process of MEPCVD has been extensively reviewed by a number of authors including [Spear 1994, Moustakas 1994, Goodwin 1998, Gicquel 1998, Hassouni 1998]. The following sections present a brief

summary of the main points, for further details the reader should consult the above reviews and the many references therein.

Figure (3.2) summarises the main features which comprise a typical CVD diamond process taking place in a microwave activated gas of methane diluted in hydrogen (typically 1% CH_4 in H_2) and includes gas phase chemistry, complex heat and mass transport, nucleation, surface chemistry, bulk chemistry and diffusion and temporal dynamics.

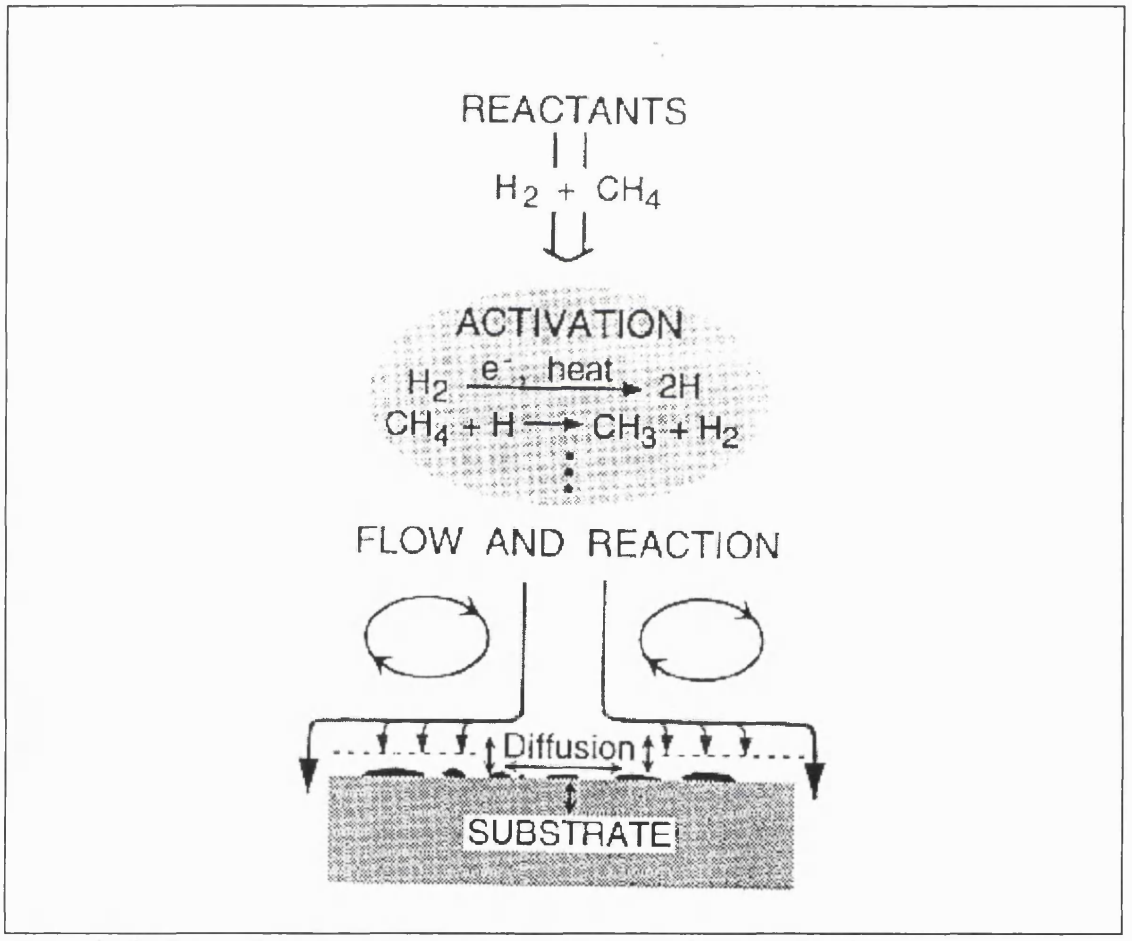

Figure (3.2): Schematic showing the main processes occurring in a typical CVD diamond environment, [Redrawn from Butler and Woodin 1993]

The simplified process can be summarised as follows; the intense, high frequency microwave electric field rapidly heats the few free electrons in the H_2-CH_4 gas which are always present at a finite temperature. The electrons undergo elastic and inelastic collisions transferring energy to the neutral species in the background gas; provided the electric field strength is sufficient some of these collisions are ionising and produce

ions and further electrons. The electron density rises rapidly to an equilibrium value at which point the energy supplied to the electron population by the electric fields is equal to the total rate of energy loss through a range of mechanisms including radiation and various types of collision. The ions produced are too massive to respond to the high frequency microwave field and gain no net energy from it; the energy supply to the plasma is mainly determined by the interaction of the electron population and the fields of the microwave radiation. At steady state three kinetic temperatures can be defined; T_i, T_N and T_e which correspond to the ion, neutral and free electron temperatures respectively. Inelastic dissociation collisions between electrons and the dominant H_2 neutral generate large quantities of the highly reactive atomic hydrogen radical which then initiates a large number of chemical reactions. These in turn generate a range hydrocarbons and carbon groups through a combination of dehydrogenation, hydrogenation and polymerisation reactions. At steady state a large number species exist but the most important (in terms of mole fraction) are H•,CH_3• and C_2H_2•. Active species are transported by diffusion and convection to the vicinity of the substrate where they give rise to nucleation sites by mechanisms which are as yet unclear. Following nucleation the diamond seed sites grow by consumption of active species; the full details of the growth mechanisms remain unclear, however a possible simplified mechanism involves the stabilisation of active carbon surface sites by atomic hydrogen which saturates the surface. Further incoming H• can then remove a terminating H• leaving an active surface site which can 'capture' a highly reactive CH_3• radical. After a length of time sufficient to allow the formation of a complete layer at the substrate the entire substrate-plasma system will at state of dynamic equilibrium.

3.2.4 The Microwave Plasma.

Much of this thesis is concerned with biased nucleation and growth from a microwave plasma and the nature of bias induced changes to the plasma and the sheath region; therefore the plasma component of the CVD process is considered in detail below and represents a summary of current state of knowledge drawn from plasma texts and the work a number of authors who have recently reviewed the subject in the CVD diamond field including; [Chapters in Prelas 1998, Huddlestone 1965, Lochte-Holtgreven 1968, Dendy 1993, Ferreira 1993, Proud 1985, Hutchinson 1987].

A plasma can be considered as a gaseous collection of ions, electrons and neutral particles in which the negative and positive charge densities are equal; this is termed a state of *quasi-neutrality*. Under these conditions charge imbalance and external electric fields are rapidly compensated for by movement of the free charges which constitute the plasma. The electrons with a mass $\sim 10^{-3}$ that of the ions can respond much more rapidly than the ions and are the dominant charge carriers; to a first approximation the positive ions can be treated as immobile. The distance over which a small potential (ϕ) can disturb the plasma is called the self-shielding or *Debye* length (λ_D) and can be found by solving Poisson's equation relating electric field and charge in a medium, which yields:

$$\lambda_D = \left(\frac{\varepsilon_0 k T_e}{n_e e^2} \right)^{1/2} \qquad (3.1)$$

where; ε_0, n_e, k, e, T_e are the vacuum permittivity, unperturbed electron density, Boltzmann constant and the electron charge and temperature respectively. The electrons cannot respond instantaneously to changes in potential or charge density; the result is that electrons tend to 'overshoot' resulting in an oscillatory motion with a frequency which is the inverse of the time to move a distance λ_D . The frequency of this motion is called the *plasma frequency* (ω_p) and it determines the maximum frequency of an applied electric field which will be shielded out by the plasma and is given by:

$$\omega_p = \left(\frac{n_e^2}{\varepsilon_0 m} \right)^{1/2} \qquad (3.2)$$

where m is the electron mass and other symbols are as previously defined. The electron energy distribution can be approximated as a Maxwellian function which describes the fraction of the total electron density (n_e) with an energy in the range E to $E + dE$. The electron energy distribution can be characterised by a mean electron temperature (T_e); typical values of kT_e for many process plasmas are in the range 1-10 eV, which can be compared with typical inelastic process threshold energies for many molecules and atoms which lie in the range 0.1- 20 eV.

The electrons in a plasma are more mobile than the ions. Therefore when a plasma is confined within a volume such as a chamber which has grounded walls there is initially a higher flux of electrons to the walls than ions. At equilibrium the plasma becomes slightly positive with respect to the wall to ensure that the ion and electron flux becomes equal. The potential which forms is called the *plasma potential*. Similarly an electrically floating surface in a plasma rapidly becomes slightly negatively charged to a potential, called the *floating potential*, which is typically the negative of the plasma potential. It turns out that the floating potential is approximately proportional to the electron temperature.

The tendency of a plasma to shield itself from fields and regions of charge gives rise to the concept of a *sheath*. This is a region of space which forms between a plasma and nearby walls or surfaces; quasi-neutrality does not hold in this region and it can support significant electric fields. Such regions are typically dark in appearance due to the low electron density there which considerably reduces the excitation rate. High electric fields and large currents can exist within the sheath region, particularly if the conducting surface is held at a large potential with respect to the plasma. The principal components of the sheath currents are:

(i) ions and electrons within the sheath.
(ii) secondary electrons generated at the surface by ion impacts there.
(iii) collision of charged-neutral species which can generate further ions and electrons in the sheath by impact ionisation.

It can be shown that the maximum current which flows in the sheath is primarily determined by the sheath thickness and potential. In an idealised model which considers the sheath as two conducting planes at potentials of 0 and V_b, separated by a distance d, with one emitting particles of mass m and charge $-e$, the space-charge limited current j is given by the *Child-Langmuir* law:

$$j \propto \left(\frac{V_b^{3/2}}{d^2} \right) \qquad (3.3)$$

These relations apply approximately to many processing plasmas; however more detailed analyses which account for collision processes such as ionisation can be developed.

Energy transfer in typical CVD diamond plasmas occurs primarily through collisions [Gicquel 1998]; these are classified as primary collisions (electron-neutral; e-n) and secondary collisions (neutral-neutral and ion-neutral; n-n, i-n). Collisions can be elastic, inelastic, reactive and superelastic and are characterised by quantities such as collision rates, cross-sections (σ) and if inelastic, energy thresholds (E_t). In general collision cross-sections, which express the probability of an interaction, are energy dependent and may increase or decrease with energy depending on the collision type. Considering the primary collisions first (e-n) the most important are the elastic and inelastic collisions and these are summarised as follows:

Elastic Collisions:

The total kinetic energy and momentum of the interacting particles is conserved, no change in internal states occur, however the individual particles may change direction and kinetic energy. The collision cross-section depends on the velocity and details of the interaction potentials. An example is the elastic collision of an electron with hydrogen which has a cross-section which peaks at around 1 eV as shown in figure (3.3). For the case of a sheath region which is collision dominated, elastic collisions are an important mechanism allowing electrons to gain significant energy from the sheath fields because energy transfer between the electron and ions or neutrals is small since the mass ratio is at least of the order of ~1/2000.

Inelastic Collisions:

These result in a change of state of the ion (i), neutral (n) or radical (r) partner in an e - X collision. A number of reactions are possible, the most important are summarised below:

Electron Excitation.

$X + e \rightarrow X^* + e$

where species X is excited from (usually) the ground state into a higher energy electronic state, an example is atomic hydrogen excited into the (n=3) state which may then emit a photon at ~656nm. The reverse of the above reaction is de-excitation by quenching or photoemission.

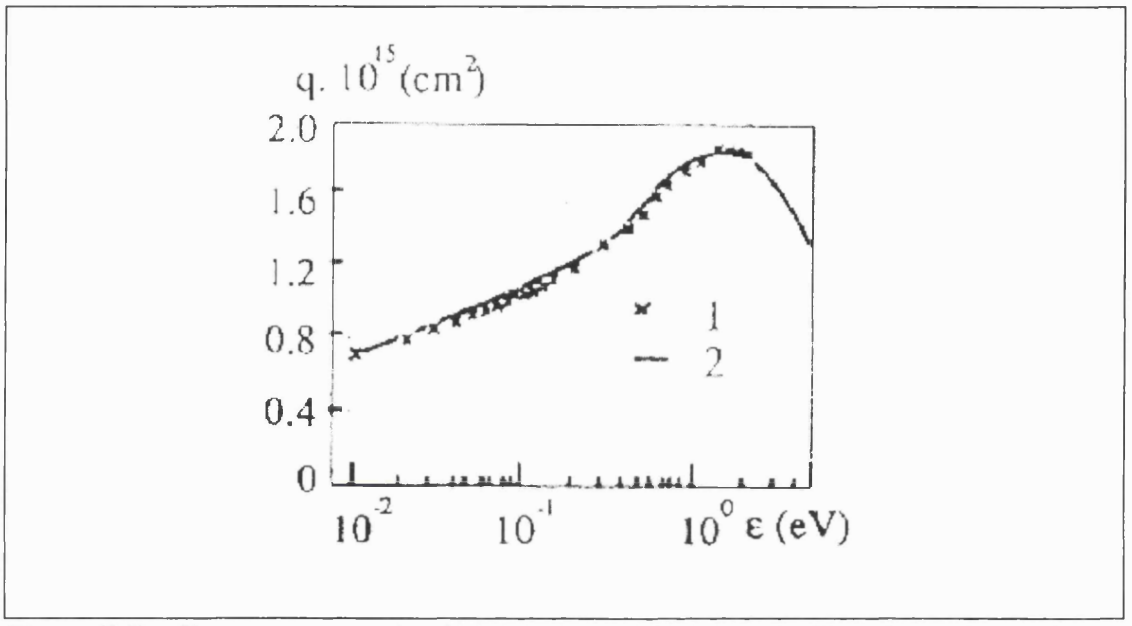

Figure (3.3): Transport cross-section for the scattering of electrons by H_2 molecule; 1=experiment, 2=calculation [Reproduced from Gicquel 1998].

Ionisation

$X + e \rightarrow X^+ + e + e$

This process has a threshold which is usually the ionisation potential of species X, however stepwise ionisation is possible at a lower energy if X is in an excited state and becomes more probable if X possesses long lived metastable states. Generally ions have a much larger ionisation energy than neutrals and in plasmas with a modest T_e (~few eV) the probability of X^{++} creation is low, hence in a typical diamond CVD plasma the assumption $n_e = n_i$ is reasonable.

Vibrational Excitation.

$X + e \rightarrow X(v) + e$

Some of the electron energy is transferred to vibrational states of the molecule X, which may include rotational modes.

Dissociation

$X^* + e \rightarrow Y + Y + e$

Typically an already excited molecule (electronic or vibrational) breaks up into two smaller fragments which may or may not be in an excited state. An example is the electron dissociation of hydrogen: $H_2 + e \rightarrow H + H + e$, which is the primary source of atomic hydrogen in typical MW diamond plasmas [Goodwin 1998, Grotjohn 1998].

Secondary Collisions:

These are the neutral-neutral, ion-neutral collisions and may include elastic, inelastic and reactive collisions and lead to a large number of processes. A complete analysis is complicated by the likely probability that the colliding species have considerable internal energy which influences the reaction rates and probabilities of many of the available processes. Inelastic collisions are the most important as these lead to significant amount of chemistry between colliding species. Similarly to e-X collisions, X-X collisions have energy dependent cross-sections and energy thresholds, however transfer modes exist and energy can be transferred between V-V, V-R, V-T and e-e (quenching) modes where the symbols mean V:vibrational, R:rotational, T:translational and e-electronic. The most important secondary collision processes are:

Quenching

$X^* + Y \rightarrow X + Y^*$

This reaction can lead to the loss of metastable and radiative species and is most important under conditions of moderate to high pressure.

Charge Transfer

$X^+ + Y \rightarrow X + Y^+$

occurs when an electron is transferred between an ion colliding with a neutral species; if the species Y is an excited state of species X then the process is called *resonant charge transfer* and at low energies the cross-section for this reaction can become very large and may dominate over other types of collision. The result of a charge exchange collision of a fast ion with a neutral is a slow ion and a fast neutral. This collision is an important source of fast neutrals especially in a sheath region above a negatively biased substrate where the process can result in a significant flux of fast neutrals to the substrate (cathode). It is only recently that the importance of this source of fast neutrals has been recognised [Dendy 1995].

Chemical Reactions.

$X + YZ(v,j) \rightarrow XY(v',j') + Z$

A very large number of such reactions can occur in a typical diamond plasma which contains a relatively high density of highly reactive atomic hydrogen and hydrocarbon radicals. The details of these reactions are very complex and depend on the details of the gas temperature, identities of the X and YZ species, together with their vibrational and rotational excited states. An example of such a reaction which occurs in a diamond plasma is $H + CH_4 \rightarrow H_2 + CH_3$.

Radiative Processes:

These are responsible for electro-magnetic radiation from the plasma volume. The main contributions are atomic and molecular transitions which result in line and band spectra together with a large continuum component which arises from the free-bound interaction in which an ion captures an electron and free-free interactions which generate Bremstrahlung radiation from the acceleration of electrons in the potential field of ions.

Diamond CVD Microwave Plasmas:

A typical diamond microwave plasma (~ 25mB, 1% CH_4/H_2, power density~$10Wcm^{-3}$) has approximately the following plasma characteristics [Gicquel 1998, Grotjohn 1998]: electron temperature of ~ 1-3 eV, an electron density between 10^{10} and 10^{12} cm^{-3}. A typical value is ~10^{11} cm^{-3}. An upper limit of $10^{12}cm^{-3}$ is imposed by the requirement that the 2.45 GHz microwave field must be able to penetrate the plasma. The diamond plasma can be described as a weakly ionised gas, with an ionisation fraction of less than 10^{-4}, characterised by two temperatures T_e and T_h for the electron and heavy particles respectively. Simple estimates have given a plasma frequency of ~ 3-9 GHz, collision frequency of ~20 GHz ; an electron-neutral mean free path of ~30 μm, neutral-neutral mean free path ~20 μm and a Debye length of 8-25 μm.

The main inelastic processes are summarised in table (3.1) which includes approximate rate constants and threshold energies. It can be seen from this data that the main routes for H production are via H_2 dissociation and a fast reaction following H_2 ionisation

which results in H_3^+ being the dominant ion in the plasma. Clearly changes in T_e and n_e can significantly affect these reactions altering the species balance in the plasma. Introduction of a small fraction of CH_4 to the plasma (~1%) opens additional pathways for the production of ions and atomic hydrogen via:

$CH_4 + e \rightarrow CH_4^+ + e + e$ and

$CH_4 + e \rightarrow CH_3 + H + e$

which represent ~ 51% and 39% of the results of inelastic electron collisions with methane. However n-n collisions are much more likely than e-n collisions and this leads to considerable chemistry which is important in establishing the concentrations and chemical species which exist within the plasma. There are many hundreds of reactions possible and the following paragraphs give a brief summary of those which are considered to be most important [Goodwin 1998].

Reaction	Expression	Threshold energy (eV)	Rate coefficient (m^3s^{-1})
ionisation	$e + H_2 \rightarrow H_2^+ + 2e$ $H_2^+ + H_2 \rightarrow H_3^+ + H$	15.4 0	$\sim 10^{-14}$ H_3^+ dominant
excitation	$e + H_2 \rightarrow H_2^* + e$	12.0	$\sim 6.5 \times 10^{-15}$
dissociation	$e + H_2 \rightarrow e + H + H$	10.0	$\sim 10^{-14}$
recombination	e + ion $\rightarrow$ neutral	0	$\sim 10^{-14}$

Table (3.1): Main inelastic processes in an H_2 plasma, [reproduced from Grotjohn 1998].

Hydrogen

Hydrogen is critical to the growth of diamond from the gas phase; it has been shown that without some source of atomic hydrogen diamond will not grow under CVD conditions [Bachmann 1998]. Atomic hydrogen is highly reactive and its presence drives much of the chemistry which occurs in the plasma phase. The concentration of atomic hydrogen in the plasma is determined by the balance of the H-atom production rate and the destruction rate from wall recombination and homogeneous chemistry. The mechanisms for creation were discussed above. Homogeneous recombination of hydrogen requires a third body to carry away the excess heat and is therefore a slow

process under typical CVD conditions with a characteristic time of around 1 second; this is sufficient to allow a diffusion distance of around 35 cm. Since the reactor walls and substrate are within a few centimetres of the plasma, H-atoms are able to diffuse and recombine there with minimal losses from homogeneous recombination. The introduction of a small CH_4 fraction can reduce the homogeneous recombination time to about 50 ms, but this still corresponds to a diffusion length of ~8 cm and under most conditions homogeneous recombination of atomic hydrogen can be ignored. However if the CH_4 fraction is raised above a few percent this is no longer true and homogeneous recombination can influence the atomic hydrogen concentration.

Atomic hydrogen is mainly lost by recombination at the walls and on the substrate which acts as a strong sink for this species. Wall recombination is characterised by the recombination coefficient γ_H defined as the ratio of the H• loss rate to the H• collision rate at the surface. For a surface at temperature T (Kelvin) γ_H can be estimated from an expression given by Goodwin [Goodwin 1998]. For typical CVD diamond deposition conditions at a substrate temperature of 1200K, a value of $\gamma_H = 0.16$ is obtained which is quite close to measured values of 0.12 and indicates that there is a high recombination rate at the substrate during CVD diamond growth.

Hydrocarbons

Introducing CH_4 into the plasma allows a very wide range of reactions to occur which generate C_1 and C_2 hydrocarbon species. The chemistry is dominated by neutral reactions such as dehydrogenation, hydrogenation and polymerisation. These generate the full range of C_1 species (CH_x x=0-4) through hydrogen shift reactions such as:

$$CH_x + H \quad \Leftrightarrow \quad CH_{x-1} + H_2$$

These reactions are typically very fast due to low activation energies; for the case of a few percent of atomic hydrogen the CH_3 radical is the most abundant product. C_2 species can be produced by reactions such as:

$$CH_3 + CH_3 \rightarrow C_2H_6$$
$$\rightarrow C_2H_5 + H$$
$$\rightarrow C_2H_4 + H_2$$

Once created C_2 species are rapidly converted to C_2H_2 through rapid H-abstraction reactions.

In summary, it is clear from this simplified discussion that the typical diamond microwave CVD plasma is a very complex system characterised by the detailed balance of a large number of different physical and chemical processes. The literature is very extensive and it is emphasised that for a more complete discussion the reader should consult the reviews listed earlier and original references therein.

3.3 Scanning Electron Microscopy.

Scanning electron microscopy utilises an electron beam to provide a magnified image of an object, similar to the principle of an optical microscope. The power of the technique arises from the high magnifications and resolutions available, combined with a very large depth of field. This enables very simple and effective visualisation of sample topographies to be carried out in real time accompanied by relatively minimal sample damage[Brundle 1992]. An additional enhancement is the inclusion of energy dispersive X-ray spectroscopy (EDX) which allows spatially resolved analysis of the near surface elemental composition, for non-trace elements [Brundle 1992]. For these and other reasons discussed below SEM has proved to be the most widely used and useful imaging technique for the study of diamond film morphology [Zhu 1993].

In an electron microscope a primary electron beam is focused and scanned across the surface of a sample [Schroder 1990]. An image, typically displayed on a CRT, can be formed from either back-scattered electrons (BSE) from the primary beam or secondary electrons (SE) generated by the interaction of the primary beam with the surface. Magnifications of between 10-300 000 can typically be obtained with resolutions of 2.5

- 10 nm's; the ultimate resolution is determined by the minimum spot size which is theoretically limited by the electron wavelength but in practise is limited by local surface charging effects. The secondary electrons have a relatively low energy and hence short escape depth and images formed from the SE beam display a high surface sensitivity. Back-scattered electrons, which have energies > 50 eV, have a larger escape depth and because they result from elastic scattering events tend to emphasise regions containing high Z elements. A by-product of irradiating the surface with the high energy primary e-beam is the generation of X-rays in the near surface region, ~100 nm - 5 μm depth. The resulting X-ray spectrum is characteristic of the elemental composition of the near surface and incorporation of an EDX unit within the SEM chamber can provide an elemental analysis which can be superimposed on the SEM image of the sample surface. However, the EDX analysis is restricted to non-trace elements with atomic numbers greater than 3 due to the poor efficiency for X-ray generation of low Z elements. Typical primary electron beam energies can range between 0.5 - 50 keV, although 20-30 keV beam energies are most commonly used during the study of diamond films. The system employed during the studies described in this thesis was a Hitatchi S-800 SEM with a magnification of 20-300K and a resolution of 20 nm utilising the secondary electron emission mode.

SEM, which is usually combined with Raman spectroscopy in the diamond field, has proven to be the most widely used technique for the characterisation of the quality and surface morphology of diamond films. Film preparation is minimal; however it is advisable to sputter a few nm's of gold onto the insulating diamond surface prior to measurement to avoid the effects of excessive charge build up which can lead to poor focusing and instability. Alternatively very low beam voltages (< 2 keV) can be employed to similar effect. Samples can be mounted easily in any orientation allowing the study of film surface as well as the fracture cross-section. Film morphology is easily identified from surface scans while cross-sections allow the study of the developing texture and clearly reveal defects such as voids, cracks and grain boundaries. Typical examples of SEM scans taken during this work can be found in chapters 4 and 8 of this thesis.

3.4 Atomic Force Microscopy

Atomic force microscopy (AFM) is a scanning probe microscopy which is able to provide three dimensional images of solid surfaces down to near atomic resolutions and is similar to many respects to Scanning Tunneling Microscopy (STM). In most case AFM samples require virtually no preparation and particularly do not require the provision of a conductive surface as is the case for STM [Rutledge 1998]. The first use of AFM was reported in 1986 by Binnig *et al.* and has seen subsequent rapid development [Binnig 1986]. More detailed discussions of the AFM technique can be found elsewhere e.g. Burnham [1991] and Brundle [1992].

The principle of the AFM technique relies on the ability to scan across a surface to be studied, at a very high precision, an atomically sharp tip. The vertical displacement required to maintain a constant force between the tip and surface is measured to a very high resolution as a function of the scanning position of the tip; the positional and displacement data is integrated by a computer to generate a high resolution 3-D image of the surface being scanned; AFM's can be used in either contact mode or attractive (non-contact) mode [Burnham 1991]. Contact is defined as being when the force between tip and surface acquire a repulsive component due to the extreme proximity of the tip and surface and offers the prospect of higher resolutions. Non-contact mode relies on purely attractive forces which occur when there is a relatively large distance between the tip and surface. In this mode resolution is reduced but the possibility of tip and sample damage is removed. AFM tips are typically produced on silicon cantilevers by highly precise bulk and surface micromaching techniques. A simplified schematic diagram showing the important components of an AFM system is shown in figure (3.4). The instrument used during these studies was a Park Scientific AFM operated in contact mode. The AFM scans presented in chapter 7 of this thesis were obtained at the Department of Theoretical and Physical Chemistry at the University of Oxford and the Author acknowledges the help of Dr R.D Marshall, Dr. J Foord and the AFM technical staff in obtaining these images.

AFM measurements require clean surfaces and are often carried out under UHV conditions. The presence of contaminants and adsorbates, such as water or hydrocarbons, on the surface can influence the acquired image especially if these significantly affect the surface energy in localised regions of the surface [Burnham 1991]. With very fragile samples, care has to be exercised as it has been shown that the AFM tip can cause damage to such surfaces. In addition some caution is required when interpreting images acquired at the highest resolutions as 'tip effects' can influence the results [Baranauskas 1992]; this is less of a problem when the instrument is used in contact mode [Burnham 1991].

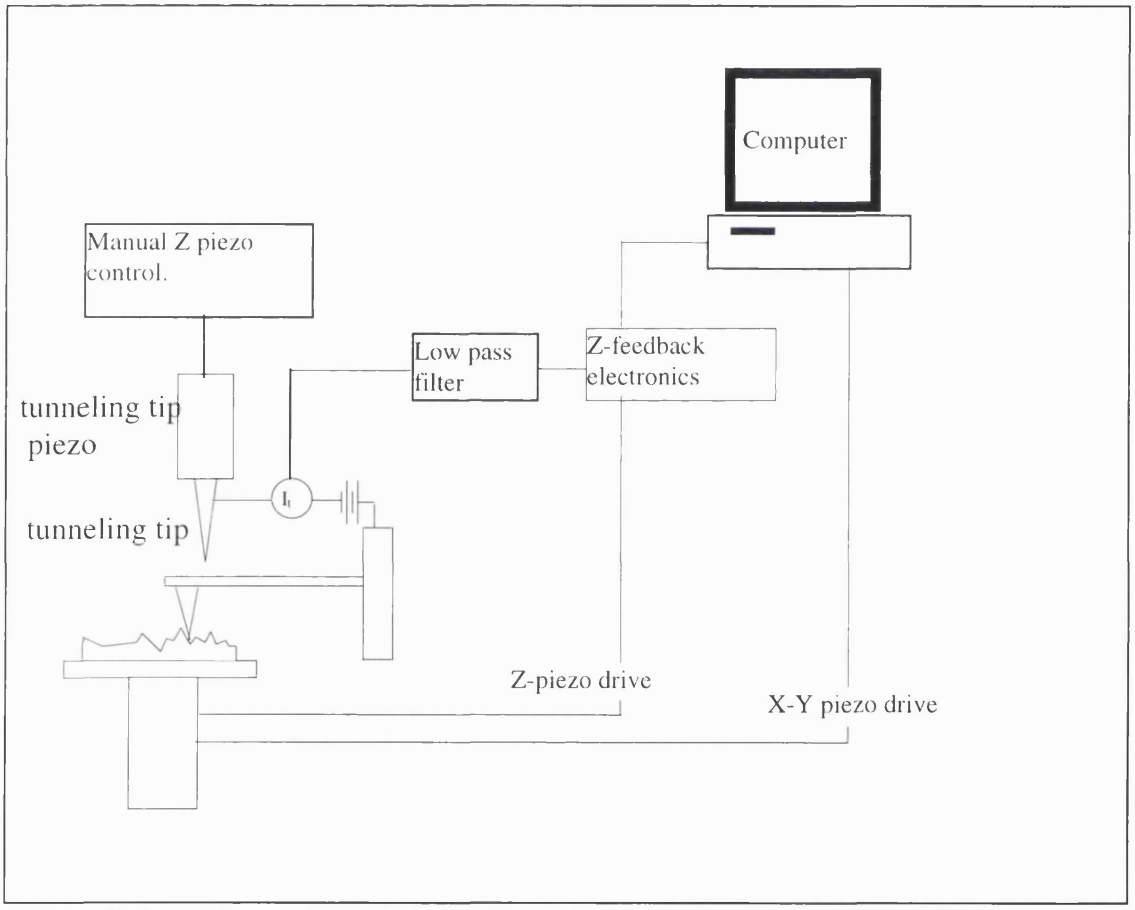

Figure (3.4): Diagram of simplified AFM microscope system configured for constant force measurement showing the key components. [Redrawn from Burnham 1991].

In the field of CVD diamond the AFM technique is a useful addition to the SEM but to-date has been much less widely used, probably due to its much more recent development and the higher cost of the initial set-up. In addition the SEM has had

many years to evolve from highly specialised research tool to the status of almost 'everyday' technique and certainly most research organisations even small companies now have access to SEM; the same is not yet true of the AFM. Although a very clean surface and UHV conditions for measurement are to be preferred; to date all diamond AFM measurements have been carried out under ambient conditions with little or no advanced surface preparation [Rutledge 1998]. The diamond surface is very stable and this is particularly true for the case of the (100) surface which has been most commonly observed in AFM studies; for example, Sutcu [1992a] saw no differences in the AFM images for diamond samples before and after cleaning in boiling sulphuric acid. None-the-less this does not indicate that normal scientific standards of sample cleanliness do not have to be adhered to for AFM measurements on diamond !

On homoepitaxial diamond AFM has been employed to study the orientation of the (100) face with respect to the diamond substrate [Sutco 1992a, Karasawa 1993]; the effect of CH_4 fraction on the surface roughness has also been examined [Maguire 1992, Sutco 1992a,b], 0.3% methane fraction resulted in micron scale roughness while a 1.6% fraction produced much smoother surfaces with nm scale roughness. On polycrystalline CVD films AFM has mainly been employed to study the early stages of nucleation, particularly the effect of bias on the orientation of nuclei on (100) silicon substrates. Jiang *et al.* [1993a] observed an intermediate layer on (100) silicon following BEN and later used AFM to assess the tilt distribution of the (100) facets of BEN nucleated crystals [Jiang 1996]. The etching of the silicon surface by atomic hydrogen which occurs prior to diamond nucleation has also been observed using AFM [Sanchez 1996], while Sattel and co-workers used AFM to study nuclei with diameters of 50-200 nm's which develop in the early stages of nucleation [Sattel 1996].

AFM is a useful complementary technique to the SEM characterisation methods commonly employed in the diamond field. A brief survey of the literature indicates that it has primarily found uses in the study of the early stages of nucleation where the very small size of features and low contrast may make SEM studies more difficult.

3.5 Raman Spectroscopy

Raman spectroscopy is a vibrational technique which uses the spectrum of light scattered from a material to study quantised molecular resonance's [Rutledge 1998]. High energy photons, in a monochromatic beam incident on the material, interact with lattice phonons and are either scattered elastically or inelastically. Elastic scattering, also called Rayleigh scattering, results in photons with unchanged energy which form the main component of the scattered light. Inelastically scattered photons undergo a change in energy during the interaction and the process is called Raman scattering. In Raman scattering, photons which lose energy to the lattice phonons emerge with a lower energy and hence lower frequency forming the Stokes lines, while photons which gain energy from the interaction with phonons emerge with a higher energy (frequency) and form the anti-Stokes component of the scattered spectrum. Since the original molecular energy levels obey a Boltzmann distribution, the intensity of the Stokes lines is much greater than the intensity of the anti-Stokes frequencies and in practical Raman spectra it is the Stokes lines which are usually observed. The phonon modes in the lattice depend upon the details of the atomic bonding and hence the Raman spectrum is characteristic of the bonding types existing in the sample being studied [Zhu 1993, Knight 1985].

Raman spectroscopy is non-destructive, reasonably quick and easy to carry out and does not display the charging effects commonly observed with other electron or ion based methods for characterising insulating materials. Raman spectroscopy is also extremely versatile and has found many uses particularly in chemistry where it is used to elucidate the bonding details of many different compounds [Williams 1980]. Raman is particularly sensitive to the different bonding configurations of the carbon atom and this, combined with its relative simplicity and low cost has, when used in conjunction with SEM resulted in its virtual dominance as the accepted technique for evaluating the quality of diamond and DLC films [Rutledge and Gleason 1998]. Raman scattering systems consist of four main parts [Baranska 1987]; (i) monochromatic excitation source - usually a laser, (ii) illumination and collection optics, (iii) monochromator and spectrograph and (iv) a detection system and recording/analysis device. The system

used during these studies was a commercial Renishaw System 2000 Raman spectrometer, with He-Ne laser source (632.8 nm) together with PC storage and Renishaw spectral analysis software. The system was provided with microscope optics and was used in the microprobe configuration with a typical spot size of ~100 μm. All the measurements included in this study were carried out on this instrument by the Author at DERA-Malvern. A simplified schematic of the system is shown in figure (3.5). He-Ne radiation from the laser source is directed through the microscope onto the sample. Scattered light is collected by the same microscope optics and subsequently analysed by the Raman spectrometer, which consists of a fore-monochromator, or range selector, followed by a spectrograph.

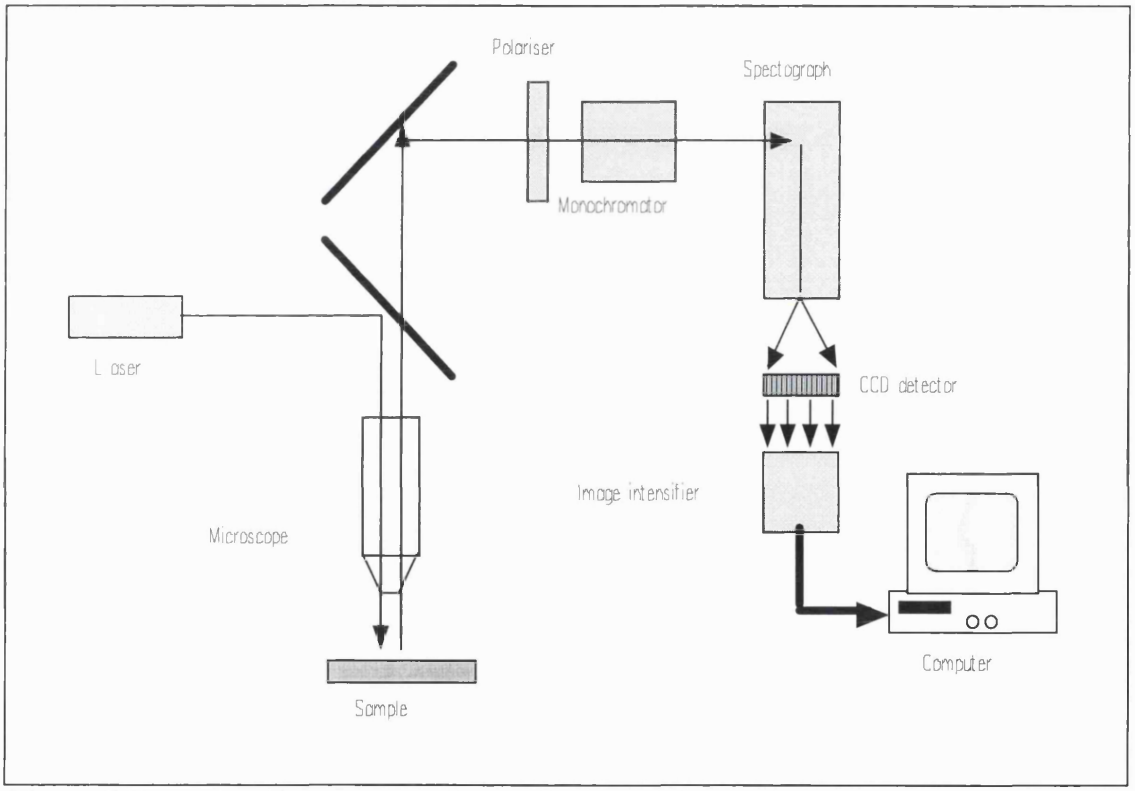

Figure (3.5): A simplified schematic diagram of a typical Raman microprobe arrangement [redrawn from Huong 1991].

The spectrograph output is directed onto a CCD multi-channel detector which is calibrated to provide optical intensity as a function of frequency. Finally the CCD data is captured by a PC, which also provides full automatic control of the instrument and includes software facilities for analysing the spectral data. The room temperature, first order Raman spectrum of natural diamond shows an unambiguous, highly characteristic

intense line at 1332 cm^{-1} and is very different from the Raman spectra of other bonding forms of carbon [Solin 1970, Knight 1985]. The diamond Raman line has a full-width-at-half-maximum (fwhm) of ~2 cm^{-1} for natural type IIa material, while for typical CVD material this can vary between 2-14 cm^{-1} [Rutledge 1998]. Although the general shape of Raman spectra obtained from CVD diamond films can vary considerably with the wavelength of the exciting radiation [M^{c}Namara 1992] the characteristic 1332 cm^{-1} diamond line remains unambiguous. The Raman scattering efficiency varies considerably between the different carbon bonding types; for example it has been shown that the scattering efficiency of graphite, which gives a Raman signal at ~1580 cm^{-1}, is some 50 times greater for 514.5 nm (Argon laser) light than the corresponding sp^3 or diamond bonded form of carbon [Wada 1981]. Furthermore excitation with He-Ne (632.8 nm) light has been shown to enhance resonantly the non-diamond Raman bands and results in an extremely sensitive tool for the evaluation of diamond films [Sails 1995]. As a consequence considerable care is needed when interpreting such spectra not to under-estimate the level of sp^3 bonded material present within the sample. Furthermore it is important to appreciate that for typical optically excited Raman spectroscopy, multi-component films present additional difficulties if quantitative assessment of the importance of the different components is required [Stuart 1993,1994]. For components with a low absorption cross-section at the excitation wavelength, e.g. diamond, Raman is essentially a bulk probe. However, for graphitic components, which have high absorption cross-sections, Raman is essentially a near-surface probe. Contributions to the Raman spectrum from different bonding components are therefore a rather complicated function of both excitation efficiency and absorption coefficient.

Figure (3.6) shows an example of a Raman spectrum obtained from a film which contains multiple carbon bonding environments [Knight 1985]. Generally Raman scattering directly above the one-phonon diamond band has been attributed to sp^2 bonded forms of carbon and typically three types can be distinguished [Shroder 1990]; crystalline graphite which gives rise to a single Raman band at ~1580 cm^{-1} [Knight 1985], defective or microcrystalline graphite showing two broad bands at 1580 cm^{-1} and 1350 cm^{-1} [Wright 1976, Knight 1985] and amorphous carbon which has a broad,

asymmetric band with a peak at around 1500±40 cm^{-1} [Knight 1985]. Some Raman spectra also show a band between 1120 cm^{-1} and 1140 cm^{-1} [Shroder 1990], however this has not yet been definitely assigned. Raman peaks below the one-phonon diamond band are also observed; 1315 - 1320 cm^{-1} has been associated with hexagonal diamond (Lonsdalite) [Knight 1989], a peak between 1200 - 1230 cm^{-1} has been tentatively assigned to the presence of an amorphous form of diamond [Yoshikawa 1988], while a band at 1140-1150 cm^{-1} has been suggested as indicative of a nanocrystalline or precursor form of diamond [Nemanich 1989, Obratzsov 1994]. A number of other less common bands occurring under various conditions have been reported in the literature and a useful summary has been given by Chan [1996].

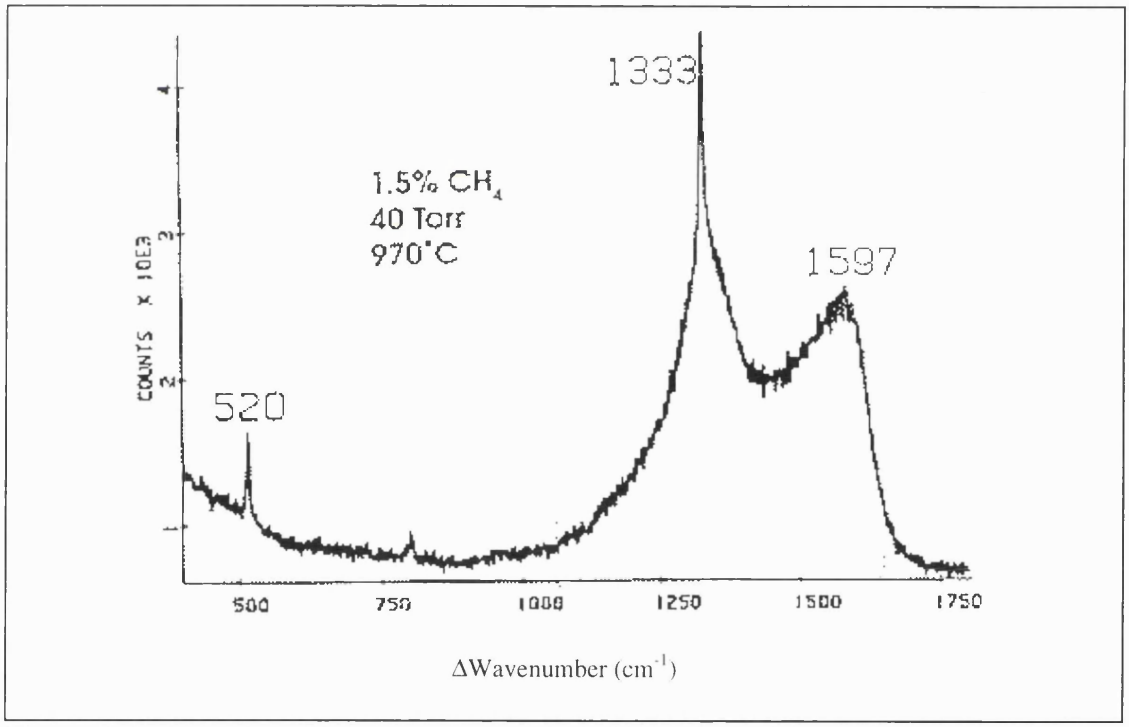

Figure (3.6): Example of a Raman spectrum obtained from a CVD diamond film containing multiple carbon bonding types. [Redrawn from Knight 1985].

The position and width of the 1332 cm^{-1} diamond line have been shown to be affected by the properties of the material and disorder in the sp^3 bonding environment and have also been shown to vary with grain size and sample temperature [Bachmann 1992]. The Raman shift is related to the inverse of the reduced mass, therefore the proportion of the ^{13}C isotope can affect the peak position, shifting it to lower wavenumber for

increasing ^{13}C, down to 1280 cm^{-1} for pure ^{13}C diamond [Chrenko 1988]. A linear shift of the 1332 cm^{-1} diamond line with temperature has been measured for CVD diamond between 300 - 700 K [Bachmann 1992]. Hence caution is needed in micro-Raman studies as the high power density can lead to local heating of the sample; this problem can be minimised by keeping spectrum acquisition time to the minimum needed to achieve reasonable count statistics. Stress has also been shown to influence the 1332 cm^{-1} peak position [Gheeraert 1992] and negative and positive wavenumber shifts have been observed which have been associated with net tensile and compressive stresses respectively. The shifts are typically of the order of a few wavenumbers corresponding to stresses of the order of a few GPa and Raman can thus offer an effective means to estimate the residual stress in diamond films [Ralchenco 1985].

In summary; Raman spectroscopy has become the pre-eminent technique within the CVD diamond field for assessing the quality of diamond films in terms of the different carbon bonding components present. The reasons for such widespread acceptance of the technique are speed, simplicity - i.e. no vacuum and minimal sample preparation, combined with relatively modest system costs and most importantly a high sensitivity to the different carbon bonding types. The utility of the technique is confirmed by its continued rapid development; for example, recently an in-situ Raman spectroscopy method has been demonstrated which allows Raman to be carried out in real time on a film as it is being grown within a CVD chamber [Bernadez 1993, Fayette 1994].

3.6 Optical Emission Spectroscopy (OES).

Optical emission spectroscopy is powerful technique which provides information on the properties and processes occurring in an emitting source via a study of its optically emitted spectrum; being a passive technique it is particularly useful for the study of plasmas. Detailed discussion of the theory of emission spectroscopy of plasma sources can be found in; [Hutchinson 1992, Lochte-Holtgreven 1968,]; reviews specific to the emission spectroscopy of *microwave plasmas* in [Kunze 1986, Ferreira 1993]; methane-hydrogen diamond plasmas [Lang 1995, Gicquel 1998 and many references

therein]; while general discussion of techniques and theory are given in [Huddlestone 1965, Mavrodineanu & Boiteux 1965].

Visible OES as used here is typically taken to include the range ~ 200 - 900 nm, i.e. deep UV to the infra-red. At wavelengths shorter than 200 nm absorption by the air becomes a serious problem and apparatus must be evacuated or purged with a less absorbing gas, e.g. nitrogen; the use of special UV optimised optical components is also necessary. While at longer wavelengths (> 900 nm) weak emissions, blackbody interference and low sensitivity detectors become a problem. Such complications detract from the simplicity and modest system costs which are key benefits of the OES technique over many of the alternatives, which suffer from being either invasive, e.g. mass spectroscopy, ion/electron spectroscopies or electric probe measurements, and/or complex and difficult e.g. CRDS, TALIF, CARS, REMPI. Invasive techniques by their very nature to some extent perturb the local plasma environment and interpretation of the data in terms of the unperturbed plasma can be difficult. Complex methods tend to be expensive, requiring specialist equipment and expertise often not easily accessible workers in the diamond field. Of course, the quantitative utility of the data obtained from a technique is often directly related to its difficulty and cost; none-the-less the use of these techniques is usually confined to very specific measurements where a high degree of confidence in the data in needed; wide ranging studies are often prohibitive in terms of time and cost.

OES can in principle be used to study any object in any form (solid, liquid, gas, plasma) emitting within the above spectral range. In this thesis OES has been used to study a diamond plasma and the rest of this discussion is confined to this type of emitting source. OES has been widely used in the fields of DLC and diamond deposition from DC, RF and MW plasmas; hydrogen emissions have been studied by a number of authors including [e.g.Lang 1996, Mucha 1988, Schreck 1996, Jubber 1996, Plano 1991]; hydrocarbon emissions, particularly CH and C_2 have been examined by [e.g. Gicquel 1993, Ballestrino 1993, Pastol 1989]; while actinometry (described below) has been employed to examine atomic hydrogen concentrations by [Gicquel 1998, Lang 1996, Donnelly 1995]; many other studies have been carried out in similar process

plasma environments but under different gas chemistries [e.g. Kampas 1982, Conner 1992]. Some studies under conditions of substrate bias during diamond nucleation have also been made, including [Shigesato 1993, Kulisch 1996, Schreck 1996, Jubber 1996, Beckmann 1994, Barshilia 1996] while Plano *et al.* [1991]have used OES to study the cathode fall of a DC diamond plasma. Some of these measurements are discussed in more detail in chapters 5 and 6. A range of OES experimental arrangements have been used depending on the aims of the measurements; for example, high spectral resolutions are needed for measurements of Doppler broadening or Stark splitting of the atomic hydrogen lines, which can be used to obtain information on translational energies of neutrals (Doppler) or electric field strengths (Stark) [Shreck 1996]. Lower resolutions and either rapid scanning monochromators or linear detector arrays are needed if widely spaced (in wavelength) spectral features are to be studied simultaneously, as was the case in these studies. However the general components of OES systems are similar and a typical OES system is illustrated schematically in figure (3.7).

Radiation from the source is sampled and collimated and then passed to a dispersive element e.g. prism or grating which produces angular dispersion of the different wavelengths in the beam generating a spectrum in which different components are spatially separated. A photographic plate, or a slit and detector arrangement, can then be used to measure the intensity of the different components in the spectrum. Comparison with wavelength standards, e.g. mercury lines from a suitable lamp, enables wavelength calibration, while comparison with known intensity standards, e.g. tungsten lamp, can allow calibration of the emission intensity; more detailed descriptions of arrangements and components can be found in the references given at the beginning of the section. Spectral features can be identified from tables of standard lines and bands, [Hertzberg 1950, Pearse 1976, Baskin 1978], together with a knowledge of the plasma constituents and previous publications of measurements in similar systems; this was the approach taken during the current studies.

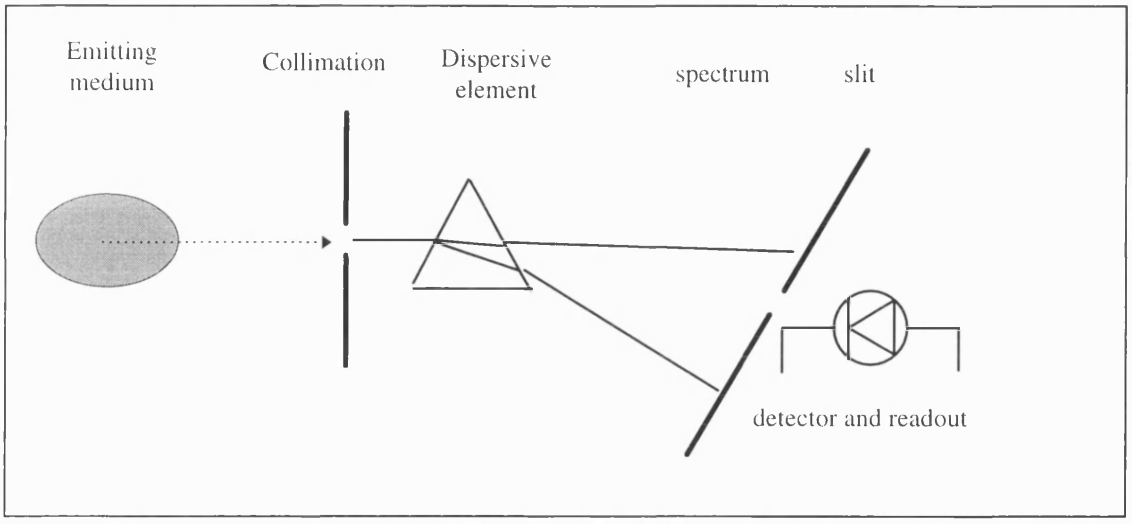

Figure (3.7): Schematic of a generic OES system showing the basic components required to make spectral measurements.

In the course of the work described in this thesis the generic system illustrated in figure (3.7) above was realised in the form of an OMA-III (EG&G-Princeton 1460) multi-channel analyser in conjunction with a 1024 element linear photodiode array (model 1453), 3-grating spectrograph (Jarerell-Ash MonoSpec 27) and a multi-frequency optical fibre bundle; the system was used to study a microwave plasmas in the ASTeX HPMS and RFA rectors described previously. Two configurations were used allowing motion of the optical fibre probe with respect to the plasma at different spatial resolutions; further details and diagrams are given in chapters 5 and 6.

The fraction of a plasma species (x) excited into an optically emitting state (j) is a function of both the species concentration and the electron energy distribution function (*eedf*) via [Kampas 1983]:

$$I_x(i \rightarrow j) = \frac{k_{x,i} n_e n_x A(i \rightarrow j) g(\lambda)}{\sum_m \left[A(i \rightarrow m) + N(i \rightarrow m) \right]} \qquad (3.5)$$

Where; $k_{x,i}$ is the rate constant for the excitation of the species x to the state i; n_e is the electron density; n_x is the concentration of species x; $A(i \rightarrow j)$ the radiative rate constant for decay to state j ; $N(i \rightarrow j)$ the non-radiative decay constant and $g(\lambda)$ the probability that the resulting photon will be collected and counted by the optical system. Changes

in the plasma parameters will generally effect both the electron energy distribution function (*eedf*) and the species concentration and it is not therefore easy to interpret emission intensities directly as changes in the concentration of the species of interest; although in practic e it is very often the case that there is a strong qualitative trend between recorded intensity and concentration [Lang 1996]. To overcome this problem a technique called actinometry was invented by Coburn and Chen and first reported in their widely referenced paper of 1979 [Coburn and Chen 1979]. Actinometry is a technique which enables the extraction of additional information, which can be quantitative, from OES spectra over and above that which can be obtained from the consideration of line intensities alone. By referencing the emissions from the species of interest to the intensity from a noble or monatomic species of known or fixed concentration, called an 'actinometer', the dependence of emission intensity on the electron temperature and density can be accounted for and the absolute concentration of the ground state species under consideration can be determined. Suitable gas species are Argon, Xenon, Helium etc. which possess an excitation level with an energy threshold and cross-section similar to the transition being used to monitor the species of interest within the plasma.

According to equation (3.5), the intensity of an emission line is proportional to the species ground state density, the electron density and electron temperature. In general changes to plasma parameters e.g. power, pressure, flow etc. may result in changes to all three quantities. Therefore the emission intensity of a given spectroscopic line is not necessarily simply related to the variation of the ground state density of the species responsible for it. However, provided: (i) the actinometer concentration is insufficient to perturb the plasma, (ii) the emitting levels in both species arise from electron impact, (iii) the excitation thresholds are similar and (iv) the respective cross-sections are a similar function of electron energy then actinometry can be used. Following Coburn and Chen, if x denotes the reactive species, y the actinometer, n_i denotes concentration and ε_l excitation efficiency then assuming:

$$\varepsilon_y = k\varepsilon_x$$
$$I_x = k_x n_x \varepsilon_x$$
$$I_y = k_y n_y \varepsilon_y$$

then:

$$\frac{I_x}{I_y} = \frac{k_x n_x \varepsilon_x}{k_y n_y \varepsilon_y}, \quad \text{let } K = \frac{kk_x}{k_y}$$

hence;

$$\frac{I_x}{I_y} = K\frac{n_x}{n_y}$$

where k_x, k_y are instrumental constants, k is a constant relating ε_x to ε_y. Under these conditions there is a simple relationship between the ratio of the species to actinometer intensity and the ratio of their respective concentrations. Hence if the actinometer concentration n_y is known, then the reactive species concentration, n_x can be determined. Alternatively, provided the actinometer concentration is kept constant, as was the case in the current study, then relative changes in n_x can be tracked. For full details of the above analysis the interested reader is referred to the original paper by Coburn and Chen [1979], while for an in depth discussion of the validity of actinometry under the plasma conditions typical during MEPCVD of diamond the reader is referred to a recent detailed study by Gicquel *et al.* [1998] which includes comparisons of the technique with other methods such as CARS and TALIF and concludes that OES argon actinometry is strictly valid over a wide range of reactor conditions typically used to deposit diamond. Even under conditions where actinometry is not strictly valid, it has been noted that the technique still returns trends which are qualitatively correct [Lang 1996].

It is possible to monitor relative changes in the effective electron mean energy or temperature (T_e) of the plasma by monitoring the intensity ratio of two lines from the same species which have different excitation energy thresholds from the ground state [Lochte-Holtgreven 1968]. Typical line ratios which have been used to monitor this quantity in diamond microwave plasmas, are the H_β/H_α and Ar_{750}/Ar_{811} ratios, both of which have been used during the current work.

3.7 Laser Ultrasonic Acoustic Wave Analysis

Ultrasonic waves have been widely used for material characterisation; several methods exist including Brillouin scattering, acoustic microscopy, piezo-electric acoustic transducers systems and laser ultrasonics. The latter technique has been used during the current studies to examine the propagation of acoustic waves in free standing CVD diamond samples. Though not previously used in the CVD diamond field this method is well established in the fields of ultrasonics and non-destructive testing (NDT) and has been extensively reviewed by other authors [Scruby 1989, Davies 1992, Hess 1993 and many references therein]. The treatment here will be restricted to the general principles. A description of the actual laser set-up, which is somewhat complicated, together with details of the various acoustic modes which can propagate, appropriate theory and interpretation are given in chapter 8 together with details of the experiments undertaken.

Laser ultrasonics, in the form employed here, is a fully non-contact, non-destructive technique in which a high power, pulsed laser (pump beam) is used to generate acoustic waves at the surface of a sample, which then propagate across the surface. Detection takes place nearby and is achieved by use of a laser interferometer arrangement (probe beam) which monitors the displacement of the sample surface as the acoustic waves propagate past the detection point. The general idea is shown simplistically in figure (3.8). The high power pump beam ($\sim 10^{7}$ Wcm^{-2}) typically derived from a pulsed ($\sim 10^{-10}$-10^{-9} s) Nd-YAG laser is line focused onto the sample surface. Absorbed power leads to a very rapid local rise in temperature which generates transient thermoelastic stresses and strains in or near the surface launching a propagating acoustic pulse into the substrate.

The initial pulse can be bipolar or monopolar depending on the nature of the surface source; in the thermoelastic power regime it is typically bipolar and the amplitudes of the compression, shear and surface waves increase linearly with power density. At higher powers the plasma regime is entered in which part of the surface is ablated generating a plasma; the momentum of the expanding plasma is transmitted to the

surface enhancing the generation of surface and compression waves; the initial acoustic pulse then typically appears monopolar.

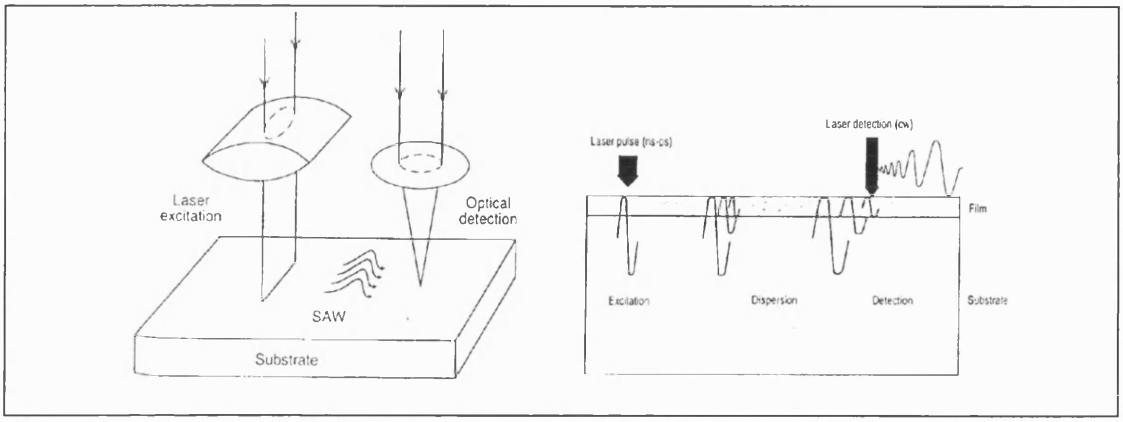

Figure (3.8): Schematic illustrating; the laser generation and detection of surface acoustic waves and the development of the initial pulse in a dispersive medium; [Reproduced from Hess 1993]

In this latter regime the method is not completely non-destructive, however the surface damage is very small. The precise details of the surface source and nature of the initial pulse are rather complicated functions of the power density and the optical and thermal properties of the substrate; these aspects have been examined in detail by Wu *et al.* [1995]. In principle, the acoustic pulse which is launched can be broad-band ~200-300 MHz; if the medium is non-dispersive then this pulse will propagate unchanged, except for a diminished amplitude, to the detection point. If the medium is dispersive then the various frequencies within the pulse travel at different velocities through the substrate and the pulse spreads out in time becoming a frequency modulated wavepacket by the time it reaches the detection point.

In the configuration shown in figure (3.8) detection is carried out by a single Michelson interferometer probe laser (typical He-Ne) arrangement which monitors the relative displacement of the surface via a suitable optical system. The probe beam is sensitive mainly to the normal component of the acoustic disturbance and can typically detect surface displacements of a few nm's depending on the details of the system. This type of detection system is also wideband, extending from DC to ~GHz frequencies, limited essentially by the speed and sensitivity of the high speed photodiodes used to monitor the interference fringes of the interferometer; a significant benefit is that, unlike piezoelectric based acoustic detectors, this system does not load the surface which

simplifies interpretation of the data. Usually the acoustic trace is captured onto a high speed storage scope (> 500 MHz) and then transferred to computer where it can be analysed using fourier transform or other methods. More detailed descriptions and diagrams of real optical arrangements can be found in the above references or in [Monchalin 1986]. Acoustic velocities can be determined from the probe and pump beam separation together with the pulse transit time. Dispersion information can be obtained by analysing the frequency spectrum of the dispersed pulse and extracting the phase function [Hutchins 1989]. The instrument used in the current studies is shown in detail in chapter 8 where it will be noticed that a dual interferometer arrangement is shown. This was a rather novel instrument which can in principle be used to determine velocity, dispersion and attenuation data simultaneously; however for reasons noted below, in this work it was primarily used in a single beam configuration which has signal-to-noise advantages when attempting to make measurements on samples with poor optical surfaces, such as the diamond films studied in this work.

The ultrasonic method just described has a number of benefits and drawbacks which have been summarised by Scruby [1989]. The benefits include: non-contact, non-destructive, remote measurement and therefore samples at high temperature or in hostile environments can be studied, broadband-generation and reception, high spatial resolution (in principle diffraction limited), also the interferometer can determine absolute surface displacement easily as the He-Ne laser wavelength acts effectively as the reference. The disadvantages are: the sensitivity of the He-Ne probe beam is much lower than a piezoelectric probe unless a very high power interferometer laser is used, the probe requires a smooth, clean and reasonably reflective surface, the systems are rather bulky, complex and expensive when compared to piezoelectric alternatives and finally the high power of the YAG laser is a serious hazard to the human eye and safety must be considered carefully.

In use there are a few experimental points to note. Typically the acquired trace is the result of 50-100 individual pump laser pulses each separated by a few milliseconds. The resulting detected pulses are averaged by the storage scope; the interpretation of a single pulse can be misleading. It is usual to collect a number of these averaged traces

for comparison. The accuracy of the absolute velocity measurements are mainly determined by the precision with which the pump-probe separation is determined. Usually the separation is ~10-20 mm and a micrometer translation stage allows this to be determined to better than ±10 μm. However for the studies carried out here, the stage at NMRC-Cork was unsuited to the diamond samples and a purpose built fixed stage was used. Consequently, separation could only be determined to ~±0.5 mm; however, as relative measurements were the main concern this was considered to be acceptable; future work would benefit from a more sophisticated approach. Generally it was very difficult to obtain sufficient acoustic amplitude to make these measurement on diamond; this was mainly attributed to poor absorption in the diamond of the frequency doubled YAG laser beam (~532nm), coupled with the extremely high thermal conductivity of the diamond when compared to more usual ceramic substrates for which the system is normally used. For these reasons the pump beam power was raised so that generation was in the plasma regime and the instrument was used in a single probe beam mode which significantly improves its sensitivity.

3.8 References.

Bachmann P.K. [1998], in *Handbook of Industrial Diamonds and Diamond Films*, eds. Prelas M.A., Popovici G. and Bigelow L.K., (Marcel Dekker Inc.), New York, USA.

Bachmann P.K. and Wiechert D.U., *Diam. and Relat. Mater.*, **1**, 422.

Bachmann P.K., Drawl W.,Knight D., Weimer R. and Messier R.F., [1988] in *Diamond and Diamond-like Materials*, MRS Symposium Proceedings, **EA-15**, 99.

Baranauskas V, Fukai M., Rodigues C.R., Parizotto N. and Trava-Airoldi V.J., [1992], *Appl. Phys. Lett.*, **60**, 1567.

Baranska H., Labudzinska A. and Terpinski J., [1987], *Laser Raman Spectroscopy: Analytical Applications*, (Ellis Horwood), West Sussex, UK.

Bashkin S and Stoner J A, [1978], *Atomic Energy-Level and Grotrian Diagrams vol II*, North Holland Publishing Company, Amsterdam.

Bernardez L.J. and M^{c}Carty K.F., [1993], *Diam. and Relat. Mater.*, **3**, 22.

Binnig G., Quate C.F. and Gerber Ch., [1986] Phys. Rev. Lett., **56,** 930.

Bou P., Vandenbulcke R., Herbin R. and Hillion F., [1992], *J. Mater. Res.*, **7**, 2151.

Brundle C.R, Evans C.A and Wilson S (eds.) [1992], *Encyclopedia of Materials Characterisation*, Butterworth-Heinemann.

Burnham N.A., Colton R.J. and Pollock H.M, [1991], *J. Vac. Sci. Tech. A.*, **9**, 2548.

Butler J.E. and Woodin R.L., [1993], *Philos. Trans. R. Soc. London*, **342**, 209.

Chan S.M., [1996], PhD. Thesis, *Electronic Device Fabrication fron Thin Film Diamond: Surface Preparation, Patterning, Metallisation and Characterisation.*, University College, University of London, UK.

Chrenko R.M., [1988], *J. Appl. Phys.*, **63**, 5873.

Coburn J.W.and Chen M., [1980], *J. Appl. Phys.*, **51**, 3134.

Conner W.T. and Sawin H.H, [1992], *Appl. Phys. Lett.*, **60**, 557.

Davies S.J., Edwards C., Taylor G.S. and Palmer S.B., [1993], *J. Phys. D: Appl. Phys.*, **26**, 329.

Dendy R., [1993], *Plasma Physics: An Introductory Course.*, Cambridge University Press, UK.

Fayette L., Marcus B., Mermoux M., Rosman N., Abello L. and Luczeau G., [1994], *J. Appl. Phys.*, **76**, 1604.

Ferreira C.M. and Moisan M., [1993], *Microwave Discharges: Fundamentals and Applications*, NATO ASI Series B: Physics Vol 302, Plenum Press, New York and London.

Field F.H. and Franklin J.L., [1957], *Electron Impact Phenomena and the Properties of Gaseous Ions.*, Academic Press Inc., New York.

Gheeraert E., Denueuville A., Bonnet A.M. and Abello L., [1992], *Diam. and Relat. Mater.*, **1**, 525.

Gicquel A. [1998], in Chapt. 11, *Handbook of Industrial Diamonds and Diamond Films*, eds. Prelas M.A., Popovici G. and Bigelow L.K., (Marcel Dekker Inc.), New York, USA.

Goodwin D.G. and Butler J.E., [1998], in Chapt. 11, *Handbook of Industrial Diamonds and Diamond Films*, eds. Prelas M.A., Popovici G. and Bigelow L.K., (Marcel Dekker Inc.), New York, USA.

Grotjohn T.A., [1998], in *Handbook of Industrial Diamonds and Diamond Films*, eds. Prelas M.A., Popovici G. and Bigelow L.K., (Marcel Dekker Inc.), New York, USA.

Hassouni K, Scott C.D. and Farhat S., [1998], in chapt.18, *Handbook of Industrial Diamonds and Diamond Films*, eds. Prelas M.A., Popovici G. and Bigelow L.K., (Marcel Dekker Inc.), New York, USA.

Herzberg G, [1950], *Spectra of Diatomic Molecules 2 edn.*, D Van Nostrand Company Inc., NY

Hess P., [1993], *Ber. Bunseges Phys. Chem.*, **97**, 1680.

Huddlestone R.H. and Leonard S.L., [1965], *Plasma Diagnostic Techniques*, Academic Press, New York.

Huong P.V., [1991], in *Analysis of Microelectronic Materials and Devices*, eds. Grasserbauer M. and Werner H.W., (John Wiley), New York, USA.

Hutchins D.A. and Lundgren K., [1989], *J. Acoust. Soc. Am.*, **85,** 1441.

Hutchinson I.H., [1987], *Principles of Plasma Diagnostics*, Cambridge University Press, USA.

Jiang X., Paul M. and Klages C.-P., [1996], *Diam. and Relat. Mter.*, **5**, 251.

Jiang X., Schiffmann K., Westphal A. and Klages C. -P., [1993a], *Appl. Phys. Lett.*, **63**, 1203.

Kamo M., Sato Y., Matsumoto S. and Setaka N., [1983], *J. Crystal Growth*, **62**, 642.

Kampas F.J., [1983], *J. Appl. Phys.*, **54**, 2276.

Kampas F.J., [1982], *J. Appl. Phys.*, **54**, 2276.

Karasawa S., Mitsuhashi M., Ohio S., Kobayashi K., Watanabe T., Hirai K., Horiguchi K. and Togashi F., [1993], *J. Cryst. Growth*, **128**, 403.

Knight D.S. and White W.B., [1985], *J. Mater. Res.*, **4**, 385.

Knight D.S. and White W.B., [1989], *J. Mater. Res.*, **4**, 385.

Kunze H.-J., [1986], in *Radiative Processes in Discharge Plasmas*, (eds. Proud J.M. and Luessen L.), NATO ASI Series B: Physics Vol. 149, Plenum Press, New York.

Lang T., Stiegler J., Kaenel Y.von and Blank E., [1996], *Diam. and Relat Mater.*, **5**, 1171.

Lochte-Holtgreven (ed), [1968], *Plasma Diagnostics*, North-Holland Publishing Company, Amsterdam.

Maguire H.G., Kamo M., Lang H.P. and Guntherodt H.-J, [1992], *Appl. Surf. Sci.*, **60/61**, 301.

Mavrodineanu R. and Boiteux H., [1965], *Flame Spectroscopy*, John Wiley & Sons, New York, London, Sidney.

M^{c}Namara K.M., Gleason K.K., Butler J. and Vestyck D.J., [1992], *Diam. and Relat. Mater.*, **19**, 1145.

Monchalin J.P., [1986], *IEEE Trans. on Ultrasonics, Ferroelectrics and Freq. Control,* **33**, 485.

Nemanich R.J., Glass J.T., Lucovsky G. and Shroder R.E., [1988], *J. Vac. Sci. Technol.*, **A6**, 1783.

Obratzsov A.N. and Pirogov V.G., [1994], *Diamond Films. Technol.*, **4**, 243.

Pearse, R.W.B and Gaydon A.G. [1976] The identification of molecular spectra 4th ed.

Prelas M.A., [1998], *Handbook of Industrial Diamonds and Diamond Films*, eds. Prelas M.A., Popovici G. and Bigelow L.K., (Marcel Dekker Inc.), New York, USA.

Proud J.M. and Luessen L., [1986], *Radiative Processes in Discharge Plasmas*, NATO ASI Series B: Physics Vol. 149, Plenum Press, New York.

Ralchenko V.G., Smoli A.A., Pereverzev V.G., Obraztsova E.D., Korotoushenko K.G., Konov V.I., Lathotkin Yu. V., and Loubnin E.N., [1985], *Diam. and Relat. Mater.*, **4**, 754.

Rutledge K.M. and Gleason K.K., [1998], in Chapt. 4, *Handbook of Industrial Diamonds and Diamond Films*, eds. Prelas M.A., Popovici G. and Bigelow L.K., (Marcel Dekker Inc.), New York, USA.

Sails S.R., Gardiner D.J., Bowden M., Savage J. and Rodway D., [1995], REF DF95

Sanchez G., Servat J., Gorostiza P., Polo M.C., Wang W.L. and Esteve J, [1996], *Diam. and Relat. Mater.*, **5**, 592.

Sattel S., Gerber J. annd Ehrhardt H., [1996], *Phys. Stat. Sol.*, **154**, 141.

Schroder D.K, [1990], *Semiconductor Material and Device Characterisation*, (John Wiley & Sons Inc.), New York, UK.

Scruby C.B., [1989], *Ultrasonics*, **27**, 195.

Shroder R.E., Nemanich R.J. and Glass J.T., [1990], *Phys. Rev. B*, **41**, 3738.

Solin S.A. and Ramdas A.K., [1970], *Phys. Rev.* **1**, 1687.

Spear K.E and Frenklach M., [1989], in *Diamond and Diamond-like Films*, The Electrochemical Society, Pennington, NJ, 122.

Stuart S.A., Prawer S. and Weiser P.S., [1993], *Diam. and Relat. Mater.*, **2**, 753.

Stuart S.A., Prawer S. and Weiser P.S., [1994], *Appl. Phys. Lett.*, **65**, 2248.

Sutcu L.F, Chu C.J., Thompson M.S., Hauge R.H., Margrave J.L. and D'Evelyn M.P., [1992a], *Appl. Phys.*, **71**, 5930.

Sutcu L.F, Chu C.J., Thompson M.S., Hauge R.H., Margrave J.L. and D'Evelyn M.P., [1992b], *Appl. Phys. Lett.*, **60**, 1685.

Wada N. and Solin S.A., [1981], *Physica B*, **105**, 352.

Williams D.H. and Flemming I., [1980], *Spectroscopic Methods in Organic Chemistry* 3rd ed., M^{c}Graw-Hill Book Company, UK.

Wright R.B, Varma R. and Gruen D.M., [1976], *J.Nuc. Mater.*, **63**, 415.

Wu L., Cheng Jian-chun and Zhang Shu-yi, [1995], *J. Phys. D: Appl. Phys.*, **28**, 957.

Yoshikawa M., Katagiri G, Ishida H., Ishitani A. and Akamatsu T., [1988], *Solid State Comms.*, **66**, 1177.

Zhu W, Kong H.S and Glass J.T, [1993]. in *Diamond Films and Coatings*, ed. R.F Davis., (Noyes Publications), New Jersey, USA.

Zhu W., Stoner B.R., Williams B.E. and Glass J.T, [1991], *Proc. IEEE,* **79**, 621.

Chapter 4

The Nucleation and Growth of Diamond on Tungsten

Bias enhanced nucleation (BEN) is the most promising recent development for the production of high quality CVD diamond films. Although the technique has been studied intensely most of the attention has concentrated on silicon substrates. However, alternative substrates are worthy of study as they may be beneficial in their own right and could lead towards a more general understanding of the BEN technique, which remains difficult to control and poorly understood. This chapter presents the results of a phenomenological study of the nucleation and growth of thin film diamond on tungsten substrates by microwave plasma enhanced chemical vapour deposition (MPECVD). Single crystal and polycrystalline forms of pure tungsten were used to examine the effect of reactor parameters on the nucleation and growth of the diamond film; particular attention was given to the effects of substrate biasing during the nucleation phase.

4.1 Introduction.

At the time of writing much of the work which has been undertaken by the CVD diamond community has concentrated on nucleation and growth issues of diamond on silicon. The reasons for this are understandable; silicon is both reasonably cheap and easily available in a convenient, pure single crystal form. Silicon is one of the most fully understood and well characterised materials available in bulk and diamond nucleates and grows well on it. Furthermore, the range of applications which would become available, if electronic grade CVD diamond can be grown on silicon, is a powerful incentive to pursue this line of research. However, silicon is not the only material of interest there are a number of other materials which can benefit from CVD diamond coatings. An important example is the refractory metal tungsten, which is widely used in cutting tools, filaments, bearings and other mechanical components. Many of these applications could benefit from the properties of a CVD diamond thin film coating [Lunn 1998, Shi 1995]. Refractory metals such as tungsten can usefully provide an interlayer allowing the deposition of diamond coatings on ordinary steel tools; which are very common and otherwise exhibit very poor coating characteristics [Qui Hua Fan 1997]. Tungsten may also be a useful candidate for the growth of free standing diamond films, for e.g. optical window applications, as it is reasonably easy to release thick films from the substrate following growth. This often not true of silicon which is usually back-etched to produce a free standing diamond film, a process with both environmental and cost consequences [Rodway 1994]. Considerable promise has also been shown for new types of composite materials based on fine tungsten fibres re-enforced with a diamond coatings [Nicholson 1997].

To this authors knowledge relatively few in depth studies have been carried out on substrates, other than silicon, which have examined both nucleation and the growth of high quality films. Typically, alternative substrates to silicon, such as tungsten, have been included as one of many, in single issue studies, in which workers have sought to improve the understanding of growth and nucleation mechanisms by comparison to the results for silicon - the most extensively studied substrate. Historically, substrates have been divided in the literature, into two groups [Wolter 1994]; those which form carbides and those which do not. Tungsten is one of the refractory metals, all of which are carbide forming

materials. Important early work was undertaken by Joffreau *et al.* [1988] who studied carbide formation during the growth of diamond on a number of the refractory metals, including tungsten. They identified common stages which appear to occur during growth on all carbide forming substrates which can be summarised as:

(i) Carbide/sub-carbide formation.
(ii) Diamond nucleation on the carbide.
(iii) Diamond crystal growth.

Step (i) is responsible for the well known 'incubation time' which occurs prior to diamond nucleation and varies for different substrate materials [Liu 1995, Joffreau 1988]. The authors show that the length of incubation is determined by the time for the formation of a critical carbon concentration at the surface, which is in turn controlled by a balance of carbon diffusion rates between at least three competing processes occurring at the nucleation surface: the diffusion rate of carbon in the metal, the diffusion rate of carbon from the gas phase and diffusion away from diamond nuclei forming on the surface. Carbide formation on tungsten was observed to be slow (approximately 2 μm in 24 hours) and subsequent nucleation densities were low, (approximately 1.2×10^4 cm^{-2}) with the nuclei showing no evidence of well defined habits. The short incubation time was attributed to a low carbon diffusion rate for tungsten, resulting in rapid formation of the critical carbon concentration at the surface and subsequent nucleation.

The importance of carbide formation during biasing has been demonstrated by Wolter *et al.* [1994]. They studied the effects of BEN on copper, which does not form a carbide but is a better lattice match to diamond than is silicon, and found only a very small enhancement of the nucleation density compared to silicon which exhibited an enhancement factor of around six orders. In a later paper [Wolter 1995b] they compared bias-enhanced nucleation on a range of carbide forming metals with BEN on silicon, noting that silicon forms a rather thin carbide layer, of ~100 nm, contrasting with the usually much thicker (several microns) layer formed on refractory metals. Tungsten however, is an exception as noted by Zhu *et al.* [Zhu1995] in that it only forms a rather thin carbide layer, of some 200-400 nm, closer to that of silicon. These authors measured the total residual stress of diamond films grown on carbide forming materials and found a correlation between stress and adhesion.

They speculated that the carbide layer may improve adhesion by allowing some relaxation between film and substrate; and then the rather thinner carbide layer, which forms on tungsten, could explain the relatively poor adhesion of films grown on this material compared to the other refractory metals. On the other hand silicon can exhibit reasonably good adhesion between substrate and film despite only a thin carbide layer .

The rather thin carbide layer which forms on tungsten is reflected in the relatively short incubation time which occurs prior to nucleation on this substrate compared with the other refractory metals [Wolter 1995a]. The same study shows that the incubation time is clearly related to the carbon diffusivity in the substrate which is low for tungsten, substrates with higher carbon diffusivities showed longer incubation times. In addition there is a strong correlation with the energy of formation of the carbide (ΔH_f) and the subsequent nucleation density achieved on the substrate, those substrates with the highest carbon affinity gave the highest nucleation densities for a given bias period. Unfortunately, once again silicon does not fit the trends of these data well, which the authors take as indicating that the crystal structure of the substrate may also play a role in the nucleation phase. This observation lends emphasis to the need for detailed studies of alternative substrates to silicon.

The general characteristics of a diamond film on a given substrate are determined by a combination of factors, most important among which are: film quality in terms of the sp^2 to sp^3 ratio, the dominant film morphology either (100), (111), (110) or a mixture of these (random polycrystalline) and the mean crystal size, particularly at the surface. Microscopic and macroscopic film stress are also important; macroscopic stress will can influence film integrity and its propensity to delaminate from the substrate, while microscopic stress within individual grains can influence electronic and optical properties. Of considerable importance, particularly in economic terms, are the nucleation times and growth rates which can be achieved on a particular substrate. These parameters can all influence the characteristics of a diamond film and different applications typically favour a different balance among these variables. For example, optical windows require high strength, optically clear material, typically satisfied by fine grained high quality (low sp^2 and low impurity levels) diamond films [Savage 1997, Ravi 1994]. Electronic applications however, require large grained, high quality material to maximise electronic transport characteristics and often benefit from (100) textured and oriented films [Dreifus 1998,

Chan 1996]. Wear resistant coatings can usually be accommodated by lower quality (higher sp^2), nano-crystalline forms of the material which do not need to be optically clear.

For a particular substrate it is obviously important to have a clear understanding of the influence of the various reactor parameters on both the nucleation and growth stages, particularly when attempting to optimise films for different applications. To date a systematic study of diamond nucleation and growth on pure forms of both single and polycrystalline tungsten has not been reported in the literature. Information on this substrate has typically been restricted to a brief mention in studies of the nucleation of diamond on carbide forming materials in which workers have mainly been interested in examining the role of carbide formation rather than assembling a coherent study of tungsten as a special case. The main aims of the study reported in this chapter were; to address this gap in the literature, demonstrate growth of high quality films on this substrate, examine nucleation and study the details of the bias process for this substrate by making use of both single crystal and polycrystalline forms of the material. Previous work has been restricted to the polycrystalline form. A key aim was to determine (100) texturing conditions and examine the possibility of obtaining highly oriented and textured films similar to those which have been shown possible for the silicon substrate. Much of the motivation for a detailed study of tungsten as a substrate material was provided by the requirements of the Defence Evaluation and Research Agency (DERA) at Malvern in the UK. DERA have supported this work through a CASE award and provided access to the facilities at Malvern where the work reported in this chapter was carried out by the author.

4.2 Experimental Details.

A range of experiments were undertaken to study the nature of nucleation and growth of microwave CVD diamond on tungsten substrates using a conventional H_2-CH_4 gas chemistry. All experiments were carried out in a standard ASTEX 1.5 kW CVD microwave reactor (located at DERA-Malvern) modified to allow independent substrate biasing; a more complete description of the system and gases used has been given in chapter 3. During the studies a small quantity of argon was added to facilitate OES measurements which are described elsewhere (chapters 5 & 6). Raman and SEM analyses were used to

characterise the effect on the nature and quality of the films resulting from systematic variation of reactor growth parameters. Experiments were carried out on both polycrystalline and single crystal forms of tungsten. Polycrystalline substrates consisted of ~50mm diameter discs with a thickness of ~6.3mm. Single crystal samples consisted of small cylinders of (100) oriented tungsten, thickness 6.3mm, cut and finished to a tolerance of ±0.5° . Typically; the polycrystalline substrates were polished to a mirror finish with 3 μm diamond grit. For the single crystal studies cylindrical holes were drilled slightly off-centre by a spark erosion method in some of the polycrystalline discs. The single crystals samples were then placed in the drilled poly-discs and held in place by small tungsten foil 'springs'. The aim was to try to minimise any changes in the plasma environment which might arise from the large difference in diameter between the polycrystalline and single crystal samples reducing any variations which might arise from growing the two films in separate reactor runs. The two sample arrangements used are shown in figure (4.1).

Prior to growth, all samples were cleaned using a standard method involving ultrasonic degrease in solvents, (5 minutes ultrasonic agitation in each of; inhibisol → acetone → de-ionised water, finished by drying in flowing N_2). This procedure was followed by a 30 minute hydrogen plasma etch carried out *in-situ* in the CVD reactor (~3% Ar/H_2, ~412 sccm flow, T_s~600°C -thermocouple indication, pressure ~15T, power ~800W). This type of cleaning regime is typical of procedures used by other workers in the field [e.g. Wolter 1994], and it is designed to ensure removal of surface contaminants and any surface oxidation which may have formed on the sample prior to loading into the reactor.

During these experiments several of the reactor parameters known to most influence the growth of diamond films on silicon were examined e.g. substrate temperature, gas composition and nucleation conditions. Prior to carrying out the main experiments some simple 'commissioning' reactors runs were made to determine a set of 'standard conditions' which could be relied on to yield reasonable quality, random polycrystalline diamond films on the polycrystalline tungsten substrates.

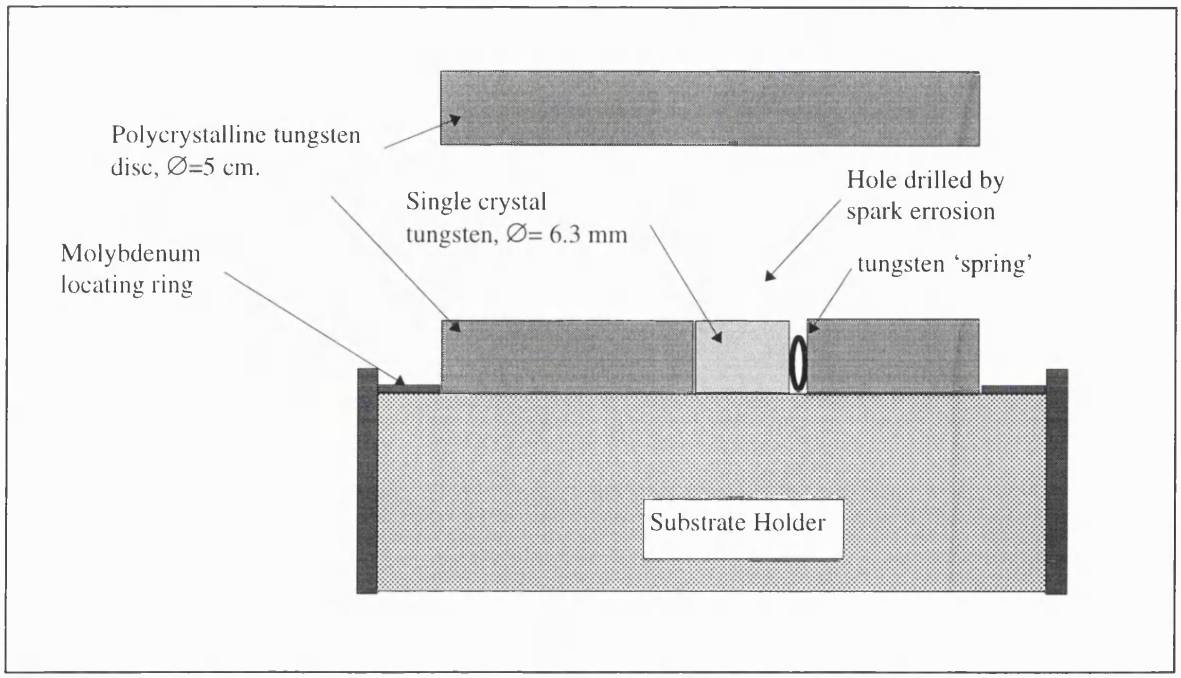

Figure (4.1): Showing the two arrangements used during this work for studies on polycrystalline and single crystal tungsten substrates; and location on substrate holder.

These 'standard conditions' were used as a reference and are given in table (4.1). In the following text, unless otherwise stated, changes in film characteristics arising from the variation of one of the standard parameters are referenced to the film grown using the full set of 'standard conditions'.

Microwave power	800 Watts
Substrate temperature	600 °C (t/c indication)
Hydrogen flow	392 sccm (typical)
Argon flow	11 sccm (typical)
Methane flow	8 sccm (typical)
Pressure	30 Torr (typical)

Table (4.1): Standard reactor conditions used to grow the reference films.

Substrate current and voltage were monitored during BEN experiments and at all other times the substrate platen was grounded. During the electrical studies of biasing on tungsten, which are described later in section (4.3.3), some measurements were made for the purposes of comparison with BEN on silicon. In all cases 76 mm diameter standard p-type, C-Z grown silicon wafers were used. The wafers were used as finished by the manufacturer, i.e. 'mirror finish' quoted as [100] oriented ±0.5°, thickness 525±15 μm

with a resistivity of 12-20 Ω-cm. The silicon wafers were subjected to the same cleaning procedure used for tungsten samples, including a 30 minute H-plasma etch. To accommodate the larger diameter of the silicon wafers a molybdenum locating ring was removed from the substrate holder and replaced with a 76 mm diameter molybdenum disc on which the silicon was placed. The disc thickness was chosen so that the silicon surface was at the same height in the reactor as the thicker 6.3 mm tungsten samples.

Optical microscopy, SEM and Raman techniques were typically used to study the substrates following nucleation and/or growth. The SEM and Raman methods have been discussed in chapter 3. Unless otherwise stated, the substrate temperatures quoted in this work are the temperatures as monitored by the *in-situ* thermocouple (t/c), located in the holder beneath the substrate. To establish the true temperature, the substrate surface was monitored using an optical pyrometer (Minolta Cyclops-241), with and without the plasma running under the standard conditions listed in table (4.1), assuming an emissivity (ε_t) for tungsten of 0.3. With the plasma running, the pyrometer-determined substrate temperature was ~70-100 °C higher than the equivalent thermocouple measurement; while without the plasma, but with the normal gas flows maintained, the pyrometer temperature was ~25 °C lower than the thermocouple temperature. Differences between the pyrometer and thermocouple values were approximately constant over the range 600-800°C. These values are in close agreement with previous pyrometer measurements carried out during earlier growth studies at the DERA in this reactor under similar conditions [Rodway 1994]. Optical pyrometer measurements were rather difficult due to the restricted view of the substrate and unless otherwise noted the nominal substrate temperature determined by the thermocouple is reported in these studies; the different measures are noted as (t/c) or (pyro) where necessary.

4.3 Experimental Results.

The experimental results of the study are presented here in three sections. The first deals mainly with effects of reactor variables on the growth and characteristics of the films. The second presents the results of the nucleation studies which were carried out on both polycrystalline and single crystal substrates and include a study of the effect of biasing.

The final section presents the results of the electrical measurements which were made during biased nucleation and includes some comparative studies which were made on silicon.

4.3.1 Diamond Growth on Tungsten.

A number of growth experiments were carried out on identically prepared polycrystalline substrates to examine the nature of the CVD diamond film as a function of growth parameters. The effect on the film of methane fraction, substrate temperature and growth time were studied as well as the variation of the film with position across the substrate. For these experiments no BEN stage was included. Figure (4.2) shows an SEM overview of the structure of a typical film grown for 20 hours under the standard conditions given in table (4.1). The nucleation or substrate side, cross-section and growth face of the film are shown as (a),(b) and (c) respectively in the figure. The Raman spectrum obtained from the as grown surface is shown in (d). The film consists of a randomly oriented mixture of well developed (111), (100) and (110) grains which have grown in a columnar manner, clearly visible in (4.1b), from uniformly distributed, almost spherical nucleation sites (4.1a), which although initially well separated have then grown together. A closer SEM examination, not shown here but see figure (4.8b), indicates that the nuclei are 'cauliflower-like' with no visible sign of facetting. The imprints of scratches left on the substrate by the polishing process are clearly visible as lines in figure (4.1a).

The film is approximately 5 μm thick, as estimated from the cross-section, yielding a mean growth rate of ~ 0.25 μm/hour. A close examination of the cross-section, (4.1b), reveals that the grains of the film possess a coarse, granular nature which can also be seen in the SEM of the growth surface, figure (4.1c).

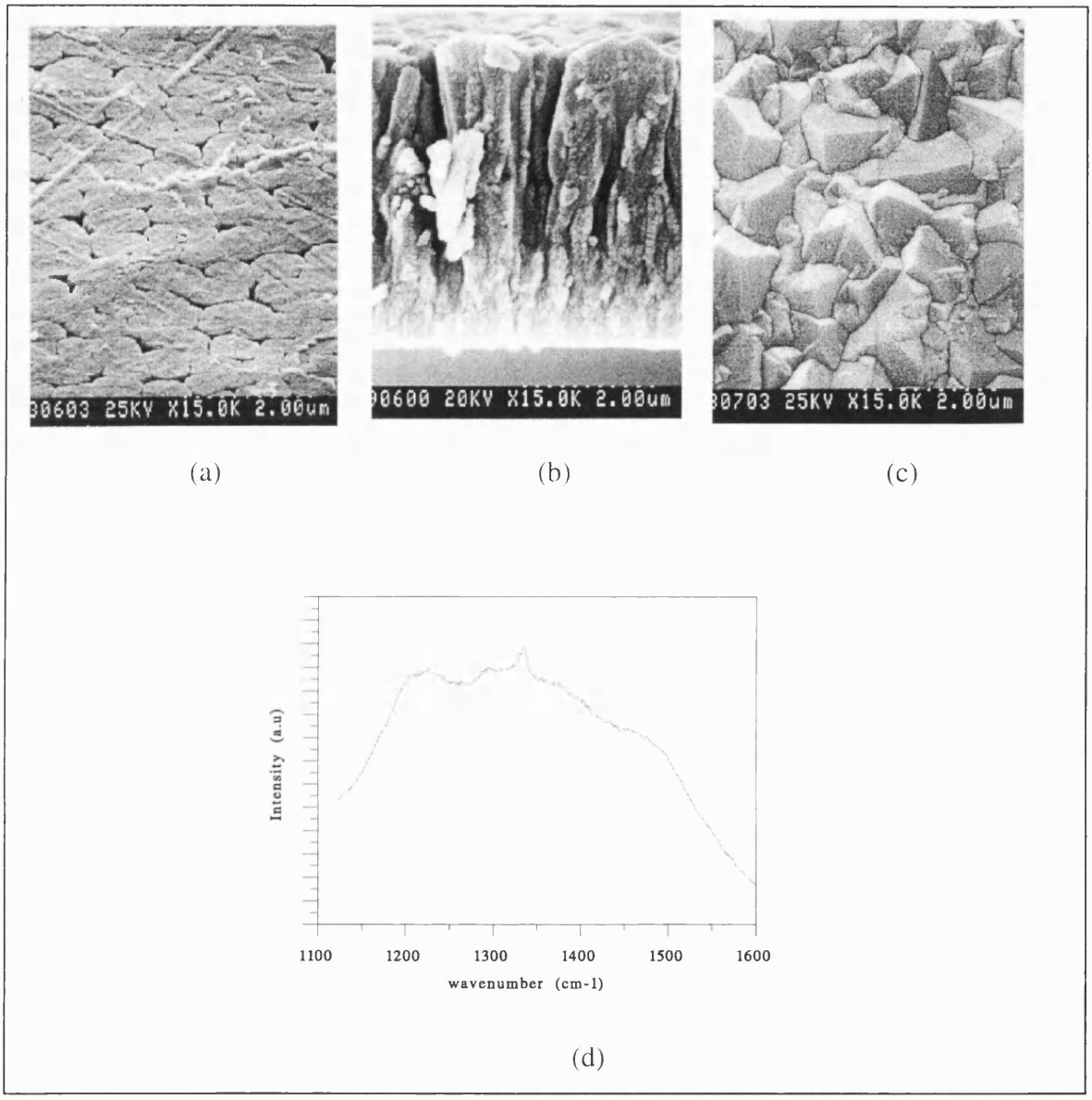

Figure (4.2): The structure of a typical film nucleated and grown for 20 hours on polycrystalline tungsten under the standard conditions described in table (4.1); (a) nucleation face (b) cross-section, (c) growth face and (d) associated Raman spectrum.

The Raman shows the characteristic diamond peak which is analysis shows is shifted up from its customary position at 1332 cm^{-1} to 1334 cm^{-1}. Upward shifts in the Raman peak may indicate that the film is under significant thermal compressive stress, due to mismatch in the thermal coefficients of diamond and tungsten, which develops as the film cools from the growth temperature of ~600 °C to room temperature prior to removal from the reactor. Ralchenko *et al.* [1995] observed shifts to higher wavenumbers for the Raman peak of diamond films grown on tungsten carbide. They associated the shift with thermal compressive stress and gave a simple expression allowing the approximate stress to be estimated from the magnitude of the shift. Using their expression, a value of ~1.1 GPa can

be estimated for the film shown in figure(4.2) from the 2 cm^{-1} shift seen in the Raman peak position. The *theoretical thermal stress* (σ_t) is given by:

$$\sigma_t = \frac{E}{1-\nu}\int_{20}^{T}(\alpha_f - \alpha_s)dT \qquad (4.1)$$

Where E =1143 GPa and ν =0.07 are the Young's modulus and Poisson's ratio for diamond averaged over different crystallite orientations and α_f and α_s are the temperature dependent thermal coefficients of the film and substrate respectively. Assuming constant room temperature values of 0.8×10^{-6} K^{-1} and 4.5×10^{-6} K^{-1} for diamond and tungsten thermal coefficients respectively [Ralchenko 1995]; an approximate value of σ_t= -2.6 GPa can be obtained from equation (4.1) for the deposition temperature of 600°C used here. The presence of sp^2 carbon within the film together with the compliance of the interface layers (carbide and α-carbon) would allow the film to relax to some degree, so the measured stress in the film would be expected to be lower than the predicted value. Zhu *et al.* [1995] reported compressive stress values of ~2 GPa for diamond films deposited at ~900°C on tungsten foils during a study to examine film adhesion for a range of substrate conditions. They noted that stress of this magnitude combined with a thin compliance layer can lead to poor film adhesion. It was observed, during the current studies, that fine cracks rapidly spread across the film from an indentation point made with a sharp implement. Within a few seconds the film would then delaminate into small pieces which 'curled up' growth side inward; this is indicative of considerable compressive stress and qualitatively confirms the analysis determined from the shift of the 1332 cm^{-1} Raman peak shown in figure (4.2d).

The full width at half maximum (FWHM) is about 8 cm^{-1} and is indicative of good quality diamond considering that at this point the layer is rather thin. Additionally, broad features can be distinguished in the Raman spectra at around; 1200-1240 cm^{-1}, 1340-1360 cm^{-1} and 1440-1500 cm^{-1}. These features have previously been associated by other authors with amorphous diamond-carbon, disordered microcrystalline graphite and amorphous carbon rich SiC material respectively, for diamond films grown on silicon [Yoshikawa 1988, Knight 1989a,b & Nemanich 1988]. As in this case there was no silicon present, the latter

feature at 1440-1500 cm^{-1} might be associated instead with a similar carbon rich tungsten carbide phase.

The effect on the film of varying the methane fraction in the range 0.5-6.0 % is shown in figure (4.3a-e); other parameters were kept constant at the standard values. A strong effect on the film morphology is evident; moving from heavily twinned mixture of (110),(100) and (111) facets at 0.5% CH_4 , to mainly pyramidal (111) facets at 2%. As the CH_4 fraction is increased to 3% (100) facets clearly begin to emerge and these are dominant at a methane fraction of 4%. Any further increase in the methane fraction beyond this point begins to degrade the film morphology and by 6% CH_4 any visible crystallinity is lost and the film appears to be a featureless, fine grained material. It is interesting to note the difference in the texture of the material which comprises the crystallites, when comparing the films grown at 0.5 % and 2 % CH_4. At high SEM magnifications (not shown) the 2% crystallites appear to be made of clusters of very small particles whereas the 0.5% film crystallites appear smooth at the same magnification. The growth rate of the 2% film is about a factor of two higher than the 0.5% film and the Raman spectra for these films, which are shown in figure (4.4), indicate that the 0.5% film may contain significantly less graphitic material than the films grown at the higher methane fractions.

The Raman spectra obtained from the as grown films at different methane fractions in the plasma are shown in figure (4.4a-e). The spectra are shown with an arbitrary count scale, however the relative intensities of the spectra are correct i.e. the vertical displacement of the spectra reflects a true difference in count rate and are not just an arbitrary displacement made for viewing convenience. The 1332 cm^{-1} diamond peak is clearly visible at the lower methane fractions reducing in size with increasing CH_4 percentage. A closer examination shows that the peak is shifted to higher wavenumbers with increasing methane fraction. The size of the peak shifts, estimated using Renishaw Raman analysis software, were approximately 2 cm^{-1} at 0.5% increasing to 7cm^{-1} at 6% CH_4. The shift was reasonably linear with increasing CH_4% as shown in the plot given in figure(4.5). On thin diamond films Raman is effectively a bulk probe; therefore the increase in count rate with methane fraction suggests that the films grown at higher fraction are thicker than the films grown at lower fractions and may as a result experience higher thermal stress.

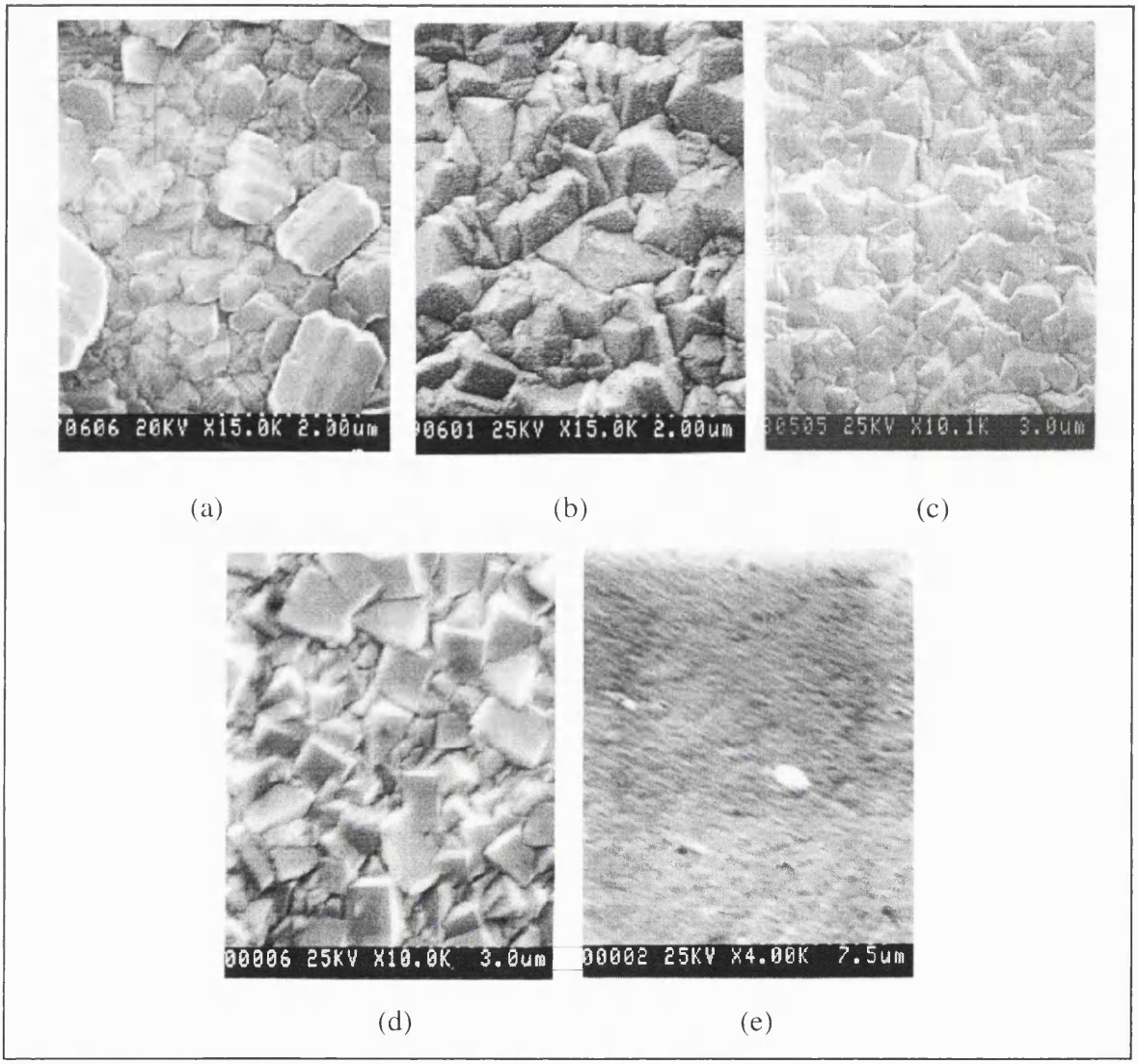

Figure (4.3): The effect on film morphology of varying methane fraction in the growth plasma; (a) 0.5%, (b) 2%, (c) 3%, (d) 4% and (e) 6% methane fractions respectively.

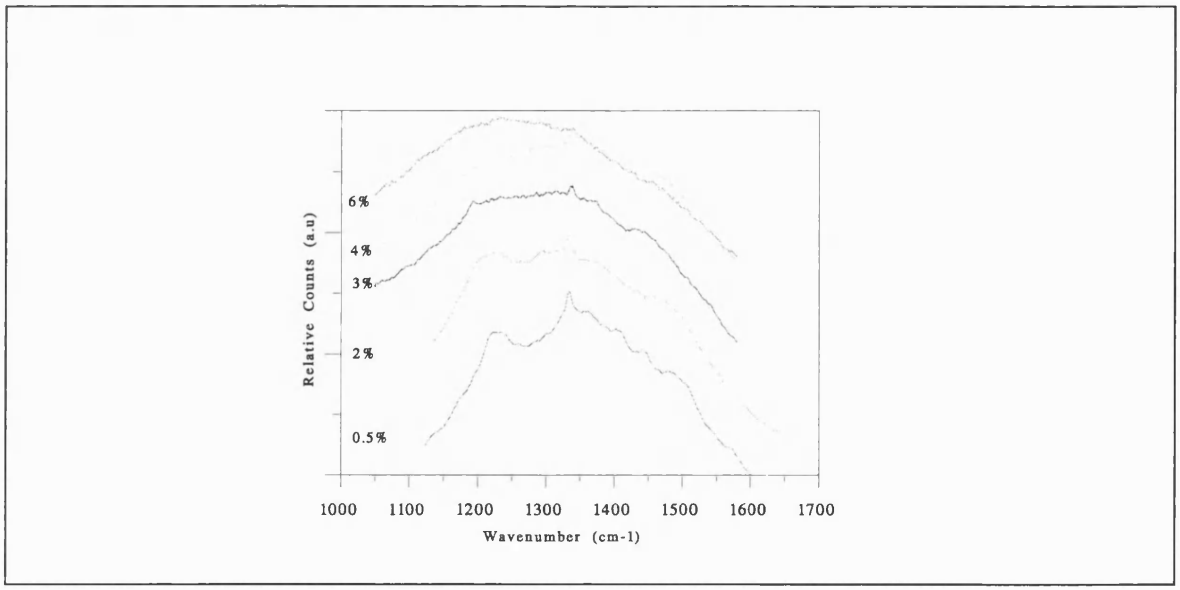

Figure (4.4): Raman spectra for films grown at varying methane fractions of: 0.5%, 2%, 3%, 4% and 6%; other growth parameters were kept constant.

A direct measurements of film thickness for the 0.5% and 2% films yielded values of 2.8 and 4.8 microns respectively; this confirms that an increase in the methane fraction can lead to thicker films; supporting the interpretation that the higher Raman intensity represented increased film thickness for these *thin* films. Unfortunately, only two films were available for direct measurement of thickness and while the ratio of the percentage change between the two thickness' to the change in methane fraction is similar to the gradient of the plot in figure(4.5) more data points are needed to establish any relationship unambiguously.

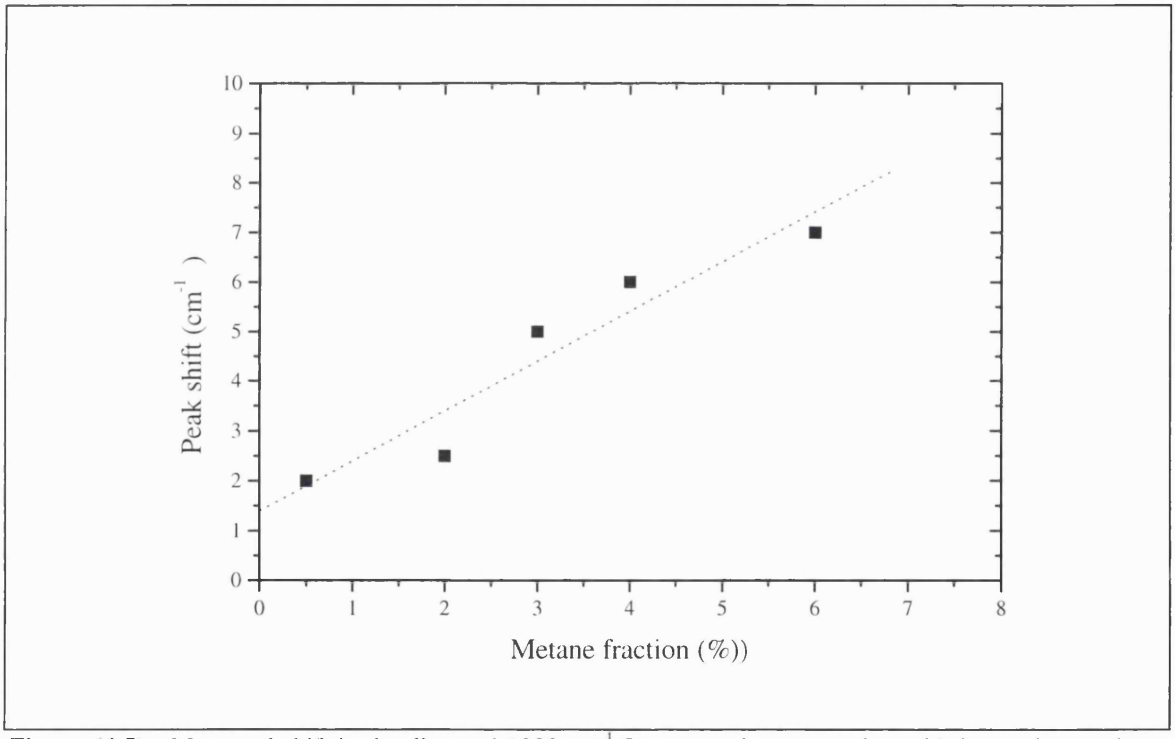

Figure (4.5): Measured shift in the diamond 1332 cm^{-1} Raman peak wavenumber with increasing methane fraction in the growth plasma.

Finally, from the Raman spectra shown in figure(4.4) it can be seen that the feature at 1230 cm^{-1} increases in importance as the CH_4 fraction increases; at the same time the average background broadens and shifts towards lower wavenumbers. This may be indicative of an increasing proportion of amorphous diamond and/or a disordered diamond pre-cursor present within the film as the methane fraction increases in the plasma [Knight 1989a,b]. Also it can be seen that the background to the right of the diamond peak increases with CH_4 percentage and this could be explained in terms of an increasing proportion of diamond-like carbons (DLC) within the film [Knight 1989a, Yoshikawa

1988]; it is well known from work on silicon that high methane fractions during growth can result in higher incorporation of graphitic and DLC material into the diamond film. The DLC band is formed from several overlapping components which can be seen reasonably clearly in the spectrum for 0.5% CH_4, which shows three distinct bumps in the spectrum between 1400 cm^{-1} and 1500 cm^{-1}. It has been shown [Knight 1989a] that these bands tend to broaden with increasing disorder in the deposited material, indicated here by the loss of the individual features as the methane fraction increases and the development of a much broader structure in the 6% case.

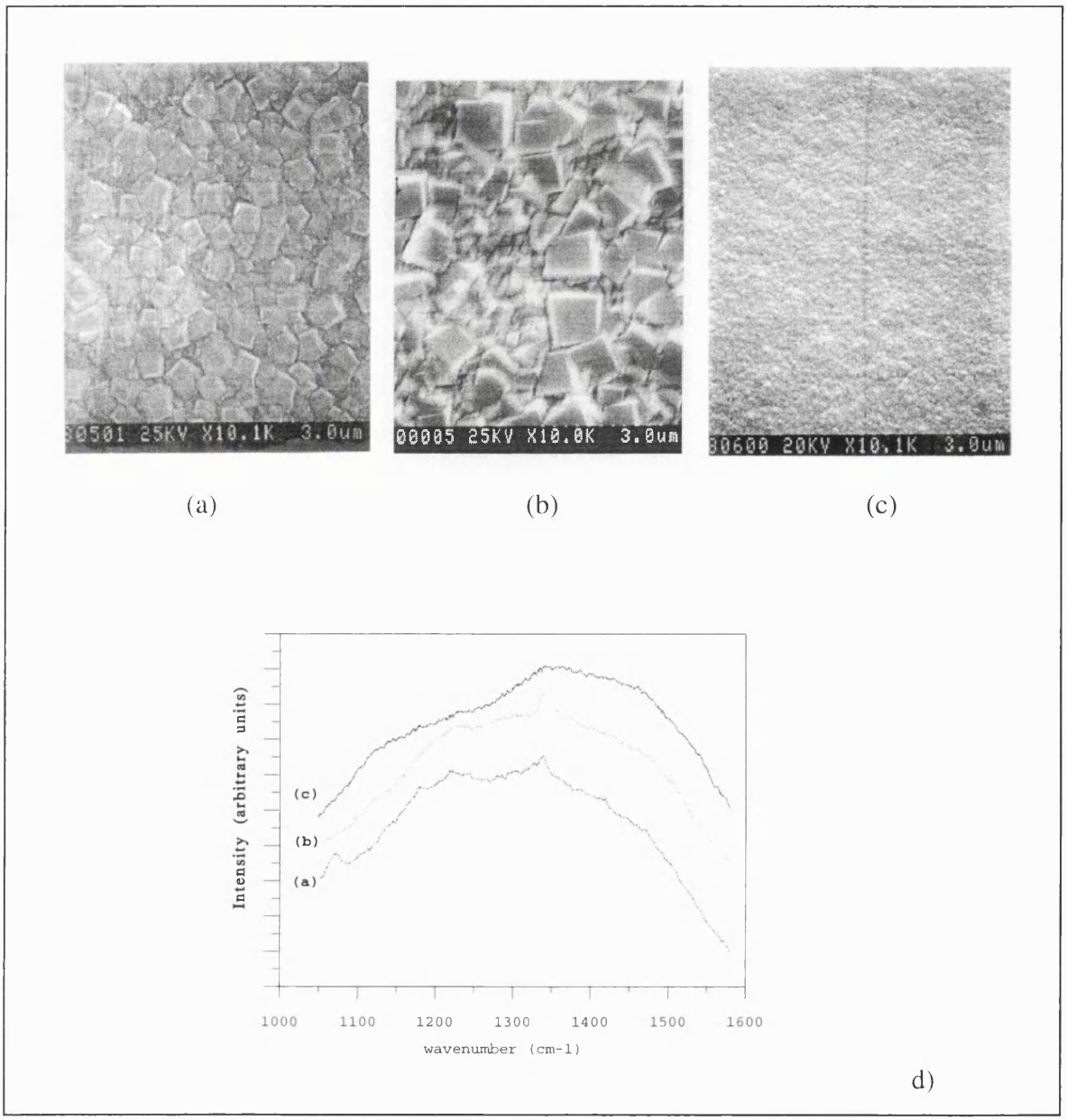

Figure (4.6): The effect of varying substrate temperature on the growth of diamond on tungsten; (a) 560°C, (b) 600°C, (c) 680°C and (d) associated Raman spectra (5 point smoothed.)

Many studies on silicon have shown that film texture and growth rates are sensitive to substrate temperature as well as methane fraction. To examine the influence of temperature the 'standard conditions' shown in table (4.1) were altered to include a methane fraction of 4% which promotes (100) texturing on the tungsten substrate as was shown by the earlier experimental results. The other 'standard parameters' in table (4.1) were left unchanged. The results of film growth on polycrystalline samples are shown in figure (4.6a-c) for substrate temperatures from 560-680 °C, together with the results of the Raman analysis shown in figure(4.6d). In each case the films were grown out for approximately 18 hours to stabilise the film texture prior to removal from the reactor.

The temperatures shown are as recorded by the thermocouple; the pyrometer measurements described earlier have indicated that the true surface temperature with the plasma in place is ~100°C higher. It is clear that the growth temperature has a marked effect on films grown under these conditions on tungsten. The morphology at 600 °C, which is mainly (100), retains this texturing for a drop in temperature of 40 °C to 560 °C, however there is about a factor of two reduction in the crystal size. This is may due to reduced film thickness arising from slower growth rates at the lower temperature [Chu 1992]. Increasing the temperature by only 80 °C to 680°C causes a complete loss of crystalline morphology giving a dark featureless film which has no clear diamond Raman signal at 1332 cm^{-1}. The Raman spectra show a small shift of ~2 cm^{-1} in the 1332 cm^{-1} peak to higher wave-number with *increasing* temperature, probably due to increased thermal compressive stress arising from the higher deposition temperature, together with a component from increased film thickness due to higher growth rate expected at higher substrate temperatures. More detailed analyses show slight broadening of the 1332cm^{-1} diamond line at temperatures above and below 600 °C coupled with the development of two opposite trends: (i) diminishing significance of the broad feature at around 1220 cm^{-1} with increasing temperature, together with (ii) a small increase in the broad shoulder above 1332 cm^{-1}, centred around 1450 cm^{-1}. The decreasing 1220 cm^{-1} feature may be indicative of a decrease in the fraction of amorphous or disordered diamond within the film, while the increasing broad background feature, centred around 1450 cm^{-1}, could indicate that the DLC component is increasing.

Total growth time and position across the substrate with respect to the plasma centre can both influence the characteristics of the deposited film. Figure (4.7) shows the effect of growth time and position across the substrate for a film grown out under (100) texturing conditions. SEM's (a) and (b) in the figure show the same film after 18 and 112 hours growth taken at *approximately the same position about half way from the centre of the sample towards the edge.* The film thickness was around 4 and 25 microns respectively, estimated from SEM cross-sections, giving a mean growth rate of ~0.22 μm/hour in both cases. A considerable improvement in texture together with increase in crystal size by a factor of ~2 is evident for the film at 112 hours as compared to the same film at only 18 hours. The third SEM, figure (4.7c), was taken close to the centre of the sample where the plasma is most intense and when compared to figure(4.7b) provides an indication of the effect of position on the as grown film. The growth rate is highest at the centre resulting in the best (100) texturing; it can clearly be seen that individual crystals have coalesced, (4.7c), as compared to the case in (4.7b) and the size of individual grains has increased considerably. The amount and spread of tilting of the (100) facets with respect to the substrate plane was reasonably small (< 10-15°) as judged qualitatively from SEM's (not shown) taken at 45° angle to the substrate normal.

A Raman scan taken from a free standing piece of this film from close to the centre of the sample is shown in figure (4.7d). This Raman signature is typical of diamond films generally considered to be of reasonably high quality; the reader is reminded that that all the Raman analyses were carried out using a 632nm excitation source which emphasises the sp^2 components with respect to sp^3 material. The Raman shows a clear, sharp diamond peak at 1332 cm^{-1}, showing no detectable shift and a fwhm of ~3.3 cm^{-1}; this compares quite well to natural diamond fwhm~2 cm^{-1} [Rutledge 1998] and also to examples of similarly thick, CVD grown (100) textured films grown on silicon which have been reported in the literature e.g. 4 cm^{-1} for ~30 μm (100) film [Haq 1994]. The absence of any significant shift in the 1332cm^{-1} peak indicates that once the film has been removed from the substrate (as in this case) it is substantially free from the macroscopic stresses arising from the mismatch in the thermal expansion coefficients of the deposited film and the underlying tungsten substrate; any remaining shift in wavenumber is probably due to intrinsic film stress [Knight 1989a].

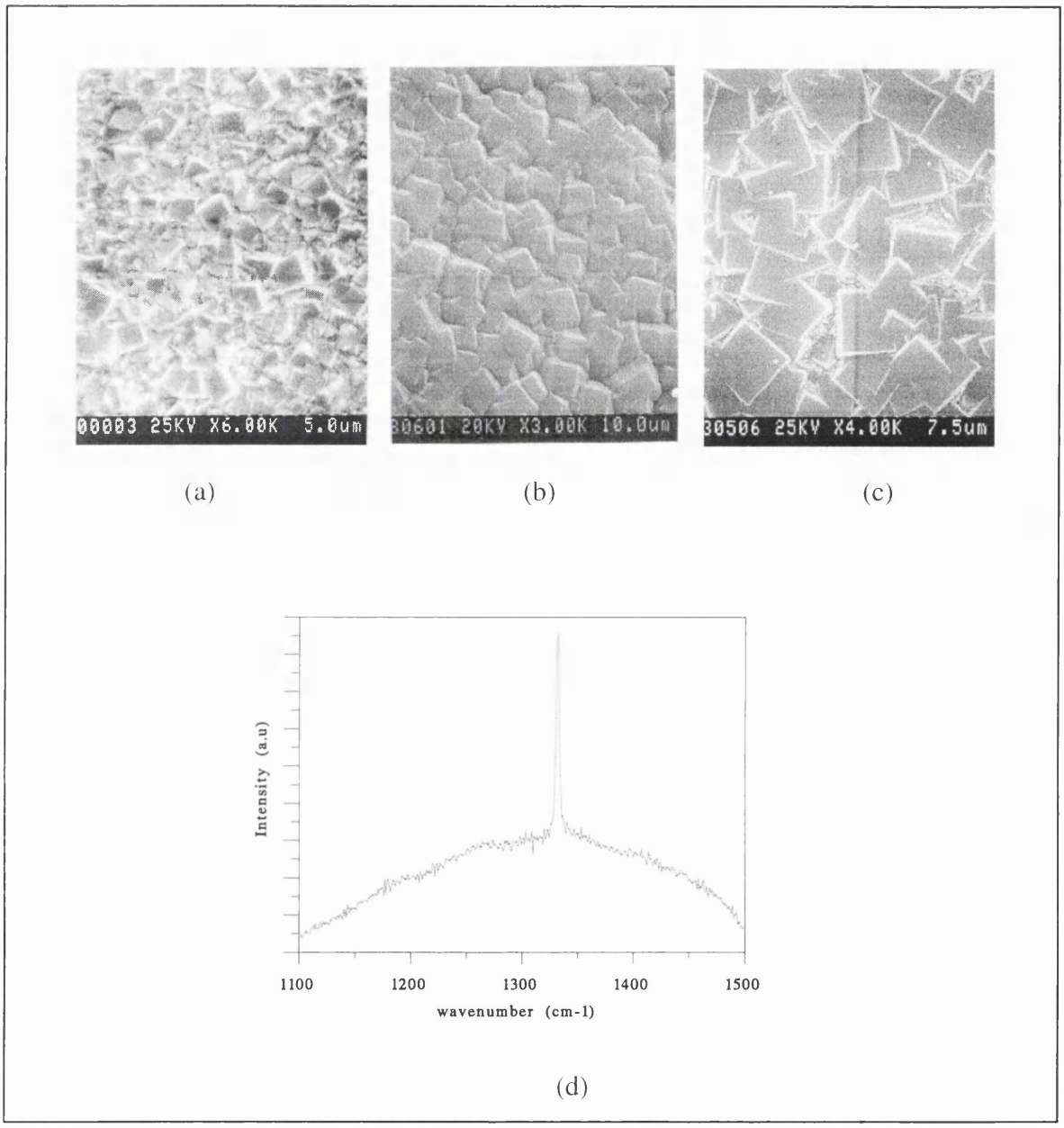

Figure (4.7): The influence of growth time and position across the substrate on film morphology; for a position approximately half way from centre (a) after 18 hours and (b) after 112 hours, (c) after 112 hour at the centre of the substrate, and (d) Raman associated with the film at substrate centre.

4.3.2 Nucleation of Diamond On Tungsten Substrates.

The nucleation phase of diamond growth is an important stage which as was discussed in the introduction can influence factors such as film morphology, crystallite density, orientation and to an extent film quality particularly for very thin films. The details of the nucleation method used e.g. scratching, can strongly influence the quality and integrity of the film-substrate interface. Biased nucleation offers the advantages of a mechanism which

is entirely *in-situ*, low in damage and amenable to automatic control while at the same time allowing a wide range of nucleation conditions to be realised. For example, on silicon, biasing allows control of the nucleation density over at least five orders of magnitude and under certain conditions can promote a degree of orientation between nuclei on this substrate [Yugo 1991, Schreck 1996]. To explore the nucleation phase of diamond film growth on tungsten a range of experiments were carried out on both single and polycrystalline forms of the pure material. The effects of applying a substrate bias on nucleation density were also characterised and these results were then combined with the growth experiments described in the previous section to examine the possibility of obtaining (100) highly oriented and textured diamond (HOD) films on tungsten. It has been recently demonstrated [Jiang 1996] that there may exist some form of registry between (100) silicon and oriented (100) diamond films which have been bias nucleated on the silicon. It is important to establish if this property is special to silicon or is a more general feature of biasing on non-diamond substrates. Studying biased nucleation on a range of substrates may help to achieve a more general understanding of the BEN process. As was mentioned in the introduction, as regards diamond growth, tungsten is in certain respects similar to silicon. For example, both substrates form relatively thin carbides, show low carbon diffusivity and have a similar carbon affinity. Tungsten is therefore a reasonable choice to study in respect of BEN and HOD diamond films.

Unless otherwise stated, in the experiments described in the following section, samples were first nucleated under the conditions of interest and then 'grown out', typically for around 20-30 minutes, to render the nuclei visible under SEM examination. Where applicable, Raman characterisation was employed and during biased nucleation both the bias voltage and bias current were monitored. Substrates were prepared and cleaned, in the manner described in section (4.2), prior to any nucleation or growth.

Figure (4.8) shows the results of typical *unbiased* nucleation on 50 mm diameter polycrystalline tungsten substrates. The film shown was nucleated and then grown out, for a total time of 1 hour under the conditions given in table(4.1), which, after longer growth times, results in the random polycrystalline film shown earlier in figure(4.2a-d). A view of the nuclei at a higher SEM magnification of 60k is shown as figure (4.8b).

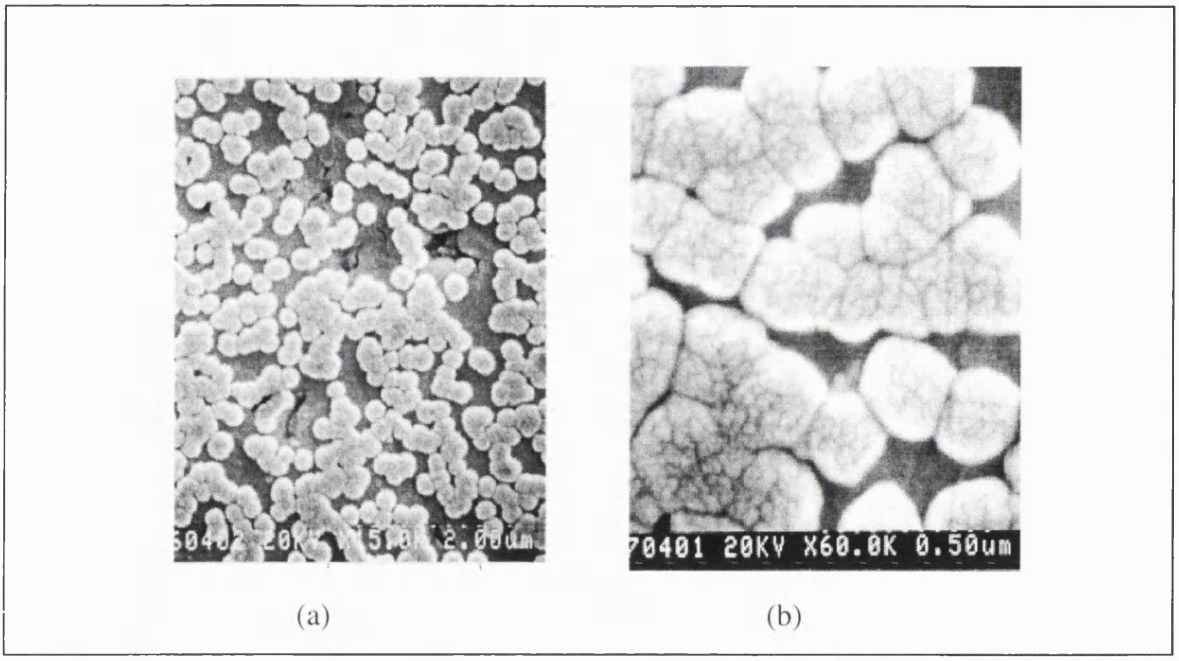

Figure (4.8): Unbiased nucleation on polycrystalline tungsten shown as (a), and (b) nuclei at high magnification showing granular structure.

Both optical and SEM analyses indicated that the nucleation density was reasonably uniform across a 2-3 cm diameter central region of the substrate, but then begins to reduce towards the towards the edges. The nuclei shown in figure(4.8a) are typical and show little variation in size, this is consistent with the supposition that the nuclei all form at a common time occurring once the critical surface carbon concentration has been reached. Under these conditions the nucleation stage appears to be a self-limiting process i.e. once a certain density is reached no further nucleation occurs and instead the existing nuclei increase in radius until they coalesce to form a continuous film across the substrate surface. The growth mode then appears to change and the spheroidal nuclei, which at this stage show no sign of crystallinity, start to grow vertically and facetting then begins to develop as the film thickness increases. Concurrently the familiar Raman signature for diamond begins to develop improving with film thickness and morphology, see for example, figure (4.2d). An SEM examination of the individual nuclei carried out at high magnifications, figure (4.8b), reveals that nuclei exhibit a distinct granular structure, appearing to be composed of clusters of much smaller clumps of material, which show up on the SEM as roughly spherical light areas separated by darker boundaries. The granular structures are approximately 20-50 nm in diameter as estimated from this SEM micrograph.

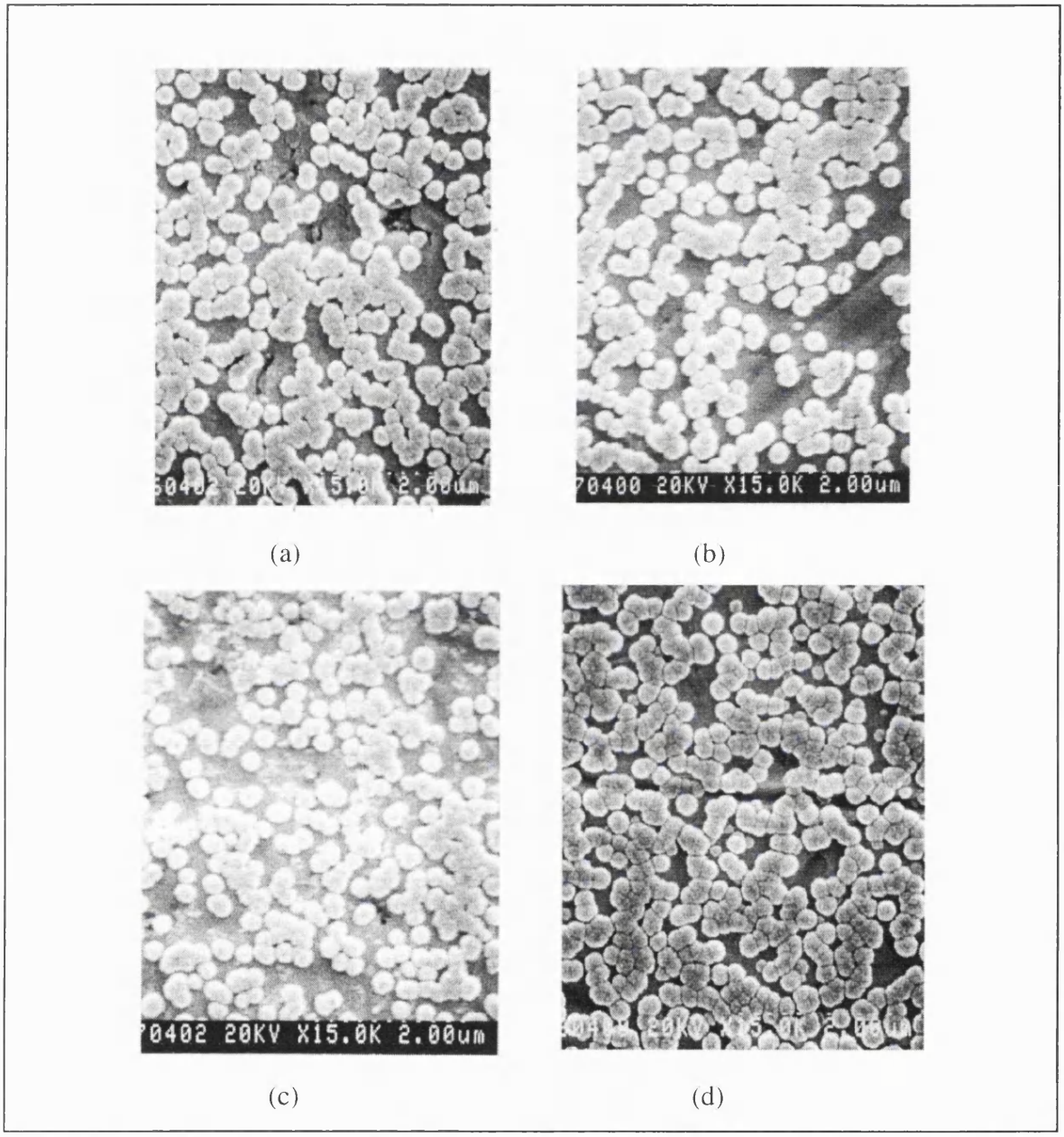

Figure (4.9): SEM's showing the effect of increasing bias voltage during nucleation on polycrystalline tungsten; (a) 0V, (b) -50V, (c) -125V and (d) -200 V. The bias period was 15 minutes in all cases.

Figure(4.9a-d) summarises the results of SEM studies of substrates which have been subjected to negative substrate biases of 0, 50, 125 and 200 V respectively. The bias was applied for 15 minutes under the standard growth conditions given in table(4.1) and the films were then grown out for a further 45 minutes under the same conditions to allow the nuclei to become visible to the SEM. There is some visual evidence from the micrographs of a slightly higher nucleation density at the highest biases, however the background nucleation density is high, of the order of 10^9 cm^{-2} in each case, which tends to mask any modest systematic changes with bias. Careful comparison of the 0 volt and 200 volt cases,

(a) and (d) in the figure, indicates that there may be a wider variation in the nuclei size in the latter film, implying that under bias conditions the generation of nuclei may be a continuous process. To establish if there is a significant increase in nucleation density with bias a more quantitative analysis was carried out in which the mean nucleation density for each film was established from SEM's taken of the central region of each substrate. The centre was examined to avoid systematic variation which could arise from the decrease in nucleation density which occurs moving from the centre towards the rim of the substrates. The results of the analyses are shown in the graph in figure(4.10) in which the mean nucleation density is plotted against substrate bias together with $\sqrt{N}$ error bars estimated from the number of nuclei counted to make the density assessments.

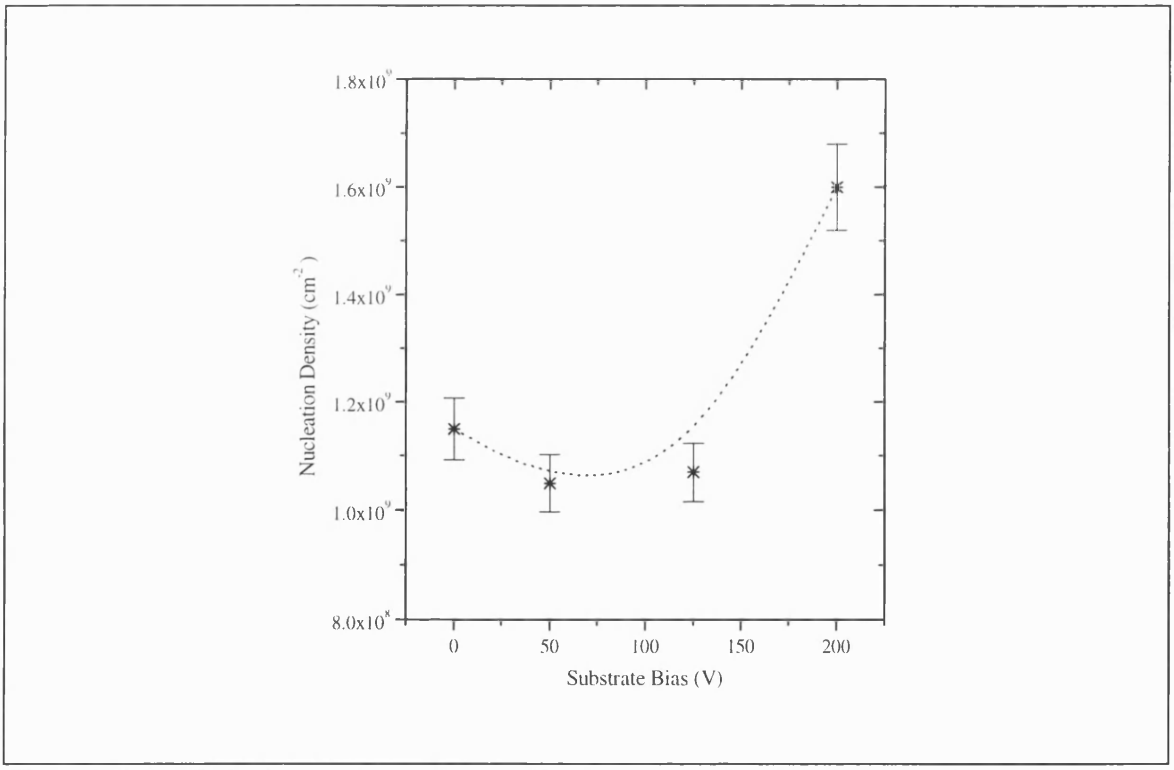

Figure (4.10) :Nucleation density on polycrystalline tungsten as a function of substrate bias (the dotted curve is intended only as a guide).

The graph shows that a -200 V bias applied for 15 minutes results in a modest 60% increase in the nucleation density on polycrystalline tungsten. A threshold for nucleation enhancement appears to occur after a bias voltage of around 125 V is reached.

It is known that nucleation densities on scratched polycrystalline substrates can be very high [Ascarelli 1992]; this maybe masking the true effect of bias on the nucleation density.

To elucidate more clearly the effect of bias, a series of nucleation experiments were carried out on single crystal samples of (100) oriented tungsten as has been described in earlier in section (4.2). To reduce systematic effects the 6.25 mm diameter single crystals were mounted within drilled examples of the polycrystalline disc samples. Table (4.2) summarises the bias conditions that were studied together with brief details of sample preparation, measured integrated substrate bias current and a summary of the SEM studies for each sample. Figure (4.11a-d) shows a set of representative SEM's taken from a series of single crystal samples that were subjected to varying bias times at a negative bias of 200 volts under nominally identical reactor conditions.

Sample [1][2] **No**	**Bias** [3] **Conditions**	**Integrated Bias Current (mA-min)**	**Nucleation density (cm^{-2})**	**Observations**
D/W332	no bias	0	10^5-10^6	*very low* density nuclei, spherical cauliflower-like
D/W348	4 min/200V	130	$1.7x10^7$	low nucleation density, spherical cauliflower like, range of diameters
D/W333	10 min/200V	208	$4.84x10^7$	cauliflower like spherical nuclei
D/W347	11 min/200V	511	$1.43x10^8$	cauliflower-like range of diameters
D/W336	40 min/200V	1167	$1.21x10^8$	cauliflower-like spherical, range of diameters apparent ~0.1-0.3μm
D/W344	25 min/200V	1874	$2.99x10^8$	cauliflower-like spherical range of diameters

(1) Substrates prepared prior to nucleation; 0.5 μm diamond polish, Al_2O_3 polish, ultrasonic degrease inhibisol, acetone, de-ionised water, 30 minute H-plasma clean.

(2) Following nucleation substrate subjected to short growth under (100) texturing conditions (table 4.1) to render nuclei visible to SEM.

(3) Biasing conditions were: 412 sccm gas flow, 4% CH_4, 3% Ar, 92% H_2, T_s 600 °C, 15.5 torr, Microwave power 800 W

Table (4.2): Summary of nucleation density experiments carried out on (100) single crystal tungsten substrates during this work.

The nucleation densities on the single crystal substrates were assessed using the method previously described and the results are shown in figure (4.12). In this case as the bias was

fixed at -200V, the nucleation density is shown plotted against integrated substrate bias current; the use of this parameter is discussed later in sections (4.3.3) and (4.4).

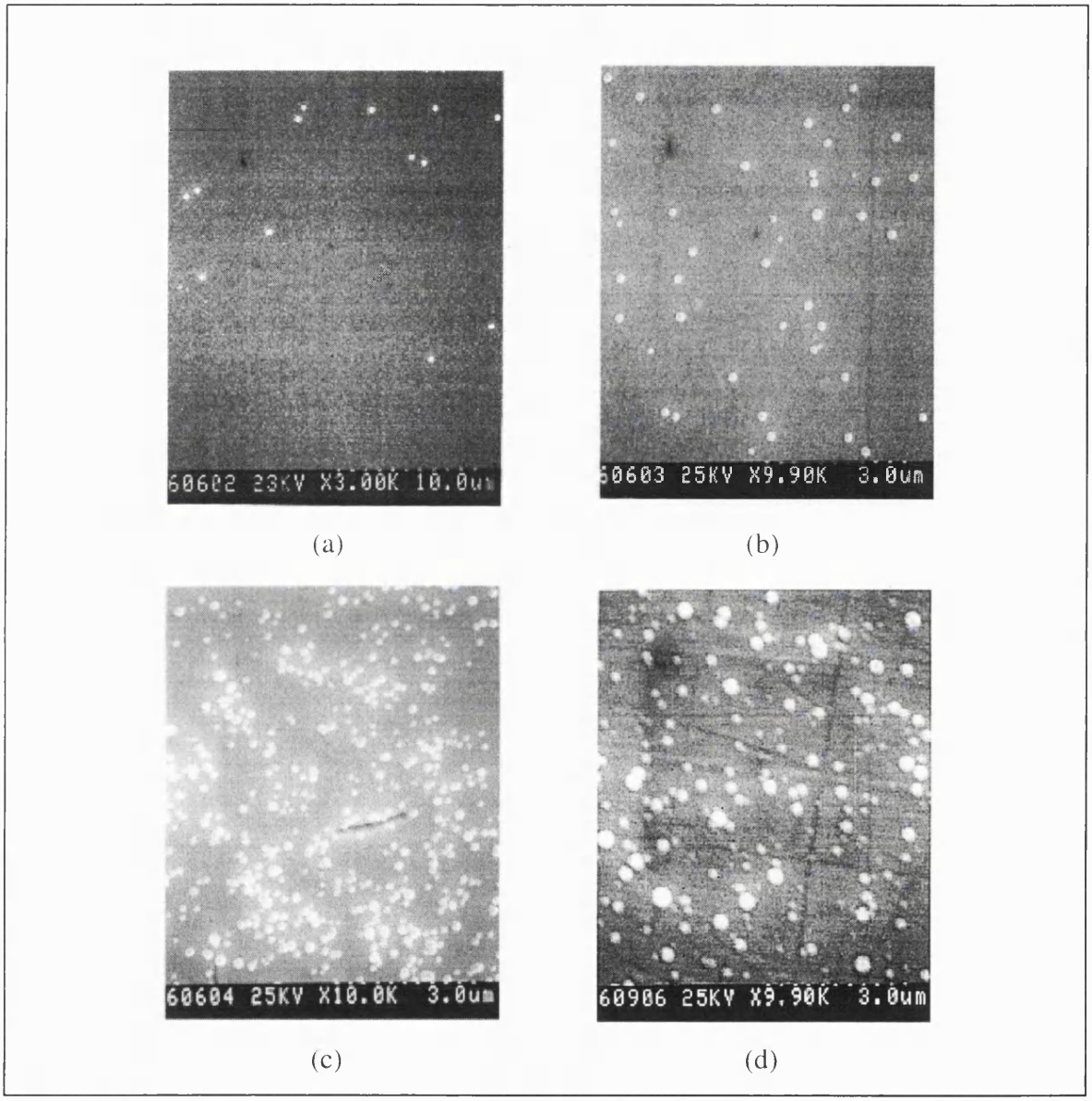

Figure (4.11): Four examples of biased nucleation on single crystal tungsten samples for increasing integrated bias current; (a) 0 mA-min, (b) 208 mA-min, (c)1167 mA-min and (d) 1874 mA-min.

The SEM's in figure (4.11) show small, nearly spherical nuclei, which were in general evenly distributed over the whole diameter (6.25mm) of the *single crystal surface*, except very close to the edges where there was a noticeable increase in the density of nuclei. This was probably attributable to an enhance bias field in this region due to edge effects. The nuclei exhibit a range of diameters, with an estimated mean of about 0.3 μm. A clear increase in the nucleation density with the integrated bias current can be seen from the

SEM's shown in the figure and this is reflected in the semi-log plot of figure (4.12), which shows integrated bias current against nucleation density.

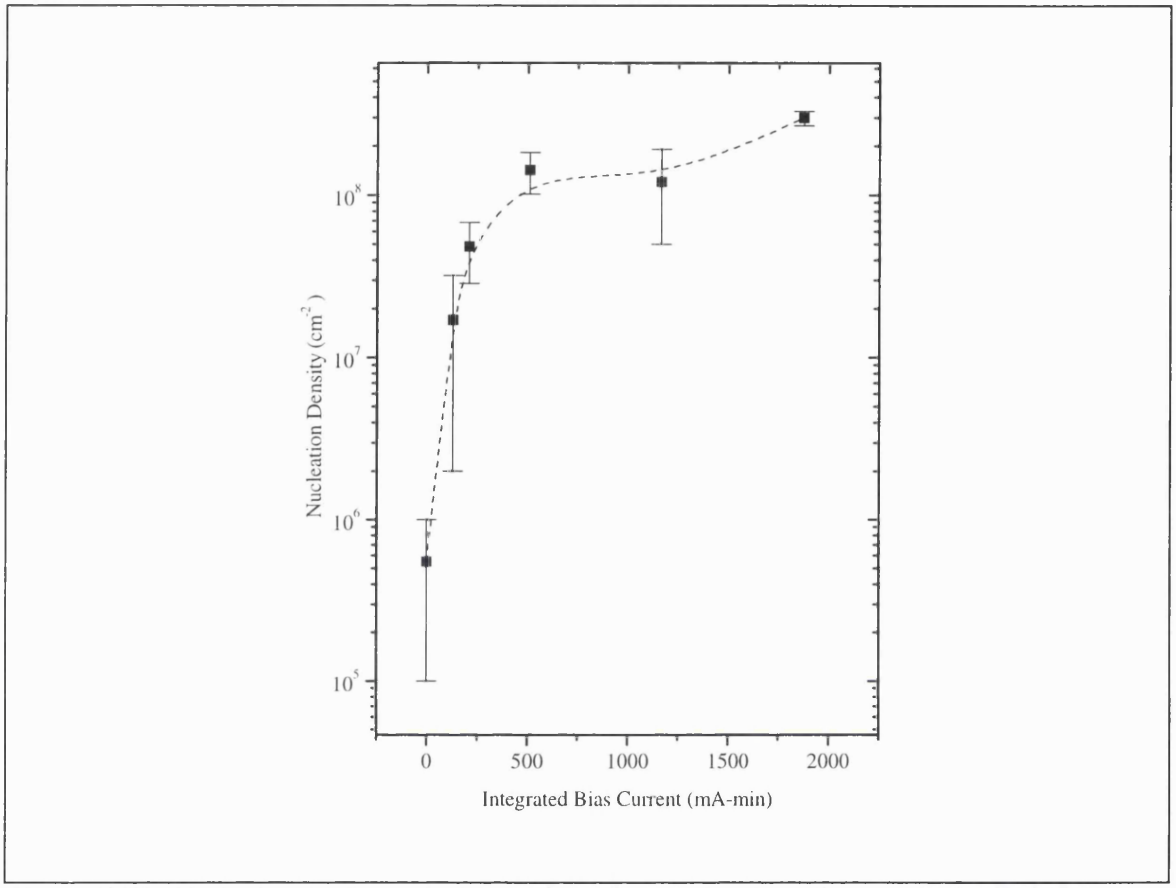

Figure (4.12): Nucleation density on single crystal tungsten as a function of integrated substrate bias current, (the dotted line is intended only as a guide).

Two regions can clearly be distinguished from the plot; first a region of rapidly increasing nucleation density for moderately low integrated currents which appears to saturate at around 400-500 mA-min. This is followed by a much slower increase in the nucleation density which remains reasonably constant out to the maximum integrated bias current of nearly 2000 mA-min investigated in these experiments. The nucleation density on the unbiased single crystal surface was extremely low and rather difficult to measure accurately with the SEM. Although the SEM micrograph shown in figure (4.11a) yields a value of around 10^6 cm^{-2} for the zero bias sample, this should be regarded as a maximum value, as for illustrative purposes this SEM was taken from an un-typical region of higher nucleation density. Most of the SEM studies on the zero bias sample showed very few nuclei and a value of between 10^5 and 10^6 cm^{-2} would be more representative of the true nucleation density for the unbiased surface; this is the value that has been plotted in figure(4.12). The

errors shown were derived from the standard deviation of 10 individual SEM estimates for each sample. The large error for the zero bias case reflects the difficulty in establishing the true nucleation density on this sample.

As table (4.2) indicates, none of the bias nucleated single crystal samples showed any evidence of nuclei possessing well defined morphology. It was therefore not possible to establish from these experiments whether there was any common orientation relationship either with respect to the (100) tungsten substrate or between diamond nuclei. To try and examine the question of bias oriented and textured films a series of longer experiments were undertaken. A small set of (100) single crystal tungsten samples were bias nucleated under a range of conditions and grown out for a period of 24 hours under the standard (100) textured growth conditions determined previously. The samples were removed and studied by SEM for signs of orientation. The modest range of bias conditions examined during this final part of the tungsten study reflected limitations in both reactor time and the number of substrates (100-tungsten is expensive) which were available to the author. The experimental conditions and results of the study are summarised in table (4.3).

At the time this work was carried out, HOD films had only recently been reported [Wild 1994, Wolter 1993,] and the relationship between bias time and 'epitaxy' on silicon was unclear; therefore the bias times shown in table (4.3) represented a compromise between the number of substrates available and the range of bias times which could be tried. It can be seen from table (4.3) that no evidence of crystallite orientation was seen on any of the subsequent films, even after onward growth of 24 hours. Typical films thickness at the termination of growth were ~5-6 μm's, as estimated from the growth rates determined previously for these reactor conditions. It would be expected that film thickness of this order would have been more than sufficient to reveal any preferential orientation of the individual grains in each film. Even after a growth time of 112 hours (sample D/W 328) no preferential orientation could be detected, although the film was of good quality and near to 100% (100) textured. The SEM study revealed virtually no differences between the films nucleated under the different bias conditions after these films were grown out. All yielded similar preferential (100) textured morphologies, however the samples with the lower bias times and consequently rather low nucleation densities exhibited large

spheroidal structures at low magnification which had coalesced in places to form a continuous film with a larger surface roughness than the other films.

Sample no[1] [2]	Bias conditions[3]	Growth time (hours)	Observations(SEM)
D/W 327	20 min/20V	18	(100) film, no orientation
D/W 328	30 min/200V	1 8 then 96 (112 total)	(100) film, no orientation
D/W 356	46 min/200V	24	(100) film, no orientation
D/W 357	11 min/200V	24	(100) film, no orientation
D/W 358	11 min/200V CH_4=1%	24	(100) film, no orientation
D/W 359	4 min/200V	24	(100) film, no orientation

(1) Samples preparation prior to nucleation: Substrates prepared prior to nucleation; 0.5 μm diamond polish, Al_2O_3 polish, ultrasonic degrease inhibisol, acetone, de-ionised water, 30 minute H-plasma clean.

(2) Following nucleation substrates were subjected to growth under (100) texturing conditions (table 4.1) to develop textured and oriented films.

(3) Except where shown in this column bias was carried out under the following conditions: 412 sccm gas flow, 4% CH_4, 3% Ar, 92% H_2, T_s 600 °C, 15.5 torr, Microwave power 800 W

Table (4.3): Summary of long growth time (100) oriented-textured film experiments carried out on (100) tungsten substrates.

At a higher magnification the large structures were revealed to be composed of agglomerations of (100) crystallites, generally similar to those comprising the smoother, higher nucleation density films. At the higher magnifications all the films appeared similar and no evidence of any orientation could be determined from the results of these studies. In addition, no differences in the general character between the films grown on single crystal tungsten and those grown at the same time on polycrystalline tungsten immediately adjacent to the single crystal samples were evident after long growth times up to 112 hours. The nature of the films grown on polycrystalline and single crystal tungsten is indicated by the SEM's shown in figure(4.13) which shows typical bias nucleated films, *grown at the*

same time on the two forms of the substrate, following onward growth times of 18 hours (a) and (c) in the figure; and 112 hours (b) and (d) in the figure.

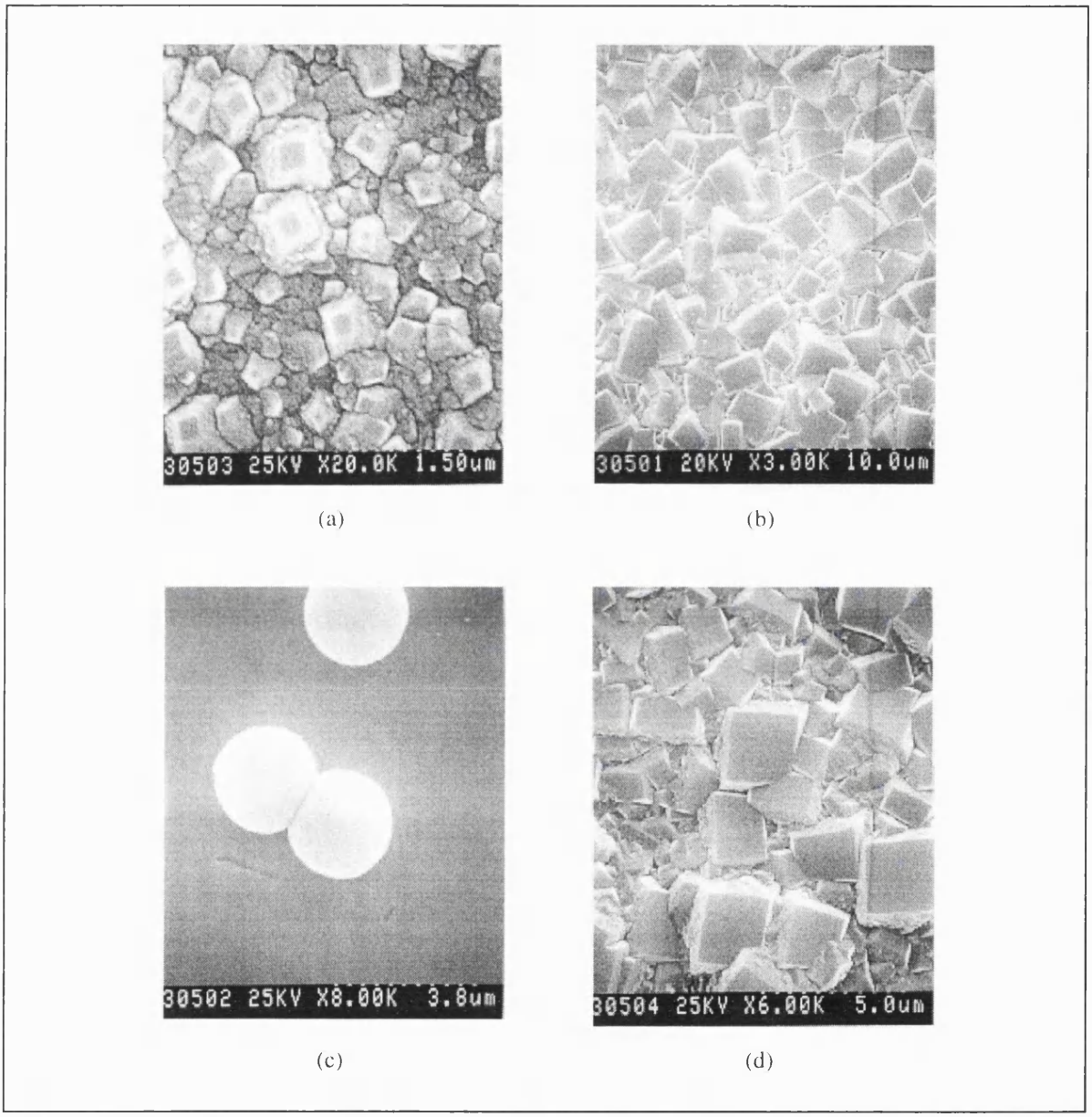

Figure (4.13): SEM's showing typical bias nucleated films grown at the same time on polycrystalline tungsten after; (a) 18 hours, (b) 112 hours, and single crystal tungsten after; (c) 18 hours, (d) 112 hours.

4.3.3 Electrical Characteristics of Biasing

A wider range of electrical studies were carried out than are presented here, the results of the more general study are discussed later in chapter six. For the work described in this chapter, the most important characteristic was the evolution of the substrate bias current with respect to time. This was because it has been shown that on silicon, the features of

this curve are closely linked with the degree of nucleation enhancement and also to orientation of the diamond nuclei [Milne 1995, Kulisch 1995]. The results of electrical measurements made during biasing of tungsten substrates are shown in figure (4.14) together with the results of similar measurements made on silicon for comparison. The details of the experiments and the silicon substrates have been given earlier in section (4.2). The plot shows bias current density against bias time for both tungsten and silicon substrates. Current density is given to account for the differing areas of the two substrates.

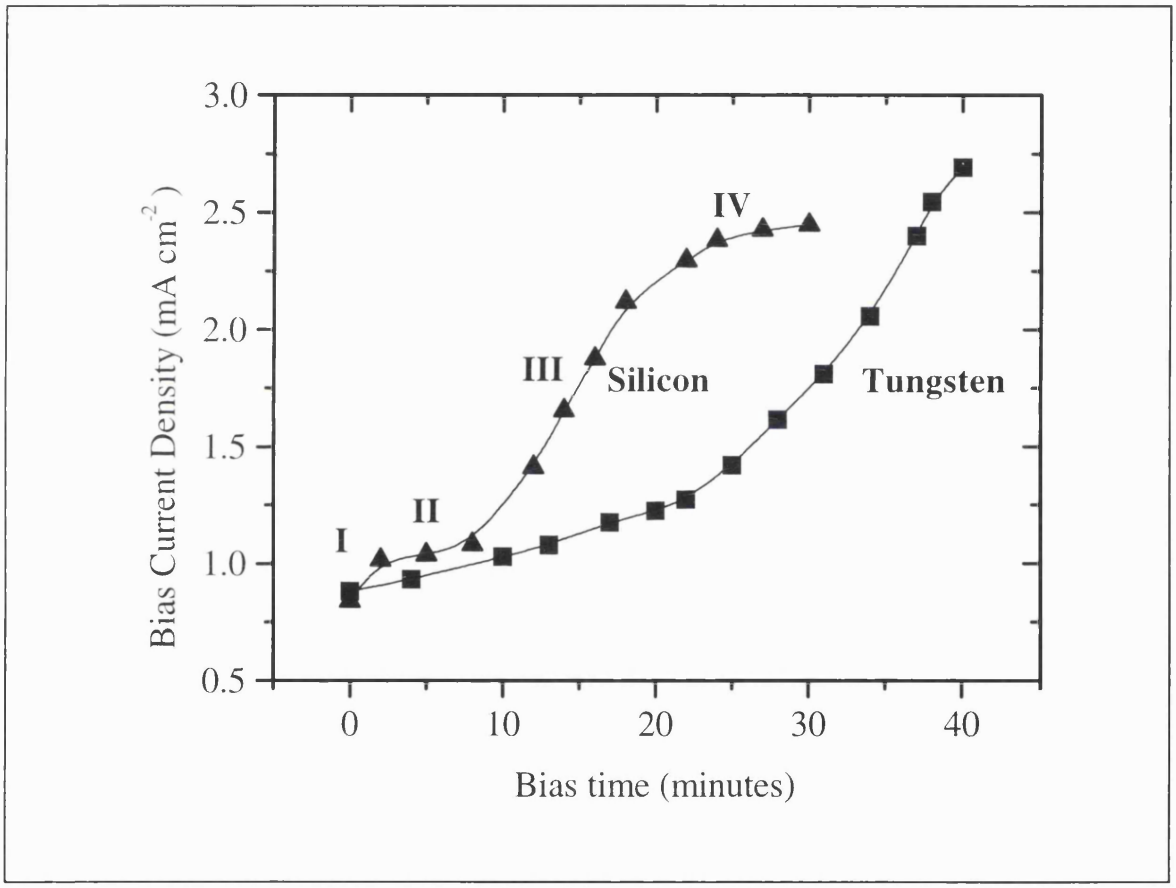

Figure (4.14): Comparison of typical substrate bias current-time characteristics for silicon and tungsten at a bias voltage of -200V. Current density is shown to account for the differing areas of the two substrates types, the solid curves are intended as a guide only.

In general it was observed that bias-time curves were rather sensitive to precise reactor conditions and over many bias runs it was clear that the curves could show considerable variation in the details of the features present. The problem of the apparent 'poor reproducibility' of bias characteristics was not clearly understood at the time this work was carried out, however this problem is now more widely acknowledged by the diamond community [e.g. Milne 1995, Kulisch 1996]; this problem is discussed in more detail in

chapter seven. The curves shown in figure (4.14) represent data that was taken close together in time and with a particular effort to ensure that reactor conditions were as alike as possible during biasing of the two substrates.

The silicon bias curve always exhibited the four distinct regions labelled I-IV in the figure, provided biasing was carried out for a sufficient length of time. The bias current increased rapidly for a short time at the start, labelled region I on the curve, this was followed by a plateau region, marked II, in which the curve was flat or the increase in current shallow, this has been referred to in the literature as the 'incubation period' [Milne 1995] and has been associated with possible SiC formation on the substrate surface. Immediately following the plateau, the substrate current showed a sharp rapid rise, region III, before finally saturating in region IV. If continued past this point the curve turned over and the bias current showed some decrease. The situation for tungsten was slightly different, for the curve shown here only two regions were readily apparent. First, an initial region of relatively slow bias current increase which persists for quite long times, around 20-25 minutes. This was followed by a region of rapid rise in bias current similar to region III in the silicon curve. There is slight evidence of slowing of this increase at around 40 minutes, however no definite saturation occurred for tungsten up to the maximum bias times examined here.

4.4 Discussion.

The results presented in the previous sections indicate that diamond growth on tungsten probably proceeds in a similar manner to that provided by the silicon model. At first the incoming carbon species react with the substrate to form carbide phases which reduce the rate of carbon diffusion into the bulk, allowing the α-carbon concentration in the surface layer to build up to some critical concentration at which point carbon clusters or diamond pre-cursor nucleation sites appear distributed over the surface commensurate with the uniformity of the plasma; the nuclei can be seen in figure (4.8) which shows the case for unbiased nucleation on a polycrystalline substrate. The absence of any significant range in the diameters of the nuclei suggests that the nucleation event is confined to short region in

time and that following nucleation most of the incoming carbon is consumed by the growing nuclei preventing further nucleation events. These observations are in agreement with the detailed model for nucleation on carbide forming substrates which has been proposed by Joffreau *et al.* [1988], who studied diamond nucleation on a range of hot-rolled, unpolished refractory metal substrates. On tungsten they observed a low nucleation density $<10^5$ cm^{-2} which allowed them to establish conclusively that further growth after initial nucleation did not increase the nucleation density with only an increase in the size of the existing nuclei occurring. The much higher nucleation density of $\sim 10^9$ cm^{-2} seen in the work reported here can be attributed to the 3 μm diamond grit polish used to prepare the substrates, together with the polycrystallinity of the substrates. After 5 hours the same group observed nuclei with a diameter of around 10 μm which exhibited no defined morphology similar to the nuclei studied in this work. However, the SEM's presented in this study are at a higher resolution than previous work and show the nuclei much earlier in their development, after only 1 hour of growth, when individual nuclei have a mean diameter of around 500 nm and are cauliflower like in appearance. Figure (4.8) clearly shows that the nuclei are comprised of tight clusters of much smaller clumps of material around 20-50 nm in diameter. No morphology develops until the nuclei coalesce and the growth mode shifts from island to film growth. It is speculated that the smaller clumps may be regions of high sp^3 content separated by boundaries of high sp^2 content, an observation which is supported by the lower secondary electron emission yield evidenced by the dark appearance of the boundaries under SEM examination. Figure (4.2) shows the structure of a typical film (grown at 2% methane) from which the columnar nature of the film development is clear, but it can also be seen that the granular nature of the original nuclei persists and at high magnification even the well developed morphology of the film remains granular. It is interesting to note that similar films grown at a much lower methane fraction e.g. 0.5% as shown in figure (4.3a) do not appear to show this granular sub-structure at least at the magnifications used here. It is known from similar work on silicon that films grown at higher methane fractions contain significantly higher sp^2 fraction which may account for the granular structure observed here [e.g. Williams 1989].

The likely growth of diamond under the gas mixture conditions used here conforms to the C-H-O scheme described by the Bachmann diagram [Bachmann 1998]. That the

morphology and film quality are strong functions of deposition conditions is expected. The general trends measured here in respect of substrate temperature and methane fraction are qualitatively similar to those observed for silicon [e.g. Williams 1989, Stoner 1993, Wild 1990 & 1994], i.e. the higher degree of twinning at lower methane fractions, figure (4.3a) and the change in the dominant morphology from (110/111) at low methane fraction to (100) at intermediate methane fractions and loss of morphology at the higher fractions. This change in morphology which occurs with increasing methane fraction has been explained in terms of the growth competition between (111) and (100) faces characterised by the alpha (α) parameter proposed by Wild *et al.* [1990,1994]. Conditions of high methane fraction favour a high value of alpha leading to (100) textured growth. Once a complete covering of the substrate is achieved it would not be expected that the substrate would significantly influence the mechanisms of subsequent diamond growth which should then proceed in a similar manner for all substrates [Zhu 1995].

The (100) textured growth which has been demonstrated on tungsten during the course of the work reported here, occurs under conditions similar to those observed for silicon with some allowance for differing reactor design and configuration. Figure (4.7c) shows that films of a similar quality to the best which can be obtained on silicon can also be grown on tungsten. The relatively narrow band of deposition conditions in terms of substrate temperature and methane fraction which give high quality (100) growth on tungsten are in qualitative agreement with the trends which have been identified for silicon from a set of statistically designed experiments by Stoner *et al.* [1993]. They found that good growth, as judged by a narrow 1332cm^{-1} Raman peak, combined with a reasonable growth rate was only attained for a narrow temperature band with a maximum at around 700 °C. At the same time moderately high methane fractions, greater than ~1%, were required. The quality of the best (100) sample grown during this work can be appreciated from the SEM shown in figure (4.7c) and the corresponding Raman spectrum (4.7d). The low background in the spectrum is indicative of a film with high phase purity - especially given the high sensitivity of the 632.8 nm excitation source to sp^2 compared to sp^3 bonded material. The FWHM of ~3.3cm^{-1} can be compared with the value of ~2 cm^{-1} quoted for natural diamond and also compares well with CVD films grown on silicon to a similar thickness [e.g. Haq 1994 4cm^{-1}, Lee 1990 5cm^{-1}]. The conditions under which films were grown for this work

were not exhaustively optimised and it is not unreasonable to conclude that films grown on tungsten could match the best which has achieved on silicon, with the possible exception of crystallite orientation which will be discussed later in this section. A rapid loss of (100) texture quality with temperature for films on tungsten is clearly shown in figure(4.6) where a temperature rise of only 80 °C from the standard growth temperature of 600 °C leads to strong degradation in film quality as judged by both Raman and SEM analyses. On silicon an upper limit for good (100) texturing has also been observed with marked changes in morphology occurring for a similar temperature *range*, e.g. $\Delta T \sim 150°C$ [Stoner 1993], which can be compared to a range of ~100°C for the films grown during the current studies. The dominance of a given texture has been well explained in terms of the growth rate competition between different facets [Wild 1990], characterised by a growth parameter α, which is a strong function of growth conditions particularly substrate temperature and methane fraction [Wild 1994].

It is of interest to consider the possibility of controlling the initial nucleation density as this can influence the surface grain size for a film of a given thickness. One of the practical motivations for this is the possibility of growing optical, thick film diamond windows on metal substrates; the grain size of a polycrystalline film can influence the strength and optical properties of such windows [Savage 1997]. The results of the bias study on *polycrystalline* tungsten samples carried out here, indicate that bias has a modest effect on the nucleation density and provides some indication for a threshold value of ~100-120 volts before this effect becomes significant. On polycrystalline samples the effect of bias is small resulting an increase of about 60% against a very high background nucleation density of $\sim 10^9$ cm^{-2}. The threshold observed during the current study was similar in magnitude to bias values typically required to show the BEN effect on other substrates including silicon. The suspicion that high background nucleation on the polycrystalline samples was masking the bias effect is confirmed by the studies carried out on the highly finished single crystal tungsten substrates which show that a negative bias of 200V can increase the nucleation density by at least four orders of magnitude, as shown in figure (4.11). The shape of the curve is broadly similar to those measured for a range of carefully finished *polycrystalline* refractory metal substrates including tungsten in the study by Wolter *et al.* [1995] carried out at the same time as this work. It is interesting to compare the unbiased nucleation

figure (4.11a) with the biased nucleation in figure (4.11d), the biased nuclei show a larger range in diameter in contrast to the unbiased case where nuclei were all of similar diameter. This implies that nucleation is a continuous process during biasing i.e. nucleation events occur all the time the bias is applied together with some increase in the size of those nuclei which appear early in the biasing period. This would suggest that under conditions of bias, nucleation is not the result of a simple critical surface carbon concentration arising from balance between; carbon diffusion into the bulk, carbide formation and carbon supply rates processes, but involves additional non-equilibrium processes. It can be seen from figure (4.12) that the initial nucleation rate is very rapid but then the rate of increase with integrated bias current becomes more shallow as the nucleation density approaches a figure at which the film becomes continuous.

The general evolution of the bias current-time characteristics measured here during biasing on silicon have been described briefly by several authors [Schreck 1995, McGinnis 1995, Jiang 1996] however, few examples of actual bias current-time curves have been presented. At around the same time as the measurements reported here were made detailed measurements of bias current as a function of time were made on silicon [Milne 1995, Kulisch 1995] which showed very similar features to those seen in this work (regions I-IV) in figure (4.14). These characteristic features have been attributed by these groups to changes occurring to the substrate surface during the BEN process. The initial steep rise , marked I, occurring at short times was not seen by all authors and may be due to incomplete removal, by the pre-bias cleaning procedure, of the native oxide which forms on silicon. The length of the H-plasma etch used by many workers to remove the surface oxide varies considerably (typically 10-30 minute treatments have been reported) and may not always be completely effective, leaving some of the oxide present on the surface. It has been shown that oxides are also effectively removed in an H_2/CH_4 plasma during the initial application of substrate bias [Stoner 1992]. Indeed some groups use a hydrofloric(HF) acid dip on silicon, just prior to insertion in the reactor, as HF is very effective in removing the native silicon oxides [Ghandhi 1994]. Removal of a partial oxide layer during biasing, might be expected to show up as an initial increase in bias current similar to the increase shown as region I in figure (4.14). The lack of a similar region for the tungsten surface could be due to a thinner oxide forming on this substrate compared with silicon. Region II

in the figure is commonly termed the 'incubation period', which occurs prior to the onset of high nucleation densities on silicon and has been associated with the formation of a β-SiC layer [Milne 1995] and/or a β-SiC + α-hydrocarbon layers [Kulisch 1995]. The 'incubation period' precedes the period of a high rate of nuclei formation characterised by a rapid rise in the bias current, marked III in figure (4.14). The length of the delay is related to the diffusivity of carbon in the substrate and the length of time taken to form the carbide layer which acts as a barrier to continued carbon diffusion away from the surface into the substrate. The carbide thickness on silicon has been shown to be less than 100 nm compared to a thickness of around 200-400 nm's on tungsten [Stoner 1992, Zhu 1995]. Assuming a similar rate of formation, this is qualitatively consistent with the observed difference in the lengths of the flat regions of the bias-time curves measured here, figure (4.14), which are a factor of 2-3 longer for tungsten than for silicon.

In principle biasing could be used to control grain size via nucleation density for films grown on highly finished tungsten substrates as evidenced by the results of this study. The general character of films grown on polycrystalline and single crystal material appear similar if grown out to large thickness. For the biasing conditions studied during this work, the films on the single crystal material have not yielded any evidence that BEN can give rise to oriented nuclei on tungsten substrates. However, it has become clear from the literature published during the course of the work for this thesis that orientated nucleation depends *very critically* on the precise nucleation and growth parameters used [e.g. Schreck 1995, Jiang 1996]. It has also become apparent that BEN suffers from significant repeatability problems, even between growth runs within single groups [Kulisch 1996, Milne 1995]. This problem is addressed in more detail in chapter seven of this thesis. Therefore the experiments reported in the current study, which have only explored a small part of the available parameter space, do not conclusively prove that oriented nucleation cannot be achieved on tungsten; to the contrary, oriented nucleation has to date been demonstrated on a range of substrates including; nickel [Sato 1991], cobalt [Lui 1995], titanium-carbide [Wolter 1995] and titanium-nitride [Chalker 1994] and oriented growth may prove to be possible on tungsten once the correct nucleation conditions are identified. However, there is one rider to this optimism; this author has noted that so far the substrates which have shown oriented diamond have also yielded nuclei with definite morphology,

even when the nuclei are very small. The author did not at any point during the course of these studies observe nuclei with regular morphology; the nuclei observed on tungsten were spheroidal, with a granular 'cauliflower-like' substructure and exhibited no morphology what-so-ever prior to coalescence, after which crystal-like morphology then began to develop.

4.5 Summary.

The work reported in this chapter is believed to be the most complete combined study of diamond nucleation and growth on tungsten substrates undertaken to date. The growth of relatively thick, high quality films on tungsten substrates has been demonstrated and the general nature and structure of the films clearly established. Raman and SEM analysis has shown that the nature of these films is strongly modified by the reactor conditions during growth; as grown films can exhibit significant thermal compressive stress arising from the mismatch in thermal coefficients and the low compliance of relatively thin interface layers which develop on tungsten during diamond growth. The conditions for (100) textured growth, an important growth mode for diamond films, have been established for tungsten. It was clearly shown that films with quality comparable with those grown on silicon, as judged by Raman and SEM, can be achieved. The nucleation phase on tungsten was characterised and the effect of substrate bias was investigated on single and polycrystalline examples of the substrate. It was shown that BEN can promote increases in nucleation density of at least four orders of magnitude on highly finished substrates in agreement with the results of other workers. The bias voltage and current characteristics for BEN on tungsten have been measured and shown to be qualitatively similar to those measured on silicon. It should in principle be possible to use BEN to control film nucleation density on tungsten provided the substrates are highly polished and cleaned prior to nucleation. No significant differences were observed between the films grown on the single crystal substrates and those grown on polycrystalline substrates, with the exception of the unbiased nucleation density which was very high at ~10^9 cm^{-2} on the polycrystalline samples compared with 10^5 cm^{-2} on the single crystal substrates. The work described in this chapter should be of use to future workers studying diamond growth on this material and to technologists and agencies with interests in using metal substrates for diamond film growth

The possibility of oriented film growth on tungsten arising from BEN was examined but remains unresolved by these experiments. The lack of any observed orientation here does not disprove the possibility but only rules out orientation for the limited range of conditions examined in this study; further experiments in this direction would be useful.

4.6 References

Ascarelli P and Fontana S, [1992], *Appl. Surf. Sci*, **64**, 307.

Bachmann P.K., [1998], Chpt. 21 in *Handbook of Industrial Diamonds and Diamond Films*, eds. Prelas M.A., Popovici G. and Bigelow L.K., (Marcel Dekker Inc.), New York, USA.

Calker P.R., Johnston C., Romani S., Ayres C.F. and Buckley-Golder I.M., [1994], *Diam. and Relat. Mater.* **3**, 393.

Chan S.M., [1996], PhD. Thesis, *Electronic Device Fabrication fron Thin Film Diamond: Surface Preparation, Patterning, Metallisation and Characterisation.*, University College, University of London, UK.

Chu C.J, Hauge R.H, Margrave J.L and Begun G.M, [1993], *Appl. Phys. Lett.* **61**, 1393.

Dreifus D.L. and Fox B.A., [1998], Chapt. 29 in, *Handbook of Industrial Diamonds and Diamond Films*, eds. Prelas M.A., Popovici G. and Bigelow L.K., (Marcel Dekker Inc.), New York, USA.

Ghandi S.K., [1994], *VLSI Fabrication Principles*, 2nd Edition, Wiley and Sons Inc.

Haq S., Tunnicliffe D.L. and Savage J.A., [1994], *Diam. and Relat. Mater.*, **3**, 593.

Jiang X and Klages C.P, [1996], *Phys. Stat. Sol. (a),* **154**, 175.

Joffreau P.O, Haubner R, and Lux B, [1988], *Int. J. Ref. Hard Metals*, **7**, 186.

Knight D.S. and White W.B., [1989a], *J. Mater. Res.,* **4**, 385.

Knight D.S. and White W.B., [1989b], *Proc. SPIE,* **1055**, 144.

Kulisch W, Ackermann L and Sobisch B, [1996], *Phys. Stat. Sol.(a),* **154**, 155.

Lee Y.H., Richard P.D., Bachmann P.K. and Glass J.T., [1990], *Appl. Phys. Lett.*, **56**, 620.

Liu H and Dandy D.S, [1995], *Diam.& Relat.Mater.*, **4**, 1173.

Liu W., Yang D.A. and Glass J.T., [1995], *J. Appl. Phys.* **78**, 1291.

Lunn B, Wright D.A and Zhang L.Y, [1998], *Diam.& Relat.Mater.*, **7**, 129.

McGinnis S.P, Kelly M.A and Hagstrom S.B, [1995], *Appl. Phys. Lett.*, 66, 311.

Milne D.K, Roberts P.G, John P, Jubber M.G, Liehr M and Wilson J.I.B, [1995], *Diam.& Relat.Mater.*, **4**, 394.

Nemanich R.J., Glass J.T., Lucovsky G. and Shroder R.E., [1988], *J. Vac. Sci. Technol.*, **A6**, 1783.

Nicholson E.D., Week J.R. and Ashfold M.N.R., [1997], *Diam. and Relat. Mater.*, **6**, 817.

Qi Hau Fan, Fernandes A. and Gracio J, [1997], *Diam. and Relat. Mater.*, **7**, 603.

Ralchenko V.G, Smoli A.A, Pereverzev V.G, Obraztsova E.D, Korotoushenko K.G, Konov V.I, Lathotkin Yu. V, and Loubnin E.N, [1985], *Diam.& Relat.Mater.*,**4**, 754.

Ravi K.V., [1994], Chpt. 14 in *Synthetic Diamond*, (eds. Spear H.E. and Dismukes J.P.), John Wiley and Sons Inc., New York.

Rodway D, [1994], DERA Malvern, Private Communication.

Rutledge K.M. and Gleason K.K., [1998], in Chapt. 4, *Handbook of Industrial Diamonds and Diamond Films*, eds. Prelas M.A., Popovici G. and Bigelow L.K.,

Sato Y., Yashima I., Fujita H., Ando T. and Kamo M., [1991], in *New Diamond science and Technology*, (eds. Messier R., Glass J.T, Butler J.E and Roy R.), Materials Research Society, 371.

Savage J.A, Wort C.J.H., Pickles C.S.J., Sussmann R.S., Sweeney C.G., M^{c}Clymont, Brandon J.R., Dodge C.N. and Beale A.C., [1997], Spie 3060.

Schreck M, Baur T and Stritzker B, [1995], *Diam. and Relat. Mater.*, **4**, 553.

Shi C.R., Aviygal Y., Dirnfelds S., Hoffman A. and Kalish R., [1995], *Diam. and Relat. Mater.*, **4**, 1079.

Stoner B.R, Ma G.H.M, Wolter S.D and Glass J.T, [1992], *Phy. Rev. B*, **45**,11067.

Stoner B.R, Sahaida S.R and Bade J.P, [1993], *J. Mater. Res.*, **8**, 1334.

Wild C, Herres N and Koidl P, J. Appl. Phys., [1990] **68**, 973.

Wild C., Kohl R., Herres N. Muller-Serbert W. and Koidl P., [1994], *Diam. and Relat. Mater.*, **3**, 373.

Williams B.E. and Glass J.T., [1989], *J. Mater. Res.*, **4**, 373.

Wolter S.D, Glass J.T and Stoner B.R, *J. Appl. Phys.*, [1995a] **77**, 5119.

Wolter S.D, Stoner B.R, and Glass J.T, [1994], *Diam.& Relat.Mater.*, **3**, 1188.

Wolter S.D., M^{c}Clure, Glass J.T. and Stoner B.R., [1995b], *Appl. Phys. Lett.* **66**, 2810.

Wolter S.D., Stoner B.R., Glass J.T., Ellis P.J., Buhaenko D.S., Jenkins C.E. and Southworth P, [1993], *Appl. Phys. Lett.,* **62**, 1215.

Yoshikawa M., Katagiri G, Ishida H., Ishitani A. and Akamatsu T., [1988], *Solid State Comms.*, **66**, 1177.

Yugo S, Kanai T, Kimura T. and Muto T., [1991], *Appl. Phys. Lett.*, **58**, 1036.

Zhu W, McCune R.C, deVries J.E, Tamor M.A and Simon Ng K.Y, [1995], *Diam.& Relat.Mater.*, **4**, 220.

Chapter 5

An Optical Emission Study of a Microwave Diamond Plasma During Bias Enhanced Nucleation.

A negative bias applied to a non-diamond substrate at the start of microwave plasma enhanced chemical vapour deposition of thin film diamond can lead to enhanced nucleation density and improved alignment of the grains in the subsequent polycrystalline film. As the plasma is the source of active species, any bias induced changes to it are of considerable interest. This chapter presents the results of optical emission spectroscopy, which has been used to study changes in the plasma species that occur as a result of applying a negative bias to a tungsten substrate. As the bias is applied the ratio of C_2 to CH emission intensities changes considerably, while actinometry indicates an increase atomic hydrogen concentration; these changes appear to be greatest near the substrate surface.

5.1 Introduction

The growth of thin films of diamond by chemical vapour deposition (CVD) methods has enabled a wide range of applications for this material to be explored. Microwave enhanced plasma CVD (MEPCVD) has become pre-eminent amongst these methods for the formation of the highest quality films [Zhu 1991]; mainly due to the efficient dissociation of the feed gases arising from electron impact reactions combined with the very clean nature of the deposition process in these types of reactor. This latter feature is due to the remote nature of the plasma which is well isolated from the reactor walls and other regions which can act as a source of impurities in the depositing film. However, the nucleation of such films on substrates other than diamond has remained difficult; nucleation densities are comparatively low and polycrystalline film evolution results. An important advance in the field, which has been discussed at length else-where in this thesis, has been the development of 'bias enhanced nucleation' (BEN) [Yugo 1990], in which a negative bias of around 200 V is applied to a silicon growth substrate for a short time at the onset of growth to promote nucleation on an otherwise untreated surface. Enhancements of the nucleation density by several orders of magnitude over other techniques have been obtained in this manner [Stoner 1992, 1993]. The effect has also been demonstrated on other substrates, most notably those metals which form carbides [Wolter 1995, Jeng 1995]. An additional benefit of this approach has been the formation of polycrystalline diamond films which display a limited epitaxial relationship with the underlying substrate material [Wolter 1993, Fox 1994]. The biasing method thus appears to be a promising approach for the realisation ofhigh quality, even electronic grade, material [Bozeman 1998].

The processes which control diamond nucleation on non-diamond substrates during CVD are still poorly understood [Frencklach 1991, Beckmann 1995]. The mechanisms which underlie BEN during MEPCVD have been even less clearly identified although its effects have been empirically established. While a number of different models have been proposed, as noted in chapter 2, contradictions exist and no single model satisfactorily

accounts for all of the experimental observations. Clearly the plasma in a MEPCVD chamber is the source of active species which give rise to diamond nucleation and subsequent growth; any changes to the plasma are likely to significantly influence these processes; simple unaided observation quickly confirms that a substrate bias gives rise to a number of changes in the appearance of the plasma, implying chemical and physical processes are being influenced. Central to understanding the BEN process is an experimental insight into the nature of the species which impinge upon the surface during the biasing step together with a knowledge of any changes which occur to the physical processes and chemistry within the plasma volume.

A range of investigational tools can be employed to try and measure changes in the plasma environment ranging from simple visible observation to complex techniques such as Cavity Ring-Down Spectroscopy (CRDS) [Zalicki 1995]. Most of the available techniques, as noted previously, suffer from being either invasive and/or complex and expensive. Optical Emission Spectroscopy (OES), which has been discussed in chapter 3, is a non-invasive technique which enables individual, optically emitting plasma species to be monitored. The method has been widely used in the field of diamond like carbon (DLC) growth where it is becoming established as a production process monitor [Plano 1991, Debroy 1994, Barholm-Hansen 1994]. OES is reasonably easy to implement, requires only modest investment and can provide rapid acquisition of data over a wide spectral range. It can also be adapted to provide spatial and temporally resolved information. In addition to providing an insight into the nature of the chemical species that occur within the plasma, it is also possible to monitor changes in the mean electron temperature (T_e) from OES data. However, as noted in chapter 3, quantitative interpretation of OES data is difficult, although this can be alleviated to some extent by the use of actinometry. In general OES is most useful for examining qualitative trends, by identifying the most interesting changes in complex environments characterised by a large number of inter-related variables, which can then be subjected to detailed quantitative study with alternative techniques. A

description of OES and the actinometry technique used in this study has been given in chapter 3.

In the following sections, the results of OES measurements made on a microwave stimulated methane-hydrogen plasma used for growing crystalline diamond are presented and discussed. Previous studies of MW methane-hydrogen plasmas have concentrated principally on the detection of emissions from atomic hydrogen species above a silicon substrate. Gomez-Aleixandre and co-workers [1993] used OES to show that the frequency of the plasma excitation source has a strong effect on the active species observed. They examined atomic hydrogen levels in plasmas excited by 35 KHz, 13.56 MHz and 2.45 GHz sources and found that the production of atomic hydrogen was most efficient for reactors employing the 2.45 GHz source. A number of workers have studied the effect of different reactor parameters on the atomic hydrogen emissions in a microwave plasma; however, although similar reactors are often used, the process parameters have tended to differ, and as the atomic H emissions vary with most of the available parameters, it can be difficult to compare results from different groups. For example, Marcus *et al.* [1991] who did not employ actinometry, used OES to study a 10 Torr, 1% CH_4 plasma and found strong variation in H_2, CH, C_2 and C_3 emissions for variation of the CH_4 fraction between 0-2%, with much smoother variation above this value. They observed rapid decrease in H_2 and H• emissions accompanied by strong increases in C_2 and CH emissions, but observed little variation in these values with pressure above about 5-10 Torr. Using argon *actinometry*, Lang *et al.* [1996] also observed a fall in H• for increasing CH_4 fraction above 1%, however their actinometric measurements indicated an *increase* in H• with both pressure and microwave power. OES measurements are often averaged over an unspecified volume of the plasma and this also does not aid the comparison of results from different groups, as most plasma parameters can be expected to show some spatial variation.

Some efforts have been made to study the role of carbon species within the plasma using OES. Clearly reported work by Balestrino *et al.* [1992] has shown that for a range of

different plasma chemistries (CH_4-H_2, CH_4-CO, C_2H_2-CO) high quality diamond growth is always correlated with a low C_2/CH emission ratio, i.e. a high value of the CH species, while the opposite case (high C_2/CH) gives rise to poor quality diamond growth with high sp^2 content. Only a few studies have considered the added complication on the plasma environment of an externally applied electric field in the form of the negative substrate bias employed during BEN. Similar difficulty in comparing data is encountered for these studies and for the same reasons described above. Beckmann *et al.* [1994] studied the effect of -170 V bias on plasma emissions in an ASTEX reactor under typical BEN conditions. They recorded a drop in atomic hydrogen concentration with increasing bias near the substrate accompanied by a slight increase in the electron temperature; they also noted an increase in electron density. However, Shigesato and co-workers [1993] reported a 20-25 % increase in the H• concentration using actinometry, together with a 6% increase in the electron temperature as monitored by the H_β/H_α ratio (the role of such ratios in monitoring electron temperature has been discussed in chapter 3). Their measurements were carried out ~1mm above the substrate, well into the sheath region of the plasma. A later study by Schreck and Stritzker [1995] examined this region (0-3 mm above substrate) using spatially resolved OES. No actinometry was employed but a large increase in the H_α signal was seen in the sheath region compared with the plasma bulk. Measurements of the Stark splitting of the H_α and H_β lines revealed electric field strengths of between 1.5-3.5 $kV\ cm^{-1}$ directly above the substrate depending on its condition (clean or diamond covered), while Doppler broadening measurements of the H_α line indicated the presence of atomic hydrogen with a least 50 eV of translational energy in this region.

It is apparent from this brief discussion that a substrate bias can influence the plasma and presumably also the balance and perhaps the identity of species incident on the substrate from the plasma. No single study has fully investigated the influence of a number of variable parameters (such as pressure, methane concentration etc.) on a wide range of optically emitting species i.e. hydrogen and hydrocarbons, whilst at the same time considering the influence of an applied substrate bias. The current study reports such

results for the nucleation of diamond on a *tungsten substrate* subjected to a negative bias and includes measurements of the spatial variation of the H•, H_β/H_α and C_2/CH plasma quantities.

5.2 Experimental Details.

The experiments to be described in this chapter were carried out in a conventional 2.45 GHz resonant standing wave reactor (ASTEX) modified to allow independent substrate biasing. This system is described in more detail in chapter 3 of this thesis and was used in the same configuration as described for the nucleation and growth experiments reported in chapter 4. Polycrystalline tungsten substrates were used throughout (50mm diameter, 6mm thick discs), prior to loading in the reactor substrates were prepared and cleaned in the manner as has already been described in the experimental section of chapter 4. The optical emission studies were carried out by varying reactor parameters, including bias, from a set of 'standard conditions' which have been given in chapter 4 but are re-stated here in table (5.1) for convenience.

Microwave power	800 Watts
Substrate temperature (t/c)	600° C
Hydrogen flow	392 sccm (typical)
Argon flow	11 sccm (typical)
Methane flow	8 sccm (typical)
Pressure	30 Torr (typical)

Table (5.1): Details of the reactor chamber conditions which are referred to in the text as the 'standard conditions'.

In separate experiments, which have been reported in chapter 4 of this thesis, this arrangement has been shown to grow good quality, randomly oriented polycrystalline diamond on tungsten and biasing at -200V shows enhancement of the nucleation density. During OES measurements, facilities to bias the substrate, in the range 0-300 volts negative with respect to the grounded chamber, were available together with digital monitoring of substrate bias and current.

Optical photography was used to record general visible changes in the macroscopic nature and geometry of the plasma. OES measurements were made using an EG&G-Princeton OMA III MCA in conjunction with a linear photodiode array and a three grating spectrophotometer. Light from the plasma was focused on the entrance slit, via a sapphire window in the chamber, by a multi-frequency optical fibre equipped with an optical lens. The head of the fibre was mounted on a slide system which allowed vertical movement of the fibre and lens assembly along the central axis of the substrate-plasma discharge; the spatial resolution was relatively low and was estimated at ~5mm from the fibre dimensions and lens arrangement. A small amount of argon (1-3%) was added to the methane-hydrogen gas mixture to act as a calibration tool for the OES studies. All the main argon lines (~811, 763, 690, 750 nm's) exhibited an approximately linear increase in intensity with argon concentration over the range 0-10%, at the same time no significant corresponding change was seen in the intensity of either the H_α or H_β lines. These observations are consistent with the requirements for actinometry noted in chapter 3 and observations by other workers e.g. Lang *et al.* [1996] who also observed linear dependence up to 5% and no effect on the atomic hydrogen emissions in a similar diamond microwave plasma.

Wavelength calibration was made using emission from the H_α, H_β and H_γ peaks, which were easily discernible, together with the emission spectra from a mercury lamp. Additional description and discussion of the optical emission and actinometry techniques used here have been given in chapter 3. The general arrangement of the experimental set-up used during this study is shown in figure (5.1).

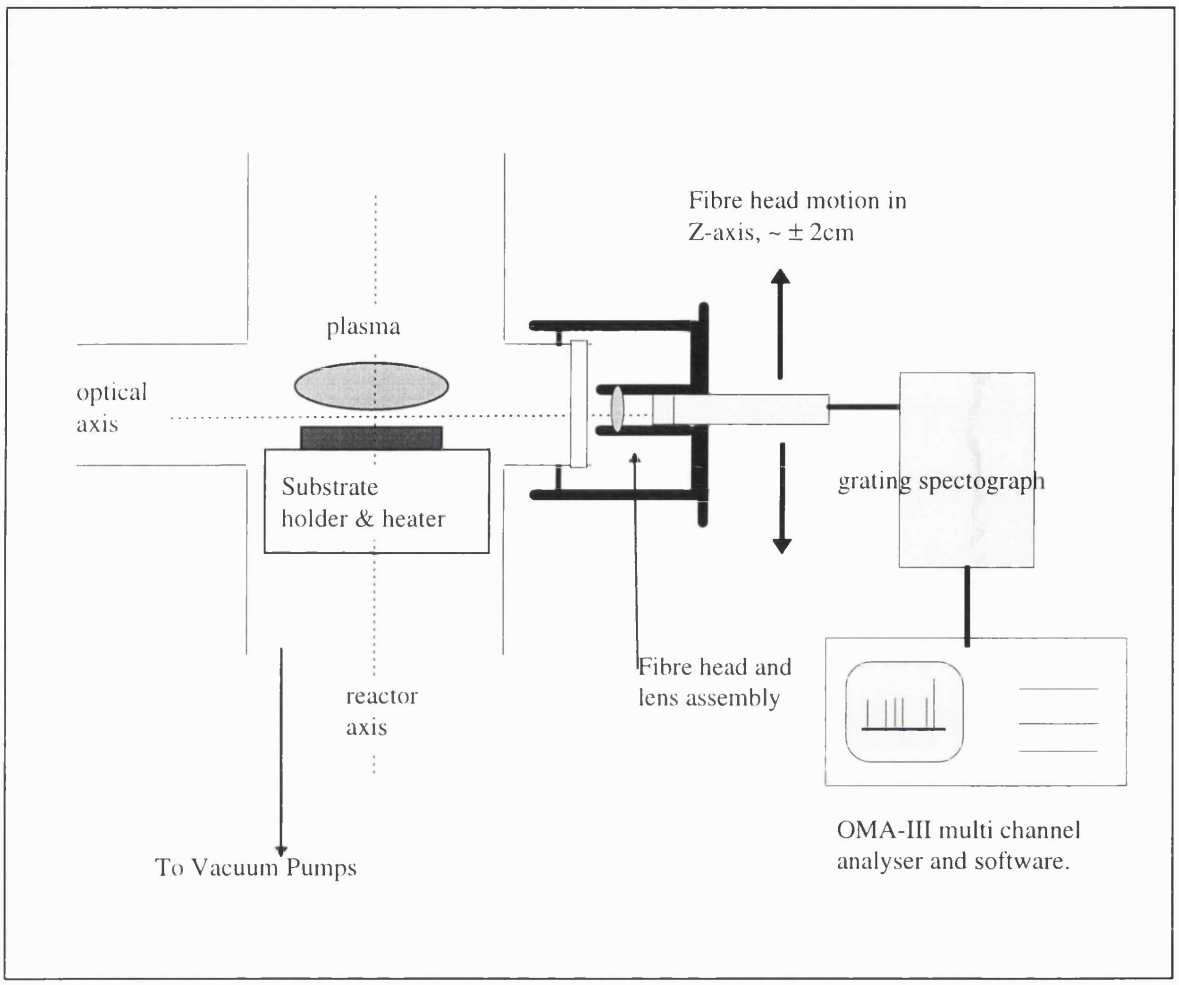

Figure (5.1): The general experimental arrangement for the optical emission measurements made in this study, showing microwave growth chamber and OES system components.

5.3 Results.

The results of the measurements made during this study are presented in the following sub-sections; first the visible changes in the plasma recorded by optical photography are given, these are followed by the results of OES measurements grouped according to the three plasma parameters mentioned previously, (H•, H_β/H_α, C_2/CH). Finally the results of spatial position measurements on these three parameters are given

5.3.1 Visible Effects.

The application of a substrate bias of -200 volts produced an immediate visible effect on the plasma ball shown clearly in the two colour photographs of figure (5.2); (a) without bias and (b) with bias. The regions of most obvious visible change are marked with roman numerals on the figure and the substrate position is identified by the arrows.

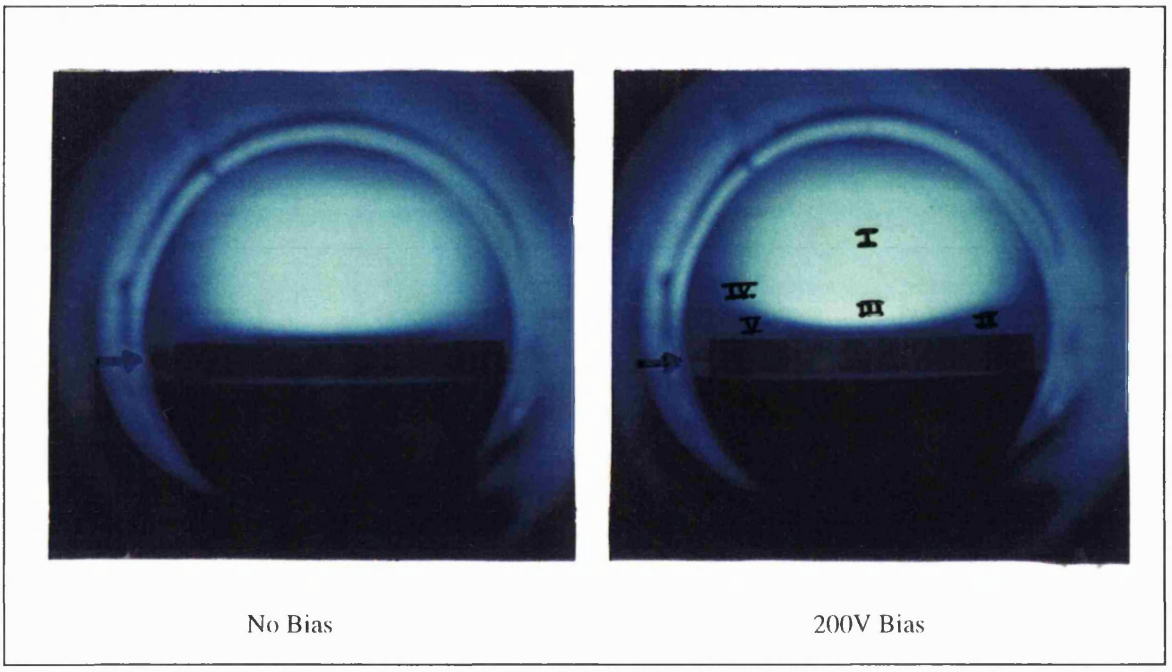

Figure (5.2): The visual effect of substrate bias of -200 V on a microwave diamond plasma; numerals indicate regions of significant change: (I) increased brightness of bulk, (II) appearance of secondary glow, (III) increased brightness near plasma base, (IV) modification to plasma shape, and (V) increase in width of dark space.

Typically the unbiased plasma appeared as a bluish coloured, flattened hemispherical, intensely emitting region centred on the substrate, confined to its vicinity and separated from the substrate by a narrow dark space a few mm's across. The detailed appearance of the plasma varied with chamber conditions; for example, the size of the plasma increased with decreasing pressure or increasing microwave power. The typical *visible* changes that occurred on application of a 200V negative bias, as indicated in figure (5.2), are summarised below:

I. A general increase in the brightness of the lower region of the plasma.

II. The appearance of a secondary glow region consisting of a bright disk within the dark-space, between the plasma base and the substrate.

III. A more marked increase in the brightness of the bulk region closest to the substrate.

IV. Modest changes in the shape of the plasma consisting of a slight flattening of the hemisphere together with some upturn of the periphery.

V. Increase in the dark space width between the plasma edge and the substrate surface.

The nature, extent and brightness of the 'secondary glow' region depended strongly on a number of factors including; the magnitude of the bias, chamber pressure and gas composition. Such visible 'gross' changes in the plasma imply that significant changes in the plasma emission spectrum can be expected.

The optical emission spectra collected over a range of chamber conditions revealed a number of sharp peaks on a broad background signal; figure (5.3) shows a typical spectrum with the principal features that were studied in this work identified. Assignments of the observed bands to emitting species were made by reference to standard molecular and atomic emission tables and previous published work as noted in chapter 3. The details of the lines and bands used in this study are summarised in table (5.2).

Emission Line (nm)	Species	Plasma Parameter
~656	H·	H_α/Ar H· concentration
~486	H·	H_β/H_α Electron temperature (T_e)
~696	Ar	Actinometer
~516	C_2	C_2/CH
~431	CH	

Table (5.2): Summary of the plasma emission lines used in this study together with assignments to emitting plasma species.

The integrated intensity of these features was monitored at a fixed point within the plasma, approximately 7mm from the substrate surface, as a function of substrate bias condition, gas pressure and methane content of the plasma feedstock gases. In addition, optical emission spectra were recorded as the probe position was moved vertically with respect to the plasma. In each case the measurements were made with and without the application of a 200V negative substrate bias. Atomic hydrogen lines were monitored at ~656 nm (H_α) and ~486 nm (H_β); actinometric calibration of the H_α signal was achieved by comparison with the Ar_{696} line [Coburn 1980]. At a given concentration of atomic hydrogen, a change in the electron energy distribution function (eedf) within the plasma can result in a change in the relative intensities of the H_β and H_α emission lines as was described in chapter 3. Thus, the ratio of H_β to H_α is commonly taken to reflect the behaviour of a mean electron temperature within the plasma, [Shigesato 1993, Lochte-Holtgreven 1968] and was also examined in this study.

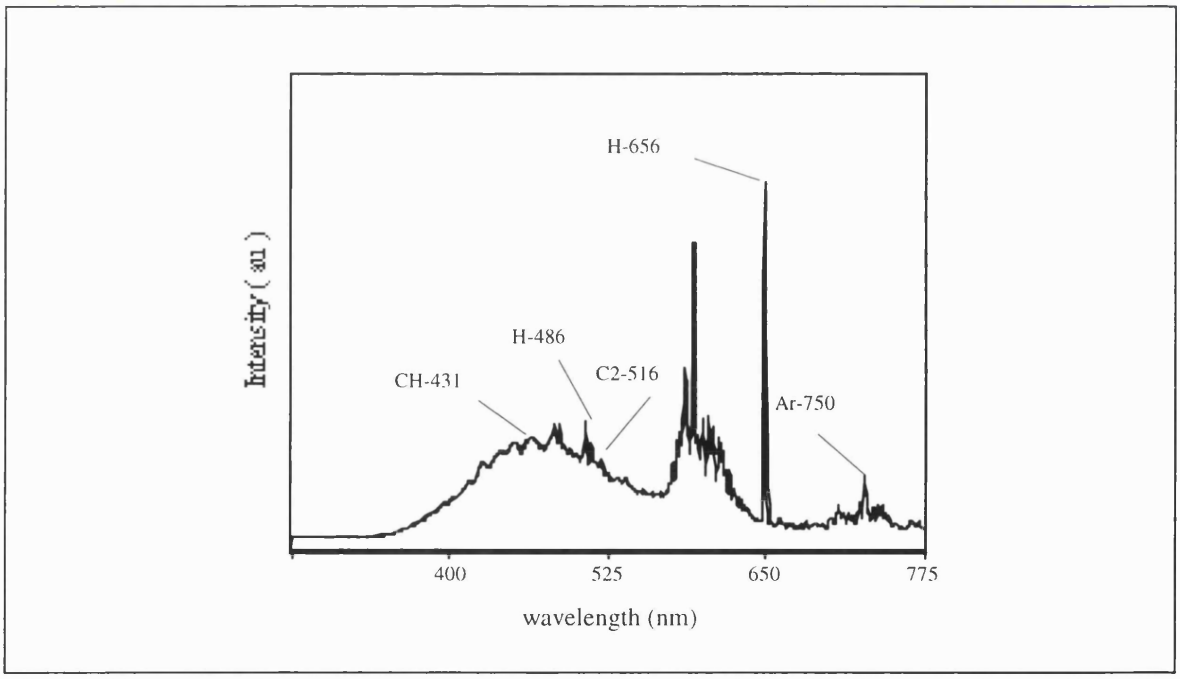

Figure (5.3): A typical optical emission spectrum recorded from a CH_4 - H_2 microwave plasma. The peaks studied in detail here are highlighted along with their characteristic wavelengths (in nm).

The role of C_1 forms (such as CH_3, CH_2 and CH) and C_2 species (C_2H_2, C_2H and C_2) during diamond CVD has been the subject of some speculation [Frencklach 1991, Beckmann 1995]. However, the primary emission lines of a number of these species, such

as CH_3, are in the vacuum ultraviolet spectral region where OES is rather difficult. As an indication of the presence of C_1 groups CH has therefore been monitored which displays a well known emission band at ~431nm; similarly, C_2 has a band at ~516nm enabling it to be studied here [Pearse 1976]. However, the use of an argon actinometer to calibrate these emissions is problematic because the excitation energies of the respective emitting states are not well matched and hence do not satisfy the requirements for effective actinometry; the results for these species are therefore presented only as ratios without this form of calibration. The implications of this approach are examined in the discussion in section (5.4). In the sections which follow, count-rates for the emitting species of interest were derived from identified emission lines and bands in the calibrated plasma spectra. Intensities were derived by determining the integrated count-rate over the peak shape with a linear background correction determined from the average intensities of a few channels either side of the peak in question. The spectral analysis was carried out with aid of a computer using the proprietary software "OMADESK" supplied with the OMA-III OES system. Where appropriate the collected spectra were corrected for background effects arising from stray ambient light and thermal noise in the detectors.

5.3.2 Atomic Hydrogen Concentration.

The results of relative changes in the measured plasma atomic hydrogen concentration, as a function of bias voltage, methane fraction and reactor pressure, are presented in figure (5.4 a-c) respectively. Figure (5.4 a) shows the H_α signal (~656nm) calibrated against the 696nm argon peak plotted for increasing bias levels at a methane concentration of 2% and a reactor pressure of 30 Torr; the plot has been normalised to the $I_{H\alpha}/I_{Ar}$ value for zero bias. A rise in the atomic hydrogen signal is apparent, with around 50% more atomic hydrogen being detected at the highest bias levels investigated here (300V). Figure (5.4 b) shows the change in atomic hydrogen concentration as the methane concentration flowing into the plasma is increased in the range 0.5 - 3%, with and without an applied bias of -200V at 30 Torr reactor pressure. Interestingly, in the absence of a bias potential the

atomic hydrogen signal falls with increasing methane concentration whilst a rather smaller fractional change occurs once a -200V potential is applied to the substrate. The effect of reactor pressure on the H• concentration measured by the $I_{H\alpha}/I_{Ar}$ signal is plotted in figure (5.4 c), again for biased and unbiased conditions at a methane concentration of 2%. In both cases, increasing the pressure from 10 to 20 Torr reduces this signal, but higher pressures lead to some recovery in the hydrogen level detected; the hydrogen signal is more intense at all pressures for the biased case. The data in figures (b) and (c) has been normalised to the unbiased value of the $I_{H\alpha}/I_{Ar}$ ratio at 0.5% CH_4 and a pressure of 10 Torr respectively; to highlight the changes in this ratio.

5.3.3 Changes in the mean electron temperature

The ratio of H_β/H_α can be used to track relative changes in the mean electron temperature in the plasma. The results of measurements to examine the behaviour of this parameter are shown in figure (5.5) in which the data have been normalised, as indicated, to the unbiased curve.

Figure (5.5a) shows the H_β/H_α ratio measured as a function of the bias voltage applied to the substrate for a 2% methane-hydrogen plasma at 30 Torr. Little change is apparent up to around 75-100V, after which a significant increase occurs up to the highest voltage investigated here (300V). The H_β/H_α ratio was also investigated as a function of methane concentration (0.5 - 3%) within the plasma feedstock gas at 30 Torr. Figure (5.5b) shows the ratio measured with and without the 200V negative substrate bias. Little change is apparent without bias, but a modest increase in the H_β/H_α ratio occurs under bias conditions, a larger increase is apparent at the higher methane concentrations.

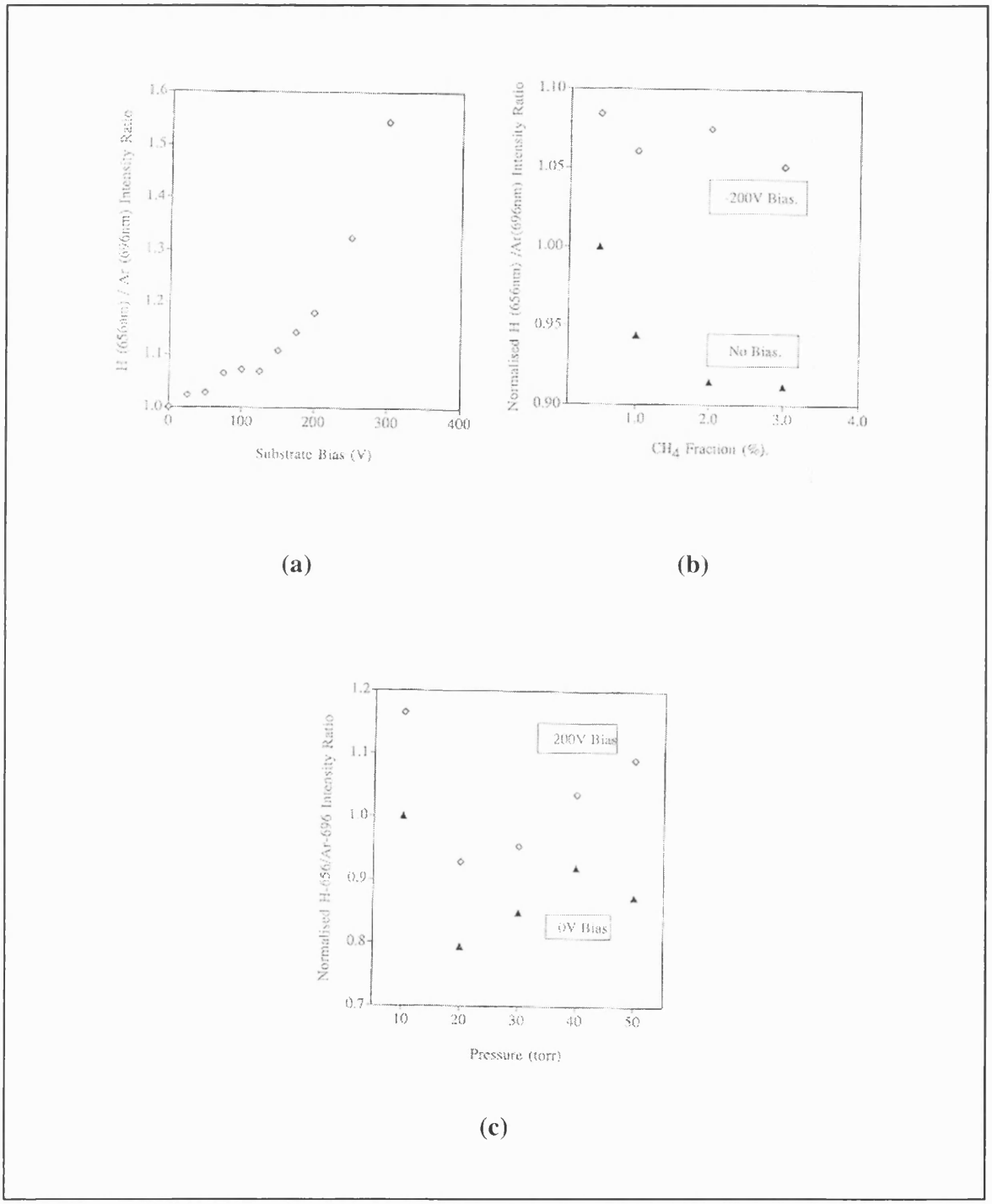

Figure (5.4): H_α/Ar_{696}emission intensity ratio (arbitary units) plotted as a function of (a) applied substrate bias (b) CH_4 mole fraction in plasma feedstock gas, for no substrate bias and a bias of -200V (c) chamber pressure, for no substrate bias and a bias of -200V.

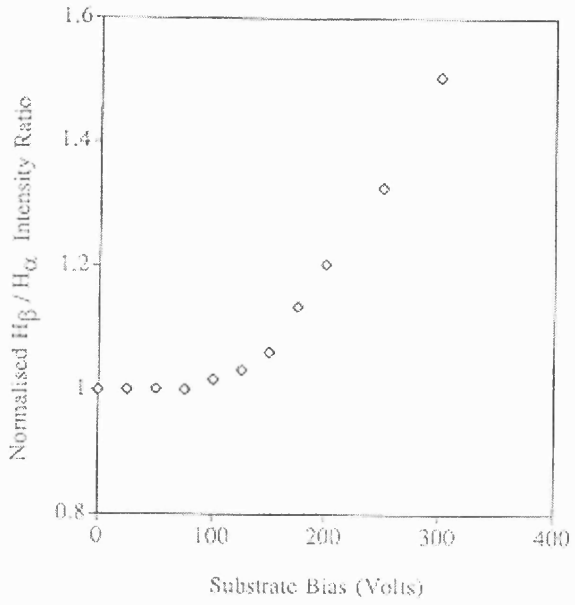

(a)

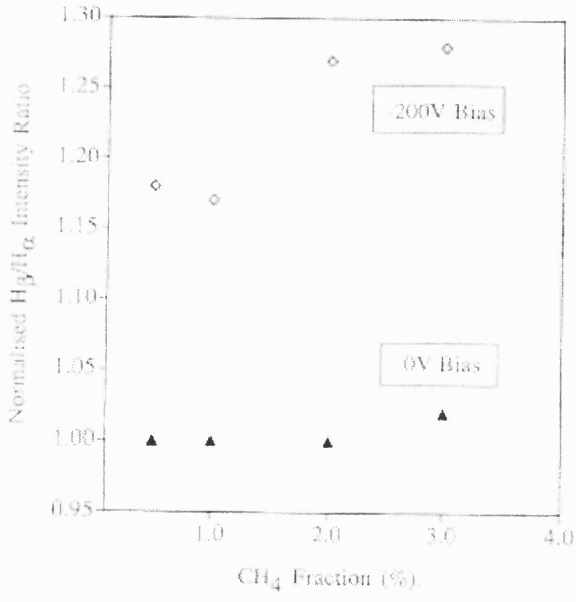

(b)

Figure (5.5): H_β/H_α emission intensity ratio (arbitary units) plotted as a function of (a) applied substrate bias (b) CH_4 mole fraction in the plasma feedstock gas, for no substrate bias and an applied bias of -200V

5.3.4 CH and C_2 emission lines

The details of the measurements made on C_2 and CH radicals are given in figure (5.6). Argon cannot be used as an actinometer for these species because the respective excitation levels are not well matched. Therefore the results are presented in the form of the ratio C_2/CH emission intensities, plotted as a function of bias voltage, methane fraction and reactor pressure. As with the previous data the figures are normalised to show relative changes in the C_2/CH parameter.

Figure (5.6a) shows the ratio of C_2 to CH emissions detected as a function of the applied bias in the range 0 to -300V; other variables were kept at the 'standard' chamber conditions given in table (5.1). A rise is apparent as the bias level exceeds 75V and at 300V the ratio has increased by more than 50%. The dependence of this ratio on methane concentration is shown in figure (5.6b), again for a reactor pressure of 30 Torr. The ratio is reduced both in the absence and presence of an applied bias over the range 0.5 - 3% methane in the feedstock gas. Variation in reactor pressure at a methane concentration of 2% gives rise to a change in the C_2/CH ratio as indicated in figure (5.6c); whilst the ratio increases for both biased and un-biased cases, a larger rise is apparent when -200V bias is applied to the substrate.

5.3.5 Spatial Dependence within the Plasma.

To investigate the changes which occurred to the CH, C_2 and hydrogen emissions near the sample surface, data was recorded as a function of probe position with respect to the substrate. In all cases the reactor pressure was maintained at 30 Torr with 2% methane in the CH_4-H_2 feedstock gas. The visible spatial effect of the bias on the plasma can be appreciated from the two photographs shown in figure (5.2); however, these changes together with the relationship of the scanned probe to the plasma are made clearer in the schematic diagram shown as figure (5.7).

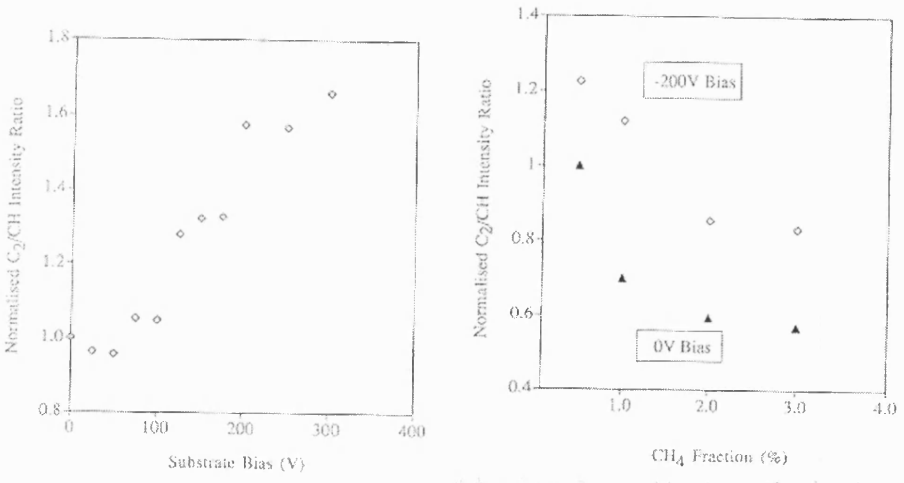

(a)

(b)

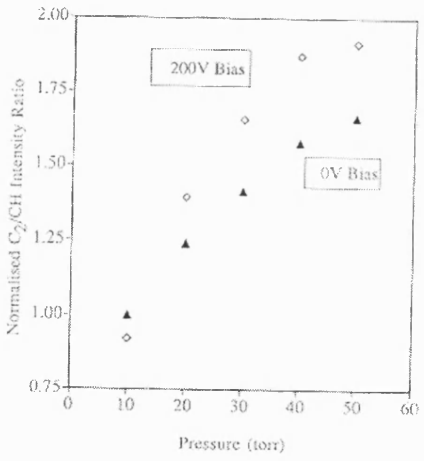

(c)

Figure (5.6): C_2/CH emission intensity ratio (arbitary units) plotted a a function of (a) substrate bias, (b) CH_4 fraction in the plasma feedstock gas, for no substrate bias and a bias of -200V and (c) chamber pressure, again for the case of no applied substrate bias and a bias of -200V.

This figure shows a scale drawing (at x2 actual size) of the plasma and was prepared from the photograph in figure (5.2 b) by careful inspection and measurement of the different luminous regions; it is by necessity a some-what idealised representation. Also marked on the figure is the approximate extent of the spatial scans, together with the position used for the fixed measurements described in sections (5.3.2)-(5.3.4), shown as a small 'X' at ~7-9 mm from the substrate surface. The data for the three principle plasma parameters, H_α/Ar_{696}, H_β/H_α and C_2/CH, as a function of position above the substrate *and with bias as a parameter* are presented in figure (5.8 a-c).

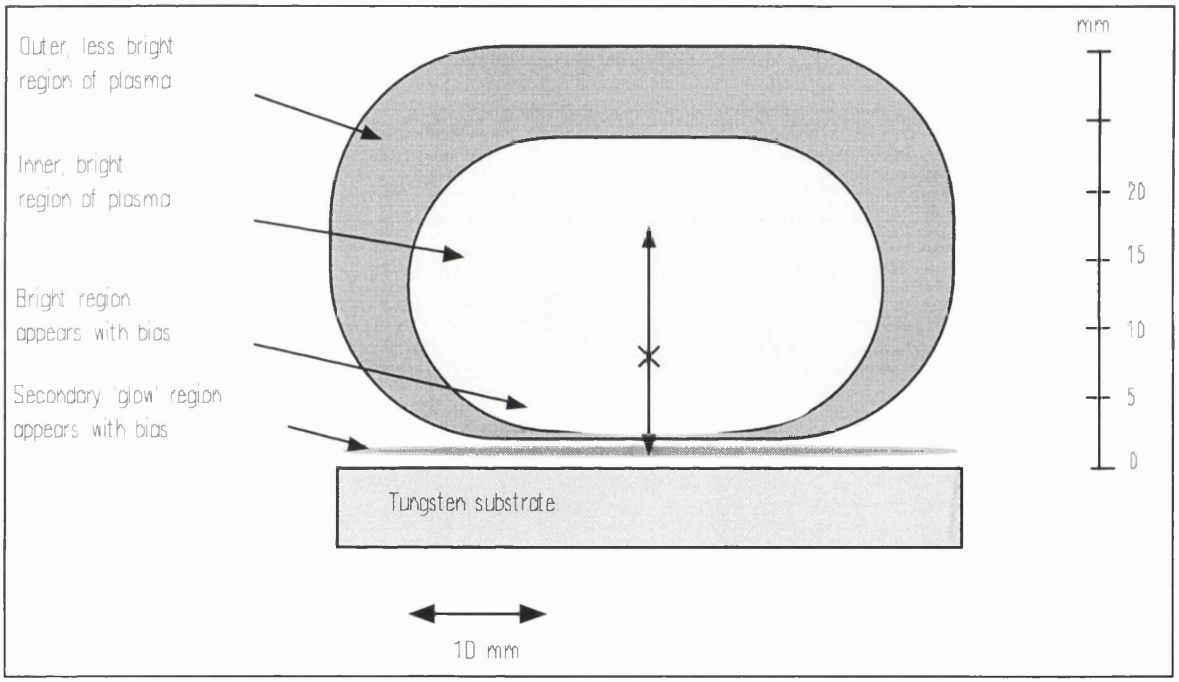

Figure (5.7): Scale drawing of the biased plasma prepared from the photograph shown in figure (5.2b); highlighting the principle regions and showing the fixed measurement position and extent of the spatial scans.

Figure (5.8 a) shows the H_α/Ar_{696} signal recorded at a distance of ~16mm from the substrate surface through to the substrate surface; the intensity of the hydrogen signal clearly declines as the substrate is approached, however at around 8-10 mm the signal recorded for the biased substrate begins to fall less sharply than for the unbiased case. Figure (5.8 b) shows the H_β/H_α ratio measured over the same distance. Whilst the unbiased and biased cases appear coincident in the bulk region of the plasma, remote from the substrate, they become strongly divergent as the volume of the plasma most visibly

affected by the bias is approached, continuing to the 'glow' region near to the surface of the substrate. In figure (5.8 c) the measured change in the C_2/CH ratio is plotted; a similar trend is apparent in both biased and unbiased cases with a peak in the ratio at around 4-6mm, but the values are consistently higher when the substrate is biased.

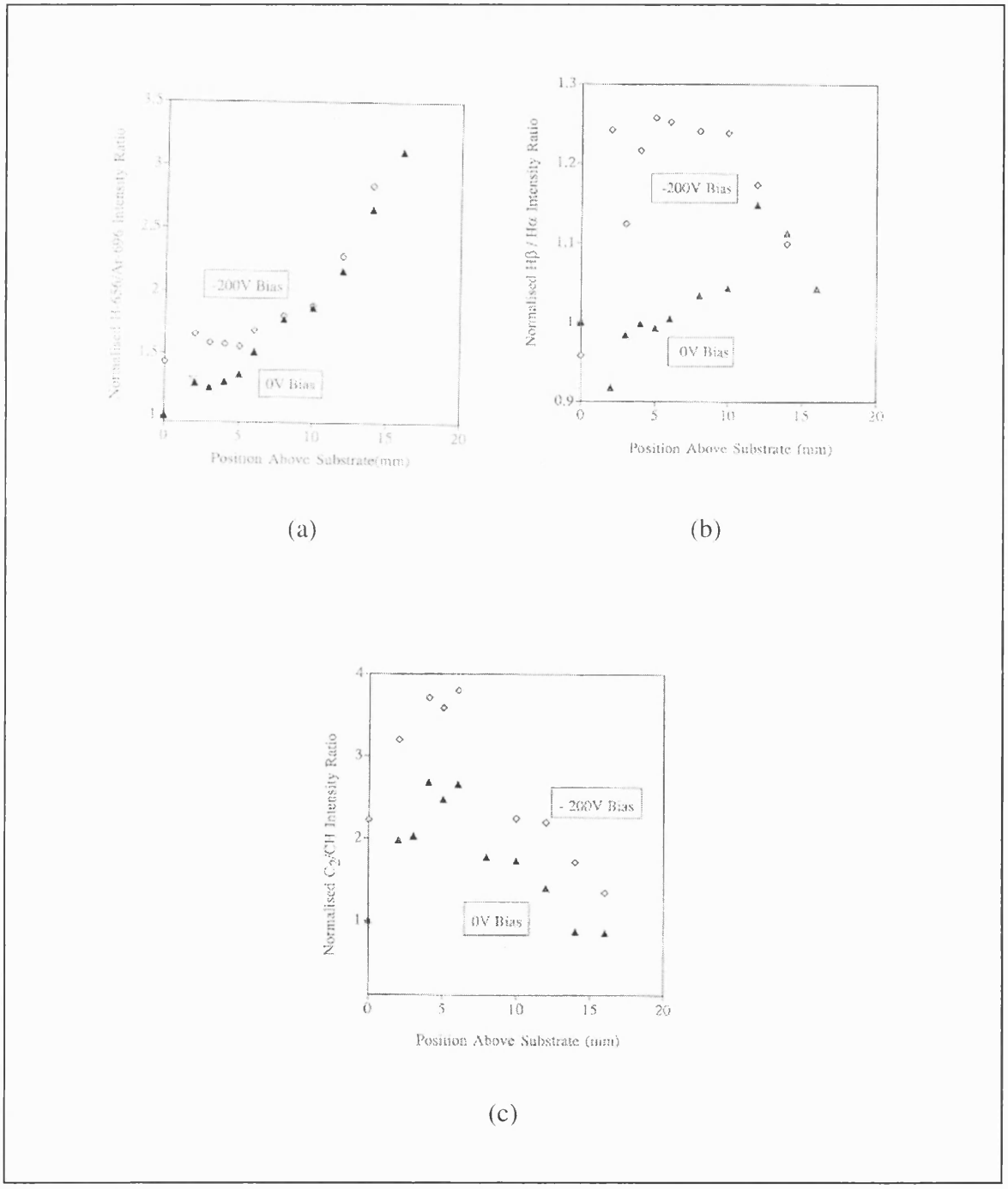

Figure (5.8): The emission intensity measured as a function of position above the substrate for (a) H_α /Ar_{696} (b) H_β/H_α and (c) C_2 / CH species (arbitrary units) with and without an applied substrate bias of -200V.

5.4 Discussion.

It is apparent from both the photographic and OES observations that the application of a negative bias to the substrate can considerably modify the plasma environment above the substrate. The intensity of optically emitting H, CH and C_2 species showed considerable changes which were most marked near to the substrate surface.

The photographs of the un-biased and biased plasma, figure (5.2), clearly show that the bias causes significant changes to the plasma, predominantly in the regions closest to the substrate. The observed changes can be understood in terms of the development of the ion rich sheath and pre-sheath regions created by movement of the free charges within the plasma volume which move to shield the plasma from the externally applied field. The electron density in a plasma falls exponentially as a charged surface is approached creating a 'sheath' region in which large electric fields exist [Dendy 1993]. Values of between 1.5-2.5 kV cm^{-1} have been have been measured directly above substrates for diamond microwave plasma conditions very similar to those studied here [Schreck 1995]. Such fields may be of sufficient magnitude to generate large numbers of electrons by impact ionisation, which could in turn significantly increase the production of active species in the nearby plasma regions driving enhanced physical and chemical processes there. Furthermore; for plasmas in which the ion temperature (T_i) is much lower than the electron temperature (T_e) and in the case of planar 'electrode-like' surfaces a pre-sheath region extends from the edge of the sheath into the plasma; significant electric fields can still exist in this pre-sheath region [Huddlestone 1965] . Above a threshold bias, the value of which depends on plasma conditions such as ionisation fraction, neutral gas density and composition; the region between the substrate (cathode-like) and the plasma edge (anode-like) resembles a parallel plate which can develop a secondary 'glow' similar to a conventional DC glow discharge; this glow can be seen very faintly in figure (5.2 b) and schematically in figure (5.7). Positive space charge regions are reported to act as 'virtual anodes' in DC glow discharge tubes [Greene 1978]. The nature of this region is considered

further in the next chapter of this thesis which reports the results of a more detailed study of this aspect of the effect of substrate bias.

Caution has to be exercised in the interpretation of OES data, especially quantitatively. However, optical emission spectroscopy has been widely used with considerable success under conditions ranging from low pressure RF discharges through to high pressure plasma-jet torches and from simple DC-glow through to microwave process plasmas [see for example, Gomez-Aleixandre 1993, Cubertafon 1995, Surendra 1992, Lang 1996]. Despite the dependence on electron temperature and density, in practice emission intensities from excited species have been broadly related to qualitative trends in species concentrations in many plasma environments including typical DLC and diamond deposition plasmas. In the field of diamond-like-carbon OES has been developed into a useful process monitor tool [Debroy 1994, Barholm-Hansen 1994]. The use of actinometry and argon actinometry in particular extends the OES technique [Coburn 1980] and allows quantitative data to be extracted from the observed trends in the emission intensities. It is important to keep the argon concentration below about 5% of the gas mix to ensure that the actinometer does not itself perturb the plasma processes being measured [Coburn 1980]. As noted in chapter 3, in the diamond and DLC fields, actinometry has been used by a number of workers to monitor changes in the atomic hydrogen concentration in the plasma. Recently a detailed study of the validity of actinometry under typical diamond growth plasma conditions has been made, [Gicquel 1998]. It was shown by comparison with absolute TALIF measurements that OES actinometry is valid for modest plasma power densities (9 - 15 Wcm^{-3}) under typical diamond deposition conditions i.e. pressure ~ 25mB and low methane fractions in an H_2 background. By comparison a value of around ~13 Wcm^{-3} has been estimated for the plasma power density in this study from the applied microwave power of 800 W and an assessment of the plasma volume made from figure (5.7). The power density of the plasma studied here is well within the range for valid actinometry, while the other conditions; pressure, flow and gas composition were very similar to those studied by Gicquel *et al.* In addition the argon level in the current study, at

3%, was well below the level of ~5% at which the actinometer may begin to perturb the plasma significantly [Coburn 1980]. In any case, even when the conditions for actinometry have not been rigorously satisfied, actinometry can still yield a useful measure of change in the true species concentration [Lang 1996].

The use of the C_2/CH ratio to characterise the emissions from carbon/hydrocarbon species in the plasma has arisen because actinometry cannot be used as the argon excitation levels are not well matched to these species. Both of the emission bands studied here; ~431 nm for CH and ~516 nm for C_2 have been studied elsewhere in the literature and changes in the emission intensities of these bands have been linked to changes in the concentrations of these species by a number of authors under a range of plasma conditions, [e.g. Ricard 1993, Balestrino 1993, Cubertafon 1995]. The C_2 and CH bands are quite close in wavelength and taking the ratio of the intensities should reduce systematic differences arising from, for example, geometry changes in the plasma and solid angle changes during spatial scanning. It would also be expected that the ratio, while not fully actinometric, would largely remove the effects of changes in the electron density within the plasma. In addition the ratio of C_2/CH emission intensity at the 516 nm and 431 nm bands has been correlated to the quality of diamond deposition in terms of sp^2 content [Balestrino 1992], under reactor conditions close to those used in this study. It was shown by these authors that a high C_2/CH ratio lead to poor deposition with a high non-diamond carbon content while a low value of the ratio occurred under conditions of high quality diamond deposition. The approach of taking emission ratios, when no suitable actinometer is available, has been reported in a number of studies [Leedy 1995, Balestrino 1992] and is a suitable approach for this study in which the primary objective was to establish the qualitative trends and relative changes caused by the substrate bias; accurate absolute measurements will require recourse to alternative techniques.

5.4.1 Atomic Hydrogen

In a previous study of a methane-hydrogen-argon plasma by Shigesato and co-workers [993] hydrogen emission spectra were recorded just above a silicon substrate (~1mm). The H_α signal was seen to increase for applied bias values up to -170V, however only a few data points were measured; the authors noted that little effect was apparent when they monitored the central region of their plasma. Schreck [1995] used spatially resolved OES, but without actinometry, and also detected a strong increase in the H_α signal near the surface of both Si and diamond substrates when a -200V bias was applied (0.4% methane, 20mbar, no argon actinometer). The data recorded here for a *tungsten substrate* (figures 5.4(a) and 5.8(a)) is in general agreement with these observations. In contrast, Beckmann *et al.*[1994] observed little change in the hydrogen concentration near the surface when a pristine silicon substrate was used and a decrease in near surface atomic H when a diamond covered sample was studied. However, the level of argon used within the plasma by these workers, at 10%, may have been high enough to modify the CH_4-H_2 plasma characteristics [Coburn 1979] and may have influenced their observations. In the current study, the concentration of atomic hydrogen shows a modest increase with bias up to around 120V, figure(5.4a), after which the level begins to increase superlinearly with bias up to 300 V, the maximum bias studied here. Beyond this bias level, under the reactor conditions used here, the plasma became unstable and DC breakdown was observed which could potentially have caused damage to the power supply. In a methane-hydrogen plasma the main sources of atomic hydrogen are from electron impact dissociation of H_2 and CH_4 via the reactions[Goodwin 1998]:

$$H_2 + e^- \rightarrow H + H + e^- \qquad (5.1)$$

$$CH_4 + e^- \rightarrow CH_3 + H + e^- \qquad (5.2)$$

The rate constants for these are nearly equal, 7.1×10^{-11} s^{-1} and 6.9×10^{-11} s^{-1} respectively [Bou 1992], therefore the dominant source of atomic hydrogen arises from the H_2 neutral supply from the background gas, as H_2 comprises over 90% of the total mole fraction.

Clearly the production rate of H• depends on the electron density and the fraction of electron population, related to $T_{e,,}$ with sufficient energy to cause dissociation. Others [Kulisch 1996, Schreck 1996, M^{c}Ginnis 1995] have suggested, based on the measured I-V characteristics of the substrate bias, that electrons can gain sufficient energy in the sheath region to cause impact ionisation resulting in electron multiplication, hence explaining the rapidly increasing bias current which has been observed by these authors. There are interesting correlation's between the shapes of the bias current-voltage curves, which have also been measured during the current study, and the bias voltage-atomic hydrogen curve shown in figure (5.4a). The details of these measurements however are discussed in the next chapter, together with the results of high resolution scans of the immediate region above the substrate. At this point it is sufficient to note that the shape of the curve in figure (5.4a) could be explained by an initial increase in the electron density, during which there is no significant increase in T_e ,as indicated by the H_β/H_α ratio, figure (5.5a). This is then followed by a rapid increase in atomic hydrogen at biases above about 120 V, possibly arising from electron multiplication in the high sheath fields. At the same time the H_β/H_α ratio increases suggesting that electrons in this region are gaining significant energy from the sheath fields. The suggestion that the electron density increases, is supported by the observation that the entire emission continuum shows a remarkably constant increase over the whole spectral range, which reaches ~15-20% for a bias of -200V; a similar increase has been noted by others [Kulisch 1996]. The relatively sharp upturn at ~120V may reflect the influence of the threshold energies, which are characteristic of inelastic reactions like those expressed in equations (5.1) and (5.2) above.

The effect of varying the methane content of the feedstock gas on the concentration of atomic hydrogen above a silicon substrate has also been explored by Beckmann *et al.* [1994]. A linear decrease was found over the range 0 - 7% CH_4 within a 20 Torr methane-hydrogen plasma, while an increase was observed with a bias of -210V, which the authors were unable to explain. Mucha and co-workers [1989] measured a decrease in the atomic hydrogen concentration within a 30 Torr methane - hydrogen plasma as the methane

concentration was increased over a similar range, but bias was not studied. Over the range examined in the current study (0.5 - 3%), a decrease in the H_α signal was also apparent when no bias was present (as may be intuitively expected), but a rather smaller decrease is measured when a -200V bias is placed on the substrate, figure (5.4b). The decrease in H• could be understood in terms of the rapid reaction, equation (5.3), which occurs between methane and atomic hydrogen to produce methyl and molecular hydrogen, when methane is introduced into a hydrogen plasma [Bou 1992]. Very recently a similar depletion (~10-20%) of H• with methane addition has been measured by actinometry [Lang 1996, Gicquel 1998] and confirmed by TALIF measurements [Gicquele 1998], under microwave plasma conditions similar to those used here. In addition the depletion effect was observed to be very much less at higher power densities and the H• mole fraction was observed to be higher at the higher powers. The authors used chemical kinetic models to demonstrate that the higher the H• mole fraction the lower the expected depletion due to CH_4 addition.

$$CH_4 + H\bullet \rightarrow CH_3 + H_2 \qquad (5.3)$$
(reaction rate $7.75 \times 10^{-14} s^{-1}$)

The reduction in the apparent loss of H• when a bias is applied may now be explained in these terms, i.e. in the regions of the plasma close to the substrate, applying a bias results in an increase in H• similar to the effect of an increase in the power density. A possible alternative explanation is that as there is much more H• present with the bias in place, then the loss due to reaction (5.3) represents a smaller fraction of the total than is the case for the no bias situation. A small downward trend of around 3% in H• level is evident when CH_4 is added in the presence of bias. These results imply that under conditions of a 200V negative bias, the measured region (centred around 7mm from the substrate surface) is not significantly depleted in atomic hydrogen when the methane content of the feedstock gas is increased. To the contrary, the increase in H• generated by the bias, more than offsets any losses due to CH_4 addition, even to quite high methane fractions.

The effect of pressure in the range 50-100 mB on the atomic hydrogen concentration has been examined using OES actinometry in a detailed study by Lang *et al.* [Lang 1996]. A near linear increase of about a factor of 2.5 was seen; measurements using all three principle hydrogen emission lines (α,β,γ) were in close agreement. Shigesato and co-workers [1993] found a similar behaviour for the α and β hydrogen lines in the pressure range ~30-45 mB, after which they observed saturation, to ~90 mB. However, they did not use actinometry and this probably accounts for the difference in observations of the these two studies. The measurements made in the current study are in qualitative agreement with these studies over the pressure range 20-50 Torr (~25-65 mB), figure (5.4 c). However, below 20 Torr an increase in H• was observed here, but this cannot be compared with the previous measurements because this pressure region was not explored in those studies. The measured pressure characteristics display a distinct minimum at ~20 Torr and the shape of the curve with bias present is very similar, with the bias provoking the expected increase in H• which is similar over the whole pressure range. The shape of the H•-pressure curve could be explained in terms of the competition between the decreasing rate of generation due to reducing H_2 density [Shigesato 1993] and the increasing rate due to higher mean electron temperature arising from the increasing mean free path at the lower pressures [Bou 1992]; it should be noted that the microwave power was held constant during these measurements. As the modelling of Bou *et al.* indicates, the increase in H•, even for small increases in T_e , can be very large and this could explain the very rapid increase in H• observed here for pressures below 20 Torr. However, the steep increase which is observed would be expected to eventually turn over as the pressure continues to reduce because the decrease in H_2 dissociation remains linear with density whereas the cross-section for H_2 dissociation peaks at electron energies of around 15 eV and drops rapidly thereafter with ionisation collisions becoming dominant at 20 eV [Saitoh 1994].

The axial variation of the atomic hydrogen concentration without bias, shown in figure(5.8a), exhibits a monotonic increase moving from the substrate to the plasma bulk (0-16mm above substrate); this plot can be compared to the scale drawing of the plasma

shown in figure (5.7). The strong decrease in H• concentration from the value in the bulk, is consistent with both the spatial variation in the electric field intensity, characteristic of microwave discharges, and also the influence of the substrate, which acts as a sink for H• due to the high surface recombination rate there [Goodwin 1998]. Variation in the ratio of the argon and H_α rate constants, ($k_{argon}/k_{H\alpha}$), which can occur under conditions where T_e varies, as is likely for spatial scans, suggests caution when interpreting the OES data in figure (5.8a). However recent measurements, in which spatially resolved axial TALIF measurements of H• were compared to line-of-sight averaged OES measurements, show extremely close agreement between the two methods as is shown in figure (5.9) redrawn from Gicquel *et al.* [Gicquel 1998].

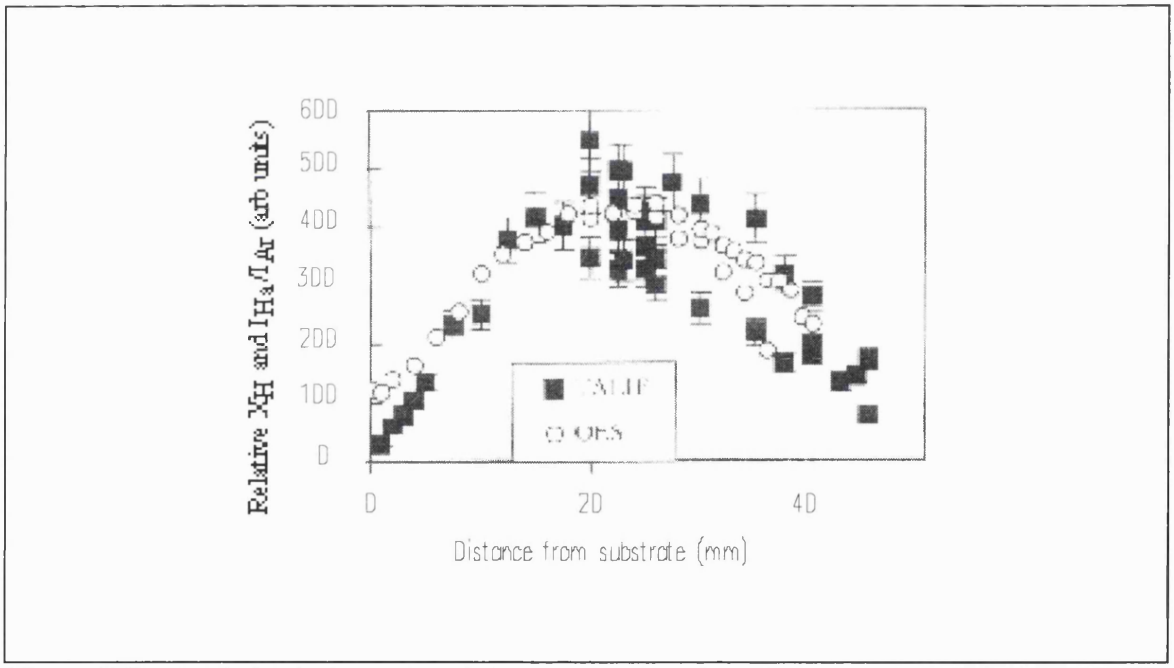

Figure (5.9): Axial distribution of the relative concentration of atomic hydrogen as measured by TALIF-solid symbols and actinometric OES-open symbols; plasma conditions were very similar to those used in the current study. [Redrawn from Gicquel 1998].

Application of the bias results in a significant change to the measured H• profile especially within a distance of ~10mm of the substrate surface and this correlates well with the increase in the brightness of the regions of the plasma nearest to the substrate, as shown in the photograph of figure (5.2 b) and highlighted in the scale drawing, figure (5.7). The influence of the bias reduces rapidly when moving towards the plasma bulk (10-20 mm). A small effect is apparent within the bulk which could be due to a small, but significant

fraction of the applied bias being dropped across the plasma instead of the sheath. Calculations by Schreck *et al.* [1995], based on their measurements of a biased diamond plasma, have indicated that up to ~40 V of an applied bias of -200 volts was dropped across the plasma bulk in their reactor,[Schreck 1996]. Given that there are not expected to be any significant radial gradients on the axis, then considering the relatively small increase in H• which is apparent in the bulk, the most likely explanation of the increase in the H• profile nearer to the surface is in terms of an increase in the H• generation rate in this region, which is consistent with the mechanisms which were discussed previously.

5.4.2 Electron Temperature

The mean electron temperature, as represented by the H_β/H_α ratio, is strongly affected by the application of a -200V bias over the region corresponding to the visible changes highlighted in figure (5.7) (~0-10 mm above the substrate) under the conditions used here, (figures 5.5a and 5.8b). These results show general agreement with the observations of Shigesato *et. al* [1993] who observed a strong increase in the H_β/H_α ratio with bias preceded by an initial flat region in which T_e showed little change with bias for a pure hydrogen plasma. The increase in T_e observed here could be explained in terms of the additional energy gained by electrons influenced by the high fields within the sheath and pre-sheath regions of the plasma which are generated by the application of the substrate bias. For a negative bias of 200 V, electric field strengths of between 1.5-3.5 kV cm^{-1} have been measured in the sheath [Schreck 1996] corresponding to around 0.2 eV μm^{-1} for an electron travelling in the sheath. Under the conditions in this study, the mean electron temperatures, without the additional bias field, are expected to be of the order of 1-3 eV [Gicquel 1998] together with a mean free path of the order of several microns. Therefore, increases of 20 - 30% in T_e due to the applied bias, for electrons in the vicinity of the sheath, as measured here are feasible. An alternative possibility is that enhanced H_2 dissociation could distort the H_β/H_α ratio via production of H(n=4), however this

possibility seems less likely as the H(n=4) level has a higher energy than the H(n=3) level and also a ratio of emission intensities taken for argon (Ar_{750}/Ar_{811}) reported a similar trend, i.e. indicate an increase in T_e, , see for example chapter 6. The spatial scans shown in figure (5.8) were made at a rather low spatial resolution and so the details of the T_e profile should be considered with caution; however, it is worth noting that the 'peak' which appears in the figure at ~1-2 mm appears to coincide approximately with the visible position of the secondary glow feature which is seen to develop between the plasma and substrate at the higher biases, figures (5.2 b & 5.7). This region of the plasma is discussed in more detail in chapter 6, where the results of higher resolutions scans are presented.

The increase in electron temperature in this region could be a contributing factor in the formation of higher concentrations of near surface atomic hydrogen when a bias is applied. Detailed plasma modelling by Bou *et al.* [1992] has indicated that a number of important plasma species may be very sensitive to the electron temperature. For example, in their model a 16% increase in T_e resulted in an increase in atomic hydrogen of around one and a half orders of magnitude. The results of the present study indicate that applying a bias results in an increase in the electron temperature together with a proportionally larger increase in atomic hydrogen concentration, in line with the trend predicted by their model. Other trends which could be identified from their work (e.g. CH concentration) are also in broad agreement with trends measured here.

Interestingly, figure (5.3b) indicates that under bias conditions an increase in the methane fraction appears to lead to a small increase in the mean electron temperature of ~5-6 %. A very speculative explanation is that a small increase in electron density occurs because CH_4 is more efficiently ionised than H_2 (e.g. threshold 12.6 eV, cross-section $4x10^{-16}$ cm^2 for CH_4 c.f. H_2 15.4 eV, $1x10^{-16}$ cm^2) [Lang 1996]. The higher plasma density should then lead to a reduced sheath width and consequently higher electric field strengths in that region which could then increase the electron temperature there. However, the change

observed is very small and in view of the low number of data points may not be very meaningful.

5.4.3 Hydrocarbons.

Recent reviews, [e.g. Goodwin and Butler 1998], have indicated that under typical microwave diamond plasma conditions there is a consensus that the growth of high quality diamond is primarily determined by the presence in the gas phase of the methyl (CH_3) radical, while C_2 forms appear more detrimental to high quality growth. As was previously discussed, the C_2/CH emission ratio has been correlated by other workers with the subsequent quality of the deposited film, with a high value leading to a poor film with high sp^2 content, [Balestrino 1992]. In lieu of suitable emissions from many of the other C_1 and C_2 species, the emissions from these two radicals have been taken as pointers to the presence of other C_1 and C_2 forms. It is widely acknowledged that bias is detrimental to film quality if continued into the growth phase,[e.g Bozeman 1998] and as shown here and by others the bias can strongly modify the nature of the plasma in the vicinity of the substrate. It is therefore of considerable interest to consider the effects of the substrate bias on the C_2 and CH line emissions. As noted earlier, a study by Balestrino *et al.* [1992] has shown that high quality deposition was correlated with high CH emissions, this was the case for a range of gas-feed chemistries for growth above a silicon substrate in the absence of any bias. In the current study, it is apparent that the application of a negative bias to the *metal substrate* considerably enhances the C_2 line intensity emanating from the plasma compared to the CH signal (figure 5.6a). This effect was observed for all of the methane concentrations within the feedstock gas measured here, but was larger for the higher methane levels (figure 5.6b); increasing the reactor pressure (20 to 50 Torr) appeared to enhance the effect further (figure 5.6c). The spatial scan, figure (5.8 c) indicates that the applied bias enhances the C_2 line intensity compared to the CH intensity and this effect is strongest in the vicinity of the substrate surface, but persists over the whole region up to

~10-12 mm above the substrate surface. If it is supposed, despite the lack of a suitable actinometer, that changes in these line intensities can be taken as representative of changes in the concentration in these species, then increases in the C_2 concentration can be understood in terms of the hydrocarbon chemistry that is likely to occur within the plasma [Frencklach 1991, Beckmann 1995, Bou 1992]. As the methane concentration is increased the likelihood of collisions between carbon containing fragments that have previously undergone atomic hydrogen abstraction increases; the formation of C_2 species will then be enhanced. A similar effect can be expected when the pressure is increased. Furthermore it has been shown that the increase in C_2H compared with CH should be faster for small increases in either or both of N_e and T_e and there are a number of possible routes for the formation of C_2 which have been listed by [Bou 1992], most of these occur via H abstraction from C_2H. It is therefore reasonable to assume that the C_2 concentration may follow changes in the C_2H concentration. Clearly these explanations for why the C_2/CH ratio may increase with bias are rather speculative, as they are based on descriptions of the plasma which are at best incomplete. Models often assume some form of equilibrium for the gas phase chemistry to keep calculations tractable, however very important species, in particular atomic hydrogen, are present in super-equilibrium amounts, especially close to the substrate and drive chemical processes would not be significant under equilibrium conditions [Goodwin 1998]. The presence of a bias which appears to elevate the atomic hydrogen levels still further could be expected to complicate this situation.

The measurements recorded here indicate that higher levels of atomic hydrogen and of C_2 species compared to CH, can be produced from a microwave methane-hydrogen plasma directly above a negatively biased metal substrate. Both of these effects appear more significant near to the surface of the substrate compared to the central region of the plasma. It is interesting to note the similarity in some of the trends observed above a metal substrate with those reported previously on silicon. It can be expected that the voltage dropped across the near surface (sheath) region will lead to ionised and other high energy species impacting upon the substrate; other studies have indicated that species with energies of ~50

eV exist close to the substrate surface [Schreck 1995]. Under these conditions secondary electron emission from the substrate could be expected and is implied by the secondary glow which appears between the biased substrate and the microwave plasma. Energetic electrons, accelerated across the sheath, could lead to enhanced inelastic ionisation and dissociation processes in this region, which could explain the elevated atomic hydrogen concentration which are indicated by the measurements made here. Atomic hydrogen drives much of the plasma chemistry and increases in the atomic hydrogen levels could account for the higher hydrocarbon signals seen here. Thus the bias enhanced nucleation process may depend upon the presence of higher concentrations of C_2 and H neutrals or energetic ionic forms of these species. It can be speculated for example, that the formation of the metal-carbide layer and the subsequent α-carbon layers, which form prior to nucleation on carbide forming substrates [Lux 1991], is speeded up by an enhanced flux of C_2 carbon species during biasing. The formation of carbon nuclei of a critical size may also encouraged by the enhanced arrival rate of carbon (from C_2 as opposed to C_1 forms) whilst the reduction in atomic hydrogen concentration that may accompany other methods for achieving this enhanced carbon flux is avoided. Since atomic hydrogen is thought to be important for the removal of non-diamond forms of carbon, complete graphitisation of the surface can thus be prevented.

5.5 Summary.

This chapter has presented the results of a comprehensive study, by optical emission spectroscopy, of the effects of bias on a typical diamond microwave plasma above a tungsten metal substrate. Atomic hydrogen concentration, electron temperature and the C_2/CH ratio were studied as a function of substrate bias. The effect of reactor pressure and methane fraction were also compared at substrate potentials of 0 and -200V. Additionally, the axial variation of these three plasma parameters was studied from substrate to plasma bulk; also with bias as a parameter. Although some studies of these quantities, under the

influence of a bias, have previously been reported, the earlier work concentrated exclusively on the effects above a silicon substrate and were not fully comprehensive. In particular the C_2/CH ratio has not been previously considered and only one report of spatially resolved measurements above a biased substrate was found [Schreck 1995]. Furthermore the total number of OES studies which have considered bias are relatively few and in some cases the results appear contradictory. However it is difficult to assess the meaning of such differences because the plasma parameters and reactor conditions vary between studies. To the author's knowledge the current study represents the first attempt to examine a wide range of plasma quantities simultaneously as a function of systematic variation in reactor parameters and bias.

The study clearly suggests that the region of the plasma within ~10-12 mm of the substrate is strongly influenced by the applied bias. The results indicate that biasing appears to promote a combination of elevated C_2/CH and atomic hydrogen concentration which would be difficult to obtain by simple variation of a single growth parameter, such as, for example, the methane fraction. The presence of C_2 species during growth is generally regarded as a sign that poor thin film material will result; that these forms are implicated during BEN underlines the differing processes that occur during the nucleation and growth phases of film formation. Comparison with reported work carried out on silicon would suggest that the BEN induced changes above a clean substrate (non-diamond) are qualitatively independent of the substrate material.

However, OES is not able to give a full picture. Only a limited number of the chemical fragments known to be present within a typical diamond growth plasma can be readily studied by this technique and a detailed insight into the energetics of each species is not possible. It must be emphasised that generally OES reports qualitative trends, although the use of actinometry and intensity ratios can improve the confidence and degree of 'quantativity' of the data. None-the-less, many of the measurements made here show good correlation with the alternative techniques and other OES measurements reported

elsewhere in the literature. Simple qualitative observations, such as the rapid onset of surface carbon saturation which occurs under bias, also would suggest that during biasing the dominant mechanism responsible for carbon deposition on the substrate is changed over the situation pertaining during high quality growth.

5.6 References.

Balestrino G., Marinelli M., Milani E., Paoletti A., Pinter I., Tebano A. and Paroli P., [1993], *Appl. Phys. Lett.*, **62** , 879

Barholm-Hansen C., Bentzon M.D. and Hansen J.B., [1994], *Diam. and Relat. Mater.*, **4**, 69.

Beckmann R., Sobisch B. and Kulisch W., [1995], *Diam. and Relat. Mater.*, **4**, 256.

Beckmann R., Sobisch B., Kulisch W. and Rau C., [1994], *Diam. and Relat. Mater.*, **3**, 555.

Bou P., Vandenbulcke R., Herbin R. and Hillion F., [1992], *J. Mater. Res.*, **7**, 2151.

Bozeman S.P., Stoner B.R. and Glass J.T., [1998], in *Handbook of Industrial Diamonds and Diamond Films*, eds. Prelas M.A., Popovici G. and Bigelow L.K., (Marcel Dekker Inc.), New York, USA.

Coburn J.W.and Chen M., [1980], *J. Appl. Phys.*, **51**, 3134.

Cubertafon J.C., Chenevier M., Campargue A., Verven G. and Priem T., [1995], *Diam. and Relat Mater.*, **4**, 350.

Debroy T., Kumar S. and Tankala K., [1994], *Diam. and Relat. Mater.*, **4**, 69.

Dendy R., [1993], *Plasma Physics: An Introductory Course.*, Cambridge University Press, UK.

Fox B.A, Stoner B.R, Malta D.M, Ellis P.J.,Glass J.T and Sivaziian F.R., [1994], *Diam. and Relat. Mater.* **3**, 382.

Frenklach M. and Wang H., {1991], *Phys. Rev. B.*, **43**, 1520.

Gerber J., M. Weiler M., O. Sohr O., K. Jung K. and H. Ehrardt H., [1994], *Diam. and Relat. Mater.*, **3**, 506.

Gicquel A, Chenevier M. and Lefebvre M., [1998], in Chapt.19 in, *Handbook of Industrial Diamonds and Diamond Films*, eds. Prelas M.A., Popovici G. and Bigelow L.K., (Marcel Dekker Inc.), New York, USA.

Gomez-Aleixadre C., Sanchez O., Castro A. and Albella J.M., [1993], *J. Appl. Phys.*, **74**, 3752.

Goodwin D.G. and Butler J.E., [1998], in Chapt. 11, *Handbook of Industrial Diamonds and Diamond Films*, eds. Prelas M.A., Popovici G. and Bigelow L.K., (Marcel Dekker Inc.), New York, USA.

Greene J.E., [1978], *J. Vac.Sci.Tech.*, **15**, 1718.

Huddlestone R.H. and Leonard S.L., [1965], *Plasma Diagnostic Techniques*, Academic Press, New York.

Jeng J.G, Tuan H.S., Salat R.F. and Fricano G.J., [1990], *Appl. Phys. Lett.*, **56,** 1968.

Lang T., Stiegler J., Kaenel Y.von and Blank E., [1996], *Diam. and Relat Mater.,* **5**, 1171.

Leedy K.D. and Rigsby J.M., [1994], *Appl. Phys. Lett.,* **66**, 676.

Lochte-Holtgreven (ed), [1968], *Plasma Diagnostics*, North-Holland Publishing Company, Amsterdam.

Lux B. and Haubner R., [1991], in *Diamond and Diamond-like Films and Coatings*, (eds. Clusing R.E., Horton L.L., Angus J.C. and Koidl P.), Plenum Press, New York, pp 579.

Marcus B., MermouxM., Vinet F., Campargue A. and Chenevier M., [1991], *Surface & Coatings Technology.*,**47**,608.

McGinnis S.P., Kelly M.A. and Hagstrom S.B, [1995], *Appl. Phys. Lett.*, **66**, 3117.

Mucha J.A., Flamm D.L. and Ibbotson D.E., [1989], *J. Appl. Phys.*, **65**

Pearse R.W.B. and Gaydon A.G., [1976], *The Identification of Molecular Spectra* 4^{th} *Ed.*, Chapman and Hall, John Wiley and Sons, New York and London.

Plano L.S., [1991], *SPIE (Applied Spectroscopy in Materials Science)*, **1437**, 13.

Ricard A., Gicquel A., Malvos H., Michel H., Bordeleau S. and Hubert J., [1993], in *Microwave Discharges: Fundementals and Applications*, (eds. Ferreira C.M. and Moisan M.), NATO ASI Series B: Physics Vol 302, Plenum Press, New York and London.

Saitoh H., Mima H., Ishiguro T. and Ichinose Y., [1994], *Diam. and Relat. Mater.,* **3**, 452.

Schreck M, Baur T and Stritzker B, [1995], *Diam. and Relat. Mater.*, **4**, 553.

Schreck M, Baur T and Stritzker B, [1995], *Diam. and Relat. Mater.*, **4**, 553.

Shigesato Y, Boekenhauer R.E. and Sheldon B.W., [1993], *Appl. Phys. Lett.*, **63**, 314

Stoner B.R, Ma G.H.M, Wolter S.D and Glass J.T, [1992], *Phy. Rev. B*, **45**,11067.

Stoner B.R., Ma G.H., Wolter S.D., Zhu W., Wang Y.C., Davies R.F. and Glass J.T., [1993], *Diam. & Relat. Mate.r.*, **2**, 142.

Surendra M., Graves D.B. and Plano L., [1992], *J. Appl. Phys.*, **71**, 5189.

Wolter S.D, Glass J.T and Stoner B.R, *J. Appl. Phys.*, [1995a] **77**, 5119.

Wolter S.D., Stoner B.R., Glass J.T., Ellis P.J., Buhaenko D.S., Jenkins C.E. and Southworth P, [1993], *Appl. Phys. Lett.*, **62**, 1215.

Yugo S., Kanai T. and Muto T., [1990], *Vacuum*, **41**, 1364.

Zalicki P., Ma Y., Zare R.N., Wahl E.H., Owano T.G. and Kruger C.H., [1995], *Appl. Phys. Lett.*, **67**, 144.

Zhu W., Stoner B.R., Williams B.E. and Glass J.T, [1991], *Proc. IEEE,* **79**, 621.

Chapter 6

Electrical and High Resolution Optical Emission Studies of a Microwave Plasma Under Conditions of Bias.

Previous OES measurements indicated that a negative substrate bias applied during nucleation of diamond can influence the plasma region directly above the substrate. At higher substrate potentials, where biasing is typically carried out, a bright secondary glow region appears in the narrow dark space between the plasma base and the substrate indicative of enhanced inelastic processes occurring there. Furthermore the sheath and hence the bias current are influenced by the state of the plasma, which in turn depends on various reactor parameters such as pressure and power. This chapter presents the results of electrical measurements and high resolution spatially resolved OES studies which have been carried out to further investigate the influence of bias on the diamond plasma in the region above a tungsten metal substrate.

6.1 Introduction

The results of the measurements described in chapter five, together with a range of studies by other workers, show that the application of a bias can have a considerable effect on the microwave plasma, particularly in the vicinity of the substrate. The plasma and substrate are coupled systems and any large perturbations to the plasma can be expected to influence the substrate; it is clear from simple visual study that considerable changes occur near to the substrate during biasing. The most dramatic example is the development of a thin brightly glowing, disc-like region, in the dark space between the microwave plasma base and the substrate surface, which appears to coincide with the onset of a significant effect on nucleation density and is accompanied by a rapid increase of the substrate bias current.

Bias enhanced nucleation has so far proved to be the only reliable method for obtaining high nucleation density, highly oriented diamond films (HOD). There is currently considerable debate as to the mechanisms underlying BEN and while a number of models have been advanced a complete understanding remains to be achieved. Furthermore it is widely acknowledged that BEN is sensitive to the precise conditions under which it is carried out and can exhibit poor reproducibility; this is especially true if HOD films are required. It has been stated that the establishment of oriented nuclei is critically dependent on the bias conditions and the possibility of orientation can be completely destroyed if BEN is carried out for only a few minutes beyond the optimum point [Stockel 1998, Schreck 1996].

In view of these discussions it is clearly important to study the plasma directly above the substrate as this appears, from visual observation, to be the region most strongly affected by the application of the bias. From a more practical point of view it is also useful to examine the variation of the bias current with reactor conditions because the bias current is the key parameter used to monitor the bias process; its magnitude and evolution have been correlated with important changes which occur to the substrate and subsequently can effect the nature of the diamond film [Milne 1995, Kulisch 1996]. There have been few attempts

to characterise the region above the substrate and only one report of spatially resolved OES measurements [Schreck 1995]. While a number of authors have studied electrical characteristics during biasing, these in the main have concentrated on the variation of the substrate current with bias voltage and time. Although variation of the bias current with some of the other reactor parameters has been reported, it appears that a comprehensive study of the variation of bias current with reactor parameters is lacking. The purpose of the study described in this chapter was to use spatially resolved OES to study the region directly above the substrate, particularly the secondary glow, and to characterise the changes which occur there under the influence of the bias. A systematic study of the bias current characteristics can provide data which may be correlated with the changes revealed by the OES study, as changes in the plasma can be expected to influence the bias current-voltage characteristics. Also, the results of the study may be useful for the purposes of process control and may indicate which reactor parameters require the closest monitoring during bias.

The BEN effect was first reported by Yugo *et al.* [1990], who argued that a DC bias could alter the sheath potential at the substrate-plasma interface, influencing the active species in that region. For example, it was suggested that an electron flux from the area of the substrate holder could enhance the dissociation of $H_2 \rightarrow H\bullet$ near the substrate surface [Lee 1990]. On the other hand, it has also been argued that a negative substrate bias can accelerate H^+ ions to the surface which could also enhance the generation of active species in the important near surface region. However, it is unlikely that H^+ would be directly responsible, as it has subsequently been shown that H_3^+ is likely to be the dominant ion species in a microwave discharge, through a fast reaction of H^+ with the neutral H_2 background molecules; this reaction also provides an additional pathway for the creation of atomic hydrogen [Grotjohn 1998, Bou 1992]. Stoner *et al.* have carried out very careful studies of the biasing process and reported bias current densities of ~15mAcm^{-2} at -250V. They suggested that altered surface/near surface chemistry arising from elevated H• levels above the substrate could play an important role; however they concluded that detailed

plasma diagnostic studies within the sheath region were highly desirable [Stoner 1992]. A number of authors have reported the distinctive variation of bias current, with both time and voltage, which occurs under biasing conditions [Milne 1995, Kulisch 1996]. For the bias current-time curve, interesting correlations have been shown between characteristic parts of the curve and critical stages in the development of the substrate surface leading up to nucleation. The shape of the bias current-voltage curve has been explained in terms of an initial mobility limited rise followed by an ion saturation region, which precedes the rapidly increasing non-linear part of the curve where biasing is usually carried out. A number of explanations, summarised by Kulisch [1996], have been advanced to explain the rapid rise in current which occurs above a threshold value of the bias voltage (~100V). These have included; thermionic emission, effective electrode area effects and secondary electron emission from the surface.

The development of a sheath region supporting strong electric fields above a negatively biased surface, immersed in a plasma with a density typical of MEPCVD systems (~10^{11} - 10^{12} cm^{-3}), can be understood in terms of established plasma physics [Dendy 1993, Huddlestone 1965]. The thickness of the sheath under such conditions would be expected to be of the order of a few mm and this is confirmed by the measurements of Schreck *et al.* who have made spatially resolved OES measurement of the H_α emissions above a biased substrate [Schreck 1995]. Stark splitting measurements of the H_β and H_γ lines indicated that fields within the sheath were of the order of 10^3 Vcm^{-1} for a -200V bias, which are sufficient to cause considerable acceleration of charged species within that region and could lead to enhanced inelastic collision processes. Ion Energy Distribution (IED) measurements by retarding field probe, situated at the substrate, have recorded ion energies of around ~80eV, which may support the subplantation nucleation model proposed by Gerber *et al.* [1994]. However these results have been questioned by Kulisch *et al.* [1996], as such measurements can perturb the local plasma environment and can be difficult to interpret under conditions where secondary electron emission is likely. Furthermore, such high ion energies would not expected at typical diamond growth pressures, at which the

sheath is collision dominated; Monte Carlo modelling of the sheath by McGinnis *et al.*[1995] has indicated rather lower likely ion energies of around ~15 eV. However, it has been suggested that recent experiments [e.g. M^{c}Ginnis 1995, Schreck 1996] indicate categorically that ions are responsible for the BEN effect (but do not necessarily support the subplantation model). These measurements rely on the observation that little nucleation enhancement is seen on regions of the substrate that are either electrically isolated from, or vertical to, the remainder of the substrate, which does show nucleation enhancement under bias. Others however, [Bozeman 1998] have cautioned that the BEN process is complex and difficult to optimise, and as these results rely on the demonstration of a negative, they should be considered with care. Furthermore, this author notes that under typical bias conditions charge exchange collisions are expected to be highly likely and possibly dominant processes within the sheath [Dendy 1993, M^{c}Daniel 1964, Manenschijn 1991]. The result of charge exchange collisions are slow ions and fast neutrals/radials; therefore the flux of energetic ions to the surface is very likely to be accompanied by a significant component of energetic neutral species and it is not clear which component (or both) is important to the nucleation process. The presence of highly energetic neutrals in the sheath region has been confirmed by Doppler broadening measurements on the H_{α} emission line. These measurements have indicated that neutral atomic hydrogen, with translational energies up to 50 eV, exists in the region of the sheath closest to the substrate [Schreck 1995]. Furthermore the importance of this source of energetic neutrals in other industrial processing plasma environments has only recently been realised [Dendy 1993].

In summary, it is clear from the above brief discussion of the more relevant literature that the mechanisms for BEN remain highly controversial; an important role for the sheath region formed directly above the substrate seems incontrovertible and a number of authors have commented on the secondary glow which forms there [Schreck 1995, Stockel 1998]; but whether this supports purely physical or chemical explanations for BEN or a mixture of both remains to be determined. Further detailed studies of this region are indicated; OES

and electrical measurements can provide useful information and jointly benefit from being non-invasive; the results of such a study are presented in the following sections.

6.2 Experimental Details.

All the experiments described in the following section were carried out using the RFA or ASTEX microwave reactors which have been described elsewhere in this thesis. Likewise the substrates used during the measurements were identical to those already described i.e. 5 cm diameter, 6 mm thick, polycrystalline tungsten. *Ex-situ* and *in-situ* sample cleaning methods were also the same. Conventional optical photography of the plasma was carried out through the same port used to make OES measurements. During biasing, which was carried out over a range 0 - 300V, the substrate was held negative with respect to the chamber, which was grounded. Bias was applied using high voltage, high current, power supplies; substrate voltage and current were recorded where appropriate. Typical chamber parameters during the experiments were; pressure ~15T, flow ~100 sccm, substrate temperature ~600°C (thermocouple indication) and power ~ 600 W. However, in general the conditions depended on the experiment and further details are included in the following sections.

Optical emission studies were carried out using the same OMA-III based multi-channel analyser and linear photodiode array which has already been described in chapters three and five. To study the region of the plasma closest to the substrate, where the greatest bias induced changes occurred, modifications were made to the optical arrangement, already described in chapter five, to allow high resolution axial scans of the substrate-plasma environment to be carried out:

(i) A rectangular to circular multi-mode optical fibre was used to couple light from the viewport to the spectrometer.

(ii) A new lens and scanning mount arrangement was designed for the fibre to image the axial plane of the plasma.

(iii) The OMA-III system was operated in a low temperature mode with forced water cooling to the detector array. This permits the Peltier cooler to reduce the CCD array

a further 30 degrees below its normal operating temperature, allowing longer integration times before detector saturation occurs and hence improving the signal-to-noise ratio.

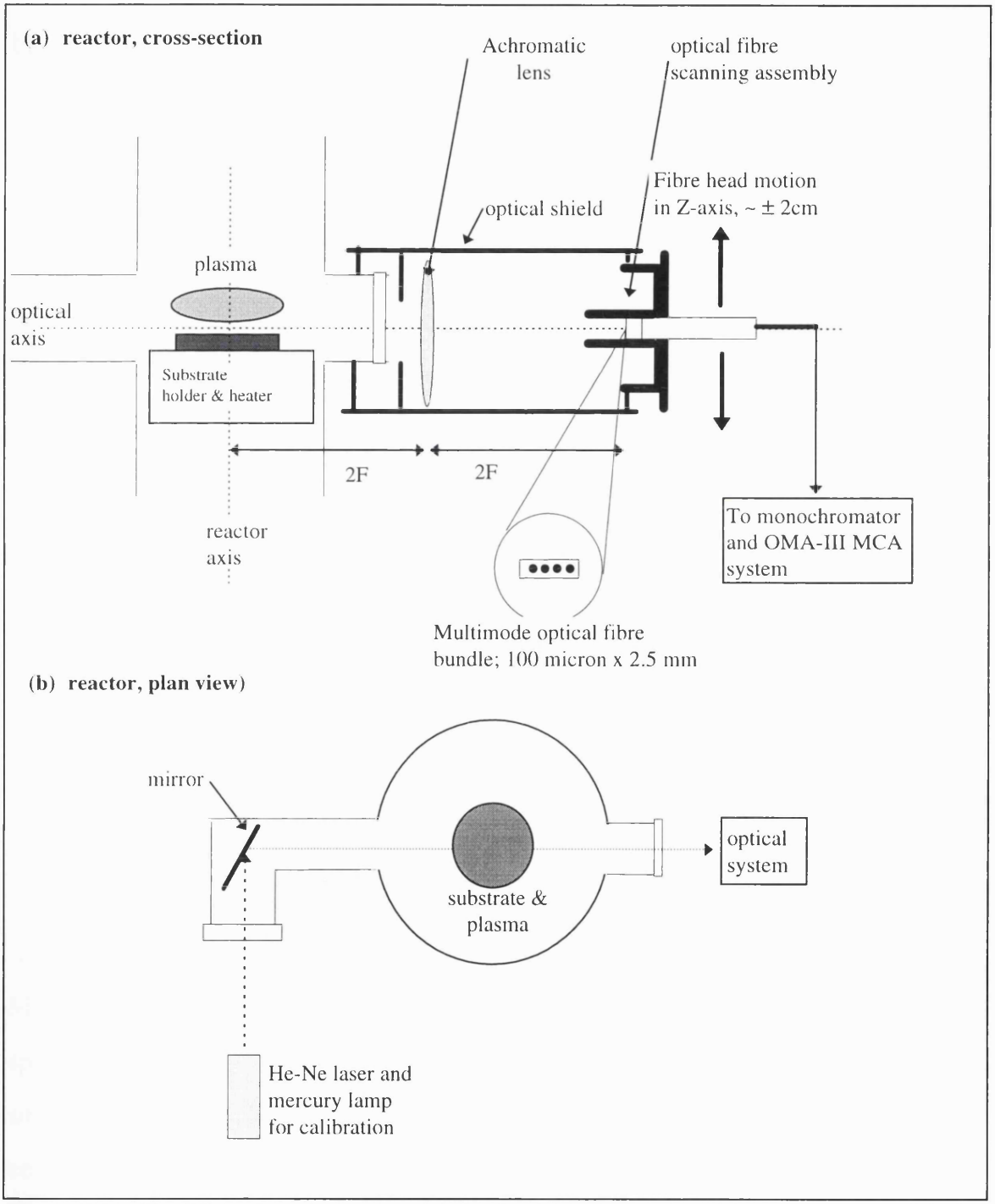

Figure (6.1): Simplified schematic (not to scale) showing (a) a cross-section of the arrangement used during high resolution spatial scanning of the microwave plasma together with details of the input end of the optical fibre, and (b) plan view showing the arrangement used to permit calibration and checking without disturbing optical setup.

The modified high resolution scanning arrangement is shown in figure (6.1), together with details of the probe end of the optical fibre.

A high quality, achromatic lens (focal length f = 9 cm) mounted in a 2f-2f arrangement forms a 1:1 image of the plasma with the image axis at the plane of the optical fibre, which is arranged with its longer dimension parallel to the substrate surface. The mechanical arrangement (not shown in full detail) consisted of a slide-mount, screw and adjustment wheel which allowed the fibre-head to be scanned in the axial direction with a positional uncertainty of ~ ±20 μm estimated from the pitch of the screw thread and the angular precision provided by a large perspex wheel and pointer. The optical system was initially set-up by imaging a sharp needle, placed at the centre of the substrate on the reactor axis, onto the entrance plane of the optical fibre. The fibre slit was set with the larger dimension parallel to the substrate by observing a fine slit mounted on the substrate axis and parallel with the substrate surface. This was then illuminated by the beam from a He-Ne laser and the optical fibre rotated in its mount until a maximum count rate was achieved on the OMA III-MCA. The approximate axial resolution of the scanning system was determined by imaging a 500 micron slit mounted at the substrate axis and parallel to its surface. The result of a scan across the slit is shown in figure (6.2), from which it can be estimated that the spatial resolution of the system is around 100 microns.

This arrangement necessarily limits the amount of light collected from the plasma and resulted in rather low count rates; to improve the sensitivity of the system the OMA-III MCA was operated in the low temperature mode described in point (iii) above. OES spectra were acquired as a function of axial position, for scans made from the substrate surface to the plasma bulk, for the cases of pure argon and hydrogen-argon plasmas under conditions of substrate bias and no bias. The emission intensities of spectral features, similar to those listed in chapter five, were studied as a function of axial position. Wavelength calibration of the optical spectra was carried out by reference to the primary

hydrogen emission lines, which were easily identified, together with the standard emission spectrum from a mercury vapour lamp and a He-Ne laser (~632nm).

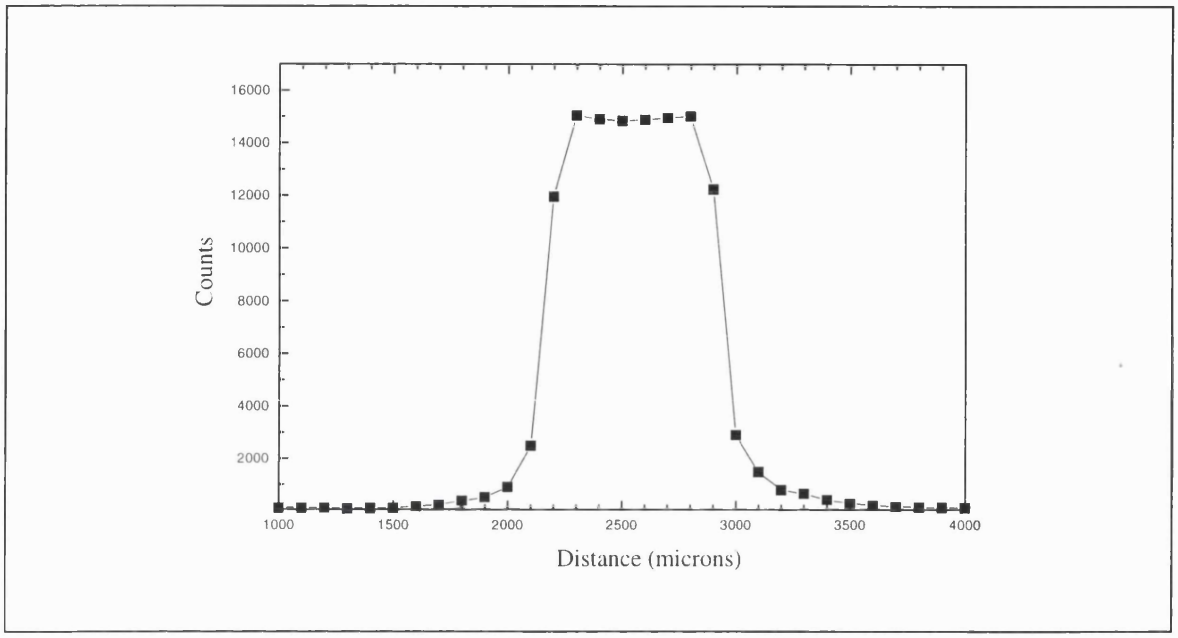

Figure (6.2): Results of axial intensity scan made on a 500 micron slit mounted parallel to the substrate surface.

To minimise disturbance to the optical system provision was made to allow checking, calibration and optimisation of the spectrograph-diode array *in-situ* via a mirror arrangement mounted in the vacuum port opposite the optical system, as shown in the lower part of figure (6.1); the system was not calibrated for intensity. Argon actinometry was employed and where it has been used this is stated in the relevant results section. The intensity of spectral features were determined using the same software and methods that have been described in chapter five. For further discussion of OES and actinometry the reader is referred to chapters three and five where more details have been given. For the electrical bias studies the variation of bias current was measured as a function of the bias voltage, methane fraction, microwave power and substrate temperature.

6.3 Results.

6.3.1 Optical Photography.

Photographic studies of typical $H_2/CH_4/Ar$ biased plasmas were made in both the RFA and ASTEX reactors. The bias induced changes were similar in each of the two reactors; a summary is given in the photographic sequences shown in figure (6.3a) and figure (6.3b). The colour plates highlight the general effects of a -200V bias compared to the unbiased substrate, while the black and white sequence records the changes that occurred to the plasma as a function of increasing applied bias in the range 0-270V. The reactor conditions were: power ~800W, pressure ~15T, 4% CH_4, 3% Ar in H_2 and the sequence shown was taken on the ASTEX reactor. The two colour photos show the general changes which occurred between the cases of 0 and -200V bias; observations can be made which are similar to those described in chapter 5, i.e. an increase in the width of the dark space occurs together with the appearance of a thin secondary glow between the plasma base and substrate. Modest changes to the plasma shape also occur and the region in the plasma bulk near its base shows an increase in brightness to a distance ~8-10 mm above the substrate. However, in this case the changes are more obvious which can be attributed to the lower reactor pressure of 15 Torr used during these studies compared to the 30 Torr used previously in chapter 5. The black and white sequence shows the development of these changes as a function of the applied negative bias up to -270V; the key points to note are the appearance of a secondary glow which becomes visible at -100V and continues to increase in brightness until at -200V it is unmistakable. This feature appears as a flat, disc-like region with a rather sharp, bright edge on its substrate side and a more gradual fall in intensity towards the plasma base from which it is typically separated by a narrow dark space. The appearance of the secondary glow region is accompanied by a small increase in the width of the space between the plasma base and the substrate. The image at a negative bias of 270 volts shows the rather extreme degree to which the bias can disturb the plasma; the dark space becomes very large and the secondary glow very bright. For higher biases

(the exact value depends on reactor and conditions) the plasma became unstable and unpredictable and could either disappear or show extreme DC breakdown usually causing the bias supply to trip out.

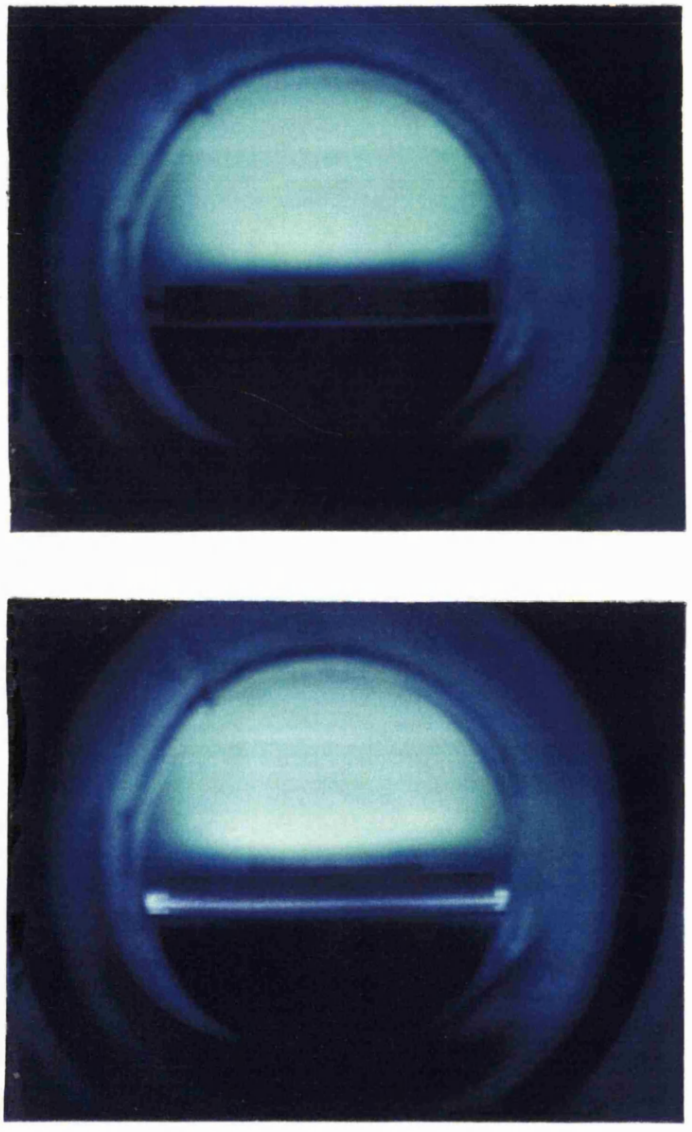

Figure (6.3a): Colour photographs highlighting the effects of a negative substrate bias of 200V above a tungsten substrate for a methane-hydrogen plasma; top: unbiased, bottom:biased.

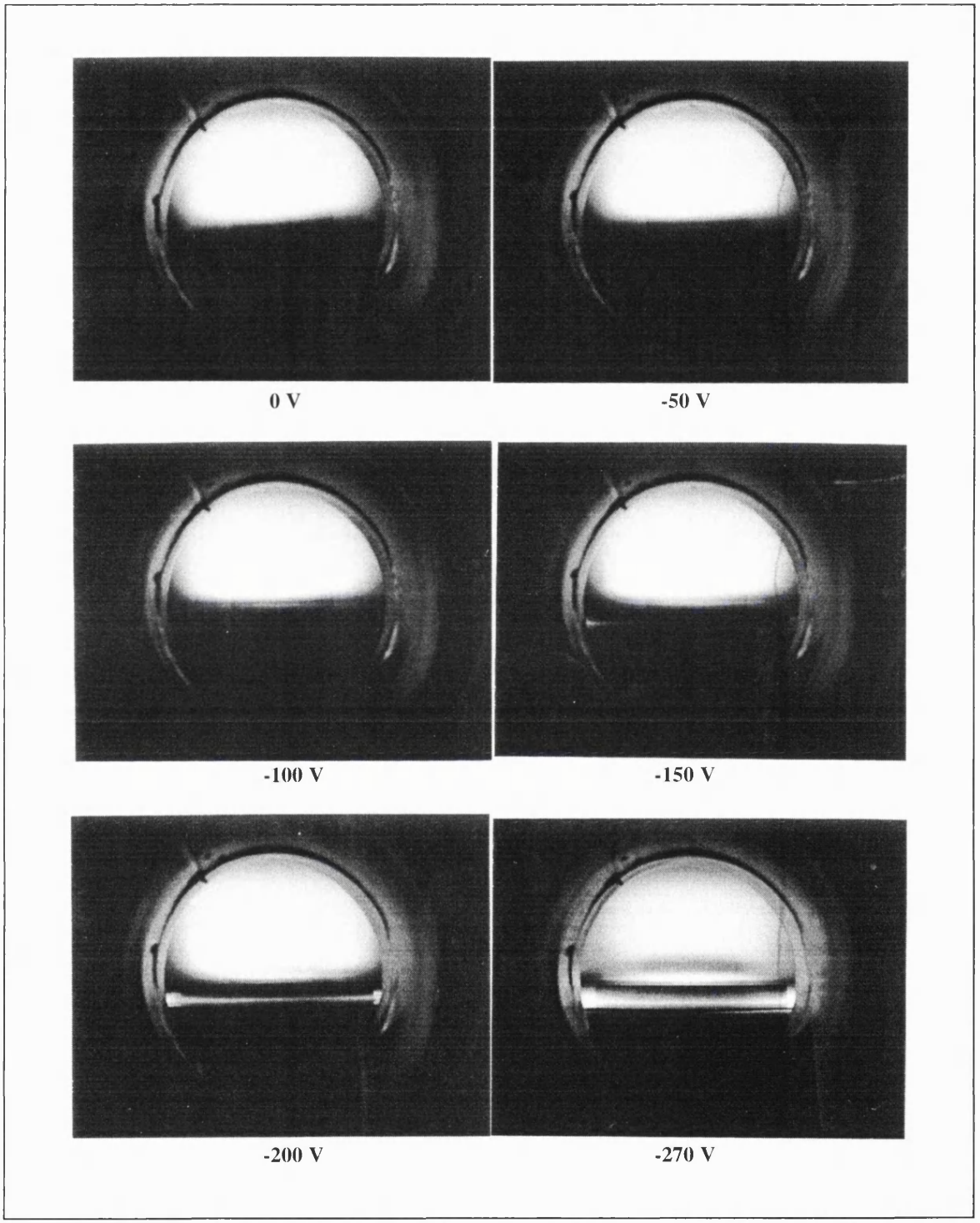

Figure (6.3b) Optical photographic sequence (black & white) showing the development of bias induced changes to the plasma above a tungsten substrate observed for an increasing negative substrate bias (0-270V).

An interesting observation is that at the higher voltages (typically ~250V) the secondary glow region persisted if the microwave plasma was turned off, appearing essentially unchanged. It was also observed that the secondary glow intensity increased with biasing time at a fixed bias voltage, as did the bias current. While for lower bias voltages e.g. ~120V or higher pressures, the glow first became visible at the substrate centre and then appeared to move outwards from the centre. However, this behaviour was dependent on both reactor and bias parameters; generally at a pressure of ~15 Torr and a bias of 200V or greater, the glow appeared almost immediately across most of the substrate although it remained brightest at the centre. The glowing ring apparent below the level of the substrate, at a bias of 200V and above, is associated with a molybdenum locating ring which was typically covered in diamond deposits. It has been reported that the presence of diamond on the substrate holder can influence the bias process, causing nucleation to proceed inwards from the substrate perimeter [Stoner 1993]. This was never observed during the current work; nucleation always started at the substrate centre and moved outwards. Under the *raised* substrate conditions used during the current studies, the substrate ring had no significant influence. It was not observed in the RFA reactor which had a stainless-steel platen which did not tend to become covered in diamond.

6.3.2 Optical Emission Spectroscopy.

High resolution OES scans were carried out to examine in detail the region of the plasma within ~10 mm of the substrate surface for the case of a pure argon plasma and an H_2-Ar plasma. However, the small size of the sampled region combined with the low optical efficiency of the high resolution system resulted in low count-rates and some spectral features of interest were either unresolved or suffered from poor counting statistics. Unfortunately time and equipment constraints prevented any redesign of the system to improve matters within the time-scale of this project. Improvements which could have been made were (i) to optimise the optical path and collection efficiency, and (ii) reduce the spatial resolution, which as designed proved to be rather higher than was useful. Despite these problems some useful scan results were obtained and these are presented here.

The results of a high resolution OES scan carried out from the substrate surface to a distance ~10 mm, encompassing the regions most affected by the bias, are shown in figure (6.4a-c) for the case of a pure argon plasma. Visibly, the geometry and appearance of the pure argon plasma was very similar to the $H_2/CH_4/Ar$ plasma shown in the previous figure. Similar changes occurred under bias; the main differences of note were that the secondary glow region appeared stronger and a lower power was required to sustain the microwave discharge, 200 watts in this case. In fact, above this power the argon discharge was unstable and tended to 'jump' to the quartz microwave window; this is a well known feature of this type of reactor and is due to the power-pressure corridor for reactor stability discussed in chapter 3. The differences in brightness and microwave power observed between the argon and $H_2/CH_4/Ar$ plasmas can be explained in terms of the additional energy loss pathways available to electrons in the H_2 plasma.

Figure (6.4a) shows the intensity profile of the unbiased plasma over the range ~0-12 mm from the substrate surface as recorded by the Ar_{750} emission line; the region of very low intensity between 0 - 3.5 mm corresponds to the dark space between the substrate and the base of the plasma. A negative substrate bias of 200 V has a considerable effect on this region as can be seen from plot (b) in the figure which also includes the data from plot (a) on the same scale (note use of log scale). The scan clearly shows the presence of the bright secondary glow, which in this case is considerably brighter than the main bulk of the plasma and is centred about 2.5 mm from the substrate surface. Relative changes in the electron temperature, as monitored by the Ar_{750}/Ar_{811} ratio, are shown in figure (6.4c) for the case of bias and no bias. This plot also includes a superimposed schematic representation of the substrate and main plasma regions.

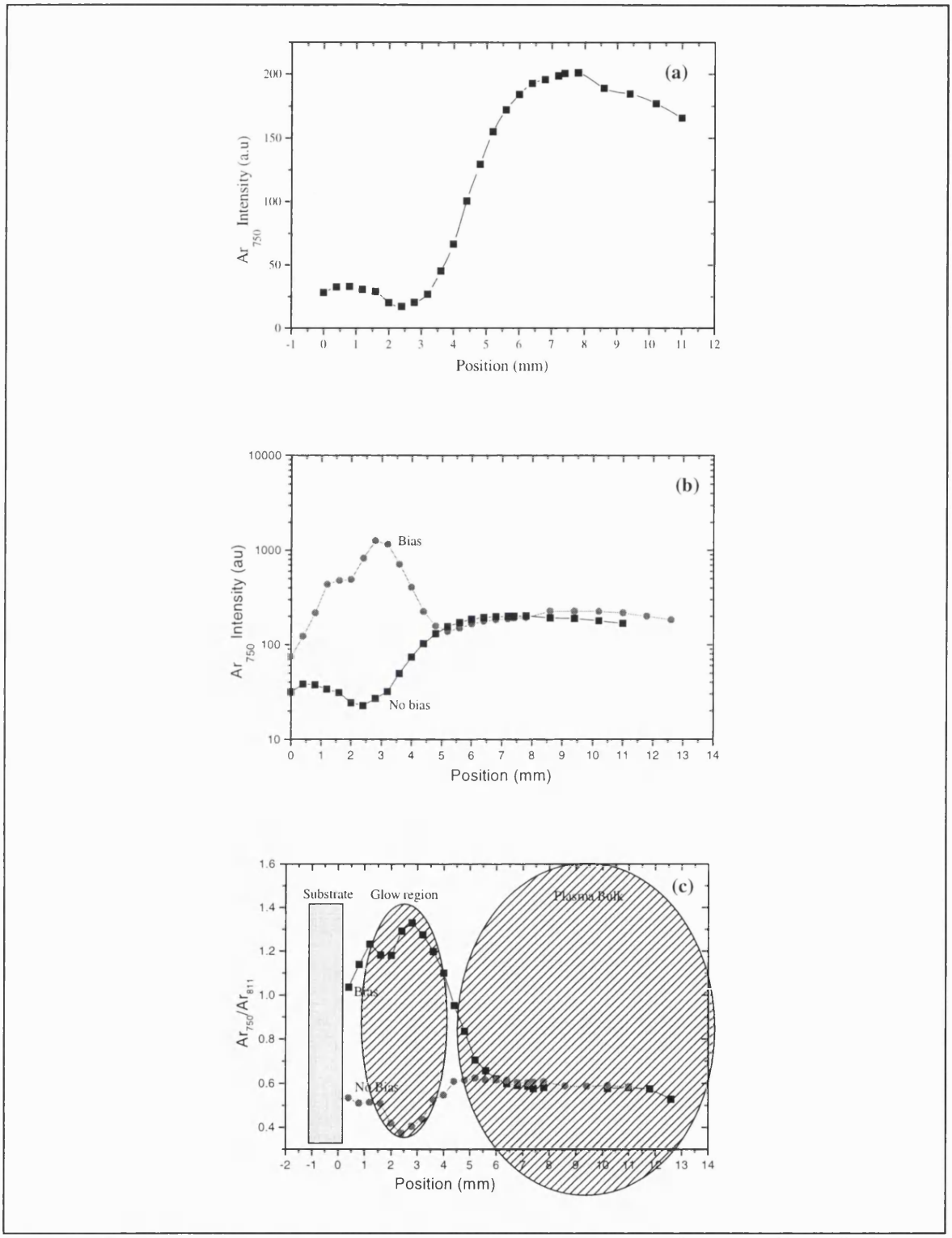

Figure (6.4): High resolution scan across near substrate region of an argon plasma; (a) Shows the intensity of the Ar_{750} peak for the case of no bias, (b) Shows the Ar_{750} for the case of both bias and no bias; (c) Shows the electron temperature T_e as monitored by the Ar_{750}/Ar_{811} ratio. Note: while the relative position of the substrate and plasma regions shown in the schematic is approximately correct, the superimposed image is not to scale.

The relative positions of the different regions were estimated from photographs and are approximately correct, although the image as a whole is not to scale. This plot clearly indicates that application of a bias strongly affects the electron temperature, as monitored by this ratio, showing an increase centred ~2.5mm from the substrate which maps closely to the bright region observed in the photographic study and the intensity plot shown in (b) of this figure. The ratio falls to its unbiased value in the plasma bulk, but an elevated value persists a few mm's into the base of the plasma.

Similar OES scans were also carried out on a hydrogen-argon plasma (9% Ar/H_2). The visual appearance of the H_2-Ar plasma was very similar to the pure argon plasma except that a higher microwave power was required to strike and maintain a plasma of similar brightness and dimensions; as noted this can be explained by differences in the electron energy loss mechanisms available between the two plasmas. For example, in a pure H_2 plasma ~58% of the electron energy may be dissipated via H_2 dissociation, [Hassouni 1998], a similar route is not available in the pure argon plasma because argon is monatomic. Application of a negative substrate bias of 200 V provoked changes similar to those which occurred in the pure argon plasma, however the secondary glow region in this case was less intense and exhibited a slight reddish tint, possibly indicative of strong atomic hydrogen H_α emission - which is in the middle of the visible red part of the spectrum (~656 nm). The results of optical emission scans on the H_2-Ar plasma are shown in figure (6.5).

Figure (6.5a) shows the axial variation of the electron temperature as monitored by the Ar_{750}/Ar_{811} ratio. A similar peak in the ratio to that seen in the case of the pure argon plasma is again apparent at around 2 mm from the substrate surface and the axial profile is qualitatively similar. Argon has been used here to monitor the relative axial changes in T_e rather than the H_β/H_α ratio because the counting statistics on the H_β peak were to low for the ratio to be considered meaningful. The relative variation in the atomic hydrogen concentration with axial position, as determined by actinometry, is shown in plot (b) and again shows a clear increase in the region associated with the secondary glow, before

returning towards the unbiased value in the plasma bulk. The axial variations of other hydrogen (H_α) and argon line intensities (Ar_{750}, Ar_{811}, A_{r696}) were qualitatively similar to the profiles shown previously in figure (6.4b) for the case of a pure argon plasma.

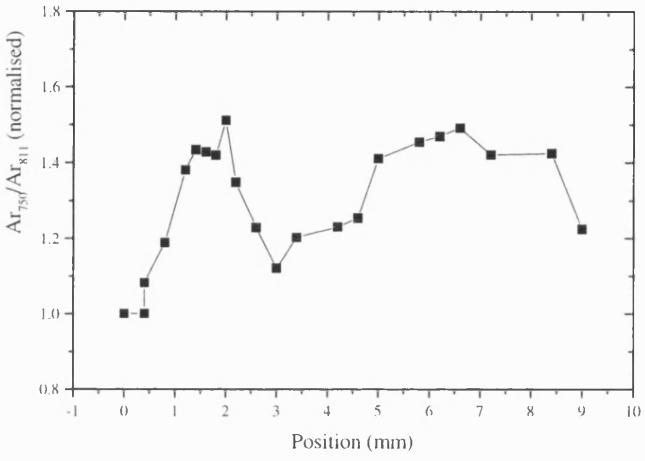

(a)

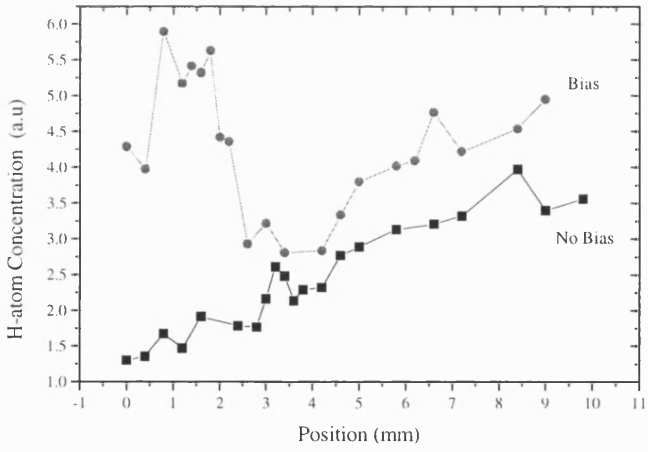

(b)

Figure (6.5): High resolution scans across near substrate region of a hydrogen-argon plasma subject to a negative bias of 200V; (a) shows the spatial variation of T_e as monitored by Ar_{750}/Ar_{811} , (b) shows the spatial variation of atomic hydrogen as determined by actinometry without substrate bias (solid squares) and with bias (solid circles).

6.3.3 Electrical Measurements.

Electrical measurements were carried out to examine the variation of substrate bias current with; bias voltage, methane fraction, reactor pressure, substrate temperature and microwave

power, for a hydrogen-methane plasma (15T, 4% CH_4, 3% Ar, 800W, 411 sccm, T_s~600 °C - typical values). The aim of the study was to provide additional data which could be correlated with the OES studies. The plasma, being the source of charged species, can be expected to influence the bias I-V characteristics. An additional aim, was to make a systematic study of the bias current in light of the reported sensitivity of the BEN process to the total integrated bias current; such data can indicate which bias parameters have the strongest influence and may also be useful for the purposes of process control.

To minimise the influence of deposits, which might be formed on the substrates during bias current characterisation, the following general precautions were adhered to:

(i) Pristine polycrystalline tungsten substrates were used.

(ii) Substrates were always cleaned prior to placing in the reactor.

(iii) Substrates were subjected to 30 minute hydrogen plasma etch to remove contaminants.

(iv) I-V measurements were carried out as rapidly as possible.

(v) Wherever possible e.g. during gas composition changes, the plasma was turned off to prevent unnecessary deposition occurring.

(vi) During longer experiments, substrates were cleaned using an extended H-plasma etch if visual inspection suggested deposition had occurred.

Clearly it is not possible to avoid completely the effects of deposition on measured bias currents; however it was judged that the above precautions minimised this influence compared to the changes arising from variation of the parameter under study. For example, it was determined that with a clean substrate in place, the bias current measured immediately on application of 200V bias was less than 5% different from that observed at 200 V after having recorded 20 data points as the bias was varied from 0 to 200V. The results of bias current measurements made as a function of bias voltage, chamber pressure, substrate temperature, methane fraction and microwave power are summarised in figures (6.6a-b) and (6.7a-c) respectively.

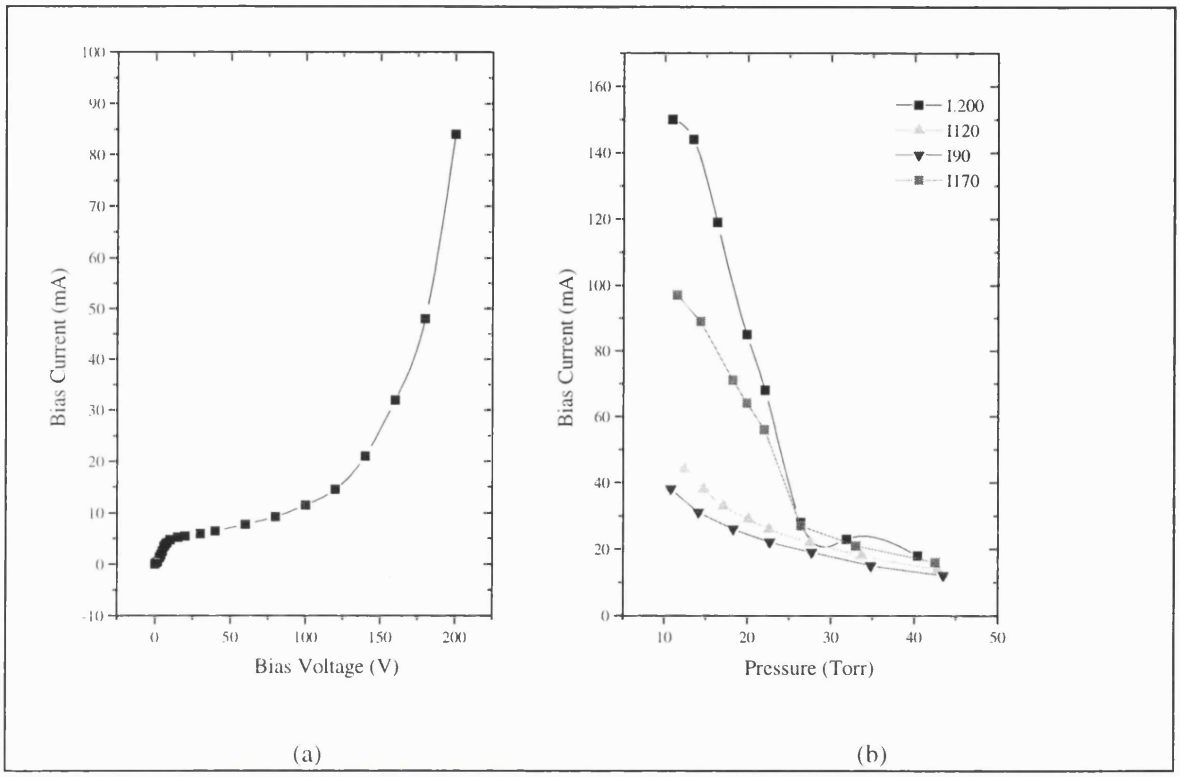

Figure (6.6): (a) Measured bias current as a function of substrate bias and (b) Bias current as a function of pressure with bias voltage as a parameter (V_b: 200, 170, 120,90 volts; squares, light squares, up-triangles and down-triangles respectively).

It is clear from these plots, that with the exception of substrate temperature, all of the parameters have a strong influence on the measured substrate bias current over the range studied. The variation with substrate bias, figure (6.6a), is qualitatively very similar to other reported measurements [Schreck 1995, Kulish 1996]; of particular note is the onset of the rapid non-linear rise which occurs at around 100-120V and coincides with the development of the secondary glow described earlier. This behaviour is also evident from figure (6.6b) in which bias was treated as a parameter and the variation of bias current with reactor pressure, for several values of fixed bias voltage, is shown. At pressures below 20-25 Torr and particularly for the higher biases, the bias current was very sensitive to the reactor pressure, showing a rapid increase with decreasing pressure to ~10 Torr, at which point there was some evidence that the rate of increase slowed. The lower pressure limit of ~10 Torr was set by the behaviour of the plasma which became unstable below this pressure.

The variation of substrate current at a fixed bias of 200V shows a strong almost linear increase with microwave power over the range studied (~ 175 W - 825 W); changing by about 25 mA for each 100 watt increase in the applied power, figure (6.7a). The methane fraction in the plasma has a strong effect on the bias current which can be seen from figure (6.7 b).

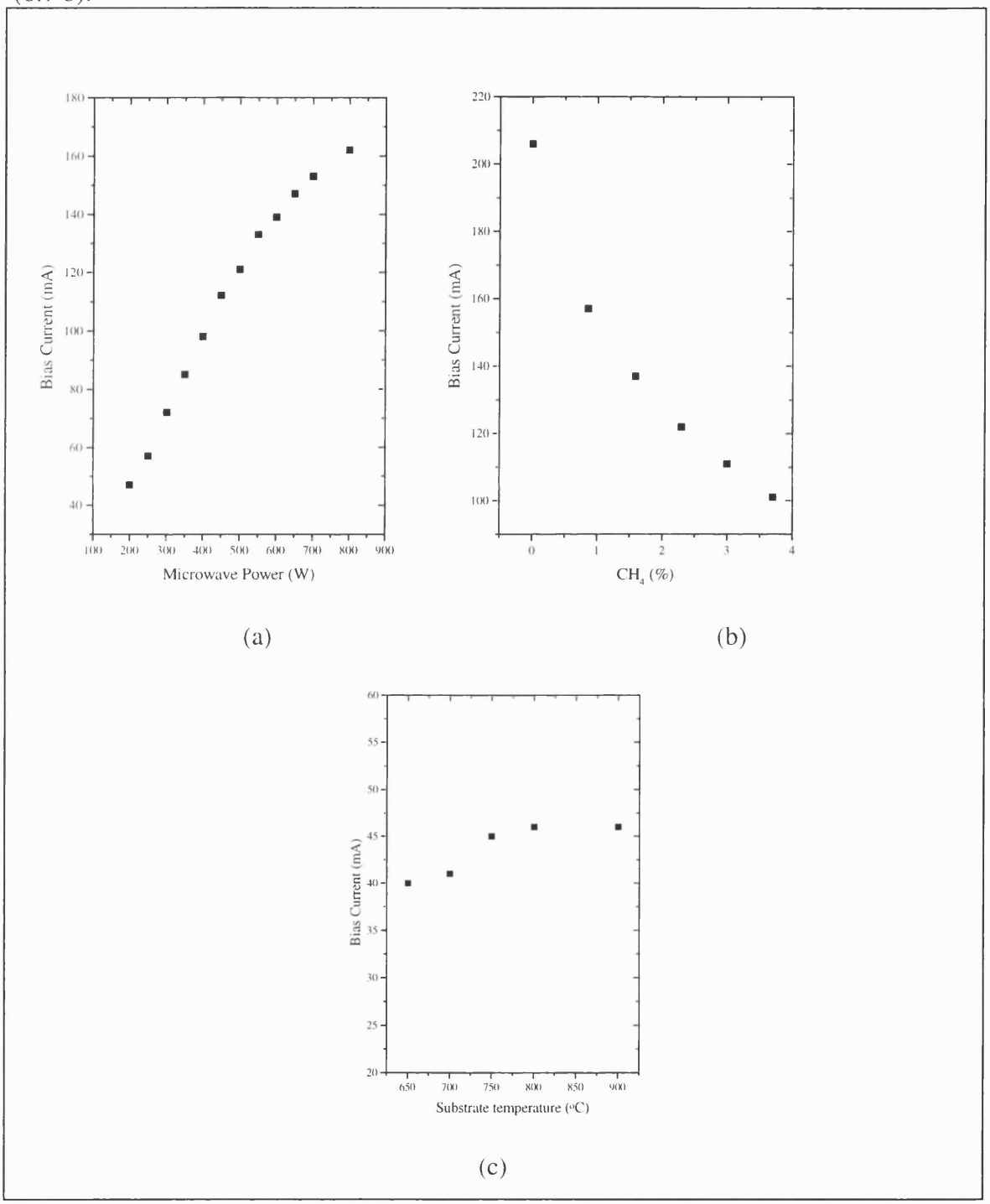

Figure (6.7): Measured variation of bias current with; (a) microwave power, (b) methane fraction and (c) substrate temperature. In all cases the bias voltage was -200V and other parameters were held constant.

Increasing the methane fraction from 0 to ~4% results in a decrease in the substrate current by around a factor of 2, with the fastest rate occurring for the first ~1.5% of methane addition. Figure (6.7c) shows the variation of bias current at 200V as the substrate temperature was varied from 650-900°C. Little variation is apparent except for a few percent increase at around 750°C.

6.4 Discussion.

Application of a negative substrate bias can lead to large increases in diamond nucleation density and under certain conditions, localised epitaxy of individual crystals with the underlying substrate e.g. (100) oriented diamond grown on (100) silicon. Coincident with the application of the bias, considerable perturbation occurs to the plasma, especially in the region directly above the substrate; a sheath supporting large electric fields develops which can accelerate charged species and influence many plasma processes. The plasma is perturbed to distance ~10-12 mm from the substrate surface as suggested by the low resolution OES measurements discussed in chapter five.

The series of plasma photographs presented in figure (6.3b) clearly show the development of the plasma perturbation as the bias voltage is increased. The dark space width increases slowly with bias and at around 100V the secondary disc-like glow, described earlier, just becomes visible; its appearance approximately coincides with the onset of a rapid increase in the bias current which also occurs at around 100 volts, as can be seen from the plot in figure (6.6a). These visual observations were made for a H_2-CH_4-Ar plasma, however very similar changes were also observed for pure Argon and H_2-Ar plasmas. The highly emitting nature of the secondary glow implies that energetic inelastic processes such as excitation, dissociation and ionisation are occurring there. Under conditions of high bias; the actual value depends on pressure and gas composition, this region is self-sustaining if the microwave source, i.e. the main plasma ball, is turned off. This is strong evidence that a high rate of ionisation can occur within this secondary glow region, implying that it also

acts as a source of atomic hydrogen since the dissociation threshold for H_2 is considerably lower than its ionisation threshold [Grotjohn 1998]. It is worth noting that the glow region showed a faint reddish tint, which may be indicative of strong H_α emission at ~656nm; the red tint was observed for both the H_2-Ar and H_2-CH_4-Ar plasmas but was not visible in the case of the pure Argon plasma. The photographic observations can be compared with the results of the high resolution, axial OES scans shown in figures (6.4a-c) and (6.5a-b) for the case of pure argon and H_2-Ar plasmas respectively. The intense nature of the emitting glow region created by the substrate bias, for the case of the argon plasma, can be appreciated by comparing the two plots shown in figure (6.4a&b). The intensity of the Ar_{750} line without bias, figure (6.4a), shows the expected axial profile consistent with the visible appearance of the plasma (five other resolvable argon lines also exhibited similar axial profiles). The data for zero bias is repeated in figure(6.4b) together with the axial profile obtained with a 200V negative bias (*note the log_{10} vertical scale*) from which it can be seen that the glow region is centred at about 2.5 mm above the substrate and is about a factor of 10 more intense than the plasma bulk. The axial profile of the electron temperature, as monitored by the Ar_{750}/Ar_{811} ratio - figure (6.4c), also shows a strong increase under the influence of bias. This closely correlates with the glow region, as is indicated by the super-imposed schematic also shown in figure (6.4c) which was prepared from the photographs. The pure argon plasma is a less complex system than a typical H_2-CH_4-Ar diamond plasma and this was reflected in the optical spectra which were more open, contain fewer bands and lines and are therefore easier to interpret. Since the argon concentration cannot increase in the pure argon plasma the very strong increase in the emission intensity in the glow region must be due to an increase in electron density and temperature in that region.

The observations made for a pure argon plasma can be qualitatively compared with measurements made on an H_2-Ar plasma under similar reactor conditions. As expected, the brightness of the glow region was reduced compared to the case for the argon plasma, otherwise visually the two plasmas exhibited similar shape, brightness and volume. The

axial intensity profiles of argon and hydrogen emission lines exhibited structure similar to that shown by the Ar_{750} profile in the pure argon case, except that the intensities in the glow region were reduced compared with the bulk. The relative changes in the electron temperature for the H_2-Ar plasma, as monitored by the A_{750}/Ar_{811} ratio - figure (6.5a), were similar to the corresponding changes seen for the pure argon plasma. The axial atomic hydrogen profile, as determined by actinometry, also shows a qualitatively similar behaviour, with a distinct increase in the region which corresponds to the position of the secondary glow. An increase in the atomic hydrogen concentration would be expected if it is accepted that significant ionisation could occur within this region under bias conditions. This possibility can be appreciated by considering the main ionisation and dissociation reactions occurring within a pure hydrogen plasma, which are shown below together with the respective threshold energies and rate constants [Grotjohn 1998]:

$$e + H_2 \rightarrow e + H_2^+ + e \qquad E_{threshold}: 15.4\ eV,\ \text{rate constant} \sim 10^{-14}\ m^3s^{-1}. \qquad (6.1)$$

$$e + H_2 \rightarrow e + H + H \qquad E_{threshold}: 10.0\ eV,\ \text{rate constant} \sim 10^{-14}\ m^3s^{-1}. \qquad (6.2)$$

Clearly, since the dissociation threshold is lower than any of the main ionisation thresholds (H_2 or Ar) and the rate constants are similar, production of atomic hydrogen within the secondary glow region can be expected. A small addition of CH_4 may change the detailed balance of reactions and can be expected to introduce additional paths for the creation and destruction of atomic hydrogen, but would not be likely to drastically modify the general picture; this point is supported by the close similarity between the visual appearances of the glow region in each of the three plasmas and the axial scans presented here and in chapter five.

These observations can also be compared with other reports in the literature; a few authors have noted the appearance of a similar secondary glow, between the main plasma ball and the substrate, on application of a substrate bias [Schreck 1995, Kalish 1996, McGinnis

1995, Stockel 1998]. Most of the OES measurements previously reported have been low spatial resolution studies which have indicated that changes to the atomic hydrogen concentration and electron temperature appear to occur directly above the biased substrate. However, Schreck *et al.* [1995] have examined the spatial variation of the H_α emission line above a silicon substrate (clean and diamond covered) from the surface out to a distance ~3.0 mm, using spatially resolved OES similar to that employed here. For a clean surface they observed a strong peak in emission intensity under bias conditions (-200V) centred at a distance of ~2 mm from the surface, showing structure very similar to axial scans made during the current study. For a diamond covered surface, the peak was increased in intensity and positioned closer to the substrate surface. A different bias configuration, compared to the more common negative biased substrate, was used in which a positive bias was applied to a ring anode above the main plasma, while the substrate remained grounded. However, the effects are similar and they also visually observed a secondary glow between the main plasma and the substrate. From Stark splitting of the H_α and H_β lines, sheath fields of ~1.5-3.5 $kVcm^{-1}$ were measured, directly above the substrate, by these authors while Doppler broadening measurements on the H_α emission line exhibited shifts consistent with translational energies of up to 50 eV for H-atoms close to the substrate surface.

Schreck *et al.* [1996] have commented on the similarity of the emission profiles above the biased substrate to those observed in the cathode fall region of a D.C. glow discharge. Actually the degree of similarity is very striking; the axial profile measurements obtained during the current study are very similar to the emission profiles measured by OES across the cathode fall of DC glow plasmas at similar pressures to those used here (~18-38 Torr) [Plano 1991]. In that work, both pure H_2 and H_2-CH_4 DC-plasmas exhibited similar profiles, showing a strong peak at 1.5-2 mm from the substrate (cathode) surface. Subsequent detailed modelling of the H_2 DC glow plasma by Surendra *et al.* showed good agreement with measured emission profiles in the vicinity of the cathode (18 Torr H_2 DC plasma, bias 355V) [Surendra 1992]. Both experimental and modelling results indicated a

cathode sheath ~2-3 mm wide, supporting electric fields of ~3 - 4 x10^3 Vcm^{-1}, just above the cathode substrate. Within this region ionisation, excitation and dissociation rates were all sharply peaked at a distance ~ 1.5 - 2 mm from the substrate surface. Figure (6.8) shows three plots extracted from their work [Suredra 1992] for the region closest to the cathode substrate; figure(6.8a) shows the predicted rates for the main inelastic processes within 5mm of the cathode, while figure (6.8b) and (6.8c) reproduces their results for the predicted and measured emission rates respectively; for the cases of two different discharge pressures. Qualitatively, the emission plot, figure (6.8c), resembles closely the profiles obtained in the current study and also those of Schreck *et al.* It is also worth noting the similarity in the magnitude of the sheath fields measured by Surendra and Schreck for the DC and biased microwave plasmas respectively.

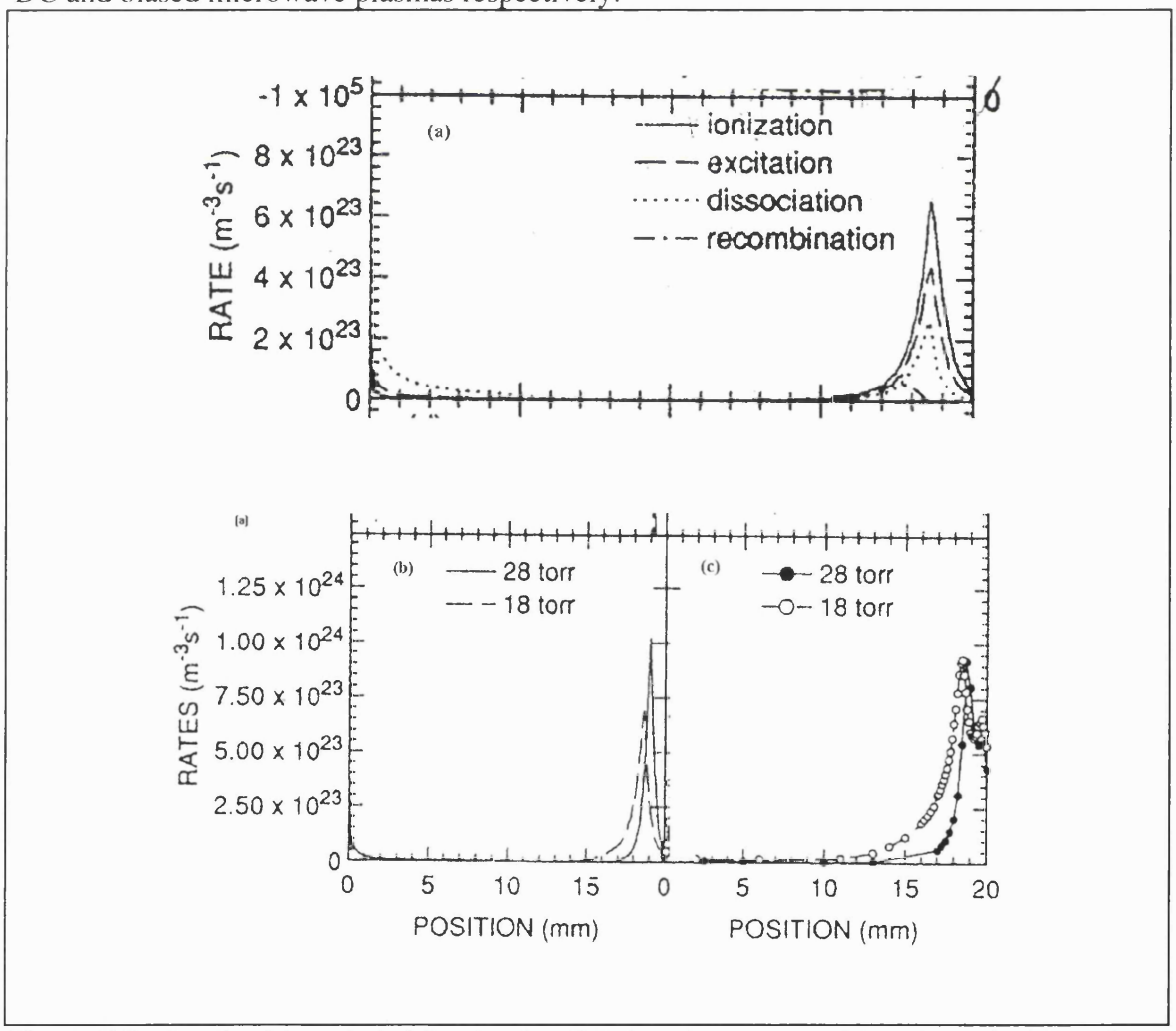

Figure (6.8): Details of the cathode fall region for a DC glow plasma extracted from the work of Surendra *et al.* showing (a) modelled inelastic process rates, (b) predicted emission rates and (c) OES measured emission rates; the x-axis is in mm and the cathode is located at 20mm in each case; [redrawn from Surendra 1992].

The possibility of significant ionisation and dissociation in the vicinity of the substrate, for the biased microwave plasma, is also apparent from a simple comparison of the maximum electric field strengths of the sheath region and main plasma ball. At around 1-2 $kVcm^{-1}$ for a 200V bias [Schreck 1996], the fields near the substrate are approximately an order of magnitude greater than the maxima predicted [Grotjohn 1998] and confirmed by measurements [Zhang 1990] for the fields supporting a typical microwave discharge, which were around $200Vcm^{-1}$; consequently, inelastic process rates similar to those occurring in the main plasma could be expected within the biased sheath.

As already noted, several authors have observed I-V characteristics similar to those which have been measured here, figure (6.6a) and a number of suggestions have previously been made to explain the rapid, non-linear increase in the bias current which occurs above a bias threshold which varies, but was around 100-120 volts under the conditions used in this study. These explanations have included thermionic emission of electrons from the hot substrate, changes in the effective electrode area and secondary electron emission from the substrate. Significant thermionic emission from a tungsten metal surface would not be expected at typical nucleation temperatures (~750°C) [Ashcroft 1981] furthermore this mechanism is not supported by measurements of the bias current made as a function of substrate temperature, figure (6.7c), which do not show significant variation as would be expected for thermionic emission. The area of the secondary plasma grows radially with bias and could allow for rapid current increase. However, the ionisation rate in the microwave plasma decreases rather rapidly in the radial direction [Grotjohn 1998] and might be expected to reduce the effect of an increase in the electrode area. Also under the conditions used in the current study the secondary glow covered the whole substrate at a bias of 200 volts; an increase in electrode area would not therefore seem able to account for the continued steep increase in bias current which was observed, up to the highest biases of 300V examined in the current studies. The most likely of these explanations is secondary electron emission arising from the collision of ions with the surface, which then leads to electron multiplication through the impact ionisation of neutrals in the sheath.

Incoming ions are neutralised very close to the surface by fast Auger type processes [Greene 1978] generating electrons in the high field region close to the substrate. The secondary electron ejection probability is quite high, typically 10-20%, for most metals and semiconductors [Greene 1978]. Electrons are therefore generated adjacent to the substrate and can be accelerated to relatively high energies by the strong sheath fields shown to exist there. That the electrons could gain sufficient energy to drive enhanced dissociation and ionisation processes, can be qualitatively understood by considering the electron mean free path (mfp) and the likely field strengths in the sheath. The electron mfp can be estimated from [Atkins 1982]:

$$mfp = \frac{k_B T}{\sqrt{2} p d^2 \pi} \qquad (6.3)$$

where, *k, T, p,d* are the Boltzmann constant, gas temperature, gas pressure and particle diameter respectively. A value of ~30 μm can be estimated from equation. (6.3) for the mfp of an electron in H_2 at 15 Torr (~20mB). The sheath fields, under similar conditions, have been measured as being of the order of 10^3 Vcm^{-1}, hence an electron could gain ~$0.1 eV\mu m^{-1}$ or a maximum of ~3 eV per mfp. Since many collisions at low energy will be elastic [Saitoh 1994] it can be appreciated that a significant fraction of electrons in the high energy tail of the *eedf* could easily gain energies of ~15-20 eV in the sheath, which is sufficient to cause dissociation and ionisation. The high ion density in the sheath may reduce the electron *mfp* e.g. McGinnis *et al.* have quoted a value of ~5-10 μm from Monte Carlo modelling of the sheath region [McGinnis 1995], however this would not invalidate the above argument. The mechanism of secondary electron emission qualitatively explains the rapid increase in bias current which is observed above a threshold voltage, at which point the sheath fields presumably become large enough to generate a significant fraction of high energy electrons able to cause further ionisation and excitation - this could account for the appearance of a secondary glow. Compared to most materials, diamond has a high secondary electron efficiency and is an excellent emitter [Dreifus 1998] which could then account for the strong increases in both the bias current and the intensity of the glow,

which have been reported to occur as the substrate surface becomes covered in diamond [Schreck 1996, M^{c}Ginnis 1995, Milne 1995, Kulisch 1996].

An interesting correlation can be made between the results obtained during the current study and the work of Saitoh *et al.* [1994], which supports the argument that the secondary glow is a source of atomic hydrogen and may also explain the position of the observed peak at 1-2 mm above the substrate surface. They carried out Monte Carlo simulations and measurements to investigate the rate of dissociation of H_2 by electrons emitted from a hot filament and accelerated to a nearby substrate by an applied field within an H_2 background. They examined a range of pressures (2-20 Torr) and fields (~0.5 - 5 kVm^{-1}) and found that the number of dissociating collisions with H_2 exhibited a strong variation with the ratio of field to gas pressure (*E/p)*; with the maximum number of dissociating collisions occurring at an *E/p* value of ~ $4x10^3$ $Vm^{-1}T^{-1}$. This was explained by the peak in the electron dissociation cross-section for H_2 which has maximum for electron energies of ~15 eV; above about 20 eV ionisation then becomes the dominant inelastic process. Estimates for this parameter can be made for the current study from the reactor pressure of 15 Torr, sheath thickness ~2-3 mm and the applied bias (assuming ~150V is dropped by the sheath) giving a value of *E/p* ~$5x10^3Vm^{-1}T^{-1}$; by comparison a value of ~$4.4x10^3$ $Vm^{-1}T^{-1}$ can be obtained from the field measurements reported by Schreck *et al.* These *E/p* values are all remarkably similar and indicate that conditions above the substrate during typical biasing are favourable for H_2 dissociation. Furthermore, Monte Carlo modelling carried out by Saitoh *et al.* indicated that under these *E/p* conditions the fraction of electrons with sufficient energy to cause H_2 dissociation did not become significant until a distance of ~1.8 mm from the thermal source. This distance correlates reasonably well with the position of the H• maximum measured in the current study - figure (6.5b), which extends between 1-2 mm from the substrate surface. It also coincides with the position of the H_α peak (1.95 mm) measured above a clean silicon substrate by Schreck *et al* [1996]. The position of the glow can be expected to be fairly insensitive to reactor conditions because the energy gained by an electron in the sheath depends on competition between the mean

free path and the electric field strength, i.e. an increase in the pressure decreases the mean free path, but would tend to increase the field strength in the sheath; this argument is supported by measurements in the cathode fall of a DC plasma which show that the emission peak moves by only ~0.2 mm, from about 1.3 to 1.5 mm above the cathode substrate, for pressures varying from 18 to 28 Torr; see figure (6.8c) [redrawn from Surendra 1992].

In the context of the above discussions, it can be speculated that bias nucleation may be possible, under the correct conditions, without the aid of the main microwave plasma. It is interesting note that in a D.C methane plasma, under conditions that grow good diamond at the anode, rather poor graphitic material is deposited at the cathode [Plano 1991]; furthermore, in hot filament deposition a strong BEN nucleation effect has been reported whenever a negatively biased silicon substrate is enveloped by a DC glow [Zhu 1995]. While a *very recent* paper [Grouzman 1998] described BEN in a hot filament rig, with the filament off, which was achieved by generating a DC plasma between a molybdenum ring biased at 500 V positive with respect to a grounded silicon substrate; a detailed description of the DC plasma has not yet been published.

The measurements of the variation of the bias current with methane, pressure, microwave power and substrate temperature, figures (6.6b) and figure (6.7a-c) respectively, indicate that the bias current is quite sensitive to the reactor conditions. Strong variation in the bias current is evident for all these parameters, with the exception of the substrate temperature which had little influence on the bias current in the range 650-900°C. As already noted the temperature insensitivity is contrary to the situation which would be expected if thermionic emission from the tungsten surface was contributing significantly to the rapid increase in current which was observed at a threshold voltage of around 100V, figure (6.6a). The strong variation with microwave power could be expected and probably simply reflects the change in plasma size, which was observed to decrease smoothly with reducing power down to ~200 W. Below this value, the discharge could not be reliably sustained and was

unstable. As has already been noted, the variation of bias current with pressure becomes very strong, most notably at the higher biases (~120-170 V), for lower reactor pressures as indicated by figure (6.6b). At reactor pressures of around 15 Torr, the variation is very strong and non-linear, with the bias current increasing rapidly with both increasing voltage and decreasing pressure. Figure (6.6b) appears to indicate that a threshold of around 20-25 Torr exists, before the onset of rapid bias current increase occurs. At pressures above this value, even for high bias voltages, only slight variation in the bias current with either voltage or pressure is apparent, with the substrate currents at around 20-25 mA. This threshold behaviour could be understood in terms of the *E/p* values required for efficient ionisation in the sheath region above the substrate. The strong decrease in bias current with increasing methane fraction shown in figure (6.7b) has been noted by other authors and it has been suggested that this could be due to a change in the balance of the contribution of different ions in the plasma to the bias current [Kulisch 1996].

These measurements underline the need to carefully control reactor parameters during biasing. Recent papers have commented on the apparent poor reproducibility of the BEN process, both between different research groups and from run to run within the same reactor [Milne 1995, Kulisch 1996]. The critical sensitivity of oriented nuclei to the total BEN time and hence the integrated current is well known [Schreck 1996, Jiang 1996, Stockel 1998]. Various suggestions have been made in the literature to explain the poor reproducibility of the BEN process, including variations in substrate resistivity, residual oxide contamination and the effects of nearby reactor surfaces already covered with diamond from previous growth runs in the chamber; these have been summarised by Kulisch *et al.* [1996]. However, the measurements presented here suggest an alternative or additional explanation arising from the strong sensitivity of the bias current to the microwave power, methane fraction and gas pressure variables. The pressure in particular is likely to be a considerable source of uncertainty, as many groups carry out biasing at a reduced pressure compared to growth pressures, with 15 Torr being quite typical [e.g. Schreck 1995, Wolter 1994, Yugo 1996]. It can be seen from figure (6.6b), that in the low

pressure range the bias current is highly sensitive to both bias voltage and pressure. Systematic variations in reactor pressure due to differences in e.g. experimental procedure, type of pressure gauge and gauge position could account for some of the biasing current variations which have been reported. It is therefore clearly important, from a process control perspective, to monitor and control these reactor parameters carefully, particularly during biasing.

6.5 Summary.

This chapter has presented the results of a detailed study of the secondary glow region which is often observed between the plasma and substrate during bias enhanced nucleation. Optical studies reveal a disc-like secondary plasma which begins to develop in a 2% CH_4-H_2 plasma for negative above biases of around 100V, under the reactor conditions studied here; the bias current also shows a non-linear increase at this point. At high biases it was noted that the secondary glow could be self-sustaining if the microwave plasma was turned off. Pure argon and hydrogen-argon plasmas exhibit qualitatively similar behaviour under similar bias conditions.

For an argon plasma, spatially resolved optical emission measurements made across the region from the substrate to the microwave plasma base, on the reactor axis, show large increases in the Ar_{750} intensity and Ar_{750}/Ar_{811} ratio. Maxima occur at a position approximately 1-2 mm above the substrate surface and the measurements can be interpreted as indicating that elevated electron processes occur in this region. Similar measurements for the case of a hydrogen-argon plasma also show peaks in the atomic hydrogen concentration and electron temperature at a similar position. Comparison with other work [Schreck 1996], together with similarities between the glow region observed here and regions present in the cathode fall of D.C. glow plasmas at similar gas composition and pressures, suggest that the secondary glow, observed during biasing in a

microwave discharge, is a D.C. glow plasma. It is likely that this is a region where high inelastic process rates occur and acts as a strong source for the production of atomic hydrogen and other energetic species during biasing; secondary electron emission from the substrate surface can explain its appearance. The importance of this region has recently been highlighted in the bias nucleation model proposed by Stockel *et al.* [1998] who concluded that the secondary glow has an important role in the formation of the oriented nuclei observed during BEN.

6.6 References.

Ashcroft N.W. and Mermin N.D, [1981], *Solid State Physics,* Holte-Saunders International Editions, Tokyo.

Atkins P.W, *Physical Chemistry,* 2nd Edition, Oxford University Press, Oxford 1982.

Bou P., Vandenbulcke R., Herbin R. and Hillion F., [1992], *J. Mater. Res.*, **7**, 2151.

Bozeman S.P., Stoner B.R. and Glass J.T., [1998] in Chapt. 25, *Handbook of Industrial Diamonds and Diamond Films*, eds. Prelas M.A., Popovici G. and Bigelow L.K., (Marcel Dekker Inc.), New York, USA.

Dendy R., [1993], *Plasma Physics: An Introductory Course.*, Cambridge University Press, UK.

Dreifus D.L. and Fox B.A., [1998], Chapt. 29 in, *Handbook of Industrial Diamonds and Diamond Films*, eds. Prelas M.A., Popovici G. and Bigelow L.K., (Marcel Dekker Inc.), New York, USA.

Gerber J., M. Weiler M., O. Sohr O., K. Jung K. and H. Ehrardt H., [1994], *Diam. and Relat. Mater.*, **3**, 506.

Greene J.E., [1978], *J. Vac.Sci.Tech.*, **15**, 1718.

Grotjohn T.A., [1998], in *Handbook of Industrial Diamonds and Diamond Films*, eds. Prelas M.A., Popovici G. and Bigelow L.K., (Marcel Dekker Inc.), New York, USA.

Hassouni K, Scott C.D. and Farhat S., [1998], in chapt.18, *Handbook of Industrial Diamonds and Diamond Films*, eds. Prelas M.A., Popovici G. and Bigelow L.K., (Marcel Dekker Inc.), New York, USA.

Huddlestone R.H. and Leonard S.L., [1965], *Plasma Diagnostic Techniques*, Academic Press, New York.

Kulisch W., Ackermann L. and Sobisch B., [1996], *Phy. Stat.Sol. (a),* **154**, 155.

Lee Y.H., Richard P.D., Bachmann P.K. and Glass J.T., [1990], *Appl. Phys. Lett.*, **56**, 620.

Manenschijn A., Janssen G.C.A.M., van der Drift E. and Radelaar S., [1991], *J. Appl. Phys.*, **69**, 1253.

M^{c}Daniel E.W., [1965], *Collisional Phenomena in Ionised Gases*, John Wiley and Sons, New York.

McGinnis S.P., Kelly M.A. and Hagstrom S.B, [1995], *Appl. Phys. Lett.*, **66**, 3117.

Milne D.K, Roberts P.G, John P, Jubber M.G, Liehr M and Wilson J.I.B, [1995], *Diam.& Relat.Mater.*, **4**, 394.

Plano L.S., [1991], *SPIE (Applied Spectroscopy in Materials Science)*, **1437**, 13.

Saitoh H., Mima H., Ishiguro T. and Ichinose Y., [1994], *Diam. and Relat. Mater.*, **3**, 452.

Schreck M, Baur T and Stritzker B, [1995], *Diam. and Relat. Mater.*, **4**, 553.

Schreck M. and Stritzker B., [1996], *Phys. Stat. Sol.(a),* **154**, 197.

Stockel R., Stammler M., Janischowsky K., Ley L., Albrecht M. and Strunk H.P., [1998], *J. Appl. Phys.*, **83**, 531.

Stoner B.R, Ma G.H.M, Wolter S.D and Glass J.T, [1992], *Phy. Rev. B*, **45**,11067.

Stoner B.R., Ma G.H., Wolter S.D., Zhu W., Wang Y.C., Davies R.F. and Glass J.T., [1993], *Diam. & Relat. Mate.r.*, **2**, 142.

Wolter S.D, Stoner B.R, and Glass J.T, [1994], *Diam.& Relat.Mater.*, **3**, 1188.

Yugo S., Kanai T. and Muto T., [1990], *Vacuum*, **41**, 1364.

Yugo S., Semoto K. and Kimura T., [1995], *Diam. and Relat Mater.*, **5**, 25.

Zhang J., Huang B., Reinhard D.K. and Asmunssen J., [1990], *J. Vac. Sci. Technol.* **A,8**, 2124.

Chapter 7

Optimising Bias Enhanced Nucleation

It is clear that bias enhanced nucleation (BEN) is a very promising development for the growth of high quality, densely nucleated diamond films. Limited orientation of the films on non-diamond substrates has also been observed and it is believed that BEN nucleated films may offer the best prospects for the eventual production of electronic grade material. However it is widely acknowledged in the diamond community that BEN suffers from poor process control leading to considerable variation in the quality and orientation of subsequent films. If BEN is to become a useful technique it is important to understand the nature of its effects and to develop *in-situ* monitoring which can be used to optimise the process, ensuring the growth of the highest quality films. This chapter presents the results of an AFM study carried out to examine the nature of BEN oriented nuclei and test simple laser reflectometry for use as an in-situ technique to determine the optimum BEN treatment time.

7.1 Introduction

Bias enhanced nucleation (BEN) has become an established technique for the formation of highly oriented, heteroepitaxial polycrystalline diamond films [HOD] grown by microwave plasma enhanced chemical vapour deposition [Stoner 1992, 1993, Jiang 1996]. In the sense used here 'heteroepitaxy' is taken to mean localised registry between substrate and film; true epitaxy is not implied. The processes by which a negative bias, applied to the substrate during the initial stages of growth, can lead to enhanced nucleation and local epitaxy are not fully understood, but several papers have discussed possible mechanisms [Robertson 1995, Gerber 1994, Milne 1995]. The status of HOD films has been reviewed in more detail elsewhere in this thesis. From these discussions it has become apparent that the conditions used during the bias step vary considerably between differing reactors and the time required to achieve optimal alignment and film quality is poorly defined [Milne 1995]. It is also the case that the area over which the highly oriented material is grown can often be limited to a rather small region of the film [Kulisch 1996]; for example, a narrow ring of highly oriented material located within a circular region of non-oriented film has been routinely reported by the group at Heriot-Watt [Jubber 1996]. Very recently Stockel *et al.* [1998] have associated this ring with the presence of the secondary plasma observed during biasing. For BEN to become a commercially important technique these problems need to be overcome; establishing a convenient means of real time *in-situ* BEN process control would be a useful advance towards achieving this goal. This chapter presents the results of a study carried out to determine if low cost optical reflectometry is a useful tool for controlling the BEN process. The results presented also provide some insight into the *limited* area of orientated material which is usually obtained under *typical* BEN conditions.

The growth of diamond on silicon and other materials by CVD methods can only be achieved once a suitable nucleation layer is produced on the substrate. Conventionally this has been achieved by scratching the substrate with diamond powder [e.g. Mitsuda 1987], but alternatively a short (typically 15 minute) period of a negative bias applied to the substrate, often combined with a modest increase in the hydrocarbon content

within the feedstock gases (typical 4% from 1%), can be used. This method can lead to a form of limited heteroepitaxy in which individual diamond crystallites show some degree of orientation with respect to the underlying substrate; however, under non-optimised conditions, BEN can result in randomly aligned polycrystalline growth. In the current study, atomic force microscopy (AFM), Raman spectroscopy and scanning electron microscopy (SEM) have been used to study the nature of the nuclei formed during the BEN process and this information is related to the results of optical studies of the BEN nucleation layer which have been made using simple laser optical reflectometry.

7.2 Experimental Details.

Bias enhanced nucleation by microwave plasma enhanced CVD of diamond on silicon (100) was carried out in a stainless steel resonant chamber reactor supplied by RFA Ltd; modified to enable bias enhanced processes to be carried out. The substrate holder was electrically isolated from, and raised above, the substrate heater. Onward growth under (100) texturing conditions was carried out in the DERA ASTeX chamber; for a more detailed description of the reactors used in this study the reader is referred to the discussion which has been given in chapter 3. Electrical bias was achieved by directly attaching a tantalum wire directly to the substrate holder. The plasma was in near contact with the substrate holder separated by the sheath region previously studied in chapters 5 and 6 and was of a flattened hemispherical shape which did not contact any other regions of the microwave chamber. A microwave power of ~1kW was used throughout at a frequency of 2.45GHz. Nucleation studies were carried out with dilute methane in hydrogen feedstock gas. The typical nucleation and chamber conditions employed during this study are shown in table (7.1).

Process Parameter	RFA Reactor		DERA (ASTEX) Reactor
	Carburisation	Bias	Growth
Power (watts)	1000	1000	800
Pressure (torr)	20	20	30
Substrate temp (°C).	800	800	600
Hydrogen (%)	98	95	93
Methane (%)	2	5	4
Argon (%)	0	0	3
Total gas flow (sccm)	100	100	418
Substrate potential (V)	grounded	-200	grounded
Process time	20 mins	30 mins	19 hours

Table (7.1): Table showing the typical carburisation, bias and growth conditions used in the two microwave reactors during this study.

Samples ~2.5 cm x 2.5 cm were cut from clean, pristine (100) silicon wafers and then subjected to a 20 minute 'carburisation' stage immediately followed by bias nucleation at -200 volt bias for times ranging from 15 to 60 minutes. The chamber conditions used during these stages were different and are summarised in table (7.1). Following biasing the samples were removed from the RFA reactor and cleaved into two equal halves, care was taken to ensure that the cut bisected the symmetrical circular deposits on the substrate which were characteristic of the BEN process; figure (7.1) indicates schematically the typical appearance of the substrates following removal from the reactor and the location of the subsequent cut. One half of the substrate was then subjected to AFM and laser reflectometry analyses, while the second half of the sample was subjected to further growth under (100) textured conditions which are listed in table (7.1).

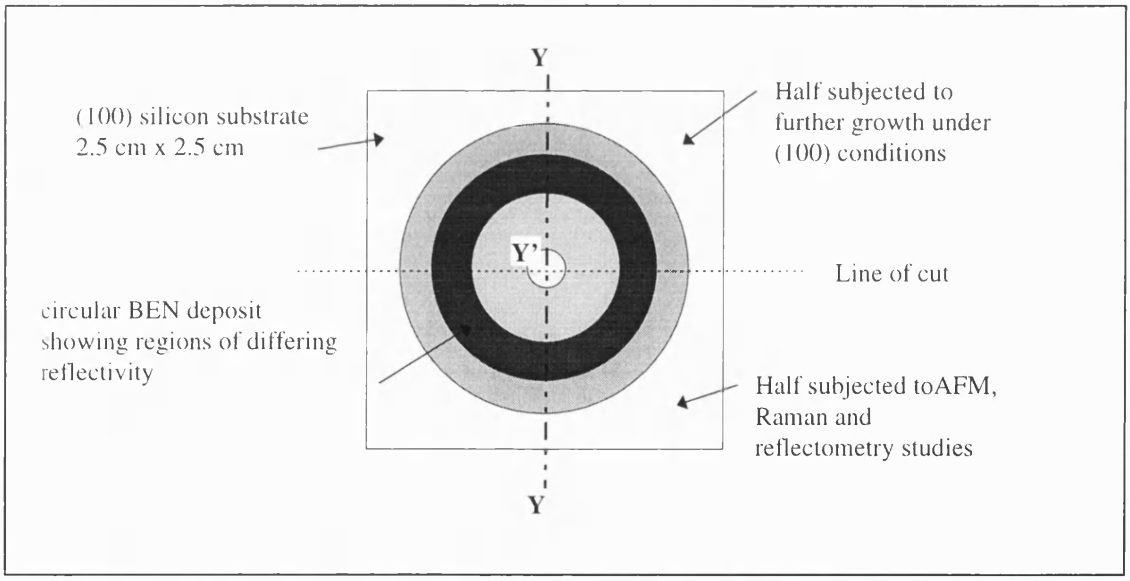

Figure (7.1): Schematic (not to scale) showing the typical appearance of surface deposits following BEN, the lightest colour corresponds to the higher reflectivity. The dotted line shows the location of the cut made to divide the substrate; Y-Y' indicates the approximate line of subsequent AFM, Raman & SEM analyses.

The AFM studies were carried out using a Park Scientific instrument operated in contact mode which has been described in more detail in chapter 3. Optical reflectometry measurements were also carried out at this time using a red (643nm) diode laser (beam diameter < 2mm) and photodiode detector. During these measurements the samples were scanned under the laser spot using a micrometer driven

X-Y stage and the photodiode trace was recorded for analysis; figure (7.2) shows a simple schematic of the arrangement used.

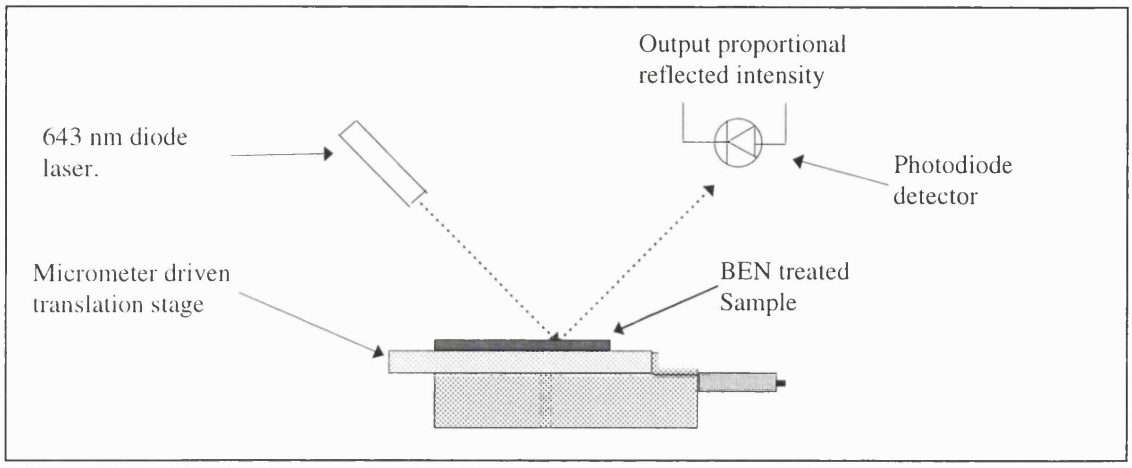

Figure (7.2): Simple schematic showing the experimental arrangement used to carry out laser reflectometry scans of silicon substrates following biasing at -200 V.

The remaining half of the cleaved, bias nucleated samples were subjected to onward growth in the ASTEX microwave chamber at DERA Malvern for ~19 hours under reactor conditions, summarised in table (7.1), which have previously been demonstrated to promote the growth of (100) textured material, see for example chapter 4. This allowed subsequent Raman and SEM analysis to be more easily carried out and enabled any orientation in the individual crystallites to be established from the SEM studies. Raman spectroscopy was carried out using a Renishaw System 2000 with red (~632 nm) He-Ne laser light previously described in chapter 3. To ensure the most uniform growth on the BEN nucleated sample, it was centred on the ASTEX substrate holder so that it was exposed as uniformly as possible to the central region of the growth plasma, which, in this reactor under the conditions used here covered the entire 5 cm diameter holder. To reduce the influence of edge effects the sample was surrounded with pieces of silicon, which had previously been carburised, to form a complete substrate covering the holder.

7.3 Results.

Bias enhanced nucleation parameters for the RFA reactor were established prior to nucleating the samples which were then used for the further studies described in the previous section. These involved a pre-bias treatment of the Si(100) substrate for 20 minutes under the conditions shown in table (7.1); a process which has been described as 'carburisation' in the literature and may aid the formation of oriented nuclei during the subsequent bias step [Wolter 1993, Stoner 1993]. The applied voltage during bias was -200V and resulted in a bias current of 20 - 40 mA. The duration of the bias step was varied between 15 and 60 minutes. For the shortest bias periods, nucleation (as judged by subsequent growth) was limited to a small central region of the substrate; appearing as a darkened circular region if examined directly after BEN, prior to any growth. The 'darkened' region was seen to move out from the centre appearing as a ring for longer bias times. For the purposes of the current study a bias period of 30 minutes was chosen as a compromise; long enough to show the dark ring, which had moved some way from the centre, but short enough that the outer parts of the relatively small (2.5 cm x 2.5 cm) samples exhibited few visible bias effects. The BEN treated region appeared qualitatively similar for the longest bias times (60 minutes) but associated with a larger area on the substrate. Figure (7.1) shown previously, indicates schematically the appearance of the substrate following 30 minutes of bias.

Following nucleation, samples were examined optically to reveal a darkened region which extended over a circular area with a diameter of ~ 20 mm. Outside of this area the silicon appeared relatively unaffected by comparison with a pristine sample. Optical reflectivity measurements were recorded as a function of distance from the centre of the circle at intervals of 1mm; the results are shown in figure (7.3). The data has been normalised to the value obtained from untreated silicon and shows that the reflectivity at the centre of the BEN-treated area is approximately 70% that of the untreated silicon wafer. Moving further out from the centre of the treated region the recorded reflectivity drops to a minimum before rising near to the untreated surface value at greater distances from the centre, outside of the affected region as apparent to the unaided eye.

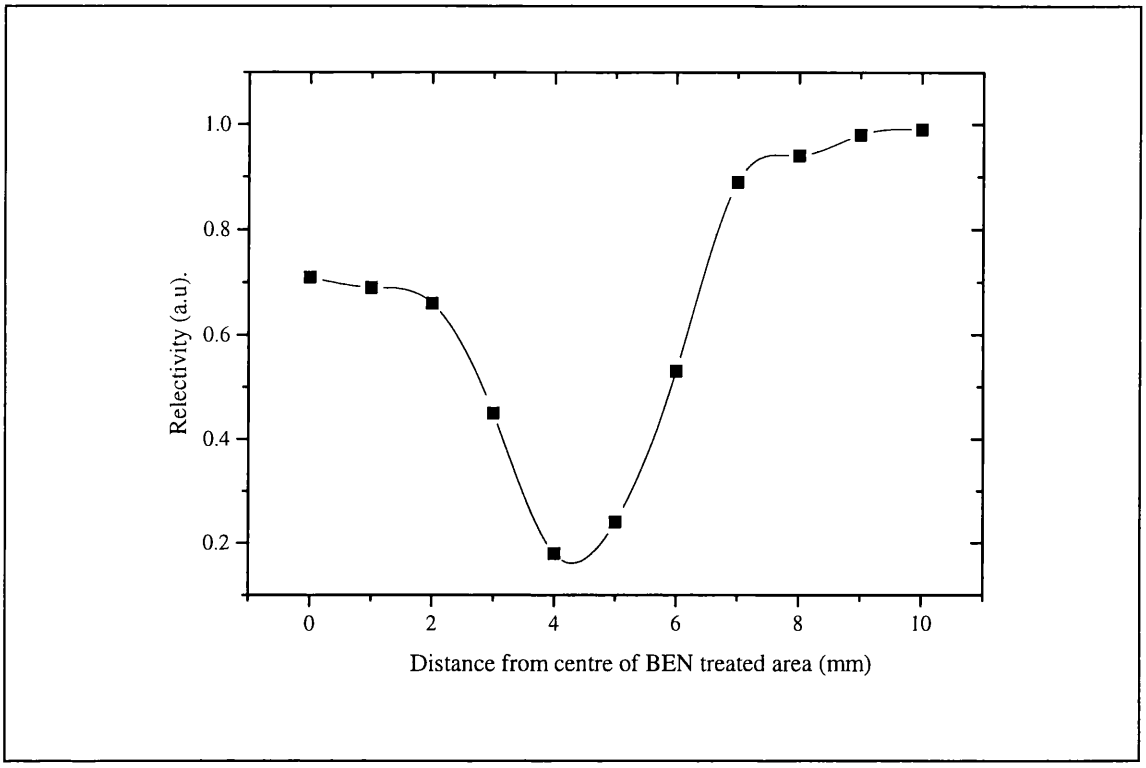

Figure (7.3): The optical reflectance signal monitored as a function of the distance of the probe beam from the centre of the BEN deposit: normalised to the value obtained from untreated silicon

To correlate the changes in reflectivity with the structure of the nucleated surface, the BEN treated samples were examined using AFM. The sample was examined along the Y-Y' line indicated on figure (7.1), images were taken at a number of locations and at a range of resolutions. Using the optical reflectometry results as a guide, the study concentrated on the centre and the region of minimum reflectivity. Representative AFM images taken during the study are shown in figure (7.4 a-d) for differing regions of the sample surface.

In figures (7.4a,b); low and high resolution images respectively of the centre of the BEN treated sample are shown. It can be seen that the BEN process produces significant surface roughening on the 100 nm depth scale. The surface features show no particular crystal faceting and are widely distributed in size within the range 20-120 nm. These images can be compared with the AFM image representative of the region of the surface which displayed low reflectivity, shown in figure (7.4c). The surface appearance is significantly different; surface features are more regular, with sizes of ~100 nm, and have a well defined morphology. Further out from the centre of the BEN treated region these features become less densely distributed and in figure (7.4d) rather

sparse features are apparent, although their size is again ~100 nm. The relatively smooth morphology of the silicon wafer in the region unaffected by BEN can also be seen in this picture.

The second half of the BEN treated sample, which had been cleaved in two, was subjected to ~19 hours of further growth under conditions leading to (100) texture as has been described in section (7.2). Following the period of textured growth, analysis of the film was carried out by SEM and Raman spectroscopy. Film thickness' of around 2-3μm were estimated, from SEM cross-sections, for the region displaying minimal reflectivity as defined in figure (7.3). SEM and Raman studies were made along the Y-Y' line indicated in figure (7.1), however these analyses were concentrated on the regions of main interest defined by the previous AFM and reflectometry measurements. Typical Raman spectra are presented in figure (7.5).

Outside the BEN region the SEM showed minimal film growth and the Raman spectra for this area show little evidence for the presence of diamond as illustrated by the absence of the characteristic 1332 cm^{-1} diamond peak in the spectrum shown as curve (iii) in figure (7.5). In the region which displayed minimum optical reflectivity, figure (7.3), the Raman spectrum, which is shown as curve (ii) in figure (7.5), clearly shows the presence of the diamond peak at ~1332 cm^{-1} . It is should be noted that the Raman spectra were acquired using 632 nm light which is considerably more sensitive to the non-diamond carbon components in the film compared to spectra that are more commonly recorded using 488 or 514 nm sources [Williams 1993]. The Raman spectrum obtained at the centre of the BEN region is shown as curve (i), the 1332 cm^{-1} peak is again visible, but is somewhat weaker than was the case for the region displaying the lowest reflectivity. The unlabelled spectra were taken as part of the scan at positions intermediate to the labelled curves.

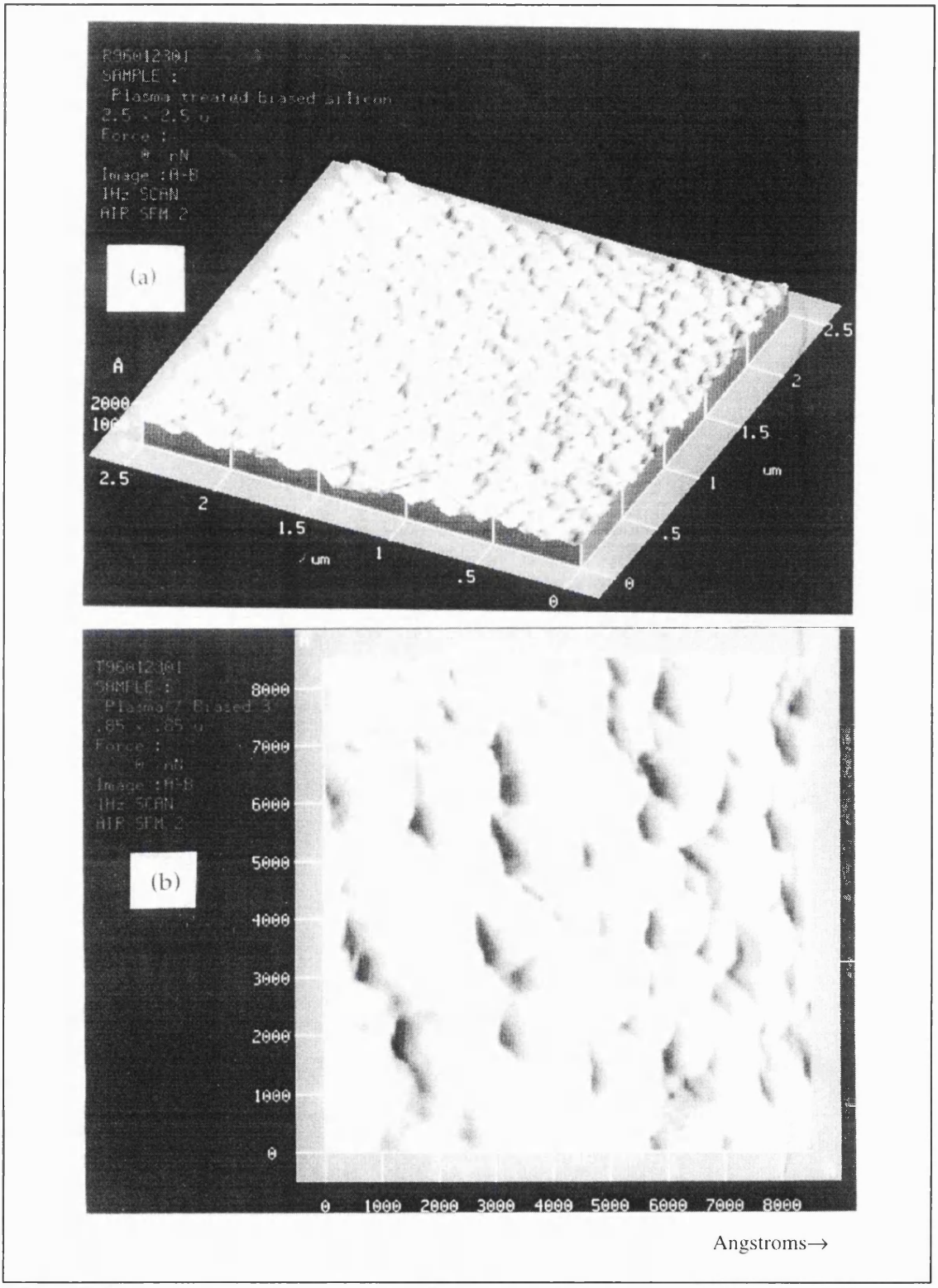

Figure (7.4): Atomic force microscope images from the central region of the sample surface (a) low resolution (scales in microns); and (b) high resolution, (scales in angstroms).

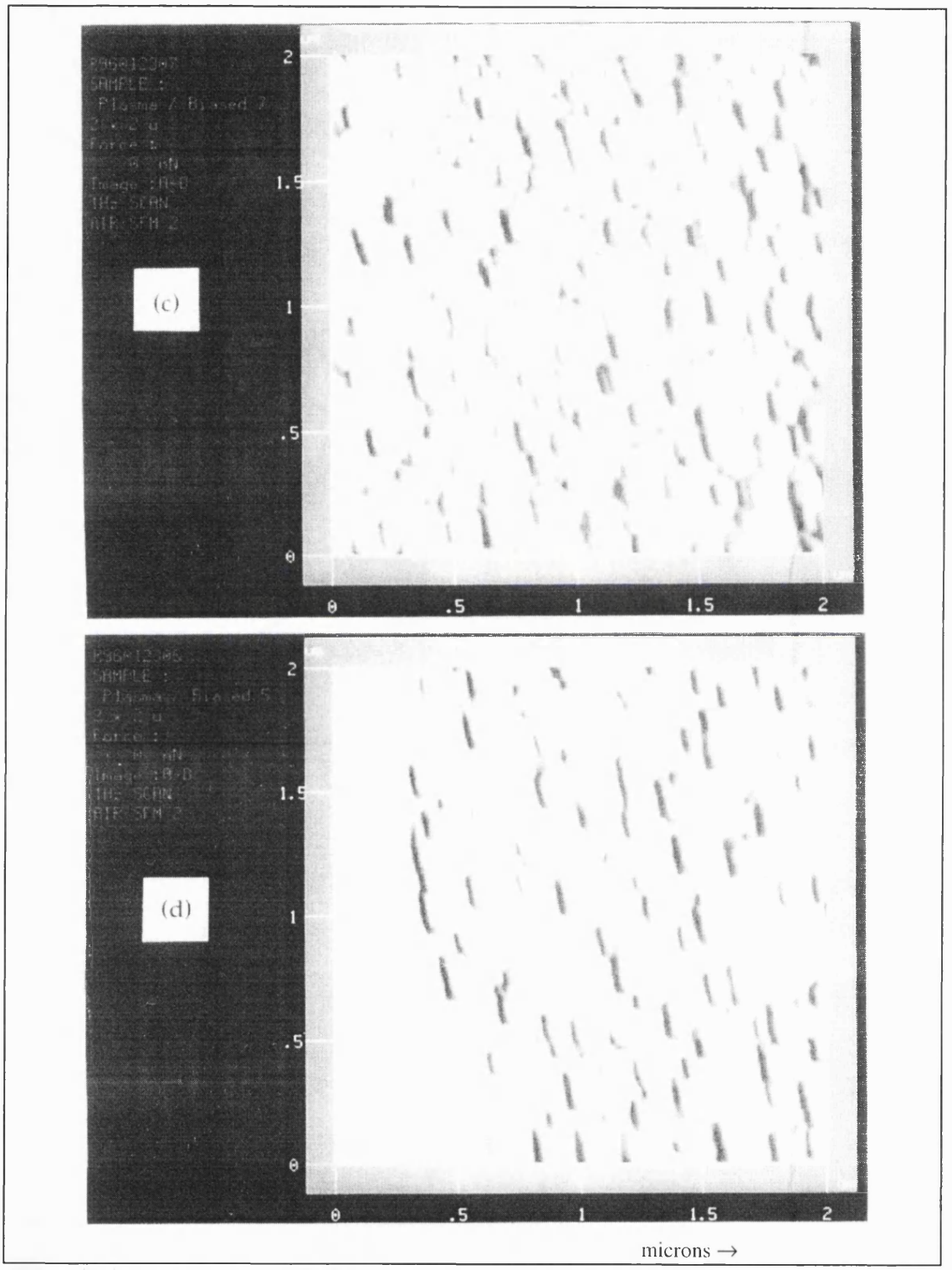

Figure (7.4): High resolution AFM from the region which showed low reflectivity is shown as (c) whilst (d) shows the AFM image far out from the centre of the BEN treated region. Scales are in microns.

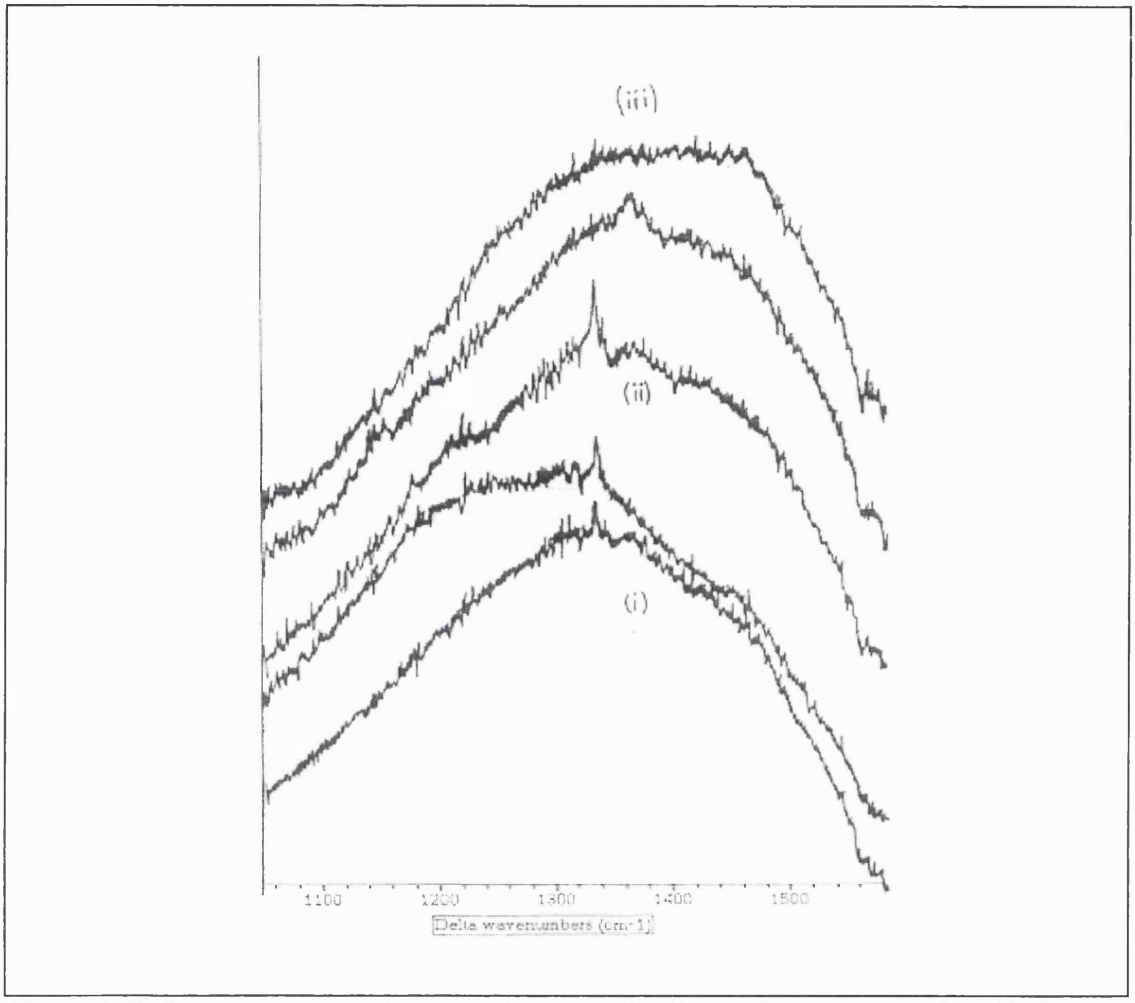

Figure (7.5): Raman spectra recorded with red (632 nm) He-Ne laser for (i) central region of BEN area, (ii) region with low optical reflectivity (iii) region outside of the BEN treated area.

To assess the degree of any common angular orientation between the (100) crystallites comprising the film and establish if there was a correlation between the nature of the starting nuclei, as revealed by AFM and reflectometry, and orientation in the subsequent film, two particular regions were examined in detail by SEM. The regions studied were the centre of the sample and part of the region which displayed minimal optical reflectivity. A simple method was developed to make an assessment of statistical orientation from the SEM micrographs The procedure involved scanning SEM photographs into a CAD software package and the details are listed and briefly described below:

i. SEM image scanned into computer at high resolution.

ii. Digital image then imported into CAD package (MacDraw Pro).

iii. An arbitrary axis was defined running 'north-south' and marked on the image using the drawing tools.

iv. Small arrowed 'vectors' were marked on the image for each crystallite, defined along an edge. Since the (100) textured grains are effectively square it is sufficient to choose a 'vector' for each grain which makes an angle to the axis of between 0° and 45°.

v. The SEM image was then removed and the vectors 'binned' in 5 degree intervals over the range 0° to 45°. The number of vectors in each angular interval were plotted as a histogram to provide a quantitative assessment of the distribution of crystallite orientations.

Figure (7.6) shows an example of one of five SEM's, taken from the region showing minimum reflectivity, the orientation vectors described above are shown on the micrograph to illustrate the description of the statistical assessment method which has been given above.

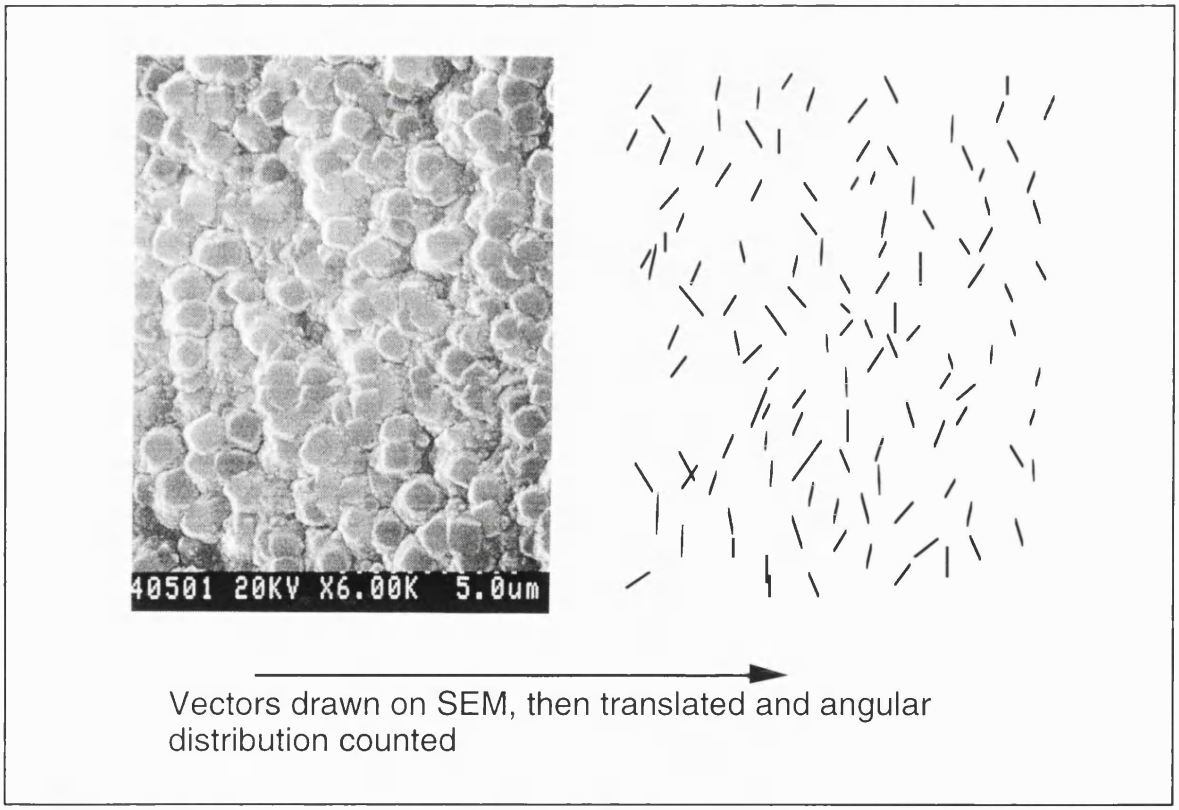

Figure (7.6): One of the SEM micrographs, taken from the BEN nucleated sample following onward growth, showing the method used to assess the degree of statistical orientation between grains. A full description of the procedure is given in the text.

The results of the orientation analysis for the centre and low reflectivity regions are plotted in the form of a histogram in figure (7.7). In the low reflectivity region it is apparent that a degree of statistical orientation exists between the grains; while in contrast, at the centre of the BEN region there is little evidence from the plot of any alignment.

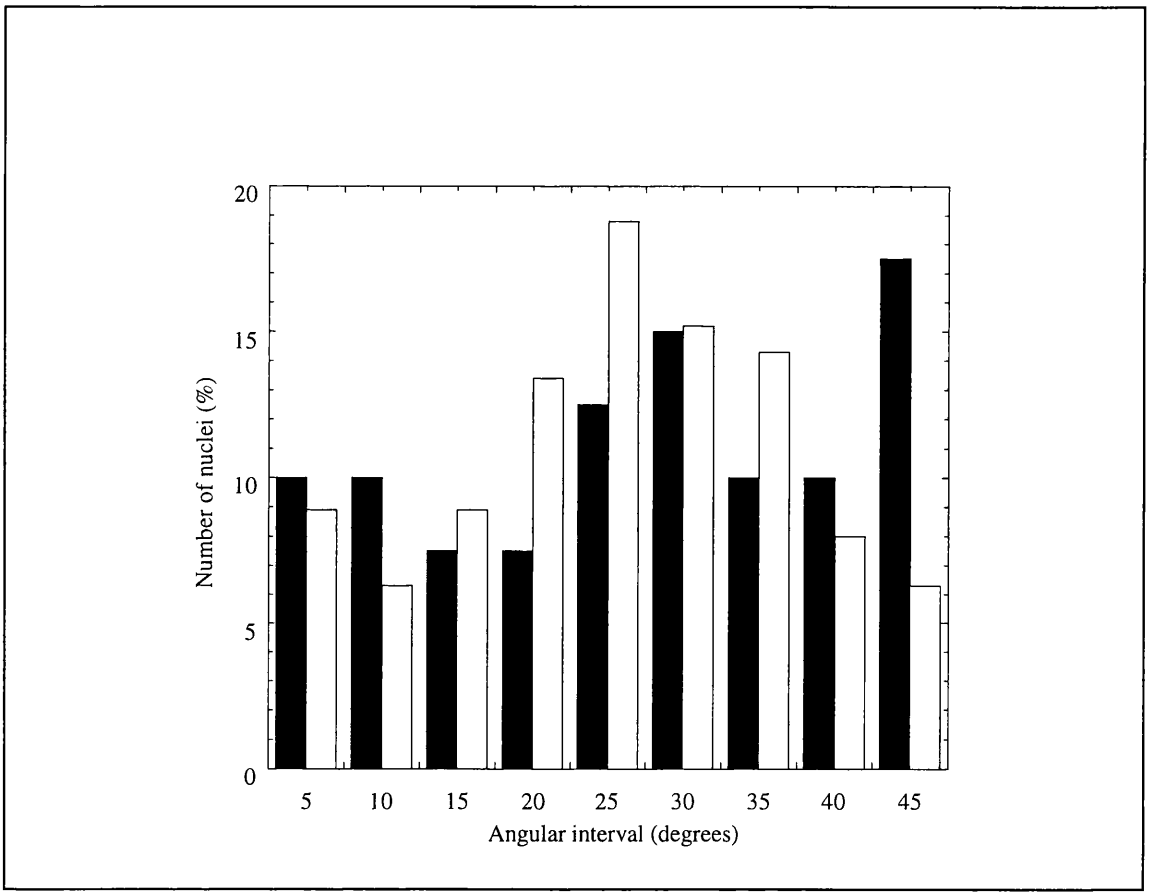

Figure (7.7): Histogram plot showing the results of the statistical orientation analysis; dark bars show the angular distribution of (100) crystallites in the central BEN region, open bars show the same analysis for the BEN region which exhibited minimum reflectivity.

7.4 Discussion.

One of the most important effects of the bias process has been the realisation that BEN nucleated films can display limited epitaxy, particularly for (100) diamond on (100) silicon. First reported on silicon in 1993, [Wolter 1993], subsequent development has refined the technique so that as of 1998 reports of wider area *polycrystalline epitaxy* are now beginning to emerge [RD Marshall 1998, Floter 1998]. The advent of such films has provided a source of smooth, high quality material with low defect densities and a

low density of low angle grain boundaries. These films show improved electronic properties over typical random polycrystalline material and offer the realistic prospect of a 'pseudo-single crystal' thin film form of diamond for the fabrication of high performance electronic and optical devices [Fox 1994]. However, despite the acknowledged importance of these developments and the very considerable world-wide research effort, which continues at the time of writing, the mechanisms which underlie the BEN process are not fully understood and a consensus is not yet achieved [Bozeman 1998]. A discussion of the literature concerned with BEN and epitaxy has been given in chapter two to which the reader is referred for further details. The discussion here will concentrate on the results of this study with emphasis on the control and optimisation of the BEN process.

Recent BEN studies have indicated that the role of energetic species incident on the substrate surface maybe of considerable importance [Robertson 1995, M^{c}Ginnis 1995]; these species may include ions, radicals and neutrals, however the relative importance and balance of these energetic components is controversial and although evidence can be presented to support the different possibilities, well defined conclusive experiments remain to be carried out. Visible inspection of silicon wafers following BEN treatment in this study indicates that a circular region of modified material evolves with an area which increases with the bias period.

It has been widely reported that microwave generated plasmas are likely to produce a non-uniform flux of reactive species to the surface [Kulisch 1996, Bachmann 1998]. This can be primarily attributed the inhomogenity of the electric fields in a typical CVD reactor which can vary by up to four orders of magnitude from the centre to the edge of the plasma [Zhang 1990]. A consequent variation in the radial distribution of active species has been confirmed by various methods including TALIF and OES measurements [Gicquel 1998]. However, the application of a negative bias during BEN can further distort the plasma, as has been demonstrated and discussed in earlier chapters of this thesis, leading to a higher flux of energetic species, including ions, to the substrate surface from the central region. This is presumably the reason why the modified surface first becomes apparent at the sample centre, and why its area increases

with time. Variations in the nature of the modified surface on moving out from the centre are likely to simply represent variations in the flux of energetic species received at particular spatial positions on the substrate, with the radial symmetry reflecting the geometry of the biased plasma. A number of studies have indicated that the exact period and conditions under which BEN treatment is carried out are *critical* to obtaining good quality orientated films [Milne 1995, Kulisch 1996] It follows that for a non-uniform flux of species, with a radial distribution, any particular BEN treatment can only create an optimal nucleation surface over a limited area of the specimen. Given the radial symmetry of the substrate-plasma, this might be expected to take the form of a ring moving outward with increasing bias time and in this sense the 30 minute biased substrates studied here represent a time evolution of the BEN process. Jubber *et al.* [1996] have also reported that within a circular area of diamond nucleated by the BEN technique, heteroepitaxial material was confined to within a single ring (3-4 mm wide, ~40 mm from centre), under the conditions within their reactor; while more recently Jiang *et al.* described a larger ring of HOD material extending from 16 mm to 27 mm from substrate centre in their experiments [Jiang 1996]. More recently, careful observations by Stockel *et al.* [1998] have indicated that the development of this ring may be closely associated with the progress of the secondary plasma which can appear during biasing and which has been studied elsewhere in this thesis.

Under the BEN conditions utilised here, the results of the AFM analysis indicate there is a strong variation in the nature of the nuclei formed within the treated area as a function of radial distance from the substrate centre. Well-defined nuclei with regular morphology were apparent in regions which then give rise to areas showing evidence of statistically oriented crystals, following subsequent growth under (100) texturing conditions. The central BEN region, identified in AFM studies as showing more irregularity subsequently lead to the deposition of film in which the crystallites showed little or no preferred orientation. The AFM results obtained in the current study can be compared with other AFM measurements which have subsequently shown that there is a reduction in the azimuthal tilt of the (100) crystallites within the HOD ring in films grown following BEN treatments similar to those studied here [Jiang 1996]. A region in which conditions were optimal for nucleation was suggested as an explanation.

AFM studies, at resolutions similar to those shown here in figure (7.4 a-d), have shown surfaces with similar features as a function of BEN treatment time, [Jiang 1993, Gerber 1996]. The Raman scan analysis, figure (7.5), carried out after the period of extra growth also shows that the nature of the film varies with radial distance from the centre as might be expected considering the radial inhomogenity of the plasma; there is some evidence from the 1332 cm^{-1} Raman peak of improvement to the film quality within the ring region which exhibited low reflectivity. A similar result has been obtained on BEN nucleated films, following growth to much greater thickness of 10-15 μm compared to the 2-3 μm used here [Jiang 1996], which showed that the sp^2 content was higher at the centre, decreased in the oriented ring and then increased again towards the edge. The Raman scans made during this study show a similar variation in quality but are more difficult to interpret; this could be accounted for by the much thinner films used here, together with the high sensitivity of the 632 nm Raman system which tends to strongly emphasise the sp^2 fractions in the film compared with any sp^3 component; at the early stages of growth when films are very thin this can lead to rather noisy spectra.

In this work only statistically oriented crystallites were observed, which exhibited rather a wide distribution about the preferred orientation as judged by the analysis summarised in figure (7.7); this contrasts with more recent HOD films which have exhibited near 100% alignment, with misorientations of only a few degrees [e.g. Floter 1998]. However, such films only result from very careful optimisation of all the bias and growth conditions and are often grown to considerable thickness (~60 μm) to select out the best grains [Floter 1998]. In the current study only modest attempts were made to optimise the nucleation and growth parameters, as the growth of large area HOD films was not the primary goal of the work; a contributory effect might have been that native oxides on the silicon surface, which can disrupt the formation of oriented nuclei, were not completely removed by the cleaning process prior to nucleation.

The observations made in this study confirm the acknowledged importance of controlling the BEN treatment period and emphasise one of the difficulties of using this technique, particularly in reactors with radially inhomogeneous plasmas. From run-to-run, differences in observed bias current and plasma characteristics tend to occur and

can lead to changes in the nature of the nucleation layer created for a given bias period; consequently the need for precise process control during BEN has been acknowledged by many authors [e.g. Milne 1995, Kulisch 1996]. The optical reflectivity measurements reported in this study ,figure (7.3), can now be suggested as a promising method for the *in situ* real time determination, of the optimal BEN treatment period needed to reduce these variations. That the surface is most reflective some distance from the centre of the wafer, can be readily understood in terms of specular reflection from the smooth unperturbed silicon. Reduced levels of reflectivity may arise because of interference effects between light scattered from the differing interfaces present in the nucleation layers and from the diffuse scattering arising from surface roughness. The exact contributions of these effects cannot be deduced from the data presented here in view of the uncertainty concerning the precise nature of the BEN layers produced; however, strong evidence that the pre-nucleation layers can vary significantly is given by the measurements of Milne *et al.* who have shown, from FTIR measurements, that the SiC layer is considerably thicker in the region which gives rise to oriented nuclei following the bias step as compared to the central region of the wafer where they observed no orientation [Milne 1996]. To establish the precise contribution of the nucleation components to the optical reflectometry signal would require further study, none-the-less the measurements do show that the reflectivity changes quite markedly with position on the substrate, exhibiting a minimum in the region where optimal BEN nucleation occurs, as judged by subsequent film growth and the higher level of statistically oriented crystallites. The magnitude of the reflectivity change is quite large and is easily measurable. It can be speculated that a system could be designed in which several probe lasers are used to interrogate the reflectivity of the growth substrate during BEN to determine, in real time and *in-situ*, the optimum BEN treatment for a given set of process conditions; this could easily be incorporated into current *in situ* systems which use laser reflectance interferometry (LRI) to monitor the film growth rate [e.g. Stoner 1991]. In addition to routine process monitoring such a system could enable the reactor to be systematically modified to encourage optimal BEN conditions over the widest possible area.

7.5 Summary.

The application of a negative bias to an otherwise pristine Si(100) surface during MPECVD of diamond creates nuclei with differing properties depending on the length of time the bias is applied. The current study, which has utilised AFM, SEM and Raman scattering, has correlated the 'quality' of the nuclei with the optical reflectivity of the surface following BEN treatment. The AFM study indicated that the orientation of crystals appears to be determined during the BEN nucleation phase and is limited to a ring of oriented nuclei which moves out from the sample centre as BEN is continued. It was shown that the spatial variation of the reflectivity of the BEN deposit can be correlated with the propensity for the formation of oriented nuclei, which then give rise to statistically oriented crystals. This outcome is likely to be most favourable in the BEN region which displays a minimum in reflectivity when monitored by laser reflectometry. Given the acknowledged radial non-uniformity of MPECVD microwave plasmas, it would seem reasonable to speculate that the question of oriented nuclei is intimately linked with integrated flux and energy of the more energetic species which the substrate receives during the biasing phase. The current studies reported in this thesis, together with recent work by Stockel *et al.*[1998], suggest that the secondary plasma observed during biasing may be a source of such species, and could have an important role in determining the effects of the bias . To obtain oriented nuclei over a larger area, a method of 'averaging' the flux of these species to the substrate during BEN may be useful, e.g. by motion of the platen or possibly the plasma during BEN and subsequent growth.

It was shown that simple optical laser reflectometry can be used to determine the optimum period of BEN treatment and therefore this technique could in principle be used as an *in situ* process control diagnostic during the production of oriented CVD diamond films.

7.6 References

Bachmann P.K. [1998], Chapt. 21 in, *Handbook of Industrial Diamonds and Diamond Films*, eds. Prelas M.A., Popovici G. and Bigelow L.K., (Marcel Dekker Inc.), New York, USA.

Bozeman S.P., Stoner B.R. and Glass J.T., [1998] in Chapt. 25, *Handbook of Industrial Diamonds and Diamond Films*, eds. Prelas M.A., Popovici G. and Bigelow L.K., (Marcel Dekker Inc.), New York, USA.

Floter A., Guttler H., Schultz G., Steinbach D., Lutz-Elsner C., Zachai R., Bergmaier A. and Dollinger G., [1998], *Diam. and Relat. Mater.* **7**, 283.

Fox B.A, Stoner B.R, Malta D.M, Ellis P.J.,Glass J.T and Sivaziian F.R., [1994], *Diam. and Relat. Mater.* **3**, 382.

Gerber J., M. Weiler M., O. Sohr O., K. Jung K. and H. Ehrardt H., [1994], *Diam. and Relat. Mater.*, **3**, 506.

Gicquel A, Chenevier M. and Lefebvre M., [1998], in Chapt.19 in, *Handbook of Industrial Diamonds and Diamond Films*, eds. Prelas M.A., Popovici G. and Bigelow L.K., (Marcel Dekker Inc.), New York, USA.

Jiang X and Klages C.P, [1996], *Phys. Stat. Sol. (a),* **154**, 175.

Jubber M.G. and Milne D.K., [1996], *Phy. Stat.Sol. (a),* **154**, 185.

Kulisch W., Ackermann L. and Sobisch B., [1996], *Phy. Stat.Sol. (a),* **154**, 155.

Marshall R.D., [1998], *Private Communication.*

McGinnis S.P., Kelly M.A. and Hagstrom S.B, [1995], *Appl. Phys. Lett.*, **66**, 3117.

Milne D.K., Roberts P.G., John P., Jubber M.G., Liehr M. and Wilson J.I.B., [1995], *Diam. and Relat. Mater.*, **4**, 394.

Mitsuda K., Y. Kajima Y., T. Yoshida T. and K. Akashi K., [1987], *J. Mater. Sci.* **22**, 1557.

Robertson J., [1995], *Diam. and Relat. Mater.*, **4**, 549.

Robertson J., Gerber J., Sattel S., Weiler M., Jung K. and Ehrhardt H., [1995], *Appl. Phys. Lett.*, **66**, 3287.

Stockel R., Stammler M., Janischowsky K., Ley L., Albrecht M. and Strunk H.P., [1998], *J. Appl. Phys.*, **83**, 531.

Stoner B.R., Chien-tah Kao, Malta D.M. and Glass J.T., [1993], *Appl. Phys. Lett.* **62**, 2347.

Stoner B.R., Ma G.H., Wolter S.D., Zhu W., Wang Y.C., Davies R.F. and Glass J.T., [1993], *Diam. & Relat. Mate.r.*, **2**, 142.

Stoner B.R., Ma G.H.,Wolter S.D.and Glass J.T., [1992], *Phys. Rev. B*, **45**, 11097.

Stoner B.R., Williams B.E., Wolter S.D., Nishimura K. and Glass J.T., [1991], J. Mater. Res. **7**, 257.

Williams K.P.J., Pitt G.D., Smith B.J.E., Whitley A., Batchelder D.N. and Haywood I.P., [1993], *J. raman Spectros.,* **25**, 131.

Wolter S.D., stoner B.R., Glass J.T., Ellis P.J., Buhaenko D.S., Jenkins C.E. and Southworth P, [1993], *Appl. Phys. Lett.*, **62**, 1215.

Zhang J., Huang B., Reinhard D.K. and Asmunssen J., [1990], *J. Vac. Sci. Technol.* **A,8**, 2124.

Chapter 8

A Laser Ultrasonic Study of Acoustic Wave Propagation in CVD Diamond Films.

Recent reports suggest that surface acoustic wave (SAW) devices will become an important application for CVD diamond. Natural diamond has the highest acoustic velocity of any material and is stable in hostile environments; it is interesting to speculate on the suitability of the CVD diamond as a substrate material for acoustic sensors. The acoustic properties of natural diamond have been well studied, however little is known about the CVD form in this respect. This chapter presents the results of a laser ultrasonic study in which the effect of properties; such as quality, morphology and orientation together with temperature, on the velocity and dispersion of acoustic waves in free standing CVD diamond has been assessed. The suitability of CVD diamond for flexural plate wave (FPW) sensors for use in harsh environments is discussed and a prototype device design is presented.

8.1 Introduction

If the research and development of CVD diamond is to continue at the current high levels it is essential that profitable near-term applications for the material are found and exploited. The material properties of diamond are extreme and recent work by Japanese groups [Yamanouchi 1989, Nakahata 1992] with CVD diamond surface acoustic wave (SAW) devices strongly suggests that the acoustic properties of this material may be a source of such applications. Diamond has the highest acoustic velocity of any material, about a factor of two faster than the nearest alternative, it is also chemically and physically very stable in hostile environments. This suggests that diamond may be useful for the fabrication of both surface acoustic wave (SAW) and flexural plate wave (FPW) devices. These devices utilise the Rayleigh and Lamb acoustic wave modes respectively but are conceptually very similar and operate using almost identical device structures. In support of the assertion that acoustic devices are an important area for CVD diamond, Nakahata *et al.* have recently demonstrated a 2.5 GHz CVD diamond SAW filter [Nakahata 1996] which they claim has applications in current and future mobile communications systems. Additionally it was reported at the recent Diamond Films 97 conference that the Japanese electronics company, Sumitomo, were preparing to ship industrial quantities of CVD diamond SAW devices developed from the work of this group.

This chapter presents the results of a study carried out to examine the propagation of acoustic waves within typical examples of 'state of the art' thin film diamond. To the author's knowledge this is the first study of its kind reported in the literature. The principle aims of the work were to study the influence of film characteristics such as morphology, quality, texture and substrate temperature on the propagation of acoustic waves within the films. The principle acoustic mode studied in this work was the flexural plate or Lamb wave mode. The acoustic measurements to be presented were obtained using a novel and flexible laser ultrasonic technique which is described in more detail later in this chapter and also in chapter 3. Although some measurements on DLC's have previously been reported, this work has been in the field of 'Ultrasonics'. The study presented here, which concentrates on CVD diamond, represents to this author's belief, the introduction of a

technique which is new to the CVD-diamond research community, and provides information in an area which has previously been relatively neglected in this field.

Acoustic wave devices typically rely on an inter-digitated transducer (IDT) to launch elastic waves within a solid with frequencies in the megahertz to gigahertz range. The properties of the material strongly influence the characteristics of the travelling wave as it propagates to a second IDT nearby where it is detected [Morgan 1985]; figure (8.1) shows a simplified illustration of an IDT acoustic device structure.

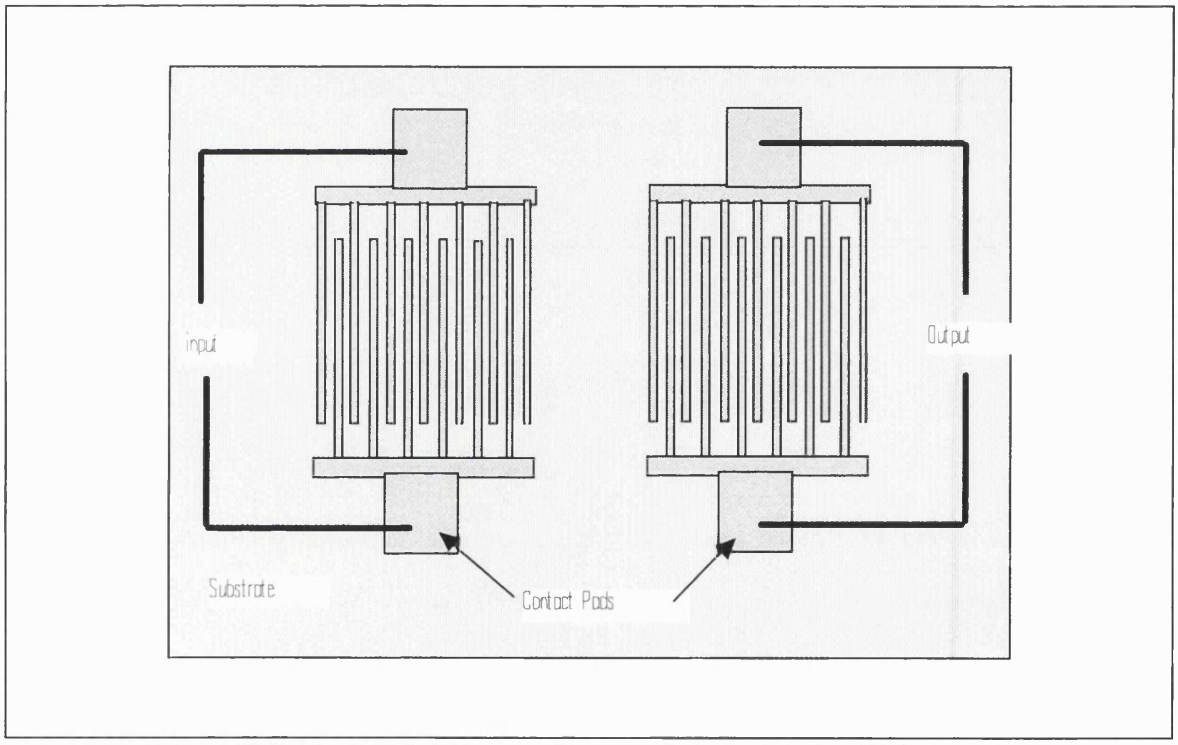

Figure (8.1): A simplified diagram of an acoustic device based on IDT structures.

Careful choice of both the IDT electrode periodicity and the material properties enable a bandpass filter to be constructed; such devices have found widespread use within the broadcast communications industry [Oliner 1978]. Alternatively, an oscillator circuit can be constructed which utilises the propagation delay time of the acoustic wave. In this configuration, acoustic wave devices can be used as sensors, since the presence of a gas or fluid on the device will modify the velocity of the acoustic wave. Surface acoustic wave (SAW) devices involve the propagation of the non-dispersive surface, or Rayleigh, wave and are capable of operation at high frequencies [Morgan 1985]. An alternative is the

Flexural Plate Wave (FPW) device which utilises the propagation of a plate like, or Lamb wave through the material. Lamb waves have wavelengths of the order of the substrate thickness or larger, and FPW devices based upon thin membranes have been used as gas and fluid sensors [Sze 1994] and ultrasonic delay lines which have been used in radar applications [Viktorov 1967].

8.1.1 CVD Diamond

Acoustic waves travelling in diamond can exhibit extremely high propagation velocities [M^{c}Skimin 1957]. In the case of SAW devices, diamond offers the prospect of very high frequency (>2GHz) bandpass filter operation, without the need for technologically challenging IDT electrode spacing [Yamanouchi 1989]. Nakahata and co-workers have reported promising filter performance characteristics from ZnO-diamond multi-layered SAW structures [Nakahata 1992,1994,1995]. The chemically inert nature of diamond, its high strength and relatively low density, allied to a high thermal conductivity, suggest it as an ideal substrate for sensing applications in hostile environments; the use of diamond for FPW sensor structures has not been previously addressed. The effective design of acoustic devices requires an understanding of the propagation of the acoustic modes within the substrate, which can be strongly affected by factors such as film structure, morphology, and quality. Well established theory [Oliner 1978] describes the propagation of many types of acoustic waves in isotropic, homogeneous elastic materials. However, CVD diamond is not isotropic or homogeneous and it is well known that its film properties e.g. morphology and phase purity depend on the film growth conditions [Williams 1989, Wild 1994]. It is therefore not clear to what extent acoustic propagation in CVD diamond can be described by simple isotropic theory.

8.1.2 Published Literature.

The following section gives a brief review of the literature covering acoustic wave propagation in diamond; very little work has been reported for the CVD form of the

material, most concerns propagation in natural diamond and arises primarily from interest in the elastic constants of the material. Natural single crystal diamond is elasticity anisotropic; its room temperature elastic constants have been measured by M^{c}Skimin *et.al.* [M^{c}Skimin 1957] from which they calculated the velocities of the longitudinal and the two shear bulk waves propagating in the (110) and (100) directions. Later they examined the influence of temperature [M^{c}Skimin 1972] and found a variation of less than 1% in the acoustic velocities over a temperature range of ~240 °C. A SAW velocity of 10860 ms^{-1} was measured on (111) natural diamond [Kushibiki 1985] using line-focus-beam acoustic microscopy. Weglein *et al.* [1991] characterised the elastic properties of diamond-like-films (DLF) films on silicon by acoustic microscopy and tentatively concluded that the existence of graphite phases had only a small influence on the propagation of SAW waves in DLF's. Around the time the work reported here was carried out, Schneider *et al.* [Schneider 1997] used a different laser ultrasonic arrangement to study the propagation of high frequency SAW waves in a composite of thin films (< 6 μm) of diamond-like-carbon (DLC) on a silicon substrate. The wavelengths were large compared to the DLC film thickness and yielded essentially the SAW velocity in silicon 'stiffened' by the presence of the DLC layer. They found that the SAW velocity increased with both layer thickness and sp^3 content; the shape of the dispersion characteristics was also strongly influenced. Some of the films were described as being diamond, however no independent evidence e.g. Raman spectra were presented from which the quality of the films could be assessed.

A small number of papers have been published which describe the fabrication and performance of high frequency SAW devices. These devices are layered structures consisting of a piezoelectric, typically zinc-oxide (ZnO), deposited on silicon supported CVD-diamond. Most of this work originates from a single Japanese group at the laboratories of Sumitomo Electric Inc. The earliest work however is by Yamanouchi *et al.*[1989] who carried out theoretical calculations to suggest that ZnO/diamond and AlN/diamond layered substrates would be able to support SAW waves with velocities as high as 12000 ms^{-1}, together with high coupling constants between the piezoelectric layer and the diamond substrate. They predicted SAW velocities of 10956 ms^{-1}, 12788 ms^{-1} and 11983 ms^{-1} for [100], [110] and [111] waves respectively, propagating in these multi-layer structures. They fabricated simple IDT SAW structures on thin (10 - 15 μm) hot filament

grown CVD diamond on silicon substrates, using a sputtered ZnO piezoelectric layer to carry out the electro-acoustic conversion. Experimental SAW velocities of up to 8000 ms^{-1} were measured in these structures. Considerable development of this early work was undertaken by the group at Sumitomo, who published their results in a series of papers [Nakahata 1992,1994,1996]. They also used hot filament grown, thin film silicon supported diamond, but demonstrated SAW filter devices with phase velocities up to 10200 ms^{-1} operating at frequencies up to 3.5 GHz. Their devices exhibited insertion losses of around 12 dB together with reasonably low values for the temperature coefficients of frequency (TCF) of around 28 ppm/°C. The same group has also published a detailed theoretical study of the dispersion characteristics of various SAW modes as a function of piezoelectric layer thickness for a range of piezoelectric/diamond combinations. These include $LiNbO_3$ which they predicted should have the highest velocities and SiO_2 which they estimate would exhibit a zero temperature coefficient of dispersion (TCD) under certain conditions. Hachigo and co-workers [Hachiago 1995] have examined the dispersion characteristics of the ZnO/diamond combination and found a reduced pole width for SAW structures on this substrate compared to bulk SAW's which they attributed to the velocity dispersion of the SAW wave which occurs in such layered structures. Adler *et al.* [Adler 1995] have shown that unexpectedly large coupling exists for the lowest order SAW modes in the ZnO/diamond structure, provided the calculations are carried out at constant frequency-thickness rather than at the more usual constant wavenumber-thickness which gives rise to anomolously low coupling values.

The velocity and dispersion characteristics of acoustic waves depend on film parameters such as stiffness, thickness, anisotropy, morphology and density etc. and directly bear on the performance and behaviour of an acoustic device. It is well known that CVD diamond films are rather variable in these respects. Film characteristics such as; morphology, texture, grain size and quality depend on the growth conditions under which a film is prepared. Hence, it is of interest to study the propagation of acoustic waves in a range of typical CVD diamond films which are unperturbed by the presence of the piezoelectric and metallic layers which are required for the fabrication of an acoustic device. Laser ultrasonics is a sensitive interferometry technique which can be used to study the propagation of acoustic wave in materials and benefits from being both non-contact and

non-destructive to the material under investigation. The following sections in this chapter present the results of laser ultrasonic study carried out to examine acoustic wave propagation in a range of CVD diamond films. The effects of quality, morphology, thickness and substrate temperature were studied and the results are discussed in terms of the application of CVD diamond films to the fabrication of Lamb wave based FPW acoustic devices for use as hostile environment sensors. To the author's knowledge this represents the first proposal that thin film diamond may be particularly suited to this type of device.

8.1.3 Simple Acoustic Theory

To facilitate the discussion of the experimental results of the work, given later in the chapter, a brief description of acoustic waves and appropriate theory is given in the following paragraphs. The applications of acoustic theory are very broad; accommodating on the one hand, seismic waves with wavelengths on the scale of kilometres and on the other hand, ultrasonic waves with wavelengths on the scale of microns. What follows is an introduction to the simplest kinds of ultrasonic wave which can propagate in solid media; we shall concentrate on Rayleigh and Lamb waves as these are most relevant to the work presented in this chapter. For detailed and authoritative treatments the reader is directed to the many excellent texts available and the author has found [Ballantine 1997], [Viktorov 1967] and [Oliner 1978] to be particularly useful. These cover in detail the general topic of acoustic waves, Rayleigh and Lamb waves and applications to acoustic wave devices. For a more detailed description and discussion of the laser ultrasonic method used during this study the reader is directed to chapter 3 of this thesis.

Acoustic waves are elastic waves which propagate in a medium because adjacent atoms in the lattice are held in an equilibrium position by the balance of attractive and repulsive atomic forces. The restraining forces are to a first approximation proportional in magnitude to any displacement of a particle from its equilibrium position and act to restore it to that position. The displacement of a particle is transmitted to neighbouring

particles by the forces between them with a phase delay determined by the strength of the forces and the mass of the interacting particles. The time evolution of the displacement through the lattice constitutes an acoustic wave. The governing equations for the wave can be derived by treating the medium as homogeneous and isotropic and then solving Newton's equations of motion for an infinitesimal volume of the medium. If this is done for an infinite medium it is found that two kinds of elastic wave can propagate independently: namely, a transverse wave in which the particle motion is perpendicular to the direction of the wave propagation and a longitudinal wave in which the motion is parallel to the propagation direction. If a boundary is introduced to the problem i.e. the medium becomes a half-space with one free surface then the equations admit an additional solution which describes a wave confined to the surface of the medium; this solution is termed a Rayleigh wave and it propagates without dispersion along the free surface, decaying exponentially into the bulk. If a second free surface, parallel to the first, is introduced the medium becomes by definition a thin plate which yields the Rayleigh-Lamb (R-L) equations relating wavenumber (k) and angular frequency (ω). For a particular value of k there are an infinite number of frequencies which satisfy the R-L equations. Each of these corresponds to a different Lamb wave mode in the plate and these waves are dispersive i.e. the phase velocity (C_p) is a function of the wave frequency. Phase velocity is defined as ω/k and for dispersive waves the relationship between k and ω is non-linear. The three kinds of acoustic or elastic waves just described are summarised in figure (8.2)

It will be seen later in this chapter that Lamb waves were the dominant acoustic mode observed this experimental study and therefore we shall consider these acoustic waves in a little more detail. Lamb waves occur in thin plates; for practical purposes a plate is considered 'thin' if its dimension normal to the direction of wave propagation is of the same order as the wavelength (λ) of the propagating wave. Consider a plate of thickness $2h$, it has been shown [Viktorov 1967] that two types of wave can propagate independently of one another in this plate: the asymmetric or flexural wave which has the dominant particle motion normal to and anti-symmetric about a semi-plane in the plate, and symmetric or extensional waves in which the dominant particle motion is parallel to and symmetric about this same semi-plane.

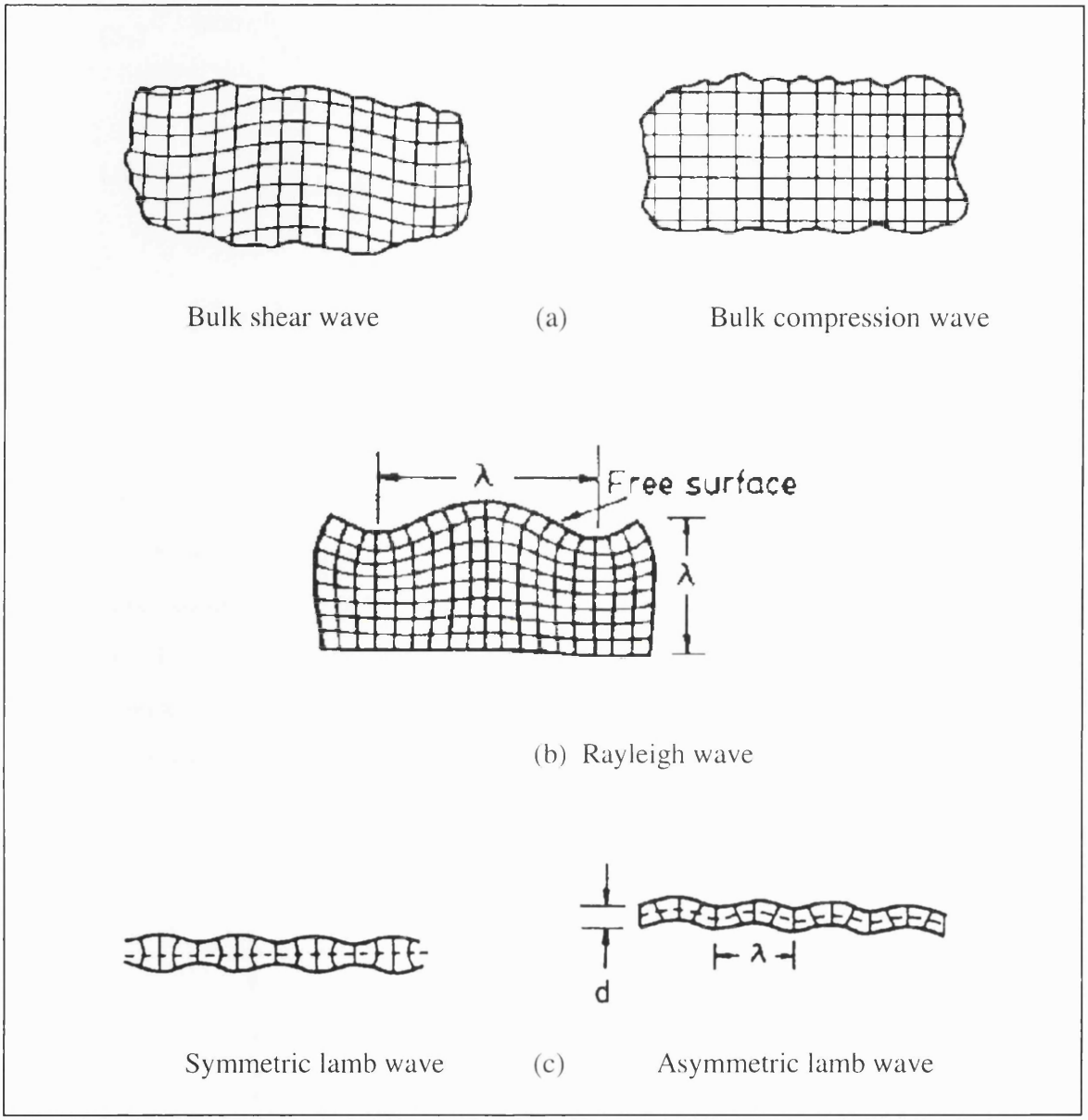

Figure (8.2): Schematic illustration of three types of acoustic waves which can propagate in solids; (a) Bulk waves, (b) Rayleigh or surface waves and (c) Lamb or flexural waves.

These two types of wave, asymmetric and symmetric, are abbreviated **a** and **s** waves respectively and their form can be found by solving the elastic wave equation subject to the requirement of stress free boundary conditions at each of the free surfaces of the plate. These solutions are the Rayleigh-Lamb equations and if k is the wavenumber of a lamb wave with angular frequency ω then the two modes are given by [Viktorov 1967]:

$$(S_0) \qquad \tanh qh \Big/ \tanh ph = 4k^2 pq \Big/ \left(q^2 + k^2\right)^2 \qquad (8.1)$$

$$(A_0) \qquad \tanh qh \Big/ \tanh ph = \left(q^2 + k^2\right)^2 \Big/ 4k^2 pq \qquad (8.2)$$

where: $$p^2 = k^2 - \left(\omega^2 \Big/ c_l^2\right) \qquad q^2 = k^2 - \left(\omega^2 \Big/ c_t^2\right)$$

and c_t and c_l are the transverse and longitudinal acoustic velocities in the medium.

As has been stated, for any given frequency ω there are an infinite number of solutions to each of these expressions. Solutions of (8.1) give the symmetrical modes s_0, s_1, $s_2...s_n$ while solutions of (8.2) give the asymmetric modes; a_0, a_1, $a_2...a_n$. These equations, which generally require numerical solution, describe the dispersion relations for each mode i.e. the dependence of frequency on wavenumber. Figure (8.3) shows the typical form of these dispersion curves for the first few modes for each type of wave.

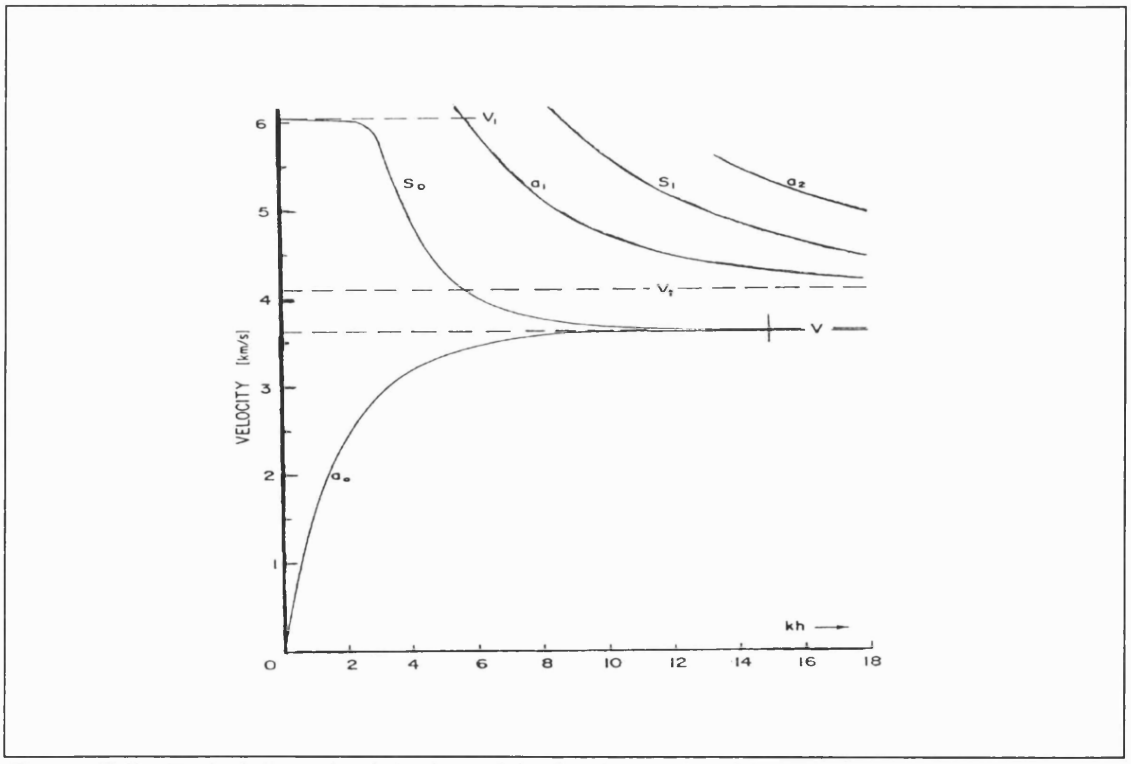

Figure (8.3): Typical dispersion behaviour of the first few modes of the symmetric and asymmetric lamb waves; v,v_t and v_l are the Rayleigh, transverse and longitudinal velocities for the material [redrawn from Oliner 1978].

It can immediately be seen that, except for the a_0 and s_0 modes, each mode has a cut-off frequency below which it cannot propagate in the medium; the a_1 mode has the lowest non-zero cut-off frequency which is given by:

$$f_c = {}^{c_t}\!/_{4h} \qquad (8.3)$$

It can also be seen from the figure that the velocities of the a_0 and s_0 modes become asymptotic to the same value for large *hk* product and this value is just the Rayleigh velocity for a half-space of the material. The Rayleigh wave for a thick, but finite substrate can be considered as the sum of two equal amplitude s_0 and a_0 modes for a plate of the same thickness. Also note from the figure, that the s_0 mode velocity varies only slowly for small values of *hk* , is called the sheet velocity C_e and is asymptotic to the bulk longitudinal velocity for $hk \rightarrow 0$. At the same value of *hk*, the velocity of the a_0 mode tends towards zero, figure (8.3), in fact in real materials residual stress forces ensure that the velocity of this mode always remains non-zero, although it may become very small [Sze 1994].

In general the dispersion relations for lamb waves given by the solutions to equations (8.1 & 8.2) are complicated. However, reasonably simple approximate expressions can be obtained for the a_0 and s_0 modes, which are valid for values of $hk<<1$, by expanding the hyperbolic tangents in the R-L equations as a Taylor series as has been shown by Hutchins *et al.* [1989], the essential results are:

a_0 mode:

$$\omega = A_1 k^2 + A_2 k^4 \qquad (8.4)$$

where: $A_1 = {}^{C_e h}\!/_{\sqrt{3}}$ $\qquad$ $A_2 = \dfrac{\left[{}^{20}\!/_{K^2} - 27\right] C_e h^3}{30\sqrt{3}}$

s_0 mode:

$$\frac{\omega}{k} = C_e = 2C_t\left(1 - \frac{1}{K^2}\right), \qquad K = \frac{C_l}{C_t} \tag{8.5}$$

where C_l and C_t are the bulk longitudinal and transverse velocities respectively and other symbols are as previously defined.

8.2 Experimental Details.

The experiments described here were broadly divided into two studies. The first was carried out on a range of samples chosen to allow an assessment of the effect on acoustic wave propagation of some of the film characteristics, such as morphology and quality, which are known to vary considerably depending on the growth conditions. The second part of the study, carried out on a large high quality wafer, was concerned with examining the propagation characteristics of the acoustic wave as a function of wafer temperature. A subsequent SEM and beam bending study, combined with a detailed analysis of the measured acoustic wave dispersion characteristics in the wafer, extended the study to include the effects of film defects on the propagating wave.

Polycrystalline thin diamond films grown by microwave plasma enhanced CVD were used throughout the experiments. To study the effect of crystal morphology, quality and thickness a sample set of seven square, free standing diamond plates were grown by MPECVD with strongly differing film morphologies and thickness. Films with prominent (100), (110) and microcrystalline morphologies were included in the sample-set. Samples with an area greater than $4cm^2$ together with a wax coating along the edges were used to minimise the influence of acoustic reflections. More detailed temperature-propagation and dispersion studies were carried out on a 50 mm diameter, free standing, translucent polycrystalline CVD diamond wafer. All samples were cleaned in boiling sulphuric acid saturated with ammonium persulphate [M^{c}Keag 1995] to ensure removal of surface contamination and residual graphite. Raman scattering analysis was carried out using a

Renishaw system 2000 instrument with (red) He-Ne laser light. Samples were coated on the backside with a thin gold layer (100-200 nm) to improve probe beam reflection during laser ultrasonic analysis which was carried out on the smooth backside of the samples

Acoustic measurements were made using a laser system which is shown schematically in figure (8.4) The line focused, pulsed, frequency doubled (532 nm), Nd-YAG laser pump beam generates thermo-elastic stresses in the sample surface which give rise to plane-acoustic wave modes propagating through the sample bulk and along the surface. Lamb waves were the dominant wave mode generated in these samples. The Nd-YAG laser pulse was of 6-10 ns duration, better than 70% Gaussian with a focused linewidth of about 100 microns. Ablation of the gold layer on the samples occurred in the first few laser pulses, subsequent pulses were absorbed by the diamond. However, the 532nm light was only poorly absorbed by the diamond and rather weak acoustic waves were generated by the laser pump beam. It was essential to use relatively large substrates, allowing reasonable separation of generation and detection points whilst minimising noise from cross-talk and reflections, along with the highest laser fluence levels available to achieve reasonable signal to noise levels. Detection of the acoustic waves was by a homodyne, path-stabilised, balanced, Michelson-type interferometer detector. Passage of the acoustic wave under the focused probe beam causes a change in the path length, resulting in an intensity modulation of the interference signal which is detected by the photodetectors and captured by a 500 MHz digital oscilloscope. Only the out-of-plane acoustic displacement, of the order of a few nm's, is monitored by the detectors which give a voltage proportional to the displacement. The recorded waveforms, figure (8.5), represent typically 90 laser pulses in rapid succession (one every few milliseconds), which are averaged by the storage scope prior to being transferred to PC where they can be analysed by time-dependent and fast Fourier transform (FFT) methods. This laser instrument can be used either in a dual or single beam configuration. This latter arrangement improves the signal strength for samples displaying poor reflectivity, as was the case for some of the samples reported here. Some further discussion of this system has been given in chapter 3 of this thesis. A general discussion of these types of laser ultrasonic systems has been given by Monchalin [1986].

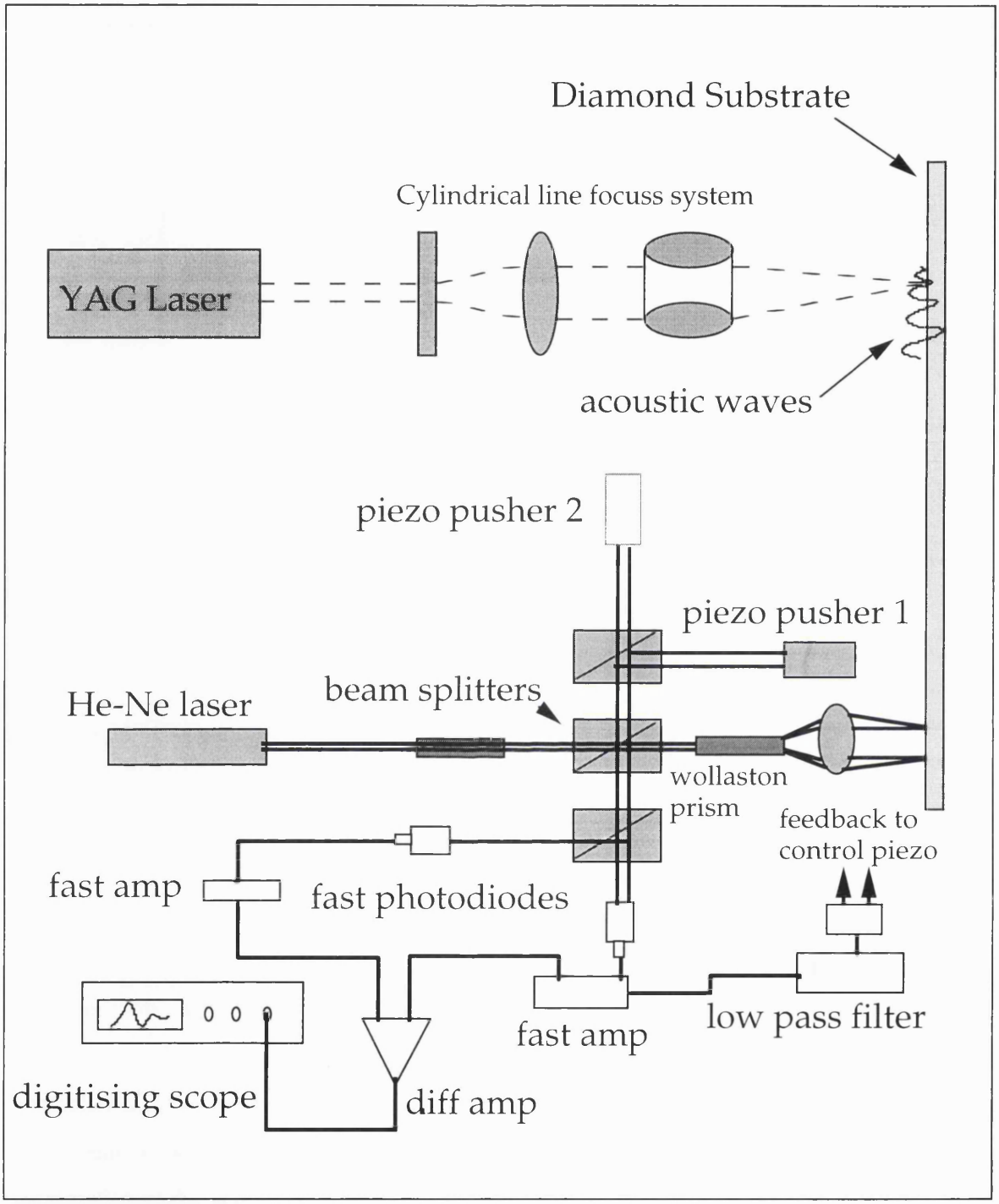

Figure (8.4): Schematic of the laser ultrasonic instrument: Acoustic waves, generated by the line-focus high power Nd-YAG laser, pulse 10nm, > 70% Gaussian, propagate to the probe position. Detection is by twin homodyne, path stabalised Michelson interferometer. Acoustic displacements (~ nm's) modulate the interference signal intensity, monitored by fast silicon photodiodes and captured by 500 MHz storage scope. Signal transferred to PC for analysis.

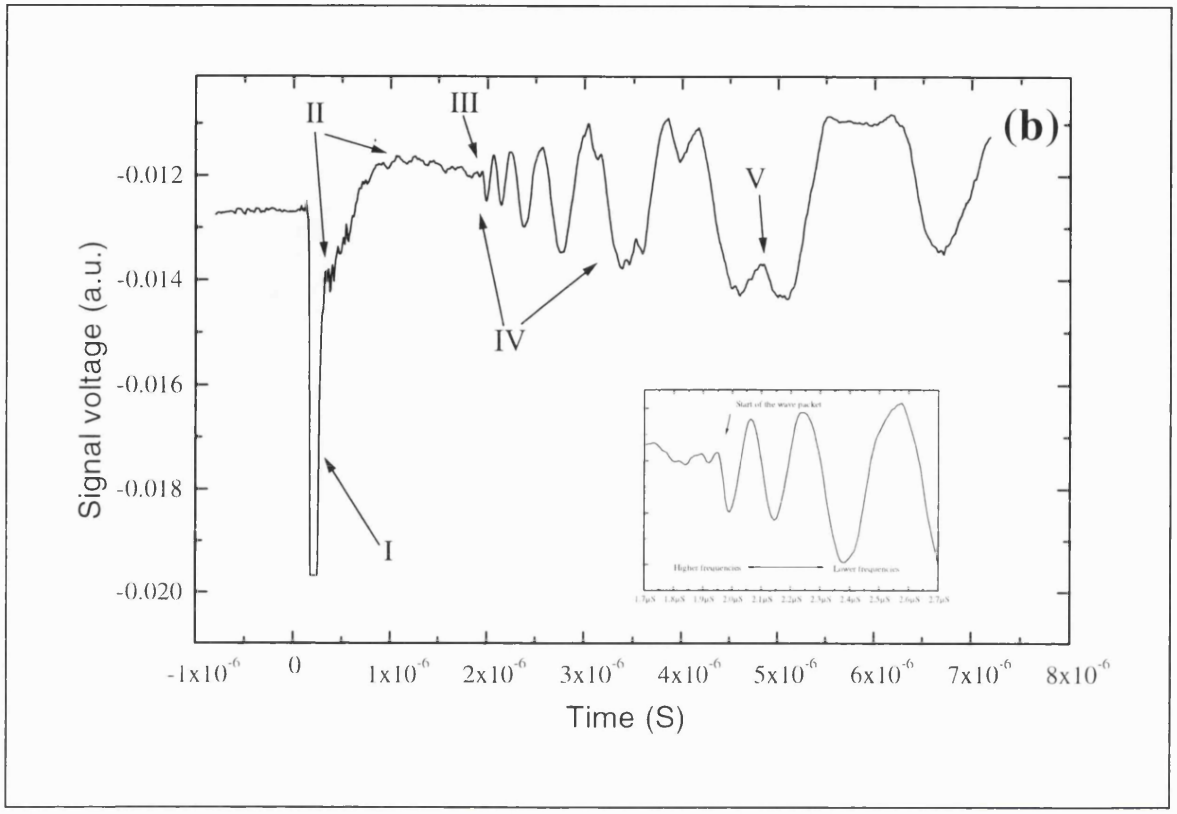

Figure (8.5): A typical trace recorded from a free standing diamond sample: The initial laser pulse, marked (I), is followed by interference associated with the Q-switched Nd-YAG laser (II), the acoustic pulse arrives between 1-2 μs (III), and develops as a decreasing frequency modulated wavetrain (IV), the higher frequencies arriving first, followed by the low frequency components at a later time. Reflections from the fastest components can be seen arriving late in the trace (V).

Laser ultrasonic studies were carried out as a function of temperature on the 50 mm diameter wafer with the aid of a simple, custom built heater set-up shown schematically in figure (8.6). The control circuit consisted of a thermocouple and Eurotherm thyristor and controller units driving two 'HotWatt' 150 watt cartridge heaters which allowed the wafer to be heated over a temperature range ~20 - 250 °C, stable to ~±1°C. During the laser measurements the wafer and heater unit were mounted normal to the optical beam path.

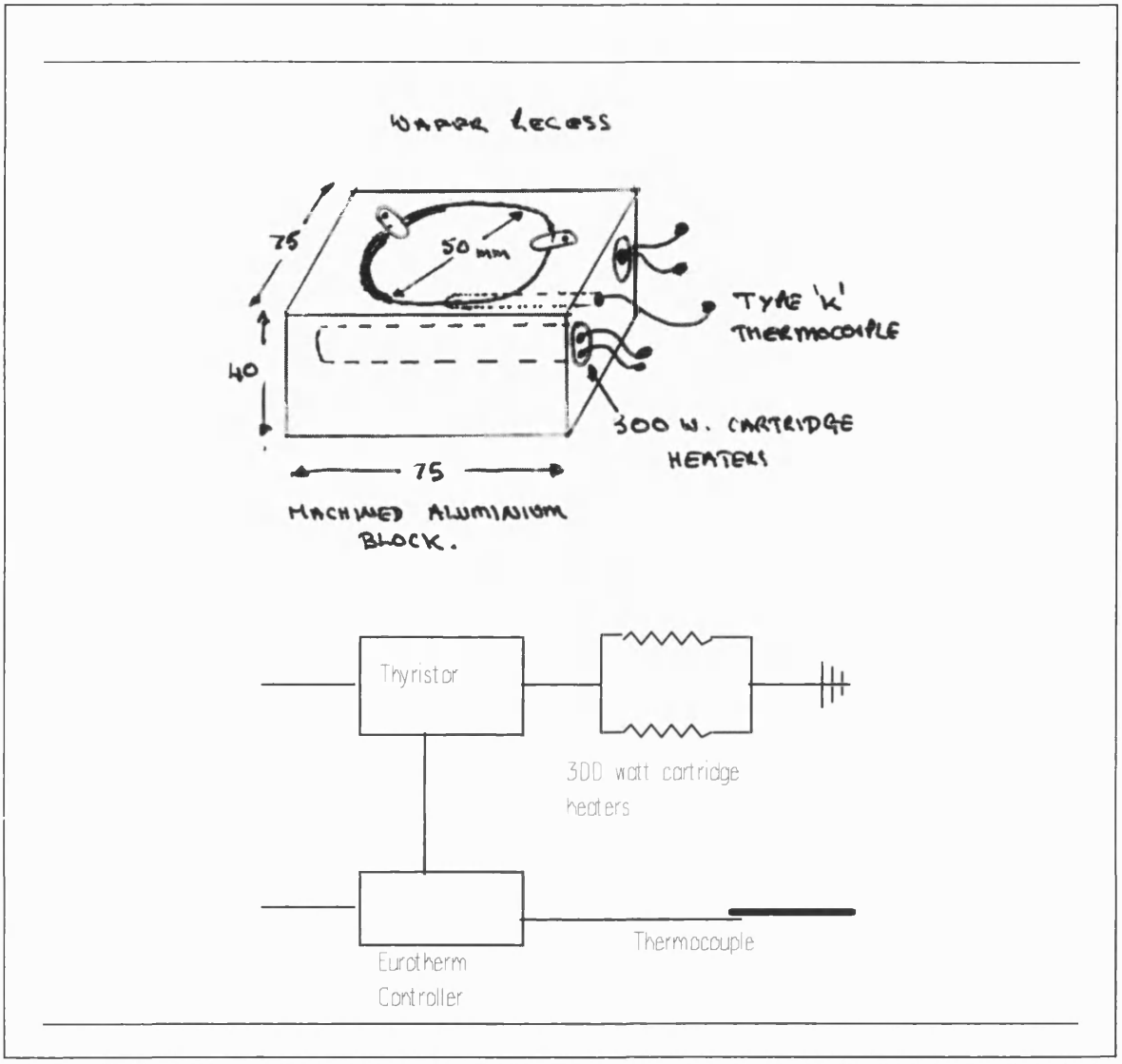

Figure (8.6): Schematic diagram of the heater block and control circuit fabricated to allow laser measurements as a function of temperature.

A value for the Young's modulus of a material can be obtained from the deflection of a fixed-free beam of the material according to simple beam-deflection theory [Timoshenko 1959, Middelhoek 1994]. For isotropic materials the value obtained will reflect the true Young's modulus of the material, however for polycrystalline samples with a strong anisotropy transverse to the plane of the beam the results of a beam bending measurement will yield an 'effective modulus' characteristic of the macroscopic stiffness of the beam. To provide an independent assessment of this parameter for comparison with values derived from the laser measurement for the 50 mm wafer (to be discussed in the following sections) the simple rig shown in figure (8.7) was fabricated.

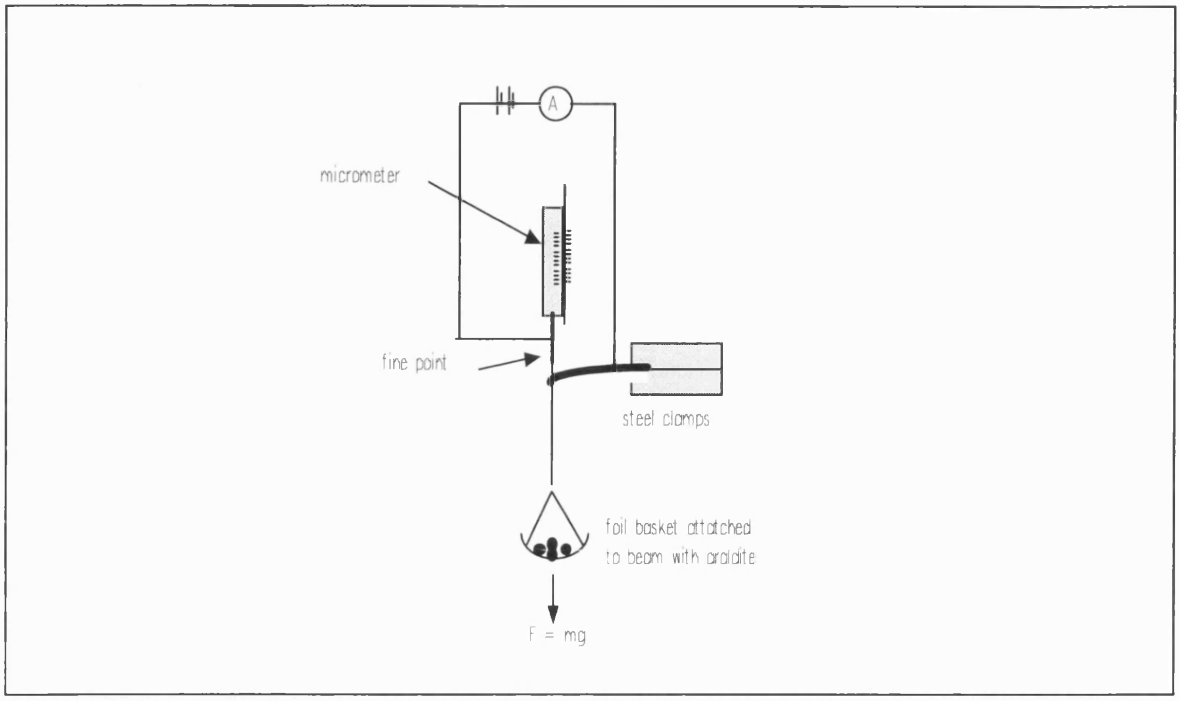

Figure (8.7): The simple beam bending test rig used to obtained 'effective Young's modulus' values for comparison with estimates extracted from the acoustic data generated by the laser measurements.

It can be shown from simple beam theory that the deflection of a beam subject to a load F applied at the free end is given by [Middelhoek 1994]:

$$d = \frac{4l^3 F}{wEt^3} \qquad (8.6)$$

where E is the Young's modulus and other symbols are as defined in the illustration below.

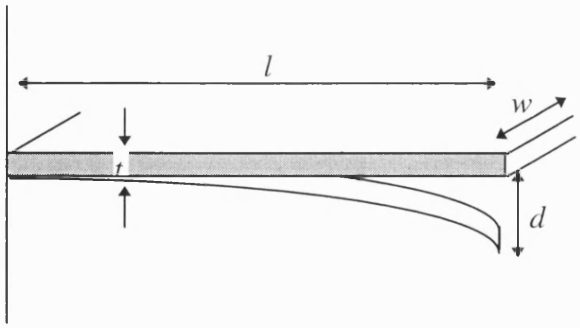

illustration of beam bending theory.

An estimate of E for the beam can be obtained from a least squares fit to a plot of deflection vs. load, provided l,t and w are known. Small beams, ~20-30 mm by 2-3 mm, were cut and mounted as shown in figure (8.7) and loaded with increasing masses. The

physical dimensions of the beams were determined by micrometer and calliper measurements. The beam deflection was determined using the micrometer-circuit combination as shown; a low applied voltage and sensitive ammeter (μA - mA) were used to maximise sensitivity . By this method it was possible to determine the deflection of the beam tip to better than 10 microns. In the case of the non-conducting diamond beam a very thin (few nm's) conducting track of silver was evaporated by shadow masking onto the upper surface to serve as an electrical contact. The efficacy of the rig was tested by making measurements on 'reference' beams cut from foils of high purity metal supplied by Goodfellow (Cambridge Science Park, UK). The results of the beam-bending tests are give in the next section.

In addition to beam bending tests, a detailed SEM study was carried out on a wide range of free standing diamond films to examine the incidence and type of defects present within these films. A total of nine examples were studied and these included samples taken from the films used here for the laser ultrasonic measurements. These films represent diamond grown under a range of conditions from three separate suppliers of free standing diamond films, (GEC, AEA T
echnology and DERA Malvern). Samples were mounted on aluminium stubs and gold sputtered to facilitate SEM examination of the fracture cross-section of each sample. The objective of this study was to obtain a qualitative assessment of the films in terms of the number and types of defects e.g. grain boundaries, microcracks and voids etc. present within the films.

8.3 Results.

In the following section the results of the acoustic studies on diamond films are presented in three sections. The first, section (8.3.1), presents the results of the study to examine the influence of film characteristics. The results of the dispersion and temperature studies on the 50 mm wafer are given in (8.3.2) while the beam-bending and SEM studies which were carried out subsequent to the laser measurements are presented in the final section (8.3.3).

8.3.1 Effect of Film Type

Optical micro-graphs of the seven square plate samples studied in this work are shown in figure (8.8 a-g); the samples are referred to by number and these correspond to the sample details which are summarised in table (8.1). The polycrystalline films displayed either (100) texture - samples 1, 3 and 7, (110) texture - samples 4,5 and 6 or microcrystalline texture - sample 2, as can be seen in figure (8.8). The grain sizes on the top face of the thickest films were in the range 100-200 μm as determined from the optical micrographs. The large spherical grains evident in sample 2 were, under higher magnification, seen to be comprised of tight clusters of many hundreds of much smaller micro-crystallites. Samples 6 and 7 were greyish in colour whilst the other films were black in appearance.

Sample	~thickness (μm)	Dominant morphology	Approximate grain size (μm)	Appearance	Maximum measured velocity (m/s)	Error (%)
1	506	<100>	35-50	Black	11041	±2
2	443	microcrystalline	300-400	Black	8719	±3
3	798	<100>	120-200	Black	11294	±6
4	694	<110>	250-300	Black	11089	±4
5	319	<110>	60-100	Black	11094	±13
6	500	<110>	30-100	Grey	12200	±5
7	510	<100>	30-80	Grey	12000	±5

Table (8.1): Summary of the data obtained for the seven square free standing CVD diamond samples used in this study.

The results of the Raman analysis are summarised in figure (8.9). All the samples exhibited Raman spectra with a strong 1332 cm^{-1} peak indicative of diamond [Fayette 1994]. The Raman spectra obtained from most samples (1,3,4,5,& 7) were very similar to the example shown as spectrum (I) in figure (8.9) which was taken from sample 3. This sample had a well developed (100) morphology. For these samples the Raman spectra showed very little other structure besides the main diamond peak at 1332 cm^{-1} indicating that these films were predominantly of sp^3 (diamond) character. This was not the case for samples 6 and 2, shown as spectra(II) and (III) in figure (8.9), which had Raman spectra that showed some additional background and structure indicating the presence of forms other than diamond in these films.

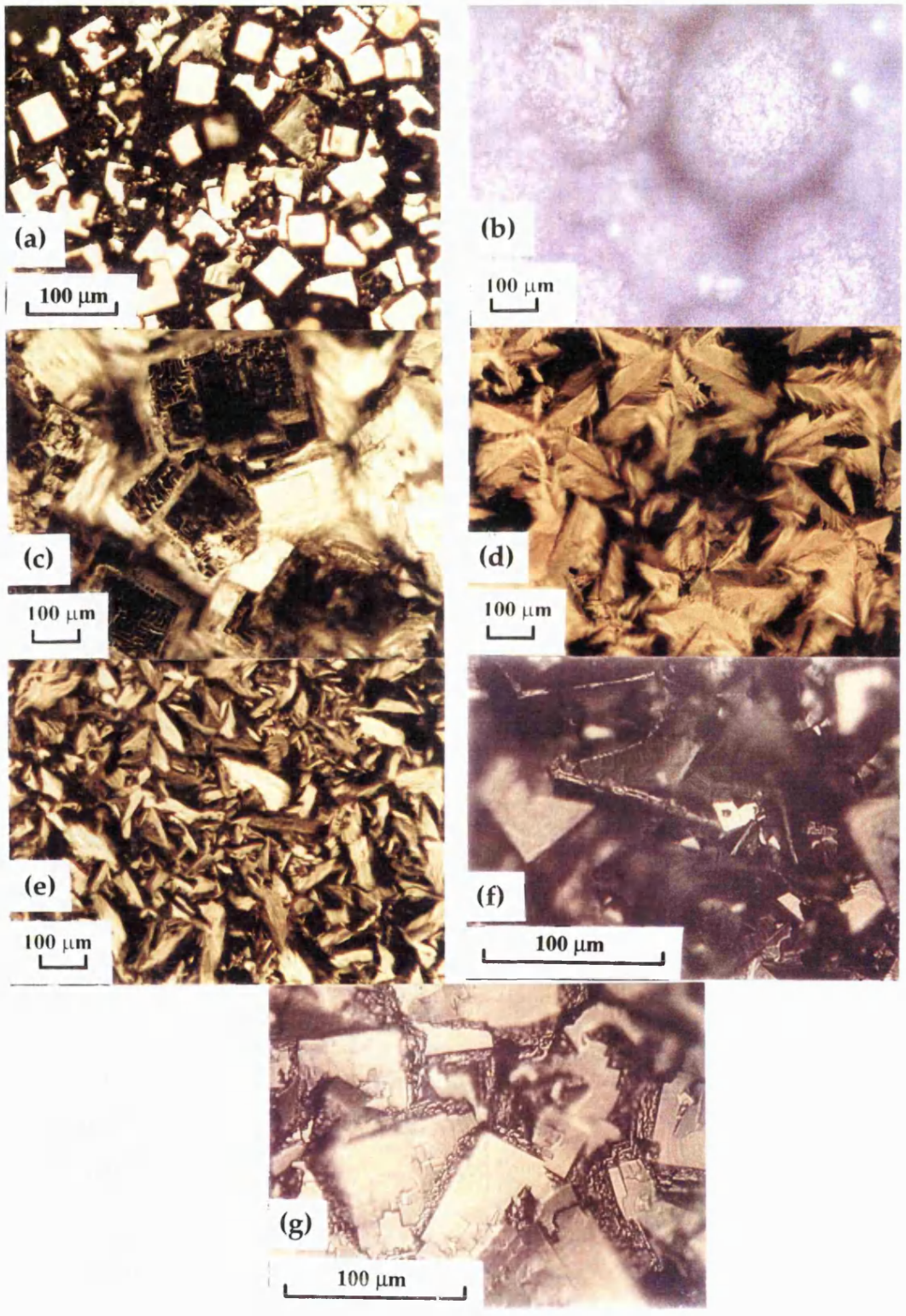

Figure (8.8): Optical micrographs (a)-(g) recorded from each of the square samples (1- 7) used to study the effects of morphology and film quality on the acoustic wave.

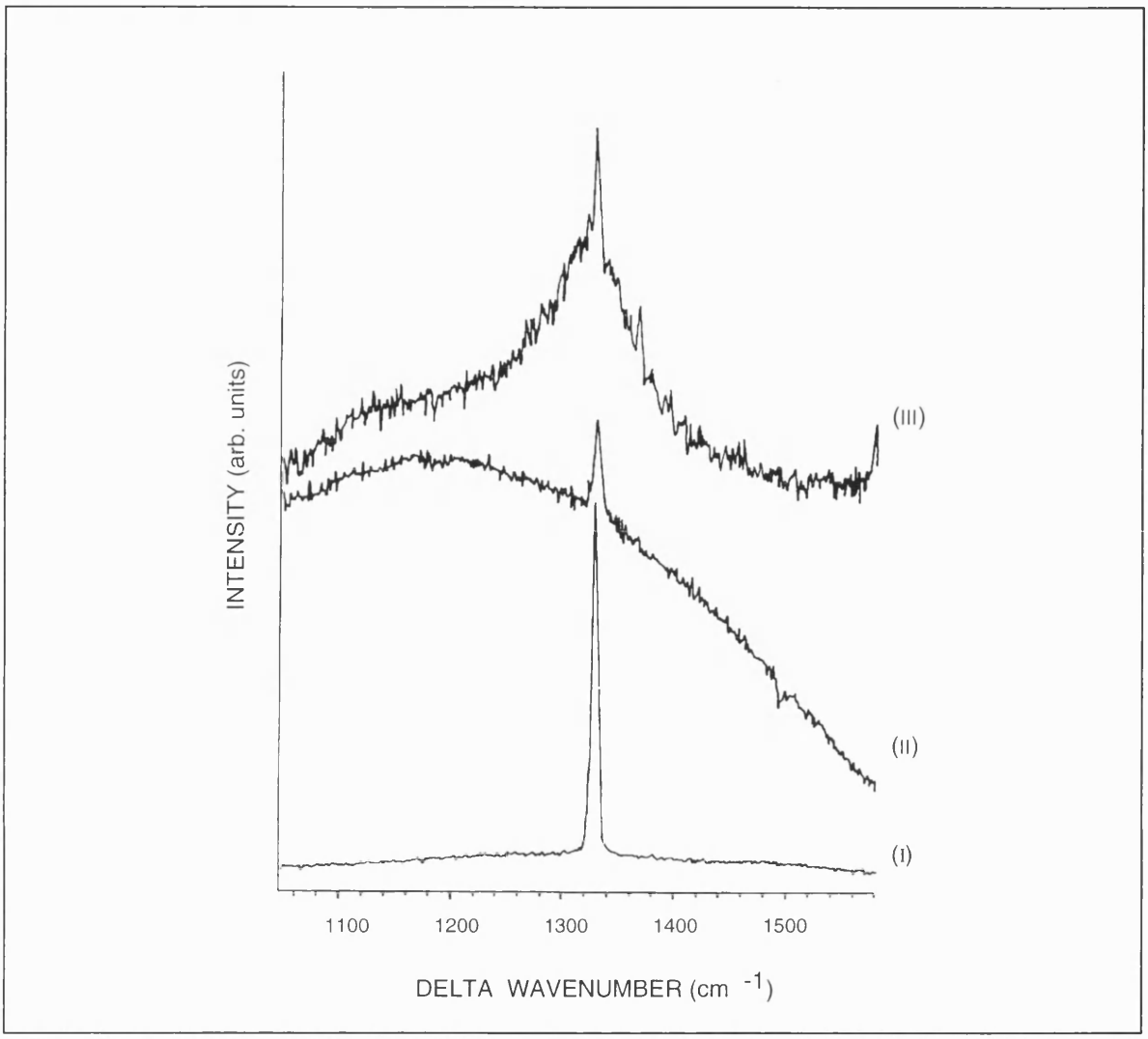

Figure (8.9): Raman scattering spectra (Renishaw system 2000 with (red) He-Ne laser light) measured on samples 1-7; curve (I) sample 3, curve (II) sample 6 and curve (III) sample 2; curves for samples 1,4,5,7 were similar to the curve (I)

Following the launch of the acoustic pulse by the pump laser the interferometer monitored the propagating, dispersive acoustic wave-packet arriving at the probe point on the surface of the diamond sample. A typical laser trace (taken from sample 1) is shown in figure (8.5), the expanded inset identifies the initial arrival time of the acoustic wave. The initial laser pulse, marked (I) in the figure, is followed by interference associated with the Q-switched Nd-YAG laser, marked (II); note that these features do not indicate actual displacement of the sample surface, they are caused by electrical and electro-magnetic interference from the large switching power supplies used to supply the Nd-YAG laser. The acoustic pulse, marked (III), typically arrives at between 1-2 μs depending on the pump-probe beam separation. The early part of the pulse contains the higher frequency components present in the signal which then develops as a decreasing frequency modulated pulse, marked (IV)

[Hess 1993], with the lower frequency components arriving later. The shape of the pulse is characteristic of a propagating asymmetric lamb wave [Dewhurst 1987]. Some interference, marked (V) in the figure, arising from sample boundary reflections and/or other acoustic modes can be seen in the later parts of the waveform. Acoustic experiments on the samples shown in figure (8.8) were carried out by making several sets of laser measurements for a range of pump beam-probe separations of typically 5-20 mm. Acoustic traces similar to the one shown in figure (8.5) were captured by the 500 MHz storage scope and then transferred to computer. The arrival time of the leading part of the acoustic pulse was determined by careful inspection with the aid of mathematical graphing software. Estimates of the maximum acoustic velocity for each sample were extracted from the gradients of least squares fits to the time-distance data determined from the laser traces. A typical example, taken from the data for sample 7, is shown in figure (8.10).

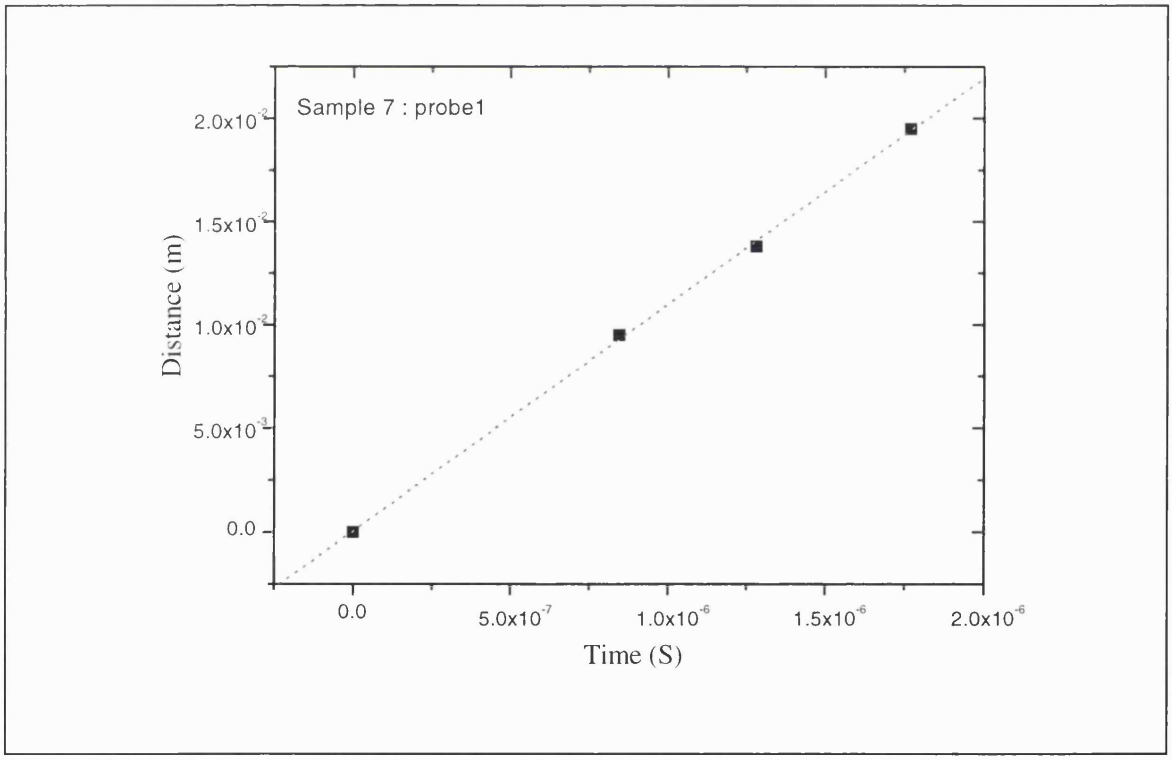

Figure (8.10): Typical example of time-distance data obtained from analysis of acoustic wave traces together with linear fit from which the acoustic velocity was determined.

A summary of the data obtained for each of the seven samples has been given in table (8.1). The velocity shown in the table represents the highest observed velocity derived

from the first arrival of the acoustic wave and includes an error derived from the regression analysis. The clearer samples (6 and 7) gave the highest velocity for the first arriving wave at around 12000 m s^{-1}, whilst the darker samples supported waves with a velocity closer to 11000 m s^{-1}. Only in the case of the microcrystalline film (sample 2) did the velocity drop significantly below this, to a value of 8700 m s^{-1}.

8.3.2 Temperature and Dispersion Measurements.

To examine the effect of temperature, laser generated acoustic pulses were monitored in a 5 cm diameter wafer of free standing, polycrystalline CVD diamond. A simple sample heater, fabricated from aluminium and incorporating a controller, thyristor and thermocouple allowed the wafer to be heated, during the laser measurements, over the range 20 - 250 °C stable to approximately ±1°C. Figure (8.11) shows an optical photograph, SEM and Raman spectrum for the wafer. The SEM shows a randomly aligned, well developed polycrystalline morphology with a grain size of approximately 20 - 30 microns. The quality is confirmed by the Raman spectrum which shows only a sharp narrow peak at 1332 cm^{-1} characteristic of diamond virtually free of sp^2 material. It should be noted that the Raman analysis was carried out using a 632.8 nm red laser source which is considerably more sensitive to sp^2 material than the more usually presented spectra obtained with green laser radiation which tend to emphasise the diamond content [Sails 1995]. The plate thickness is an important parameter which influences the dispersion characteristics for lamb waves. Micrometer measurements indicated a mean maximum thickness of 90 ±1μm, however this value was adjusted to 84 μm to account for a typical surface roughness of 12 μm assessed from alpha step measurements.

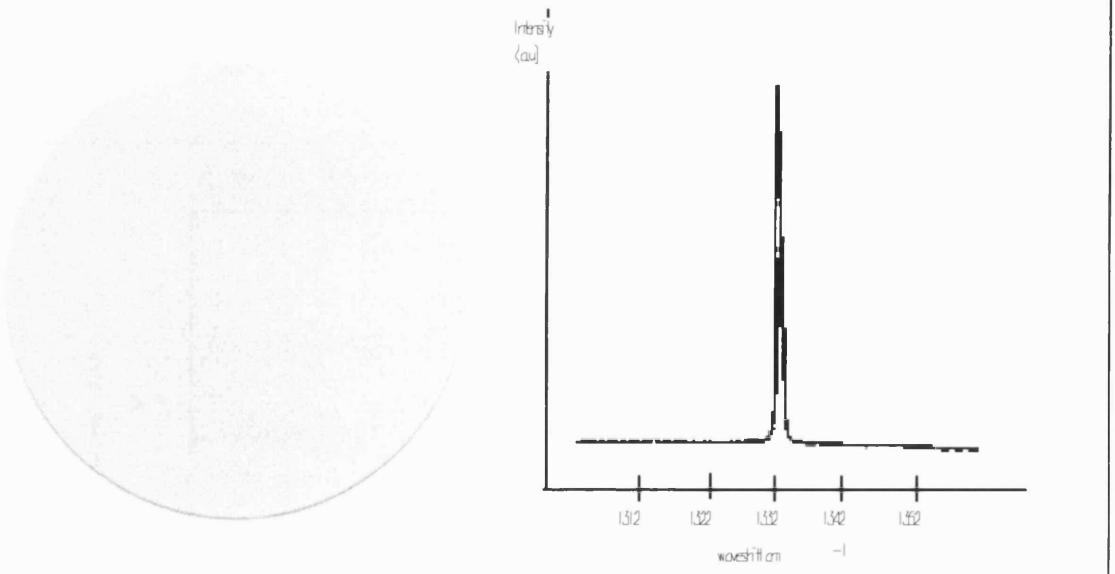

(a) (b)

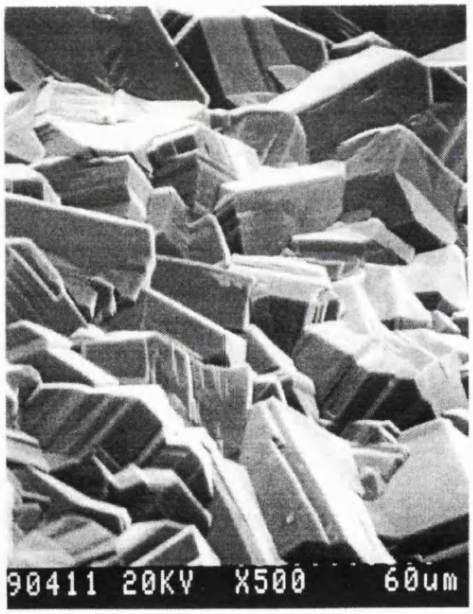

(c)

Figure (8.11): (a) Photograph of top surface of 5 cm free standing 'white' diamond wafer, (b) Raman spectrum and (c) SEM of growth side, taken from the 50mm diameter diamond wafer used to study temperature and dispersion effects on acoustic wave propagation.

The characteristic dispersive a_0 lamb wave, observed during the measurements made on the seven square samples, was also the dominant acoustic mode exited in this wafer, as is clearly shown in figure (8.12).

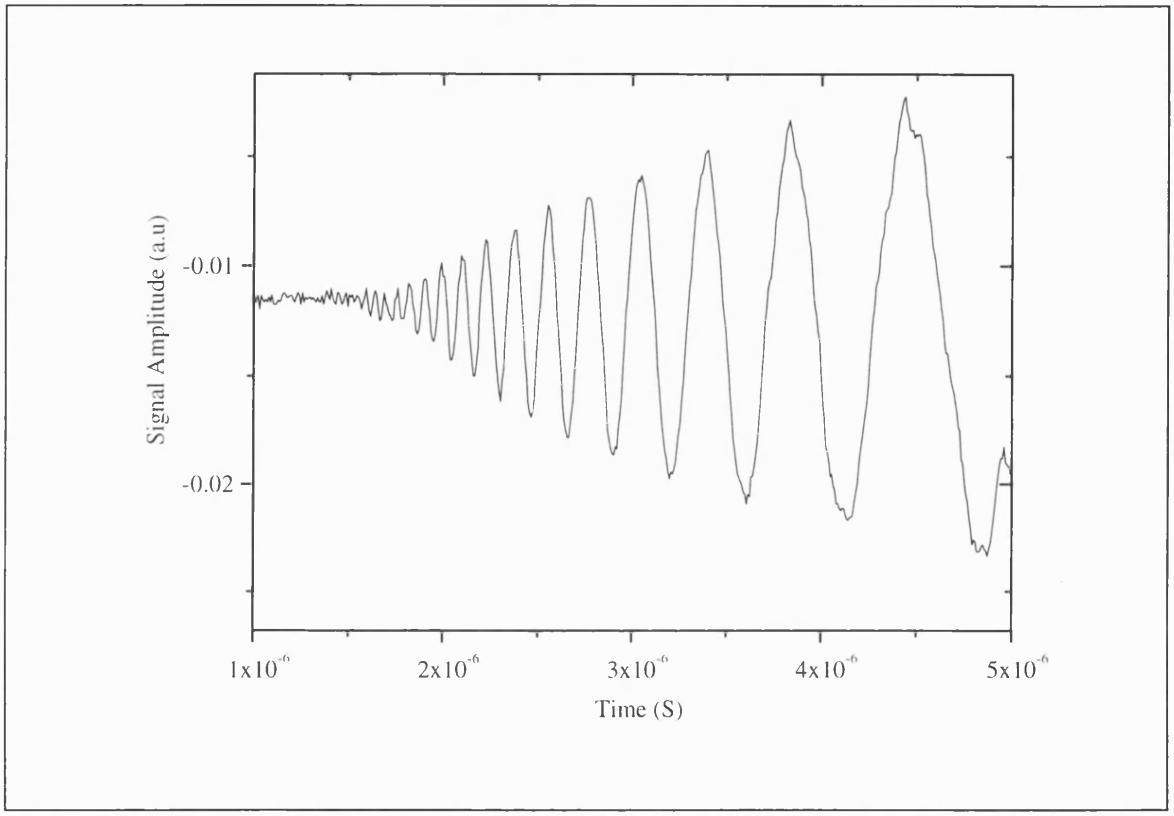

Figure (8.12): Expanded section of the laser trace from the 50mm wafer, showing the decreasing frequency modulated wavepacket characteristic of the dispersive zero order (a_0) asymmetric lamb wave.

At each wafer temperature, velocity-frequency data were extracted from the wavetrains by a variation on the method which has been described by Dewhurst *et al.* [1987] , who have studied lamb wave propagation in other materials. In this method, components of the signal were assigned a frequency based on the inverse of the period between successive maxima together with a velocity determined from the mean delay time and the source-probe separation. The results for wafer temperatures in the range 30-250 °C are shown in figure (8.13). This method determines the group velocity; so the figure indicates the group velocity-dispersion characteristics for the a_0 lamb mode in the material. It is qualitatively apparent from figure (8.13) that any variation with temperature was relatively small. The increasing 'scatter' evident for the data points at the higher frequencies reflects the increasing relative error with which it is possible to determine the frequencies and arrival times of the faster components by this method. The lower amplitudes of the faster

components, together with noise originating from the YAG pulse, also contribute to these uncertainties.

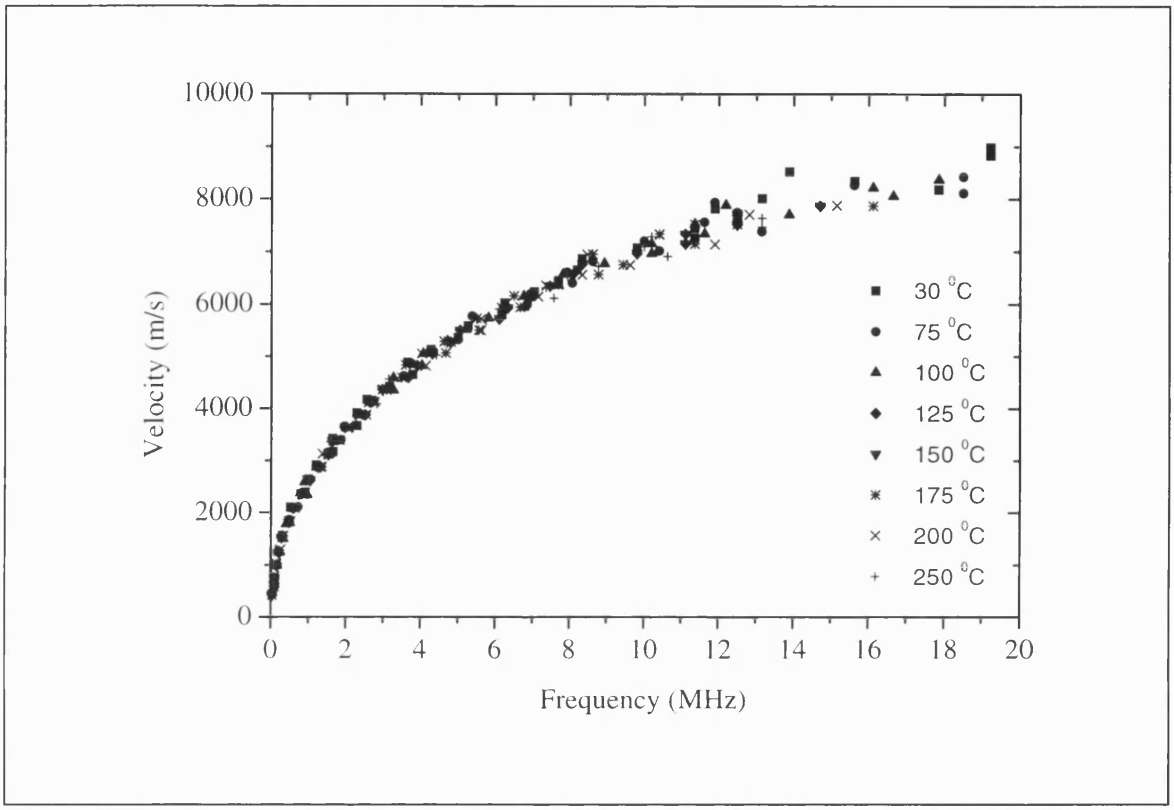

Figure (8.13): Frequency-Velocity dispersion characteristics, extracted from the acoustic data, for the a_0 lamb wave propagating in a 50 mm diameter, free standing polycrystalline diamond wafer at temperatures in the range 30 - 250 °C.

8.3.3 Beam-bending and SEM studies

To obtain an independent estimate of the 'effective' Young's modulus for the 50 mm diamond wafer simple beam-bending measurements were carried out with the purpose built rig which was described in the previous section (8.2). Figure (8.14) shows the results of force-deflection measurements made on a sample taken from the 50 mm diamond wafer; Similar plots were obtained for the 'reference' samples cut from high purity molybdenum and stainless steel foils (Goodfellows 99.95%). Estimates for E were calculated from the gradients of least squares fits to the data, as shown in figure (8.14), and equation (8.6) relating beam deflection and the applied force; the results of the analysis are summarised in table (8.2). The error shown in column 5 was assessed from the quadratic combination

(i.e. most probable) of the contributions from the least squares fit error together with the estimated error on the measurements of l, w and t for the beams

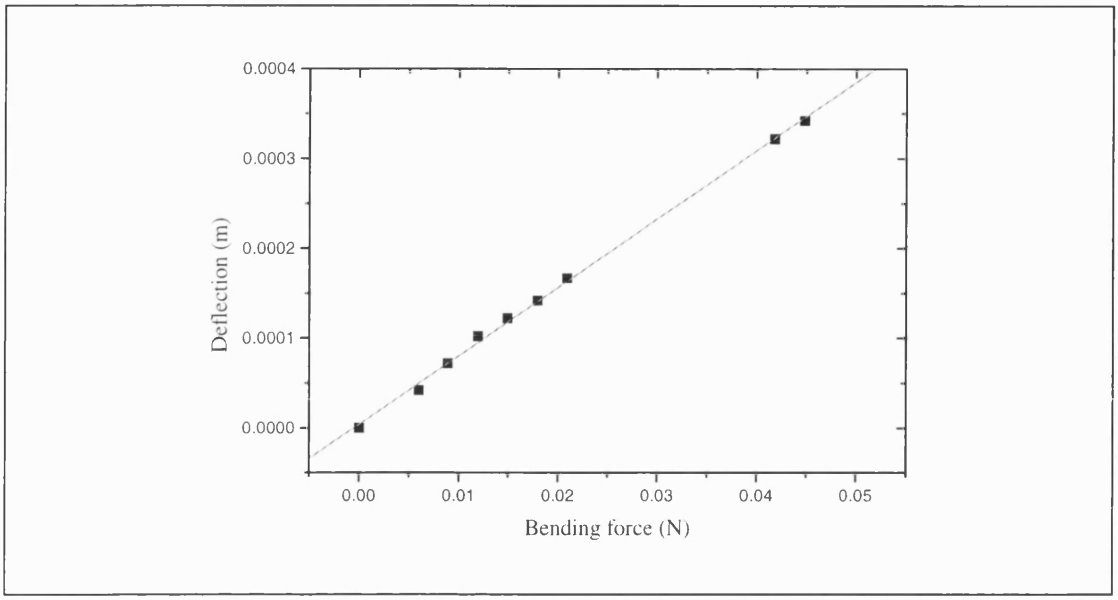

Figure (8.14): Results of the beam bending measurements for the diamond beams showing deflection of the beam tip as a function of the applied force, together with a linear fit to the data.

The reference values shown in the table are the quoted values from Goodfellow data book for stainless steel and molybdenum sheets together with the value derived from the laser measurements for the diamond film. In each case it can be seen that the measured and reference values for E agree to within the stated experimental error.

Sample	Gradient from fit (μmg^{-1})	Correlation coeff. (R^2)	$E_{measured}$	Error (%)	E_{ref}
Molybdenum	$8.67x10^{-3}$	0.998	286	20	343
Stainless steel	$8.92x10^{-2}$	0.999	237	20	210
Diamond	$7.62x10^{-3}$	0.999	328	20	306

Table (8.2): Summary of data derived from beam-bending measurements on a sample from the 50 mm diamond wafer and high purity metal reference samples.

The results of the SEM study are summarised in figure (8.15) which shows representative micrographs from two of the nine diamond film samples examined; typical examples of some of the film defects observed during the study are indicated on

the figure. Without exception, all of the films studied by SEM showed evidence of significant defect density across the full thickness of the sample. Defects consisted of large cracks (~ microns), micro-cracks, voids which varied in size and the characteristic grain boundaries, which ran vertically through the diamond films, arising from the columnar nature of the film growth. Both inter-granular and intra-granular fracture of the films was visible in the SEM cross-sections.

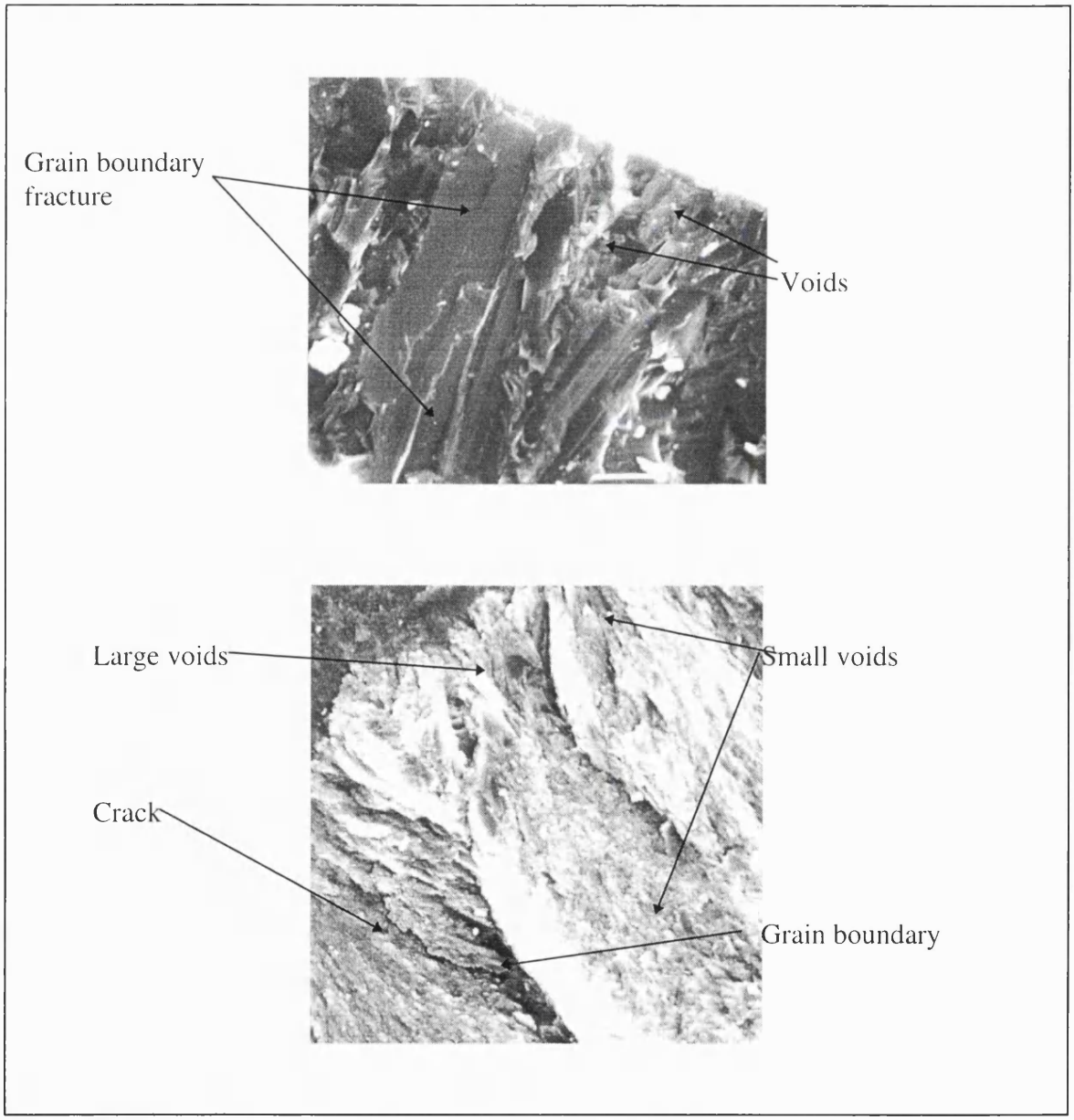

Figure (8.15): Two examples of typical SEM's taken from a cross-section study of nine free standing diamond films obtained from a selection of suppliers. The labels identify some of the defects observed during the study and it should be noted that similar defects were present to varying degrees in all of the films examined.

8.4 Discussion.

To improve the reflectivity and hence the signal-noise ratio, and to eliminate multiple scattering of the He-Ne laser probe beams arising from the polycrystallinity, a thin gold layer was evaporated onto the backside of each of the samples which have been described in sections (8.3.1) and (8.3.2). It might be expected that this layer would introduce dispersive effects of its own, influencing the measurements. This would certainly be the case for very high frequency SAW waves, which the laser system is in principle able to study. The gold layer would then introduce a characteristic dimension resulting in dispersion of the normally dispersionless SAW wave and would also mass load the surface reducing the propagation velocity. However, this study has concentrated on low frequency lamb waves with wavelengths many orders larger than the thickness of the gold layer (which was typically 100-200 nm) and well established theory [Oliner 1978] clearly shows that the effect of such a thin layer will not be significant for this type of acoustic wave. Gold was chosen as it is easy to deposit in very thin layers by argon sputtering and is reasonably stable on diamond, however aluminium, with a lower density and higher reflectivity, may be a better choice for future measurements.

As has been discussed in chapter 3 in more detail, diamond is rather a difficult substrate on which to make these types of laser measurements; a combination of low thermal expansion, very high thermal conductivity and low absorption at the pump beam wavelength (532 nm) combine to ensure that the acoustic wave generation is rather inefficient, resulting in low amplitude acoustic waves which are difficult to detect. Several strategies were examined during this work to try and improve the situation. One solution is to reduce the pump-probe separation which improves the amplitude by reducing the amount of absorption the wave undergoes prior to reaching the probe beam. However, this approach was unsuccessful with the diamond substrates used here. The reason can be traced to the very high acoustic velocity of diamond when compared with other typical substrates which have been studied by laser ultrasonics. If the probe-pump separation is reduced too much, the very fast nature of the diamond acoustic wave means that the acoustic signal begins to arrive during the period when noise from the firing of the Nd-YAG pump laser is

dominating the recorded trace. Under these circumstances it can be difficult to extract the true acoustic signal from the noise. An alternative solution is to increase the pump power until ablation of the substrate material begins to occur, at which point the amplitude of the acoustic wave being generated rises very rapidly with pump power compared to the rate during the purely thermal regime [Scruby 1989]. This is the approach that was found to be reasonably successful for the substrates studied during these experiments, none-the-less obtaining reasonable quality signals on these samples remained rather difficult. Future work might consider the benefits of using substrates finished to an optical quality, together with the use of a higher frequency for the pump beam which would result in more efficient optical absorption close to the substrate surface and should yield improved acoustic signals.

(8.4.1) Effect of Film Type.

The results of the Raman analysis are summarised in figure (8.9). The spectra are typical for large grain CVD diamond films grown by MPECVD methods [Wild 1994]. It is important to be aware that this Raman study was carried out using red 623 nm light. As a result the sp^2 content for all the films is exaggerated with respect to the sp^3 content and it should be realised that in all cases this means that the sp^2 levels in these film are relatively low. It is well known that changes to the growth conditions lead to the domination of different crystal textures and, under some circumstances, the formation of poorly defined microcrystalline material can also occur [Williams 1989, Wild 1995]. It is of considerable interest to study the influence of variations such as film morphology and quality on acoustic wave propagation characteristics. As the film thickness increases, both the symmetric and asymmetric zero order Lamb wave velocities tend towards the Rayleigh wave velocity, which for diamond is predicted to be around 11000ms^{-1} for (100) 11600ms^{-1} for (110) and 10800ms^{-1} for (111) material [Yamanouchi 1989]. It is apparent from the data in table (8.1) that all of the films studied here are capable of supporting high velocity Lamb waves. Clearly these films are of sufficient thickness that the highest frequency lamb wave components of the acoustic pulse can travel at velocities approaching the Rayleigh velocity. Experimentally, high frequency SAW velocities of up to 10000ms^{-1} have previously been measured in ZnO-polycrystalline CVD diamond layered structures

[Nakahata 1994]. The high values recorded for samples 6 and 7 are, within the experimental errors, close to the expected Rayleigh velocities for single crystal diamond. Apart from sample 2, all other films support waves with a velocity of around 11000ms^{-1}; since no trend between films with differing crystal texture or film thickness can be determined from table (8.1), the most likely explanation for the higher velocity of samples 6 and 7 is film quality. For example, compare samples 4 and 5, these are both (110) films with similar grain sizes, however the thickness' differ considerably at 694 μm compared with 319 μm respectively. The maximum velocities are however very similar 11089ms^{-1} as compared to 11094 ms^{-1}. A similar result is seen for samples 1 and 3 which both have (100) morphologies. The data in the table also shows, that for the films with well developed texture, neither morphology (compare samples 3 and 4) or grain size appears to have a significant influence on the maximum velocity measured.

The optical micrograph, figure (8.8b), clearly shows that the sample 2 film has a rather poor, microcrystalline morphology reflected in a much weaker Raman 1332 cm^{-1} signal, figure 3 curve(III). The broad background and additional structure in the Raman indicates the presence of increased levels of poor quality and/or sp^2 material compared to the samples showing Raman spectra similar to curve (I) in the figure. The presence of graphitic material within the film might be expected to reduce the stiffness of the solid medium through which the Lamb wave travels. It could then be argued that this might account for the much lower velocity measured for this film . However sample 6, which shows good (100) crystal morphology, figure (8.8f), and the highest velocity measured here, also has a rather broad background in its Raman spectrum, figure (8.9) curve (II). While the diamond peak is still strong, the broad background is indicative of the presence of non-diamond components in this film despite which the sample shows a very high velocity. Schneider *et al.* [1997] observed a correlation between the acoustic velocity and the sp^2/sp^3 fraction in DLC films, with the higher velocities occurring in the films with the greater sp^3 content. Weglein *at al.* [1991] suggest however that in diamond-like-films (DLF), the influence of the sp^2 phase on acoustic velocity is only small. The resolution of these conflicting statements probably lies in the precise amounts of sp^2 present; DLC films can contain relatively large fractions of sp^2 material, diamond films, even quite poor examples, by comparison contain much lower fractions of this form of carbon. It would

certainly be expected that large amounts of graphitic carbon distributed throughout the film would strongly reduce it acoustic velocity. The much smaller amounts present in diamond films are generally concentrated in the grain boundaries. Therefore, while it cannot be ruled out that sp^2 in the film may be partly the cause of the lower acoustic velocity seen here, it seems more reasonable to conclude from these measurements that poor morphology, in the form of micro-crystallinity, is the more likely cause of lower acoustic velocities in thin film CVD diamond. This can be understood in terms of the increase in porosity and the very high grain boundary density present in microcrystalline films which would tend to reduce the 'average' stiffness of the film. Graphitic sp^2 may also be detrimental to the velocity but this is not proven here.

Noise originating from the rather small size and non-ideal flatness of the plates contributed to experimental uncertainties in this study and may have masked variations in the acoustic wave velocity of the well developed (100) and (110) polycrystalline materials which have been studied here. However, the predicted velocities for the (100) and (110) orientations are very similar, differing by only a few hundred ms^{-1} [M^{c}Skimmin 1957] and since the Lamb wave propagates throughout the full sample thickness, any determined velocity constitutes a mean velocity measurement averaging over the variation in grain size and morphology. Unless deliberately removed, all CVD diamond films have poorly defined morphology and fine grain structure on the nucleation side of the film and this is more likely to account for the similarity of velocities for the films studied here. To determine the differences more precisely, films would need to be thinned before analysis to remove the lower quality material. The results presented here have indicated that the effects of morphology and sp^2 fraction on the maximum acoustic velocity in good quality free standing diamond films must be relatively small, however more comprehensive and careful studies are necessary to establish the precise influences of these parameters.

8.4.2 Temperature and Dispersion Measurements

The form of the velocity-frequency plot shown in figure (8.13) is typical for the a_0 Lamb wave which is a dispersive acoustic mode [Oliner 1978]. A quantitative analysis can be carried out on this data to determine any temperature dependence and which also enables

data to be extracted from the acoustic signals concerning the material parameters of the wafer.

In general both the a_0 and s_0 types of lamb wave, described by equations (8.1) and (8.2), are dispersive. However for a plate of thickness $2h$, it can be shown that at low frequencies, where the wavelength λ becomes large compared to the plate thickness, the s_0 mode velocity becomes asymptotic to a constant value which is called the sheet velocity C_e [Dewhurst 1987]:

$$S_0 \approx C_e = 2C_t\left(1-\frac{1}{\mathrm{K}^2}\right)^{1/2}, \qquad \mathrm{K}=\frac{C_l}{C_t} \tag{8.7}$$

where C_l and C_t are the bulk longitudinal and transverse velocities respectively and the other quantities are as previously defined, section (8.1.3)

For λ large compared to the plate thickness, the velocity of the zero order asymmetric mode (a_0) decreases from the Rayleigh velocity (C_r) for the material to zero and at the lowest frequencies its dispersion characteristics are approximately [Dewhurst 1987]:

$$\omega \approx \frac{Ce}{\sqrt{3}}k^2h \ , \quad kh << 1 \tag{8.8}$$

from which the group velocity ($d\omega/dk$) for the mode can be determined as:

$$C_g = \frac{\mathrm{d}\omega}{\mathrm{d}k} \approx 2\frac{Ce}{\sqrt{3}}kh \tag{8.9}$$

eliminating k by squaring and using equation. (8.8) yields:

$$C_g{}^2 \approx \frac{4Ceh}{\sqrt{3}}\omega \tag{8.10}$$

Therefore the square of the group velocity ($C_g{}^2$) is proportional to the angular frequency ω and the gradient of a plot of $C_g{}^2$ vs. ω should yield an estimate of the plate thickness ($2h$)

provided a value for C_e is known. For values of $kh<<1$ the s_0 mode velocity is asymptotic to C_e and if the mode is clearly visible in the acoustic trace it can be used as an estimate for C_e. Alternatively an estimate for the sheet velocity (C_e) can be obtained from the C_g^2 vs. ω plot provided the thickness of the plate is known. Dewhurst *et al.* [1987] have used this method to measure the thickness of thin aluminium sheets. However, it can be difficult to determine the frequencies of the different components in the signal. An improvement, described by Royer *et al.* [1989], is to notice that in equation (8.10) ω is the time derivative of ϕ the instantaneous phase of the signal, this together with the path length (L) between source and detector given by $L=C_g t$ yields:

$$\omega = \frac{d\phi}{dt} \cong \frac{\sqrt{3}L^2}{4C_e h}\frac{1}{t^2} \tag{8.11}$$

and by integration, ϕ is a linear function of $1/t$ and a plot should yield a straight line with a gradient equal to:

$$\frac{\sqrt{3}L^2}{4C_e h}. \tag{8.12}$$

As noted by Royer *et al.* these characteristics are very easy to plot because ϕ is equal to $(n+1/2)\pi$ when the signal is zero and $n\pi$ when at a maximum or minimum. This is the basis of the method used here and the procedure was first to extract the dispersive a_0 part of the acoustic signal which was then smoothed using a 5 point Savitsky-Golay algorithm to preserve the magnitude and shape of peaks in the trace. The resulting signal was then differentiated to allow easy and precise location of the maxima and minima from which phase in units of $n\pi$ and corresponding values of $1/t$ were determined and plotted graphically. Finally, a value of C_e was determined from the gradient of a linear fit to the data points corresponding to the lowest frequencies present in the signal..

Figure (8.16) shows a plot of phase against $1/t$ for the measurements taken at a wafer temperature of 30°C. It is clear that the relationship is highly linear for small values of $1/t$ which correspond to the lowest frequencies. A least squares best fit to the lowest seven data points was carried out for each temperature; in each case the correlation coefficients

were better than 0.9990. The example shown in the figure was typical of the quality of the data and the subsequent fit at each measurement temperature.

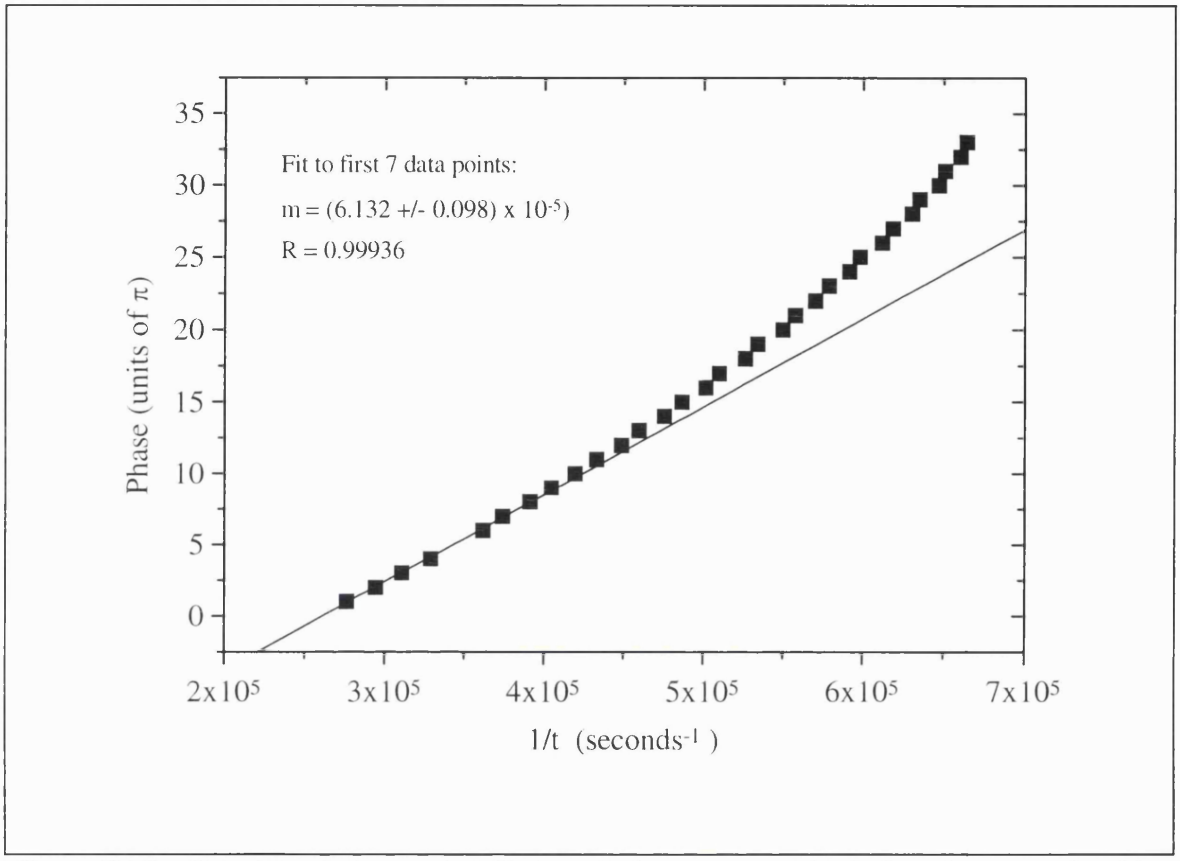

Figure (8.16): Plot of signal phase against *1/t* for a_0 lamb wave propagating in 5cm diameter wafer. Line shows least squares fit to the lowest frequency components of signal from which a value for C_e was extracted. The wafer temperature in the plot shown was 30 °C; other temperatures yielded similar quality plots.

Using equation (8.12) and the previously determined value of 84 μm for the wafer thickness, a value for the sheet velocity (C_e) was obtained for each temperature from the gradient of the linear fits to the phase vs. *1/t* plots. The results are shown in figure (8.17), together with errors determined from the least squares fit analysis. It is clear from the results shown in this plot that no variation in the acoustic sheet velocity could be determined for wafer temperatures in the range 30-250°C within the experimental errors appropriate to these measurements.

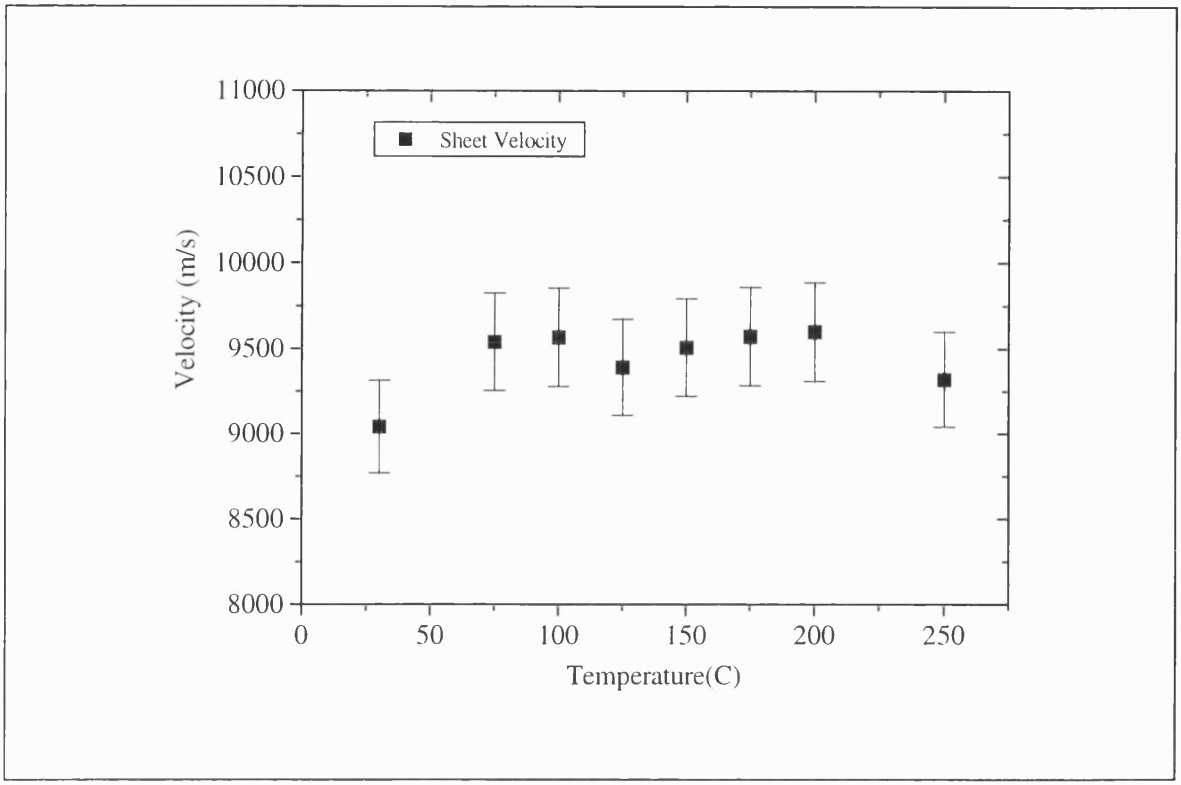

Figure (8.17): Values of C_e extracted from phase plots for wafer temperatures in the range 30 - 250 °C. The error bars were derived from the regression statistics.

A problem with this analysis is that the thickness ($2h$) is also function of temperature via thermal expansion of the substrate and this could influence the gradient determined from the $1/t$ plots. However, the Raman analysis, figure (8.11b), indicates that this sample has a very high phase purity and therefore it is reasonable to use the expansion coefficient of diamond to estimate the likely change in sample thickness with temperature. Calculation shows that for a 200 °C change in temperature the thickness variation is less than 0.02%, which is negligible compared to the other errors in the experiment.

The acoustic parameter plotted in figure (8.17) together with the velocity-frequency characteristics in figure (8.13) show virtually no variation with temperature. These results can be compared with the data of M^{c}Skimin *et al.* [1972] who calculated, from their measured elastic constants, a variation in the acoustic velocities for natural single crystal diamond of less than 1% over a temperature range of 240°C. For CVD diamond, Werner *et al.* [1996] have measured the Young's modulus of 300 μm thick plates by a three point bending technique and found negligible variation with temperature up to 600°C, implying a similar behaviour for propagating elastic waves. The CVD material used here would be

more closely represented by the properties of an *ideal isotropic polycrystalline plate* characterised by its Young's modulus (E), density(ρ) and Poisson ratio (ν); from which the *ideal* plate acoustic velocities can be determined. Klein [1992] has calculated a value of 1143GPa for the Young's modulus of polycrystalline diamond. Taking the accepted values [Wilks 1994] of ~3.51 gcm^{-3} and 0.07 for ρ and ν respectively, a value of 18076 ms^{-1} can be calculated for the sheet velocity C_e in an *ideal* polycrystalline diamond plate. This value is considerably higher than the value for C_e derived from the measurements made during this study, which yield a value of 9444 ms^{-1} (simple mean of all the measurements). For materials with a low value of Poisson ratio the sheet velocity approaches the bulk longitudinal velocity, C_l, and their ratio varies only slowly with ν; to within a few percent C_e is therefore a reasonable estimate for C_l from which an estimate of Young's modulus for the real plate can be calculated.

Werner *et al.* [1996] also measured the absolute value of Young's modulus for a number of free standing diamond plates using a beam bending technique. They found that the values of E for their plates were much lower than the value of around 1143 GPa which would be expected for an ideal polycrystalline plate. Values of E for their plates fell in the range 242 - 539 GPa, together with measured densities which were approximately 4% less than the theoretical value for ideal polycrystalline diamond. Their SEM investigation revealed the existence of significant densities of microcracks and voids within the films, while their Raman studies indicated only very low levels of sp^2 bonded material in the plates. They interpreted the less than ideal Young's modulus for the plates as an 'effective' modulus reduced by the presence of voids and microcracks within the film. An estimate for Young's modulus of around 305 GPa, for the film studied here, was obtained from the C_e velocity parameter derived from the dispersion measurements, together with a density of 3.4 $x10^{-3}$ gcm^{-3} . This value is well within the range measured by Werner *et al.* and was confirmed to within 20% by the separate beam bending tests described in section (8.3.3), where a value of 328 GPa was obtained for a sample taken from the wafer, see table 8.2. The results of the Raman analysis (figure 8.11b) also rule out the presence of any significant quantities of sp^2 material in this sample; it is worth re-iterating that Raman measurements are particularly sensitive to the sp^2 components, while the use of the red 632 nm laser excitation source would have exaggerated the sp^2 signal still further. The results

of the SEM study, described in section (8.3.3), have revealed the presence of extended defects including voids, cracks and grain boundaries within this film, see for typical examples figure (8.15).

The measurements and analysis presented here, together with the measurements on differing film types given in section (8.4.1), suggests that for *free standing* CVD diamond films, it is the quality of the films in terms of grain boundary, microcrack and void density which most significantly affects the observed acoustic velocity via the reduced 'effective' Young's modulus caused by these defects. At the levels present in these types of films the effect of sp^2 material is of little importance by comparison. Further evidence to support these conclusions can be obtained by considering the acoustic data from the square samples described in (8.3.1) in a little more detail. The data from these samples was previously analysed only in terms of the fastest acoustic components, however the acoustic pulses from these samples also exhibited strong dispersion of the signal similar to that seen for the 50 mm wafer. Although the dispersion results from these samples were not ideal, due mainly to the smaller size and much poorer optical quality of these substrates, some approximate values for the 'effective' Young's modulus were estimated from the lowest frequency a_0 components by applying the analysis described previously in section (8.4.2) . In table (8.3) the trends are compared to the results of the SEM analysis, described in section (8.2.3) and (8.3.3) and (figure 8.15), which was carried out on film cross-sections to examine quality in terms of the defects present within each film. In addition to the samples used for the acoustic measurements described here, other samples from three separate suppliers of free standing material were examined. In all cases defects were apparent which included; voids of varying size, large cracks, microcracks and grain boundaries along which fracture appeared to have taken place. It can be seen from table (8.3) that the 'defectivity' assessed qualitatively from the SEM study follows the trend for the 'effective' E derived from the dispersion data. In other words, the more defective a film appeared under SEM examination the lower the derived value for E. It should be noted that due to the relatively poor quality of the dispersion data obtained from the square samples (8.3.1) the trends indicated in table (8.3) are qualitative and a quantitative analysis would require more detailed experiments.

Sample	Film Characteristics	SEM Characterisation of X-section	C_e (ms^{-1})	'Effective' E (GPa)	E, beam bending (GPa)
50 mm Wafer	white diamond random morphology	Some defects, few voids, cracks, well formed not 'porous'	9444	305	328 +/- 20%
4	Dark (110) morphology	Extended defects, moderate voids, visible cracks, grain boundaries	7845	210	-----
7	Dark (100) morphology	Similar to sample 4	7384	185	-----
5	Dark microcrystalline morphology	Many defects, film looks porous, larger voids, cracks, very high grain boundary density throughout film.	5936	120	-----

Table (8.3): Summary of data obtained from the SEM characterisation and the analysis of velocity-dispersion curves for thin film diamond samples studied during this work.

8.4.3 Modelling of Dispersion Data.

The phase velocity-frequency and group velocity-frequency dispersion characteristics for lamb waves propagating in an ideal polycrystalline diamond plate can be modelled and compared to the velocity-frequency characteristics measured for the real CVD plate. An approximate expression can then be derived which describes the ω-k relationship over a limited frequency range for the real plate. Such an expression may be useful during the design of Flexural Plate Wave (FPW) devices which utilise lamb wave propagating in free standing thin diamond film.

For low frequency, a_0 mode lamb waves propagating in a plate with wavelengths much greater than the plate thickness ($2h$), it has been shown [Hutchins 1989] that the dispersion characteristics can be approximately expressed as:

$$\omega = A_1 k^2 + A_2 k^4 \qquad (8.13)$$

where A_1 and A_2 are constants to be determined. The group ($d\omega/dk$) and phase (ω/k) velocity-frequency characteristics can easily calculated from this expression. A common approach [Hutchins 1989, Sachse 1978] to find values for A_1 and A_2 is to obtain an

experimental ω-k curve from the phase function given by the Fourier transform of the measured acoustic signal. A non-linear least squares fitting algorithm can then be used to fit the curve to equation (8.13) yielding best fit values for A_1 and A_2. However, the procedure is sensitive to the quality of the recorded signal, the signal to noise ratio of the various frequency components and the choice of windowing function used to isolate the A_0 part of the signal [Hutchins 1989]. Attempts to carry out this type of analysis on the data recorded during the current study were only partly successful, due mainly to convergence problems with the non-linear fitting program. Instead an alternative method was used which avoided the use of non-linear fitting while yielding an acceptable fit to equation (8.13) for low frequency a_0 lamb waves. The values derived for C_e and E from the analysis presented in section 8.4.2, together with analytic expressions for A_1 and A_2 given by Hutchins *et al.* [1989] were used to calculate initial estimates for A_1 and A_2. These values were then used with equation (8.13) to obtain an ω-k relationship from which a group velocity-frequency curve was derived. The calculated curve was compared with the experimental curve using Microcal Origin 4.1 mathematical graphing software and the values of A_1 and A_2 adjusted to give a new curve. The process was repeated until, by trial and error, a qualitatively acceptable fit to the data was obtained. The results of the analysis are shown in figure (8.18); the solid curve represents the fitted equation to the experimental points (shown as solid blocks) with values of A_1=0.230 m^2s^{-1} and A_2= - 2.405 x $10^{-11}m^4s^{-1}$. The dashed curve shows the group velocity-frequency characteristics which were calculated for an ideal isotropic polycrystalline diamond plate with E,ρ and ν values of 1143GPa, 3.512 gcm^{-3} and 0.07, respectively. The fit shown is limited to frequencies up to 8 MHz because the requirement that kh is much less than unity, for equation (8.13) to be a reasonable approximation to the dispersion relation, is no longer well satisfied above this frequency. For both the real and ideal plates the phase velocity-frequency characteristics could also be obtained from equation (8.13) by simple calculation; it is worth noting that for very low frequencies, the group velocity is to a good approximation twice the phase velocity.

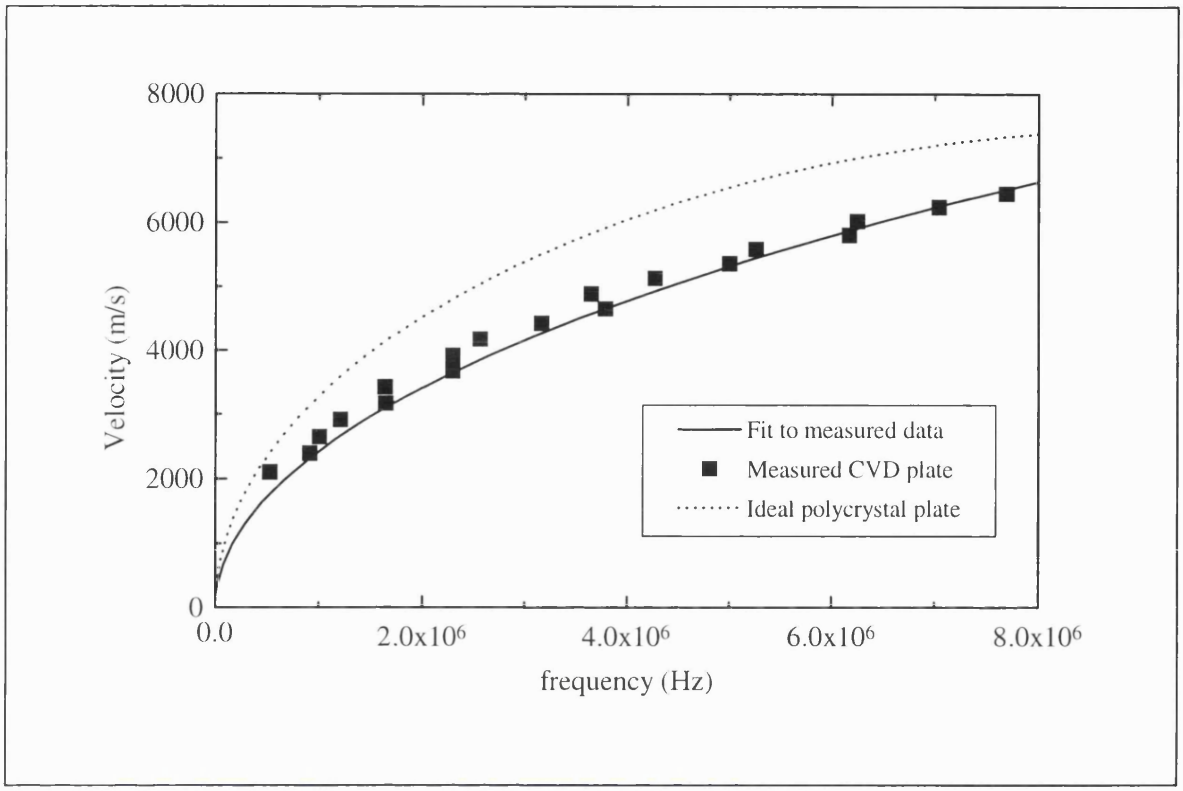

Figure (8.18): Plot showing the expected low frequency group velocity dispersion characteristics for the a_0 lamb wave in an ideal polycrystalline plate (dotted line) compared to the data for the real plate (solid blocks), together with a fit to the theoretical relationship assuming an 'effective' Young's modulus of 305 GPa for the real plate.

Some comment is required concerning the values extracted for the C_e parameter and the high maximum a_0 velocities which have been measured in the thicker films. The C_e parameter would normally be associated with the sheet velocity in an isotropic medium and would be expected to have a value close to the longitudinal velocity [Oliner 1978] considerably in excess of the Rayleigh velocity, which is the limiting value for the a_0 Lamb wave mode at large values of *hk*; this was clearly not the case here. It can be speculated that this arises from the strong vertical anisotropy which is characteristic of CVD diamond films. The cross-sections of such films clearly exhibit columnar growth and also a high density of grain boundaries running vertically through the full thickness of the film. As has been demonstrated by the beam bending test made on the sample considered here and confirmed by similar independent measurements on a range of CVD diamond plates [Werner 1996], the macroscopic or 'effective' Young's modulus derived from such measurements is very much reduced from the value of 1143 GPa expected for an ideal polycrystalline plate. A value of around 300-330 GPa was obtained for the plate studied

here. This low 'effective' E then results in the low value of the extracted C_e parameter which is derived from the low frequency dispersion characteristics of the asymmetric lamb wave mode. The a_0 mode is primarily a flexural wave dominated by the 'effective' stiffness of the plate. As the frequency of the lamb wave increases the acoustic wavelength becomes shorter and the wave will be more influenced by the microstructure. It also travels closer to the plate boundary and is therefore less affected by defects in the plate bulk. Indeed Jiang *et al.* [1991] have shown that the properties of individual crystallites in polycrystalline diamond films are close to the ideal natural crystal values; hence it is not surprising that at higher frequencies the behaviour of acoustic waves deviates significantly from that which would be expected from consideration of its low frequency behaviour alone. It is likely that a complete description of acoustic propagation over the whole frequency range in a material as complex as CVD diamond will require consideration of the microstructure and in particular careful modelling of the strong vertical anisotropy which is a characteristic feature of these films.

8.5 Applications

The acoustic wave measurements undertaken during the course of this study have lead the author to propose that CVD diamond films may be an ideal candidate for the fabrication of FPW based sensors which utilise the lamb wave modes [Whitfield 1998]. Such devices are not new but it believed that this is the first time that it has been suggested that CVD diamond films may be useful for this class of devices. This suggestion has resulted in an ongoing research program to study diamond acoustic devices with a particular aim of fabricating the lamb wave sensor which was outlined during these studies. Therefore the following section presents a brief discussion of FPW devices and includes the proposed device.

Acoustic wave propagation in diamond can be utilised to construct a wide range of devices; most recently research has concentrated on the use of diamond to fabricate very high frequency surface acoustic wave filters (SAW) which utilise the non-dispersive Rayleigh wave propagating in the surface of the material. The simplest examples of these devices utilise two interdigitated transducers coupled to a diamond substrate via a thin piezoelectric

layer such as ZnO. Acoustic waves are launched from the input transducer and travel in the surface of the substrate to be detected by the nearby output transducer. The operational frequency of these devices is proportional to the acoustic velocity of the material and inversely proportional to the IDT finger spacing. The very high acoustic velocity of diamond compared to other acoustic substrates therefore enables the fabrication of very high frequency devices without the need to resort to very fine (and expensive) IDT geometries. Some success has recently been achieved with these devices and CVD diamond bandpass filters operating at frequencies as high as 2.5 GHz have been fabricated [Nakahata 1996]. However the published work is at the 'proof of principle' level and much remains to be done to achieve low insertion loss, high coupling efficiencies and high mechanical integrity of deposited piezoelectric layers on the diamond substrate.

An alternative acoustic device for which, to the author's knowledge, diamond has not yet been considered is the Flexural Plate Wave (FPW) device which utilises the propagation of Lamb waves for its operation. The device is very similar to a SAW device in structure requiring two IDT transducers coupled via a piezoelectric layer to a diamond substrate. The most significant difference is that the substrate thickness and IDT geometry are chosen so that the a_0 Lamb wave is the dominant acoustic mode which propagates between the transducers. FPW devices can be used in a wide range of applications such as fluid pumping, gravimetric sensing, chemical vapour sensing and viscosity measurement, [Moroney 1991, Wenzel 1989]. A particular feature of these devices is the ability to function in electrically conductive and corrosive media by virtue of the isolating plate separating the medium from the transducers. CVD diamond would be ideally suited to the fabrication of such devices as the material is strong, electrically insulating and highly chemically and physically resistive. Many FPW devices have medical applications and diamond is particularly compatible with biological materials; the highly dispersive nature of lamb waves propagating in thin plates can be used to fabricate frequency dependent delay lines for use in chirp filters and radar applications. The use of the a_0 Lamb wave mode, which has been studied here, has a particularly interesting consequence for sensors; for a fixed frequency the phase velocity of the wave becomes very small as the thickness of the plate becomes small [Sze 1994]. In an acoustic sensor e.g. a fluid sensor, this behaviour means the design of the sensor can be chosen so that the propagation velocity of

the wave is lower in the sensor material than in the contacting fluid, resulting in very low power losses into the fluid. In contrast, high power losses of the order 1dB/λ [Sze 1994] are a particular problem for SAW based sensors.

Figure (8.19) shows a schematic of a CVD diamond based FPW gravimetric fluid sensor which is proposed for operation in harsh environments. The device consists of a thin, free standing CVD diamond membrane on which two aluminium IDT transducer structures are formed by conventional photolithography and thermal evaporation onto the smooth nucleation side of the film. The structures are then overcoated with a thin layer of a suitable piezoelectric, an interesting possibility here is ZnO deposited by pulsed laser deposition (PLD) which might help reduce the stress problems which can occur with the more conventionally sputter deposited form of this material on CVD diamond. It is worth noting, that because the lamb wave propagates throughout the thickness of the film, the lithography can be carried out on the almost optically flat nucleation side. This avoids either the need to carry out difficult work on the rough growth surface or expensive polishing of the surface to prepare it for photolithography. Access is then opened into the ZnO and contact pads deposited to facilitate external connection. A thin layer of a chemically selective material is deposited onto the opposite side of the CVD film to form the sensor. The input and output IDT's are connected in a feedback configuration and the system oscillates at a frequency determined by the propagation velocity of the lamb wave and the separation of the two IDT's; the propagation velocity being determined by the substrate material and its dispersion characteristics, with the wavelength determined by the IDT finger spacing. Chemical species of interest are selectively adsorbed in the sensing layer and result in an increase in the specific mass of the film which can be monitored as a change in the oscillation frequency of the device. Furthermore, the low reactivity of the diamond surface means that device design can concentrate on the behaviour of the active chemical layer with minimal consideration given to interactions between the environment and the diamond plate.

Wenzel *et al.* [1989] have shown that the mass sensitivity of lamb wave sensors is given by $S_m = -1/4\rho h$, which in contrast to SAW sensors is independent of the operating wavelength.

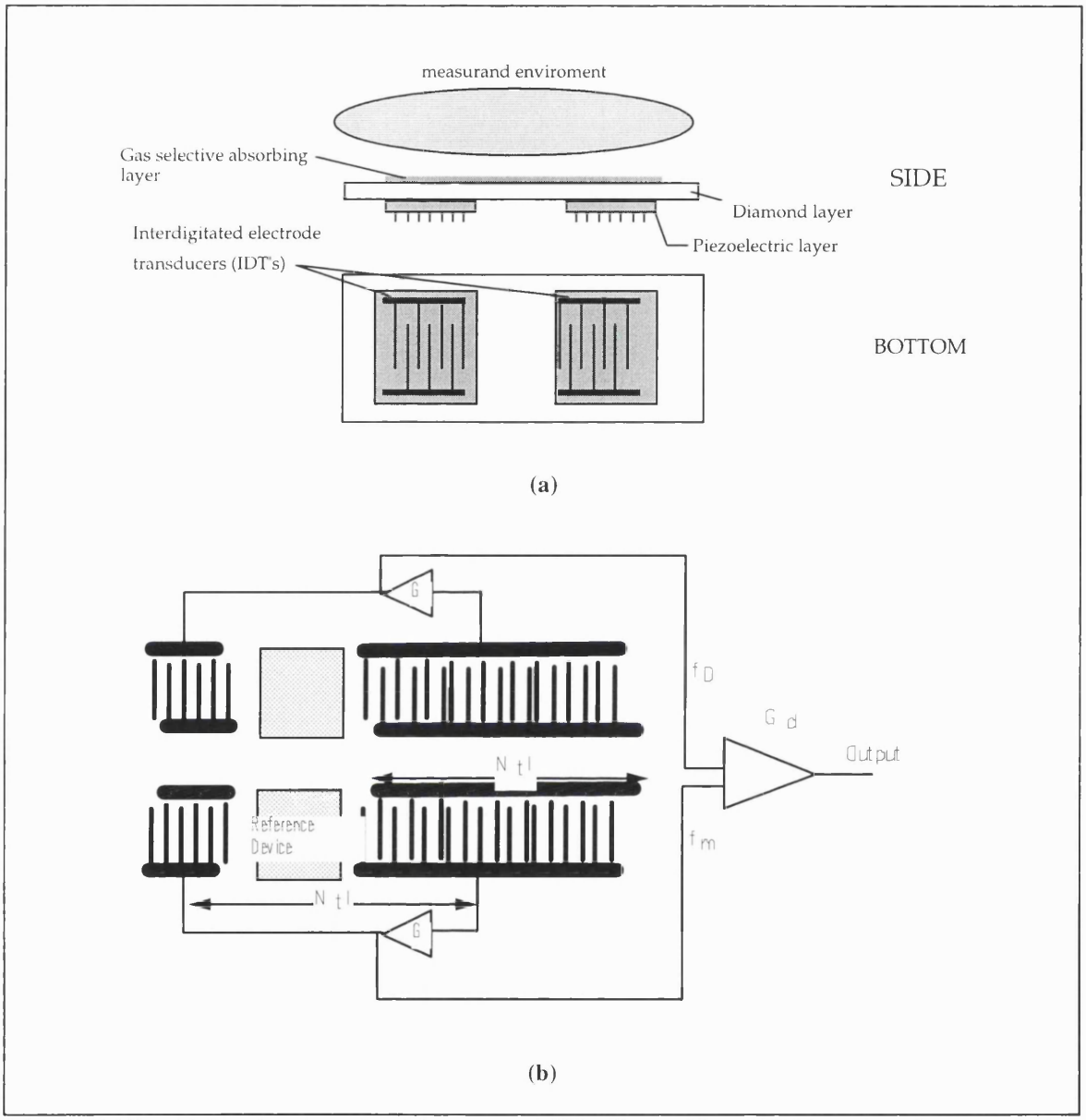

Figure (8.19): (a) Simple schematic of the proposed CVD diamond based FPW gravimetric sensor device and (b) practical implementation showing feedback circuitry and a reference device to account for systematic changes.

It can be speculated that the strength and lightness of diamond could result in very thin plates and consequently a high sensitivity at much lower frequencies compared with either SAW or Bulk wave sensors. For example; a CVD diamond FPW sensor utilising a 2 μm thick plate with mechanical properties similar to the plate studied in this chapter, section (8.4.2), and incorporating two IDT's spaced 1200 μm apart, with a wavelength of 100 μm determined by the IDT finger spacing, would operate with a phase velocity of around 700 ms^{-1}, fundamental frequency of about 7 MHz and an

oscillation frequency of 0.5 - 1 MHz depending on the total phase shift in the delay line. The mass sensitivity is estimated to be around 70 cm^2g^{-1}. Figure (8.19 b) shows a practical implementation of the sensor which includes feedback circuitry and a reference device fabricated on the same substrate to allow compensation of systematic drifts due to e.g. temperature or ageing effects.

In summary, CVD diamond is proposed as a candidate for extreme environment lamb wave sensors and a possible sensor design suggested which draws on results of Lamb wave measurements made during this study. The suggested device is the subject of an ongoing research study by the author at the Diamond Electronics Group at UCL.

8.6 Summary.

This chapter has examined the subject of acoustic wave propagation in thin film diamond in the light of recent promising progress in the use of this material as a substrate for high frequency surface acoustic wave devices. Acoustic wave propagation in CVD diamond has received little attention in the literature and there is virtually no data available to assess the relative importance of the various characteristics of these films on the propagation of acoustic waves. The studies presented in this chapter represent, to the author's knowledge, the first attempt to examine the role of film characteristics such as morphology and quality on acoustic wave propagation. It is also believed that this study introduces the technique of laser ultrasonics to the CVD diamond community for the first time.

The measurements on a range of films with strongly differing morphologies indicate that lamb waves with high group velocities can propagate in all these films. However poor quality in terms of microcrystallinity and high grain boundary density appears detrimental to the acoustic wave velocity; little difference was seen in these experiments between films with predominantly good but different morphologies e.g. (110) compared to (100). Graphitic material is not suggested as being a significant influence in *these* films, however a detrimental effect on acoustic velocity can not be entirely ruled out by these experiments in view of the generally low levels of sp^2 material indicated by the Raman spectra.

Analysis of velocity-dispersion characteristics when combined with the results of SEM studies and beam bending tests indicate that the propagation of acoustic lamb waves within these types of film are strongly influenced by the defect density in terms of voids, micro-cracks, cracks and grain boundaries, which give rise to a considerably reduced value for the 'effective' Young's modulus for the material. At the levels present within the free standing films studied here, the sp^2 content has marginal influence by comparison. The velocity-frequency characteristics were measured as a function of wafer temperature over the range 30 - 250 °C; within the experimental errors no variation in either the dispersion characteristics or sheet velocity could be determined. The measured dispersion characteristics for low frequency asymmetric Lamb waves were compared to the calculated propagation characteristics for an ideal, isotropic, polycrystalline diamond plate and shown to be reasonably well represented by an equation of the form $\omega=A_1k^2+ A_2k^4$ provided a reduced 'effective' Young's modulus was assumed for the real CVD plate. Such dispersion characteristics are an important parameter in the design of flexural plate wave sensors which utilise lamb wave acoustic modes. For the first time thin film diamond was proposed as an important material for fabrication of harsh environment FPW sensors. A simple design, which is the subject of current research, was presented as a prototype for a CVD diamond FPW device for use as a hostile environment gravimetric sensor.

8.7 References.

Adler E.L. and Solie L., [1995], *IEEE Ultrasonics Symposium*, 341.

Ballantine D.S., White R.M., Martin S.J., Ricco A.J., Zellers E.T., Frey G.C. and Wohltjen H., [1997], *Acoustic Wave Sensors: Theory, Design and Physico-Chemical Applications,* (Academic Press), San Diego, London, Boston.

Dewhurst R.J., Edwards C, M^{c}Kie A.D.W and Palmer S.B, [1987], *Appl. Phys. Lett.*, **51**, 1066.

Fayette L., Marcus B., Mermoux M., Abello L. and Lucazeau G., [1994], *Diam. & Relat Mater.*, **3**, 438.

Hachiago A., Malocha D.C. and Richie S.M., [1995], *IEEE Ultrasonics Symposium*, 371

Hess P., [1993], *Berrichte de Bunsen Gesellschaft fur physikalische Chemie*, **97**, 1680.

Hutchins D.A. and Lundgren K, [1989]., *J. Acoust. Soc. Am.*, **85**, 1441.

Jiang X., Harzer J.V., Hillebrands B, Wilde Ch. and Koildl P., [1991], *Appl. Phys. Lett.* **59**, 1055.

Klein C., [1992], *Mater. Res. Bulletin*, **7**, 1407.

Kushibiki J. and Chubachi N., [1985], *IEEE Trans. Sonics and Ultrasonics*, **32**, 189.

McKeag R.D., Chan S.S.M, Johnston C.,. Chalker P.R and Jackman R.B., [1995], *Mater. Sci.Eng B*, **29**, 78.

McSkimin H.J. and Andreatch P Jr., [1972], *J. Appl. Phys.*, **43**, 2944.

McSkimin H.J. and Bond W.L., [1957], *Phys. Rev.*, **105**, 116.

Monchalin J.P., [1986], *IEEE Trans. on Ultrasonics, Ferroelectrics and Frequency Control*, **33**,485.

Middelhoek S. and Audet S., [1994], *Silicon Sensors,* Delf University Press.

Morgan D.P., [1985], *Surface Wave Devices for Signal Processing*, (Elsevier).

Moroney R.M., White R.M., and Howe R.T., [1991], *Appl. Phys. Lett.* **59**, 774.

Nakahata H, Hachigo A, Shikata S and . Fujimori N, [1992], *IEEE Ultrasonics*

Nakahata H, Higaki, Fujii S, Kitabayashi H, Tanabe K, Seki and Shikata S, [1996] *Sumitomo Electric Technical Review*, 41.

Nakahata H., Higaki K., Hachigo A., Shikata S., Fujimori N., [1995], *IEEE Trans. Ultrasonics, Ferroelectrics and Frequency Control*, **42**, 362.

Nakahata H., Higaki K., Hachigo A., Shikata S., Fujimori N., Takahashi Y., Kasihara T. and Yamamoto Y., [1994], *Japn. J. Appl. Phys.*, **33**, 324.

Oliner A.A.,(ed.) [1978], *Acoustic Surface Waves*, (Springer-Verlag), Berlin, Heidelberg, New-York,

Royer D., Dieulesaint E. and Leclaire Ph., [1989], *IEEE Ultrasonics Symp.* 1163.

Sachse W. and Pao Y-H., [1978], *J. Appl. Phys.*, **49**, 4320.

Sails S.R., Gardiner D.J., Bowden M., Savage J and Rodway D, [1995], *Diam. Relat. Mater.*, **5**, 589.

Schnieder D., Schwarz T., Scheibe H-J. and Panzner M., [1997], *Thin Solid Films*, **295**, 107.

Scruby C.B., [1989], *Ultrasonics*, **27**, 195.

Symposium, 377.

Sze S.M., (ed.), [1994], *Semiconductors Sensors* ,(John Wiley and Sons Inc.), (1994).

Timoshenko S and Woinsky-Krieder S.,[1959], *Theory of Plates and Shells*, 2nd Edition, M^{c}Graw-Hill.

Viktorov, [1967], *Rayleigh and Lamb Waves*, (Plenum Press), New York

Weglein R.D. and Mal A.K., [1991], *Surface and Coating Tech.*, **47**, 677.

Wenzel S.M., and White R.M.,[1989], *Appl. Phys. Lett.* **54**, 1976.

Werner M, Klose S., Szucs F., Moelle Ch., Fecht H.J., Johnston C., Chalker P.R. and Buckley-Golder I.M., [1996], *Diam. Relat. Mater.*, **6**, 344.

Whitfield M.D., Audic B., Flannery C.M., Kehoe L.P., Crean G.M., Johnston C., Chalker P.R and Jackman R.B., [1998], *Diam. and Relat. Mater.*, **7**, 533.

Wilks J. and Wilks E., [1994], *Properties and Applications of Diamond*, Butterworth-Heinmann, Oxford, UK.

Wild C., Kohl R., Herres N., Muller-Sebert W., and Koidl P., [1994], *Diam. and Relat. Mater.*, **3**, 373.

Williams B.E., Glass J.T., [1989] *J. Mater. Res.* **4**, 373.

Yamanouchi K, Sakurai N and Satoh T, [1989], *IEEE Ultrasonics Symposium*, 351.

Chapter 9

Concluding Remarks

The recent and remarkably rapid development of a chemical vapour deposition method for the growth of a thin film form of diamond, from a mixture of hydrogen and hydrocarbon feed gases under condition of modest temperature and pressure, may provide a realistic opportunity for the full exploitation of many of the remarkable properties which diamond possesses. As was summarised in chapter two, the improvements to many fields of application that the use of diamond could bring, based on predictions from the properties of the natural form, are considerable. For example, diamond has by far the highest thermal conductivity of any material, some four times that of copper, and its introduction into the field of integrated electronics, merely as a thermal substrate, could solve many of the current thermal management problems which are beginning to concern ULSI manufacturers as they seek to pack transistors in ever higher densities onto silicon. However, diamond is not only a material for passive use; it also has the potential to be an excellent semiconductor, with properties far surpassing its more common competitors such as GaAs and Si. This is especially true where applications are likely to be in hostile environments of elevated temperature and radiation. The figures of merit presented in chapter two, although they should not be interpreted too literally, provide a measure of the likely benefits to be obtained from diamond if fully active electronic devices made from this material become a reality. However, it is necessary to temper all the enthusiastic predications which have been made on the behalf of thin film diamond [e.g. Yoder 1994] with some measure of reality. The realisation of fully active electronic devices, which are able to deliver the promise suggested by the FOM's discussed in chapter two, require that we are able at the least to grow reasonably large area single crystal thin film diamond substrates on which to work. Since thus far no suitable large area diamond substrates are in evidence, this means the heteroepitaxial growth of diamond is a necessity. Although there are no accessible lattice matched materials which can be considered as substrates for the heteroepitaxy of diamond, the successful growth of single crystal beta silicon carbide on silicon, despite a considerable lattice mismatch, indicates that growth of single crystal

diamond films may be possible under the correct conditions. However, despite the very promising progress which has been achieved in the growth of highly oriented diamond (HOD) films on silicon, using the bias enhanced nucleation process, this goal has not yet been achieved. It would seem that the bias nucleation approach is the most promising route along this path; However, our very poor understanding of ordinary nucleation mechanisms, let alone the more complex situation which prevails once a large substrate bias is introduced into the complex CVD environment, severely hampers progress towards the goal of heteroepitaxy for CVD diamond. Clearly it is very important, if single crystal growth on non-diamond substrates is to be achieved, that the mechanisms which underlie BEN are elucidated.

In the meantime; as was discussed in chapter two, the continued rapid development of this exciting field requires applications which can profitably utilise the *currently* available thin film material; which although polycrystalline, is in many respects excellent, equalling the performance of the natural material in some areas. This is particularly true in the thermal and optical applications, where artefacts such as 5-10 cm diameter flat and *hemispherical* optical windows, with thickness of the order millimetres, are simply not a realistic prospect from any other source of diamond. Governments and the public purse cannot be expected to fund indefinitely fundamental research of the nature required to solve the outstanding problems, particularly in the areas of nucleation and growth, that still exist in this field. It is very important that CVD diamond begins to repay the huge investments, encouraged by the initial enthusiastic assessments of the material, with some real beneficial applications. This author is firmly of the opinion, that with the realisation of active diamond electronics probably some way off, one way to achieve this goal is through intelligent use of current CVD material for novel or niche applications which make limited use of the electronic properties of diamond but also combine this with one or more of the other extreme properties of the material; such as wide bandgap, biochemical compatibility or thermal conductivity. In this way, devices which would be difficult or impossible with other material systems may be realised. Possible examples are the visible blind UV detectors, medical devices and acoustic wave devices discussed in chapter two.

With these thoughts in mind this thesis has attempted to address both the fundamental aspects of CVD diamond research, together with a practical contribution towards the realisation of the promising acoustic waves applications which have been considered in earlier chapters. Work has been carried out to characterise growth and nucleation on tungsten, an industrially important material, with many applications which might benefit from CVD diamond coatings; metal substrates may also be useful alternatives to the predominantly studied silicon as they can be machined with more ease into three dimensional shapes for use in the production of e.g. hemispherical optical windows. This thesis has presented a comprehensive study of bias enhanced nucleation and growth on both single crystal and polycrystalline forms of this material and demonstrated that high quality (100) textured diamond can easily be grown. In parallel with this work, an attempt to try and understand some of the effects of the substrate bias has been undertaken through the use of optical emission and electrical studies described in chapter five and six. The substrate bias markedly effects the regions of the microwave plasma which are in near contact with the substrate during bias as can easily be verified by visual observation; Spatially resolved OES indicates that within this region the atomic hydrogen concentration is strongly influenced and possibly the balance of C_2 and CH species; it is already known that basing promotes more rapid formation of the carbon saturation of the surface which appears to precede nucleation. The changes observed by OES appear to be closely linked with the appearance of a secondary glow between the substrate and the microwave plasma bulk; high resolution OES studies carried out in this study have indicated that this is a region where a high rate of inelastic processes occurs, resulting in the generation of additional atomic hydrogen close to the surface; the importance of this species to the processes of diamond nucleation and growth is widely acknowledged in the literature. While OES can be difficult to interpret, the approach used here, in which the effects of a bias on argon, hydrogen-argon and hydrogen-methane-argon plasmas has been compared, is of some help in this respect. The measurements have indicated that the secondary glow is very similar to the cathode fall region of a DC glow discharge and that elevated inelastic process rates, probably originating from secondary electron emission from the substrate, are likely in this region. The importance of this secondary glow region has been recognised in a very recent model which assigns it an active role during the formation of diamond nuclei under bias conditions [Stockel 1998]. However, whether the role of this region

during the bias process occurs primarily through physical or chemical means is unclear and remains to be established. Most likely it will prove to be a combination of both.

On a more practical note, the work described in chapter seven of this thesis has indicated that although the effects bias may be somewhat variable due to the critical sensitivity of the oriented nuclei to the integrated bias current, simple laser reflectometry may offer some prospects for *in-situ* process control. The ring of oriented material, typically observed during biasing, appears reasonably easy to detect using this simple technique. Remaining on a practical note; but moving on to the development of immediate applications for current CVD material; the acoustic propagation work presented in chapter eight has introduced the technique of Laser Ultrasonics, which is well known in the field of ultrasonics but new to the diamond community. The information derived from the study described in chapter eight, while far from comprehensive, should be of benefit in the emerging field of diamond acoustic devices. The study has lead the author to suggest that thin film diamond may be well suited to the fabrication of FPW based harsh environment sensors; which should be devices which can expect to find reasonably immediate applications. Being very similar to SAW devices, rapid progress for FPW devices could be expected. However, a proof of principle FPW has yet to be fabricated from CVD diamond and this could be a promising direction for future work.

Looking forward to the future, the work undertaken for this thesis suggests that in addition to further acoustic wave studies and the development of acoustic applications, the CVD diamond field would benefit from further sustained efforts to try and determine the precise mechanisms of the BEN process, which has proved so successful at advancing the goal of epitaxy. However given the difficulty of studying complex systems, such as the microwave substrate-plasma environment, rapid progress in this area can not be expected. In particular, regarding the OES measurements made here, it would be very useful to make further investigations of the secondary glow region using alternative techniques.

9.1 References.

Stockel R., Stammler M., Janischowsky K., Ley L., Albrecht M. and Strunk H.P., [1998],*J. Appl. Phys.*,**83**, 531.

Yoder M.N., [1994], in *Synthetic Diamond: Emerging CVD Science and Technology*, (eds. Spear H.E. and Dismukes J.P.), John Wiley and Sons Inc., New York

Appendix A

GLOSSARY.

BEN	Bias Enhanced Nuceation.
BSE	Back Scattered Electron.
CARS	Coherent Anti-Stokes Raman Spectroscopy.
CRDS	Cavity Ring-down Spectroscopy
CVD	Chemical Vapour Deposition.
DLC	Diamond-like Carbon.
DLF	Diamond-like Film.
EDX	Energy Dispersive X-ray Spectroscopy.
EEDF	Electron Energy Distribution Function.
FFT	Fast Fourier Transform.
FPW	Flexural Plate Wave.
He-Ne	Helium Neon (as in Laser).
HOD	Highly Oriented Diamond Film.
IDT	Interdigital Transducer.
MCA	Multi Channel Analyser
MPECVD	Microwave Plasma Enhanced Chemical Vapour Deposition.
Nd-YAG	Neodinium-Yittrium Aluminium Garnet (as in Laser).
N_e	Electron density (plasma).
OES	Optical Emission Spectroscopy.
PDF	Polycrystalline Diamond Film.
REMPI	Resonance Enhanced Multi-Photon Ionisation.
R-L	Rayleigh-Lamb equations.
SAW	Surface Acoustic Wave.
SE	Secondary Electron.
SEM	Scanning Electron Microscopy.
TALIF	Two photon Allowed Laser Induced Florescence

TCD	Temperature Coefficient of Dispersion.
TCF	Temperature Coefficient of Frequency.
TDF	Textured Diamond Film.
T_e	Electron Temperature (plasma).
TEM	Transmission Electron Microscopy.

Appendix B

Publications related to this thesis.

[1] *Microwave plasma characteristics during bias-enhanced nucleation of diamond: an optical emission spectroscopic study*, Whitfield MD, Jackman RB, Rodway D, Savage JA, Foord JS , *Journal of Applied Physics*, Oct 1 1996, Vol.80, No.7, p.3710

[2] *Biased enhanced nucleation of diamond on metals: an OES and electrical investigation*, Whitfield MD; Rodway D; Savage JA; Foord JS; Jackman RB, *Diamond-and-Related-Materials*. vol.6, no.5-7; April 1997; p.658-63

[3] *Optimising control of microwave plasma bias enhanced nucleation for heteroepitaxial chemical vapour deposition diamond*, Marshall RD; Whitfield MD; Tracey S; Thompson DJ; Foord JS; Jackman RB, Diamond-and-Related-Materials. vol.6, no.5-7; April 1997; p.676-80

[4] *Polycrystalline diamond films for acoustic wave devices*
Whitfield MD, Audic B, Flannery CM, Kehoe LP, Crean GM, Johnston C, Chalker PR, Jackman RB , *Diamond and Related Materials,* Feb 1998, Vol.7, No.2-5, pp.533- 539

[5] *Aluminium nitride/diamond and gallium nitride/diamond SAW devices.*, Chalker PR, Joyce TB, Johnston C, Whitfield MD, Jackman RB, *Diamond. and Related Materials.*1999, In Press.

[6] *Accoustic Wave Propagation in free standing CVD diamond: Influence of film quality and temperature.*, Whitfield MD, Audic B and Jackman RB, *Diamond and Related Materials.* 1999, In Press.

[7] *Characterisation of Acoustic Lamb Wave Prpagation in Polycrystalline Diamond Films by Laser Ultrasonics*, Michael D Whitfield. Barbara Audic Colm M Flannery, Liam P Kehoe, Gabriel M Crean and Richard B Jackman, *Journal of Applied Physics*, Submitted.

[8] *Spatially resolved optical emission studies of the secondary plasma region observed during electrical biasing of a diamond microwave plasma.*, Michael D Whitfield and Richard B Jackman, *Diamond-and-Related-Material*, Submitted.

[9] *Nucleation and Growth of Diamond films on single crystal and polycrystalline tungsten substrates.,* Michael D Whitfield and Richard B Jackman, *Diamond-and-Related-Materials*, Submitted.

[10] *High-performance metal-semiconductor field effect transistors from thin-film polycrystalline diamond*, Looi HJ, [13] , Vol.7, No.2-5, pp.565- 568

[11] *Enhancement mode metal-semiconductor field effect transistors from thin-film polycrystalline diamond*, Looi HJ, Pang LYS, Wang Y, Whitfield MD, Jackman RB, IEEE Electron Device Letters, Apr 1998, Vol.19, No.4, pp.112-114

[12] *UV photodetectors from thin film diamond,* Chan SS, McKeag RD, Whitfield MD, Jackman RB, *Physica Status Solidi (A) Applied Research*, Mar 1996, Vol.154, No.1, pp.445-454

[14] *Thin film diamond photodiode for ultraviolet light detection,* Whitfield MD; Chan SSM; Jackman RB, *Applied-Physics-Letters*. vol.68, no.3; 15 Jan. 1996; p.290-2

[15] *A high performance UV photodetector from thin film diamond*, McKeag RD; Whitfield MD; Chan SS; Pang LY; Jackman RB, *Diamond for Electronic Applications. Symposium. Mater. Res. Soc*, Pittsburgh, PA,

[16] *A thin-film diamond phototransistor*, Lansley SP; Hui Jin Looi; Yanyang Wang; Whitfield MD; Jackman RB , *Applied Physics Letters*. vol.74, no.4; 25 Jan. 1999; p.615-17